Conception and synthesis of the new cryptophane for the applications in xenon NMR molecular imaging

Bo Gao

NNT : 2016SACLS283

THESE DE DOCTORAT
DE
L'UNIVERSITE PARIS-SACLAY
PREPAREE A
L'UNIVERSITE PARIS SUD

ÉCOLE DOCTORALE N°571
Sciences chimiques : molécules, matériaux, instrumentation et biosystèmes

Spécialité de doctorat : Chimie

Par

M. Bo Gao

Conception et synthèse de nouveaux cryptophanes pour des applications en l'imagerie moléculaire par RMN du xénon

Thèse présentée et soutenue à CEA Saclay, le 05 octobre 2016 :

Composition du Jury :

M. Cyrille Kouklovski, Professeur, Université de Paris Sud, Président du Jury
M. Jean-Claude Chambron, Directeur de Recherche, Université du Bourgogne, Rapporteur
Mme. Olivia Reinaud, Professeur, Université Paris Descartes, Rapporteur
M. Thierry Brotin, Directeur de Recherche, ENS de Lyon, Examinateur
M. Christophe Dugave, Chercheur, CEA Saclay, Directeur de thèse
M. Grégory Pieters, Chercheur, CEA Saclay, Invité

Remerciement

Je voudrais remercier ici toutes ces personnes qui m'ont beaucoup aidé dans ces trois ans de thèse. Avec vous, j'ai passé non seulement une très belle aventure en chimie, mais aussi des moments sympathiques et mémorables.

Je tiens tout d'abord à exprimer mes sincères remerciements au Dr. Thierry Brotin, au Dr. Jean-Claude Chambron, au Pr. Cyrille Kouklovski et au Pr. Olivia Reinaud, membres du jury qui ont accepté de juger mon travail de thèse et avec lesquels j'ai eu des échanges très agréables et intéressants.

J'adresse mes remerciements les plus chaleureux au Dr. Christophe Dugave et Dr. Bernard Rousseau qui m'ont encadrée dans la réalisation de ces travaux. Leurs conseils et leur bienveillance ont très largement contribué au bon déroulement de ces trois années, aussi bien d'un point de vue scientifique que d'un point de vue personnel.

Je remercie également toute l'équipe LSDRM : Dr. Patrick Berthault, Céline Boutin, Emilie Mari, Estelle Léonce, pour leur énorme contribution dans la caractérisation des cryptophanes par RMN ^{129}Xe.

Je remercie tous les autres collaborateurs dans le projet « NSCLC » : Dr. Sofia Rivera pour les expériences cellulaires et les discussions sympathiques, Dr. Hervé Volland pour son aide dans la manipulation avec des anticorps.

Je remercie Dr. François Fenaille pour son aide chaleureux dans la spectrométrie de masse.

Je tiens à remercier toute l'équipe du laboratoire d'analyse: David Buisson, Céline Chollet, et Elodie Marcon.

Je souhaite dire un grand merci à tous mes collègues dans la « crypto team » : Dr. Emmanuelle Dubost pour m'avoir introduit au non seulement le monde du crypto mais aussi la vie quotidienne dans laboratoire, pour sa patience et son enthousiasme qui me rend vraiment agréable dans la nouvel équipe; Dr. Gaëlle Milanole pour tous les moments précieux qu'on a passé ensemble et son soutien et encouragement quand la chimie marche moins bien; Emilie Mari pour son aide en RMN ^{129}Xe et la bonne chance qu'elle m'a emmener; et finalement, Dr Grégory Pieters pour être toujours là pour moi comme un grand frère pendant tous ces trois ans.

Je remercie également Dr. Eric Doris pour sa gentillesse et attention, Dr Edmond Gravel pour ses conseils en PEG et en ma vie, Dr. Sophie Feuillastre pour son humeur et les introductions

de l’histoire française, Sébastien Garcia pour sa disponibilité et son enthousiasme, Florence Pillon pour sa patience et sa reponsabilité.

Je tiens tout particulièrement à remercier Longhui Gao pour son soutien, ses conseils, et tous les moments qu’on a partagé ensemble dans les derniers deux ans.

J'exprime mon amicale reconnaissance à toutes les personnes que j'ai côtoyées au Laboratoire de Marquage au Tritium : Dinh Vu Nguyen pour notre solidarité comme les thésards dans la même promotion, Anaëlle Doerflinger pour toutes les discussions très sympathiques entre nous, Dr. Simon Donck pour son humeur et son énergie, Dr. Serge Perato pour ses musiques hyper-cool, Dr. Damien Clarisse pour sa bière délicieuse, Dr. Isabelle George pour son encouragement dans mon cours de conduite, et Dr. Alaric Desmarchelier, Dr. Marielle Tamigney Kenfack, Dr. Emilie Nehlig, Olivia Carvalho pour leur gentillesse et leur encouragement dans ma rédaction de thèse.

Je remercie Dr. Fréderic Taran pour sa responsabilité, Dr. Davide Audisio pour notre discussion sympathique du basketball, Lucie Plougastel et Elodie Decuypere pour leurs aides dans ma vie professionnelle et personelle.

Je remercie Dr. Jean-Christophe Cintrat pour son humeur et sa collection de vin chinois, les « filles de Combi » : Dr. Karen Hinsinger, Dr. Valérie Pons, Dr. Hajer Abdelkafi pour leur gentillesse et patience. Je remercie également Dr. Thierry Le Gall pour sa gentillesse et son encadrement dans mon stage, Dr. Marie-Pièrre Heck et Dr Yves Ambroise pour leur bon accueil.

Je remercie Chantal pour sa gentillesse et responsabilité.

Je remercie l’ensemble du SCBM pour leur soutien et leur aide durant ces trois années ainsi que tous ceux que j’oublie de mentionner ici, mais qui m’ont tant apporté.

Je remercie bien mes parents et mes beaux-parents pour leur soutien quotidien, en particulier ma mère pour son encouragement régulière.

Je remercie tous mes amis chinois dans « Les Fantastiques en Plateau de Saclay » pour tous les joies et folies qu’on a passé ensemble, particulièrement Da, Lihan et Qirong pour notre grande amitié.

Pour terminer, je remercie sincèrement Chenge, ma chérie, sans qui je ne sais pas comment être dans ce monde, pour tout ce que t’a fait pour moi.

Résumé en Français

L’imagerie médicale, qui a pris un essor considérable ce dernier siècle, se tourne petit à petit vers l’imagerie moléculaire. La détection plus fiable de nombreuses cibles permettrait une meilleure compréhension et un diagnostic plus précoce de pathologies.

L'Imagerie par Résonance Magnétique (IRM) est une technique d'imagerie médicale couramment utilisée dans le milieu hospitalier pour diagnostiquer des maladies sur des organes tels que le cerveau et les poumons. Elle est basée sur le principe de la Résonance Magnétique Nucléaire (RMN) et elle repose en général sur la détection des protons (^{1}H) présents dans le corps humain. Cette technique d'imagerie se caractérise par une haute résolution spatiale/temporelle et est devenue un outil incontournable pour l'observation de tissus en profondeur.

Cependant, le principal inconvénient de l’IRM est sa faible sensibilité. L'utilisation d'agents de contraste est souvent nécessaire afin d'améliorer la qualité de l'image et donc de faciliter le diagnostic. Les plus utilisés actuellement sont les complexes de gadolinium et les nanoparticules d’oxyde de fer super paramagnétiques. Malgré l'utilisation d'agents de contraste, l'IRM ^{1}H n'est pas encore suffisamment sensible pour pouvoir faire de l'imagerie à l'échelle moléculaire. Cependant, l’observation des protons atteint rapidement ses limites. L’utilisation d’autres espèces hyperpolarisables telles que l'hélium (^{3}He), le carbone (^{13}C) ou le xénon (^{129}Xe) peut permettre l’accès à de meilleures sensibilités.

Au cours de ma thèse, nous nous sommes intéressés à l'IRM du xénon (IRM ^{129}Xe). Le xénon est un gaz de spin 1/2, inerte, non toxique et déjà connu pour ses propriétés anesthésiantes et pour faire de l'imagerie des poumons humains par IRM ^{129}Xe. Il est très sensible à son environnement et possède donc une large gamme de déplacements chimiques. D'autre part, grâce à une technique d'hyperpolarisation du xénon, il est actuellement possible d'obtenir un gain en sensibilité considérable de l'ordre 10^{4} à 10^{5}. Cependant, n’étant spécifique d’aucun récepteur biologique, le xénon nécessite d’être vectorisé. Pour ce faire, des auteurs ont proposé son encapsulation dans une cage moléculaire capable de reconnaître la cible

biologique à imager. Les meilleurs candidats pour une encapsulation optimale du xénon sont aujourd'hui les cryptophanes, qui possèdent les meilleures propriétés d'encapsulation du xénon, en termes de constante d'affinité, de vitesse d'échange entrée/sortie du xénon dans la cage et de relaxation du xénon dans le cryptophane.

Les cryptophanes, dont la structure générale est présentée ci-dessous, sont des molécules cages constituées de deux unités de type cyclotribenzylène reliées entre elles par trois chaînes pontantes (Figure I). Ils ont été synthétisés pour la première fois par l'équipe d'A. Collet au Collège de France au début des années 1981.[2] En 2001, l'équipe d'A. Pines à Berkeley a mis au point la première biosonde en RMN ^{129}Xe en détectant la complexe biotine-avidine à partir d'un cryptophane décoré par une molécule de biotine.[3] Depuis, de nombreux scientifiques se sont intéressés à la synthèse de nouvelles biosondes à base de cryptophanes pour réaliser leur application *in vivo*. Pour ce but, nous avons étudié de nouvelles voies chimiques menant à des bioconjugués à base de cryptophane avec une bonne efficacité ainsi que des quantités satisfaisantes.

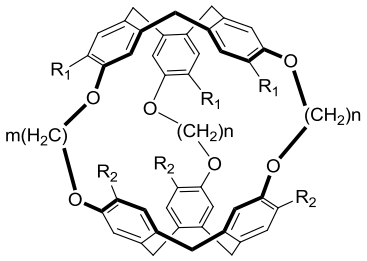

Figure I: structure générale des cryptophanes

Dans ce contexte, l'objective de cette thèse est designer des nouveaux cryptophanes qui peuvent être utilisé comme une plateforme moléculaire pour construire des biosondes en IRM de ^{129}Xe utilisable dans l'imagerie *in vivo*. Pour répondre à cette demande, deux grandes difficultés doivent être résolues.

Tout d'abord, les biosondes synthétisés sont peu solubles dans l'eau en raison de la forte hydrophobicité du cryptophane. En milieu aqueux, les cryptophanes sont enclins à former des systèmes auto-organisés qui tendent à favoriser une interaction non spécifique avec les

membranes lipidiques et l'incorporation de la sonde à l'intérieur de la membrane cellulaire. Pour éviter ce problème préjudiciable à l'application de ces biosondes *in vivo*, le groupe polyéthylèneglycol (PEG) est utilisé pour développer une synthèse efficace de cryptophanes hydrosolubles utilisés potentiellement comme plateformes universelles pour la construction des biosondes de ^{129}Xe IRM.

Deuxièmement, la haute symétrie des cryptophanes s'est avérée être un inconvénient important pour contrôler la réactivité d'une position particulière par rapport à d'autres sites équivalents. Des mélanges statistiques sont rapportés dans tous les types de voies synthétiques existantes utilisées pour désymétriser la molécule, compliquant les étapes de purification et gênant la production de grandes quantités de cryptophanes nécessaires à la synthèse de biocapteurs. Pour cette raison, il y a une discussion systématique sur la façon de casser la symétrie des cryptophanes et différentes tentatives ont été faites pour synthétiser les cryptophanes mono-fonctionnalisés.

La discussion de stratégie est basée sur la « méthode de template », qui est une méthode largement utilisé dans la synthèse des cryptophanes. Dans cette voie synthétique, 5 stratégies potentielles sont proposé pour casser la symétrie des cryptophanes comme montré ci-dessous (Figure II).

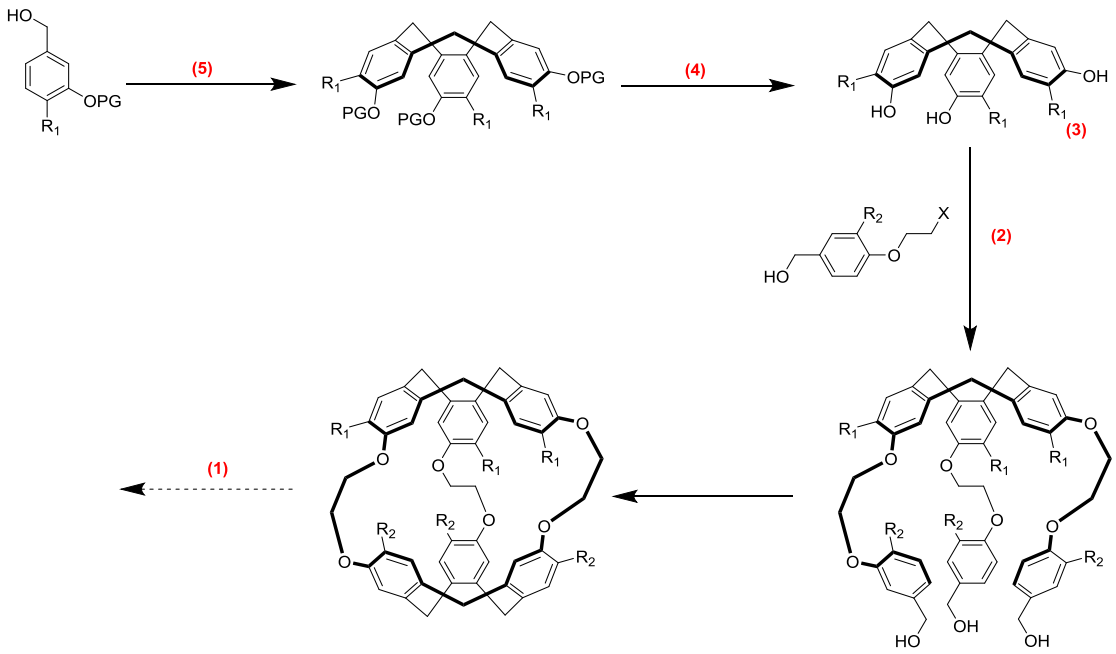

Figure II: La voie synthétique générale de « méthode de template » avec des 5 points possibles pour casser la symétrie des cryptophanes

(1) Désymétrisation d'un cryptophane symétrique.

(2) Fonctionnalisation des CTVs avec des dérivés d'alcool benzylique différents.

(3) Mono-halogénation des CTVs.

(4) Synthèse des cryptophanes basée sur des CTVs mono-protégé.

(5) Cyclotrimérisation avec des dérivés d'alcool benzylique différents pour former des CTVs asymétriques.

Dans cette thèse, nous avons concentré nos efforts sur les stratégies différentes pour réaliser la synthèse des cryptophanes PEGylés mono-fonctionnalisés. Suivi ces stratégies, beaucoup de cryptophanes et CTVs ont été synthétisés, montrant des applications potentielles très intéressantes dans la construction des biosondes de IRM du xénon *in vivo*.

INDEX

ABBREVIATION LIST

All: allyl

Ar: aromatic group

BMIM: 1-butyl-3-methylimidazolium

Bn: benzyl

Bu: butyl

CB[n]: cucurbit[n]urils

CTV: cyclotriveratrylene

CrA-da: cryptophane A diacid

DABCO: 1,4- diazabicyclo[2.2.2]octane

DDQ: 2,3-dichloro-5,6-dicyano-*p*-benzoquinone

DLS: dynamic light scattering

DHP: 3,4-dihydro-2*H*-pyran

DIEA: N,N-diisopropylethylamine

DMF: dimethyl formamide

DMSO: dimethyl sulfoxide

DNA: deoxyribonucleic acid

DNP: dynamic nuclear polarization

EDCI: 1-Ethyl-3-(3-dimethylaminopropyl)carbodiimide

EGFR: epithelium growth factor receptor

Et: ethyl

FAM: fluorescein amidite

FID: free induction decay

FLAIR: fluid-attenuated inversion recovery

HPLC: high-performance liquid chromatography

LC-MS: liquid chromatography–mass spectrometry

MALDI: matrix-assisted laser desorption/ionization

Me: methyl

mPEG 550: methoxy-polyethylene glycol 550

MRI: magnetic resonance imaging

Ms: mesyl

NBS: *N*-bromosuccinimide

NIS: *N*-iodosuccinimide

NHS: *N*-hydroxysuccinimide

NMDA: *N*-methyl-D-aspartate

NMP: *N*-Methyl-2-pyrrolidone

NMR: nuclear magnetic resonance

NSCLC: non-small cell lung cancer

OAc: acetate

OTf: trifluoromethanesulfonate (triflate)

PEG: polyethylene glycol

PET: positron emission tomography

PG: protecting group

PHIP: parahydrogen-induced polarization technique

PPh_2Li: diphenyl lithium phosphide

PPTS: pyridinium p-toluenesulfonate

PyBOP: benzotriazol-1-yl-oxytripyrrolidinophosphonium hexafluorophosphate

RT: room temperature

SPECT: single photon emission computerized tomography

SPIOs: super paramagnetic iron oxides

STCAS: 4-sulfothiacalix[4]arene sodium salt

TBAI: tetrabutylammonium iodide

TFA: trifluoroacetic acid

TEA: triethylamine

THF: tetrahydrofuran

THP: tetrahydropyran

TLC: thin layer chromatography

TMSI: trimethylsilyl iodide

TOF: Time of flight

TTEC: tris-(triazole ethylamine) cryptophane

Ts: tosyl

USPIOs: ultrasmall super paramagnetic iron oxides

GENERAL INTRODUCTION

The imaging techniques are getting more and more attention thanks to their capacity to realize a fine detection and real-time monitoring for the therapy of many diseases. With a reliable detection of numerous targets, which permits a better comprehension and an earlier diagnosis of pathology, the anatomical and functional medical imaging has turned little by little to molecular imaging in the last decade.

Among other diagnostic techniques such as bioluminescence, single photon emission computerized tomography (SPECT) or positron emission tomography (PET), magnetic resonance imaging (MRI) offers several advantages owing to its low invasiveness, its harmlessness and its spatial in-depth resolution (Figure 1). In USA, more than 25 % of diagnostic imaging is achieved by MRI, which is about 30 million MRI scans performed each year.

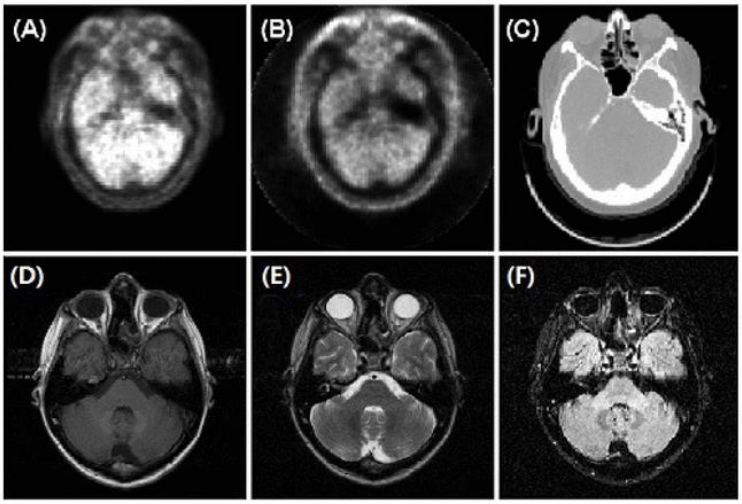

Figure 1[1]: Two-dimensional views of the common landmark (the skin) for (a) PET with attenuation correction. (b) PET without attenuation correction. (c) CT. (d) MRI : T1. (e) MRI :T2. (f) MRI : fluid-attenuated inversion recovery (FLAIR)

However, MRI suffers from poor sensitivity. To address this issue, different strategies were proposed. The contrast agents like gadolinium complexes or super-paramagnetic iron oxide nanoparticles are often engaged to improve the quality of imaging and to facilitate the diagnosis. However, despite their use, ^{1}H MRI still quickly reaches its limit in sensitivity. As a result, the utilization of hyperpolarizable species such as parahydrogen (^{1}H), helium (^{3}He), carbon (^{13}C) or xenon (^{129}Xe) shows a fascinating future by allowing a much better sensitivity.

Despite considerable advantages of hyperpolarized ^{1}H, ^{3}He and ^{13}C which can be inserted into organic or biological molecules without alteration of their structures, ^{129}Xe is undoubtedly the first choice for MRI of soft tissues which are difficult to image *in vivo*. Besides its well-known application in anesthesia, it is an inert gas with a polarizable electronic cloud which leads to an extreme sensitivity to its chemical environment. Moreover, its capacity of being hyperpolarized makes it possible to obtain a significant gain of sensitivity. Nevertheless, xenon has no specificity to any biological target and freely diffuses through biological barriers including the blood-brain barrier. Therefore it needs to be encapsulated and vectorized to reach biomarkers for molecular imaging. Different molecular cages were proposed to encapsulate xenon with a chemical function for covalent conjugation to a molecular vector for specific imaging.

Cryptophanes (Figure 2) are molecular cages composed of two cyclotriveratrylenes moieties connected by alkylenedioxy linkers. They were originally synthesized by the team of A. Collet in Collège de France in 1981.[2] In 2001, Pines and coworkers in Berkeley have developed the first ^{129}Xe MRI biosensor in detecting biotin-avidin complex based on a functionalized cryptophane.[3] Since then, many scientists have focused on this field in particular to realize the application of these cryptophane-based biosensors *in vivo*. For this purpose, we investigated new chemical routes leading to cryptophane-based bioconjugates with good efficiency as well as satisfactory quantities.

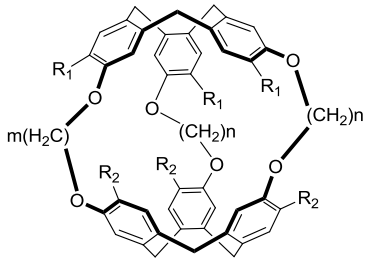

Figure 2: General structure of cryptophanes

In this context, the objective of this thesis is to design new cryptophanes which can be used as molecular platforms to construct novel ^{129}Xe MRI biosensors usable for *in vivo* MRI imaging. To meet this demand, two main difficulties should be resolved.

First of all, the synthesized biosensors are poorly water-soluble due to the high hydrophobicity of the cryptophane poly-aromatic core. In aqueous milieu, cryptophanes are prone to form self-organized systems which tend to promote a non-specific interaction with

the lipid bilayers and the subsequent embedding of the probe inside the cell membrane. To avoid this problem which is detrimental for the application of these biosensors *in vivo*, the polyethylene glycol (PEG) group is used to develop an efficient synthesis of water-soluble cryptophanes working potentially as universal platforms for ^{129}Xe MRI biosensors.

Secondly, the high symmetry of cryptophanes has been proven to be an important drawback to control the reactivity of a particular position versus other equivalent sites. Complex statistical mixtures are reported in all kinds of existing synthetic pathways used to desymmetrize the molecule, complicating the purification steps and jeopardizing the production of large quantities of cryptophanes required for the synthesis of biosensors. For this reason, there is a systematic discussion of how to break the symmetry of cryptophanes and different attempts were made to synthesize mono-functionalized cryptophanes.

In this thesis, we focused our efforts on the design of different strategies to achieve the synthesis of water-soluble mono-functionalized cryptophanes.

This PhD work was achieved in the Tritium Laboratory of SCBM in CEA Saclay in collaboration with several other research teams: P. Berthault's group for ^{129}Xe NMR experiments and the group headed by F. Fenaille for mass spectrometry analysis.

A. BIBLIOGRAPHIC STUDY

I. The Hyperpolarized ^{129}Xe MRI and Its Encapsulating Cages

Medical imaging is a set of non-invasive methods for visualizing biological processes inside the organisms. It's essential to the comprehension of the pathology, in order to achieve a better diagnosis, prognoses as well as to provide an adapted and efficacious treatment. After more than a hundred-year development since the discovery of X rays, the expectation of medical imaging is no longer the anatomic imaging and functional imaging. The new challenge in this field is now to realize a fine molecular imaging with validated biomarkers. In this thesis, we are especially interested in the application of hyperpolarized ^{129}Xe MRI to routine magnetic resonance imaging diagnosis which is largely used in hospitals.

1. General presentation of MRI

The MRI is an imaging technique based on the principles of nuclear magnetic resonance (NMR) which studies the response of nuclear magnetic moment in magnetic field. As the NMR reveals the magnetic properties of the detected atoms into the samples, the application of a specific sequence of magnetic field gradient and adapted signal treatment permit an access to *in vivo* 2D or 3D image of tissues and organs inside of body. It enables to study the soft tissues like lung, brain, and spinal cord and to provide information about the anatomic structure as well as the function of organs.

a. Principles of NMR

In the absence of magnetic field, the magnetic moments of proton spins do not have a particular orientation. Under the effect of a magnetic field B_0, they will begin to turn around the direction of B_0 at an angular velocity $\omega_0 = \gamma B_0$, which γ is the gyromagnetic ratio. Therefore a longitudinal component of the magnetization M_z is created on the Z axis. When the magnetic moments of proton spins are submitted to an oscillating electromagnetic wave at the resonance frequency of protons, an incline of the magnetization M to B_0 (in the XY plane) occurs in a perpendicular way, which is the transversal magnetization M_{xy} (Figure 3).

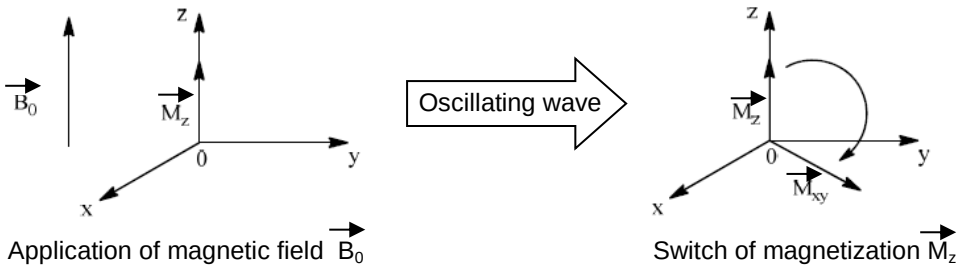

Figure 3: interaction of proton spins with a magnetic field in NMR

After the oscillating wave has stopped, the magnetization returns to its equilibrium position under the effect of B_0. This return to equilibrium takes place following a free precession movement, during which the longitudinal components M_z and the transversal component M_{xy} of the magnetization M vary over time (Figure 4).

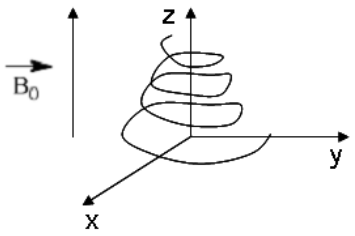

Figure 4: Return of the magnetization to equilibrium

This phenomenon, which is called relaxation, is characterized by two parameters. The first one is longitudinal relaxation time T_1, which corresponds to the time needed for the magnetic moments to get back to their alignment along the Z axis. The other one is the transversal relaxation time T_2, which describes the decrease of the signal in the XY plane.

The signal of free induction decay (FID) is recorded. And after a Fourier transform, a signal depending on the resonance frequency is thus obtained as the final NMR spectrum.

b. Principles of MRI

To obtain an image by magnetic resonance spectroscopy, the principle is to apply a magnetic field gradient in the two-dimensional or three-dimensional space so that the frequency of resonance of nuclei changes from one point of the object to another for the same nucleus. With a frequency-fixed wave, only one region will resonate and provide a signal. By shifting the detected frequency, a different region will enter in resonance and will permit to

probe another zone of the object (Figure 5). The magnetic signal which is emitted by nuclei after the resonance is recorded and then a data processing treatment allows reconstructing a three-dimensional image shown in successive cuts.

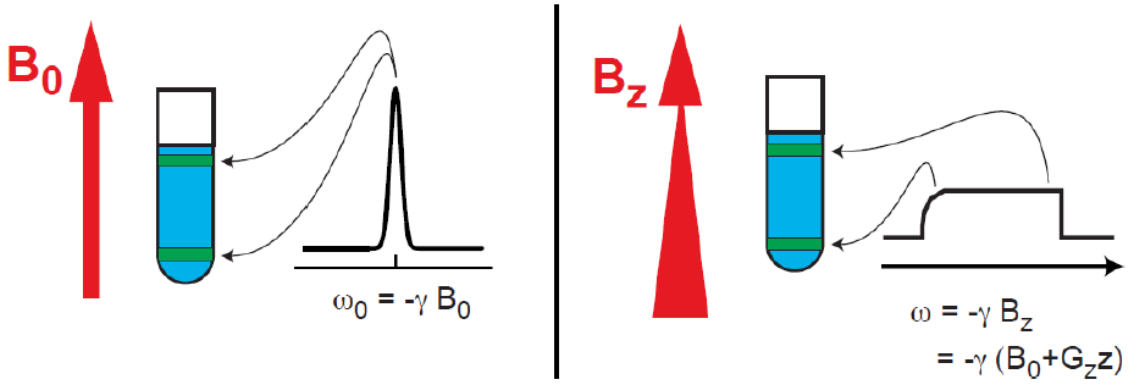

Figure 5[4]: Principle of magnetic resonance imaging in NMR spectrum (left) and in 1D MRI (right)

c. Advantages and Disadvantages of MRI

Thanks to the fast development of medical imaging, different imaging techniques including MRI are currently available in the hospital for routine diagnostic. Although different kinds of techniques can be applied at the same time to complement each other,[5] it is important to understand the advantages and drawbacks of each method to realize the earliest diagnosis of diseases as well as the best feedback of treatment for personalized medicine.

Optical imaging has unparalleled sensitivity, but it is not capable to go deep into the tissues. The positron emission tomography (PET) allows to probe all deep inside the human body, but do not possess good spatial and temporal resolution.[6] The application of computed tomography (CT) is often limited to bones and solid tumors. In addition, the utilization of these two techniques should be moderated due to the significant doses of ionizing radiations delivered during the examination which could be harmful for the patient. Ultrasound is an inexpensive technique but with a poor sensitivity.[7] The most relevant characteristics of these current imaging methods are compared in the following table (Table 1).

	PET	CT	Optical imaging	ultrasound	MRI
Spatial resolution	1-10 mm	100 µm	25-50 µm	30 µm	10-100 µm
Temporal resolution	60-1000 s	10-100 ms	1-200 ms	1-100 ms	10-100 ms
Sensitivity	pM	µM	fM-nM	µM-mM	µM-mM
Cost	+++	++	+	+	+++
Ionizing radiation	Yes	Yes	No	No	No
Other limit		Limited contrast for soft tissues	Limited in depth	Limited in depth	No analysis of solid tissues

Table 1: Comparison of common medical imaging techniques

Among all the techniques, MRI offers several advantages owing to its low invasiveness, its harmlessness and its spatial/time in-depth resolution but suffers from its expensive cost and poor sensitivity. The improvement of the sensitivity of MRI is always one of the main issues of research in this field.

2. How to improve the sensibility of MRI

The poor sensitivity of MRI results from the intrinsic poor sensitivity of NMR detection. The signal intensity is proportional to the polarization which depends on the difference of populations of spins between the two energy states (Equation 1).

$$P = \frac{|N_+ - N_-|}{N_+ + N_-} = \tanh\left(\frac{\gamma \cdot \hbar \cdot B_0}{2 \cdot k_B \cdot T}\right)$$

Equation 1

For a particle with spin I = 1/2, N_+ and N_- represent the number of spins in the two states, B_0 is the applied magnetic field, γ is the gyromagnetic ratio , k_B is the Boltzmann constant and T is the absolute temperature.

At the thermodynamic equilibrium, there is no large difference in the population of spins on the two energy levels, therefore causing a low P nuclear polarization. Different strategies

can be used to resolve this problem in particular the use of contrast agents or hyperpolarized species.

a. The MRI contrast agents

Currently, the contrast agents are delivered to the patients to improve the signal/noise ratio of MRI. They aim to accelerate the magnetic relaxation rate 1/T1 or 1/T2 of the protons in water. This leads to the shortening of the time necessary for a protons spin to return to its original state after the excitation by the radiofrequency wave. It should be noticed that the contrast agents are not visualized in MRI but that they influence the water molecule protons located around the contrast agents.

With 7 lone pair electrons in its 4f orbit, the lanthanide ion Gd^{3+} is the most widely-used paramagnetic ion as a contrast agent in MRI. This kind of paramagnetic metallic ions with a large number of free unpaired electrons (e.g. Gd^{3+}, Mn^{2+}), which are also called positive contrast agent, have mainly the effect of reducing the longitudinal relaxation time T1, resulting an increase of the intensity of the MRI signal. However, due to its strong toxicity as a competitor with calcium in all the calcium-dependent processes inside the human body,[8] gadolinium cannot be directly administered and needs to be chelated in order to limit adverse effects. Nowadays there are eight kinds of gadolinium-based contrast agents clinically approved (Figure 6).

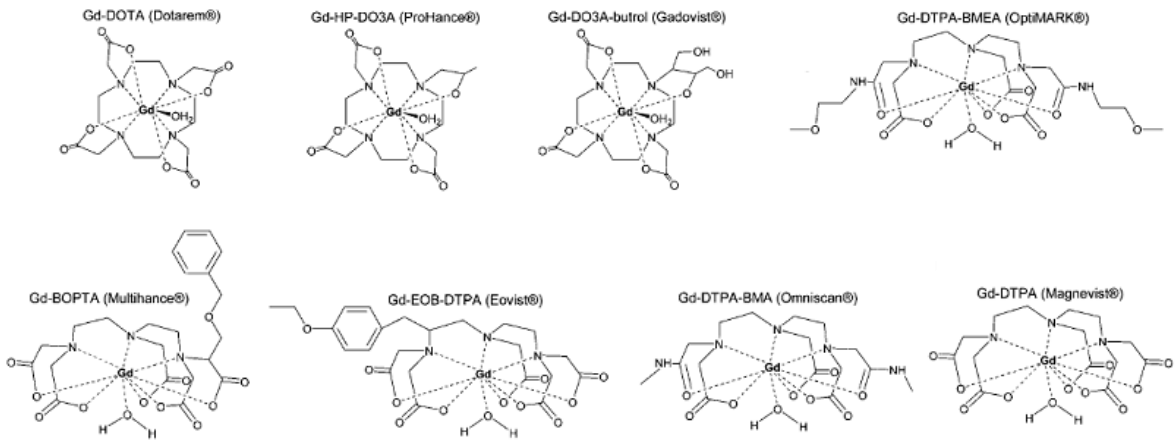

Figure 6: Commercial gadolinium-based contrast agents[9]

Unlike the gadolinium-based compounds, another category of contrast agents reduces the transversal relaxation time T2 of protons in water and thus generates a negative contrast by decreasing the intensity of the MRI signal. This kind of contrast agent, also known as

negative contrast agent, is basically the super-paramagnetic materials such as super-paramagnetic iron oxide.[10] It is called "super-paramagnetic" because of the presence of individual magnetic multi-domains within the iron oxide crystals. When a magnetic field is applied, all these micro-domains are oriented parallel to the field creating a very high magnetization within the particle (Figure 7). This magnetization will increase the relaxation of the protons in water by an order of magnitude.

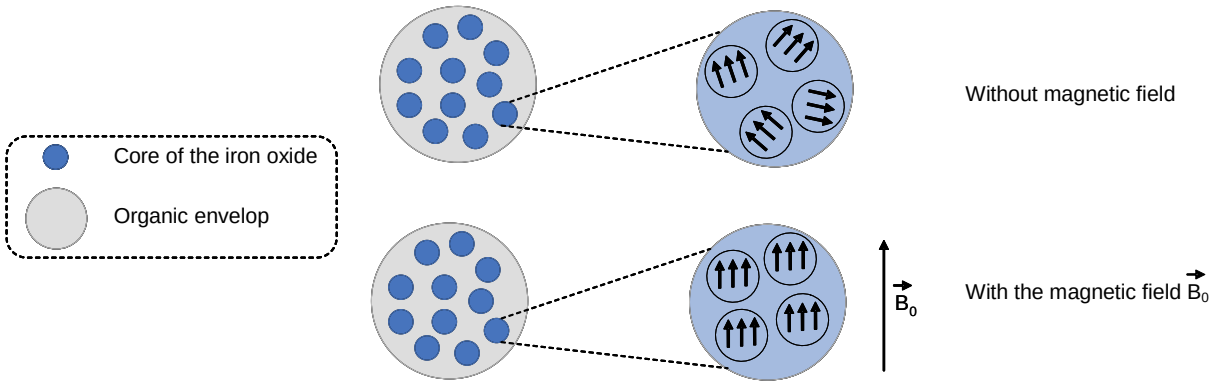

Figure 7: Magnetization of the super-paramagnetic iron oxide in the presence of a magnetic field

This super-paramagnetic particle can be classified according to the hydrodynamic size of the iron oxide core: SPIOs (Super Paramagnetic Iron Oxides) and USPIOs (Ultrasmall Super Paramagnetic Iron Oxides). The SPIOs are nanoparticles between 50 nm and 3500 nm. Normally, they will be captured by macrophages in the liver and are generally used for hepatic imaging (detection of small-size hepatic lesion). On the other hand, USPIOs have even smaller size (less than 50 nm) and will be captured by other phagocytic cells such as ganglion cells (Lymph-MRI).

Besides these two kinds of most-widely used contrast agents, there exist other potential candidates for contrast, like super-paramagnetic iron platinum particles and manganese-based nanoparticles. However, no matter which type of contrast agent is used, MRI is still not sensitive enough to achieve images at the air/liquid interface (e.g. lung epithelium) due to the presence of very few detectable atoms. To overcome this problem, several research teams focused on the use of hyperpolarizable atoms such as ^{129}Xe, ^{13}C and ^{3}He.

b. Hyperpolarization

As we can see in Equation 1, the best way to improve the sensitivity of MRI is to increase the polarization *P*, which depends on the difference in populations of spins between the two

energy states. At thermodynamic equilibrium, the Boltzmann's distribution is preponderant and consequently there is almost no difference between the two states. After an artificial modification like a polarization by laser, the difference in populations of spins is obviously augmented (Figure 8) leading to hyperpolarization.

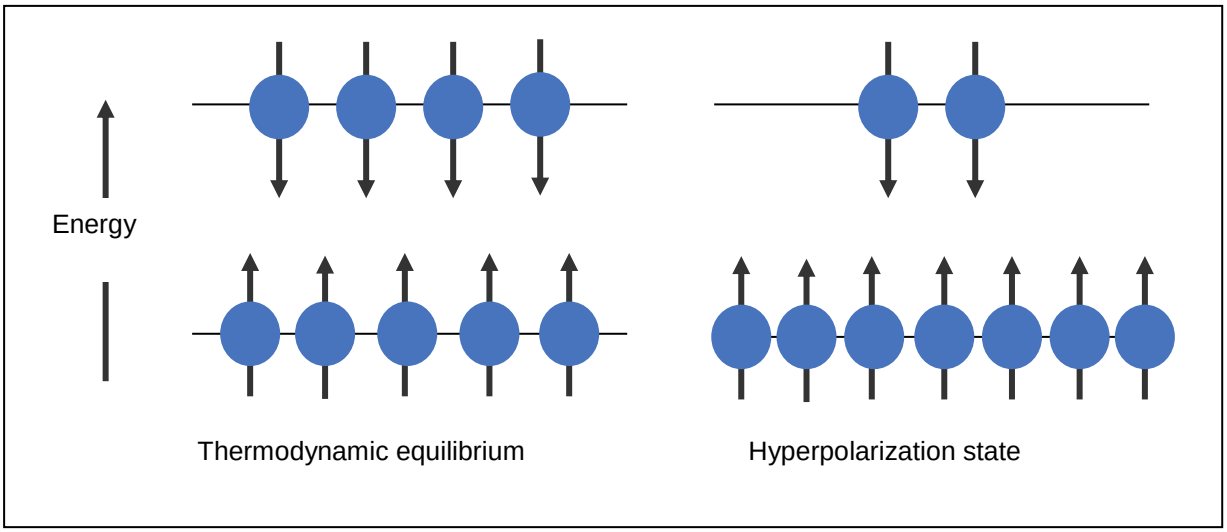

Figure 8: Distribution of spins before and after hyperpolarization

The hyperpolarized isotopes that are potentially usable for MRI are parahydrogen, ^{3}He, ^{129}Xe, ^{13}C and ^{15}N. The choice of these stable isotopes is substantially conditioned by the possibility of obtaining a longitudinal relaxation time longer than the duration of the polarization process.

i. Parahydrogen

Molecular hydrogen actually exists as four nuclear spin isomers. Orthohydrogen is used to describe hydrogen molecules that exist with one of the 3-fold degenerate spin state terms $\alpha\,\alpha$, $\alpha\,\beta + \beta\,\alpha$, and $\beta\,\beta$, whereas parahydrogen molecules exist solely as $\alpha\,\beta - \beta\,\alpha$ spin isomers. The ortho and para isomers exist in different rotational states, and their proportion is temperature-dependent when their normally forbidden interconversion is facilitated.[11, 12] If pure parahydrogen is desired, running hydrogen gas through a copper block containing silica/$FeCl_3$ catalyst at 20 K is sufficient.[13] Moreover once formed and removed from the interconversion catalyst, parahydrogen is relatively stable to spin-reequilibration. Therefore, the depolarization time is sufficiently long to enable the synthesis of molecules which can be monitored by hyperpolarized NMR methods.[14] Usually, the application of parahydrogen in

hyperpolarized NMR is achieved by parahydrogen-induced polarization technique (PHIP) which will be presented in part A-I-3-b.

i. Hyperpolarized ^{3}He

The hyperpolarized ^{3}He atom is basically used for lung imaging. The first image of lung with a hyperpolarized gas was obtained with ^{129}Xe.[15] However, helium quickly replaced xenon thanks to a larger gyromagnetic ratio as well as a better hyperpolarization yield.[16] Thus, most current human lung images are obtained with ^{3}He. However, researchers progressively come back to replace the helium by xenon. In fact, despite its intrinsic advantages, helium severely suffers from its rareness and expensive price. Moreover, unlike ^{129}Xe, ^{3}He is not very soluble in biological milieu, a drawback which drastically limits its application for molecular imaging.

ii. Hyperpolarized ^{13}C

A major advantage of using ^{13}C as the hyperpolarized atom is that ^{13}C naturally exists in small amount in numerous metabolites of living organisms. By following the evolution of the ^{13}C-labeled metabolites in enzyme-catalyzed reactions, precious information about the metabolism can be obtained.[17] In practice, the metabolites are hyperpolarized by dynamic nuclear polarization (DNP): the hyperpolarization of the ^{13}C nuclei is realized through a transfer of polarization from the lone-pair electrons of a radical species to the ^{13}C nucleus under the effect of a microwave irradiation.[18] Then the labeled metabolites are injected into the patient and their evolution is monitored by MRI.[19]

The example of $^{13}C_1$-pyruvate can illustrate this assertion.[20] Because pyruvate is at a crossroad of the major energy generating metabolic pathways, its metabolism differs in cancer and normal cells.[21] After the injection into the patient, the ^{13}C labeled pyruvate will be metabolized to give by-products such as $^{13}C_1$-lactate and $^{13}C_1$-alanine. It is known that in cancer cells, pyruvate is predominantly transformed into lactate, and therefore there will be an evident augmentation of the concentration in $^{13}C_1$-lactate as well as a diminution in the concentration of $^{13}C_1$-alanine. By measuring the ratio of each hyperpolarized metabolite signals in MRI (Figure 9), a mapping of the metabolic pattern can help the oncologist to trace and identify the tumor and to get a convenient treatment feedback.[22]

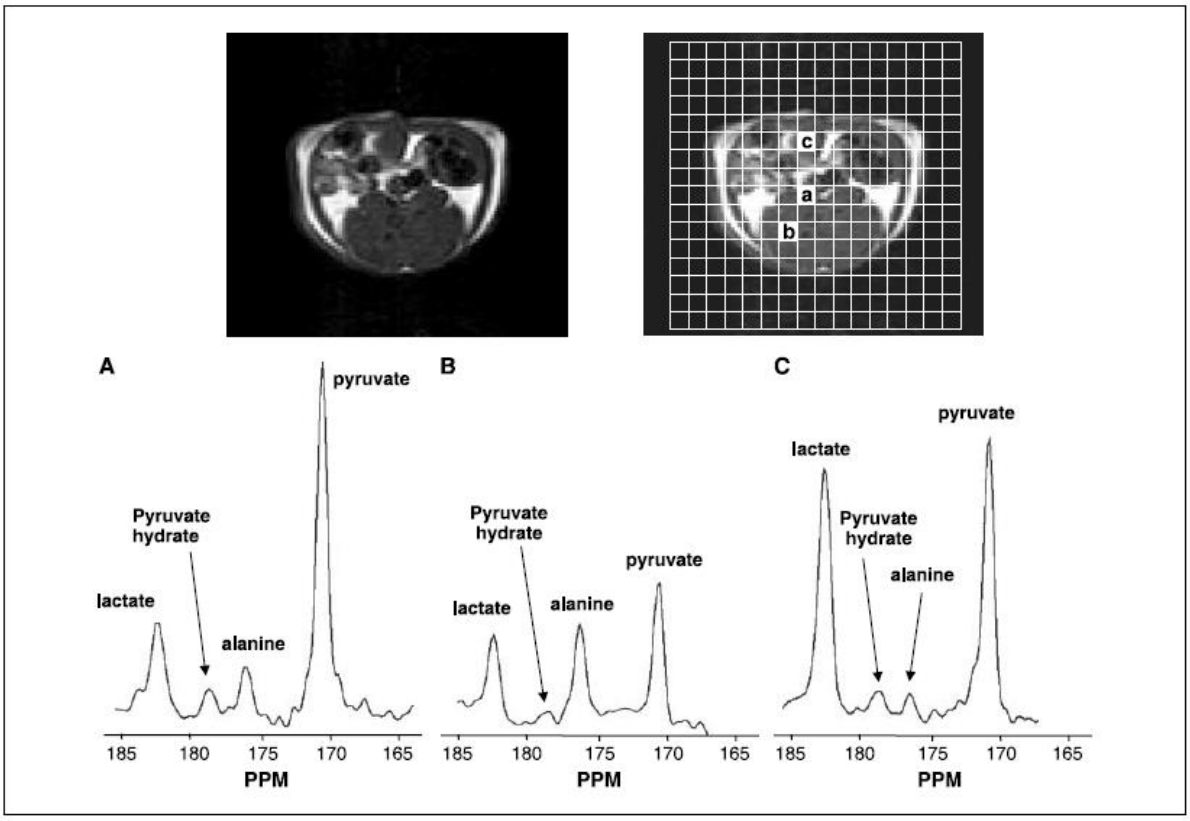

Figure 9: Change in metabolic pattern visualized by ^{13}C-MR spectra originating from the area containing vena cave (A), skeletal muscle (B), and P22 tumor tissue (C). Whereas alanine is most prominent in skeletal muscle, the tumor shows a typical lack of alanine signal and has a high lactate signal[21]

Besides, the measure of the concentration ratio between $^{13}CO_2$ and $H^{13}CO_3^-$ makes possible to measure the extracellular pH which is particularly interesting for localizing certain tumors like lymphatic tumors. Inside the tumor tissues, the pH is more acidic than in normal tissues. This study has been done *in vitro* and *in vivo*, and recently the clinical research on patients has been approved in order to study the prostate cancer.[23, 24] Now the challenge is focused on the technical development of hyperpolarization tools in order to lower MRI costs.

3. Hyperpolarized ^{129}Xe

a. General presentation of xenon

Xenon is a noble gas, which is inert, odorless and colorless. There are two major xenon isotopes which can be observed in NMR: ^{129}Xe, 26.4 % of natural abundance, 1/2 spin and ^{131}Xe, 21.2 % of natural abundance, 3/2 spin. Although the ^{131}Xe has already been applied in lung scintigraphy,[25] the best candidate for application in NMR is ^{129}Xe which is more

abundant, has a simpler signal in NMR and a longer longitudinal relaxation time T1. It is an excellent candidate for hyperpolarized NMR.

Xenon has shown no noticeable toxicity for living organism. In the human body, it inhibits glutamatergic receptors N-methyl-D-aspartate (NMDA), which accounts for its anesthetic properties. At lower concentrations, it is a neuroprotective agent by interacting with globular cytosolic proteins.[26] Only a slight dizziness and an euphoria were reported as side-effects.[27] Moreover, as mentioned before, xenon has a very good solubility in biological milieu which enables further application *in vivo*.

Practically, for *in vivo* experiments, xenon can be administrated either by inhalation or by injection. The inhalation is the simplest method to bring xenon inside body either by intubation of anesthetized animals or by an inhalation by human volunteers. It is thus possible to observe the lung[11] or even the brain[28] with the help of hyperpolarized xenon. On the other side, the injection is an invasive method but more direct than inhalation. Xenon gas should be dissolved in a biocompatible solvent for optimal solubility and limited relaxation rate. Until now, xenon was injected in saline solutions, the aqueous suspensions of lipid vesicles[29, 30], the emulsions of perfluorocarbons[31, 32, 33] and liposomes[34].

More noticeably, xenon possesses a large highly polarizable electron cloud, which makes it extremely sensitive to its chemical environment, resulting in a wide range of NMR chemical shifts (Figure 10).[35, 36, 37]

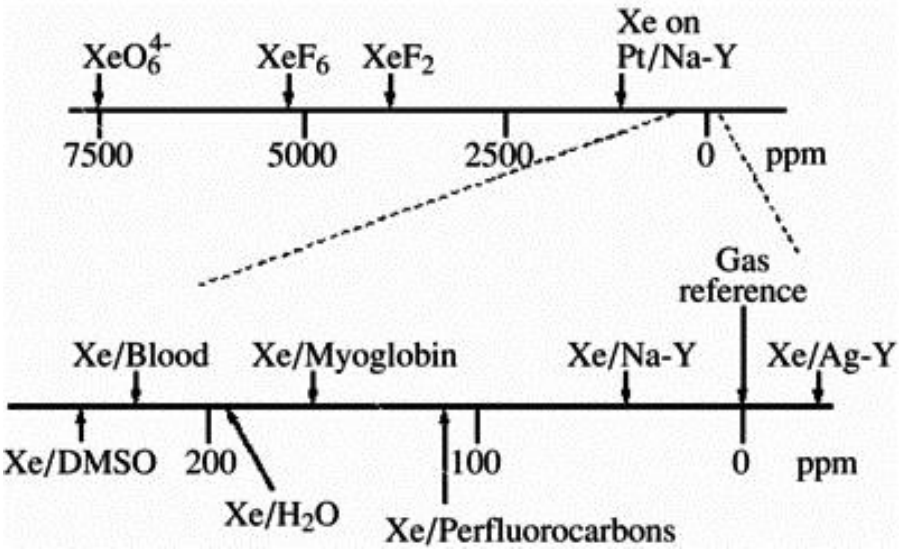

Figure 10: Chemical shifts of xenon in different environments

b. Hyperpolarization with optical pumping

Hyperpolarization enables an increase of sensitivity by several orders of magnitude. Generally, there are 3 methods for hyperpolarizing nuclei:

1) Dynamic nuclear polarization (DNP) is the most currently used method. Basically, the transfer of polarization from the single electrons to the nuclear spins can hyperpolarize a large variety of atoms in a molecule. For example, polarization of ^{15}N in the urea and ^{89}Y in the chelates of yttrium (III) has all been succeeded using DNP. However, as discussed previously, only polarized ^{13}C could be used for *in vivo* MRI applications, in particular thanks to its higher sensitivity.[38, 39]

2) Parahydrogen-induced Polarization (PHIP) is a technique which involves a chemical reaction in liquid phase or gas phase in which polarized para-hydrogen (antiparallel nuclear spins) is transferred to the molecule of interest by hydrogenation.[40, 41] Therefore, the two transferred protons become magnetically non-equivalent with a net polarization which can be transferred to neighboring nuclei by scalar coupling (spin-spin interaction). Despite the efficiency of this method, the major drawback arises from the chemical modification of the product of interest, and as a result, a limited selection of hyperpolarizable molecules.[42, 43]

3) Optical pumping is the currently-used method to hyperpolarize xenon gas, which will be introduced more in detail further.

A. Kastler presented firstly the principles of optical pumping in 1950.[44] This method enables to change the distribution of spin populations on the two energy states through an irradiation of atoms by polarized light in the presence of a magnetic field. Once the stationary state is reached, a strong augmentation of the electronic polarization is obtained. In 1959, the group of M. Bouchiat shown that alkali atoms with an increased electronic polarization could transfer their polarization to the nuclear spin of a noble gas by simple contacts in the gas phase.[45]

The hyperpolarization of ^{129}Xe is thus achieved through optical pumping of rubidium (Rb) followed by a transfer of the polarization of electrons to xenon nuclear spin, a process which clearly implies two separated steps (Figure 11).

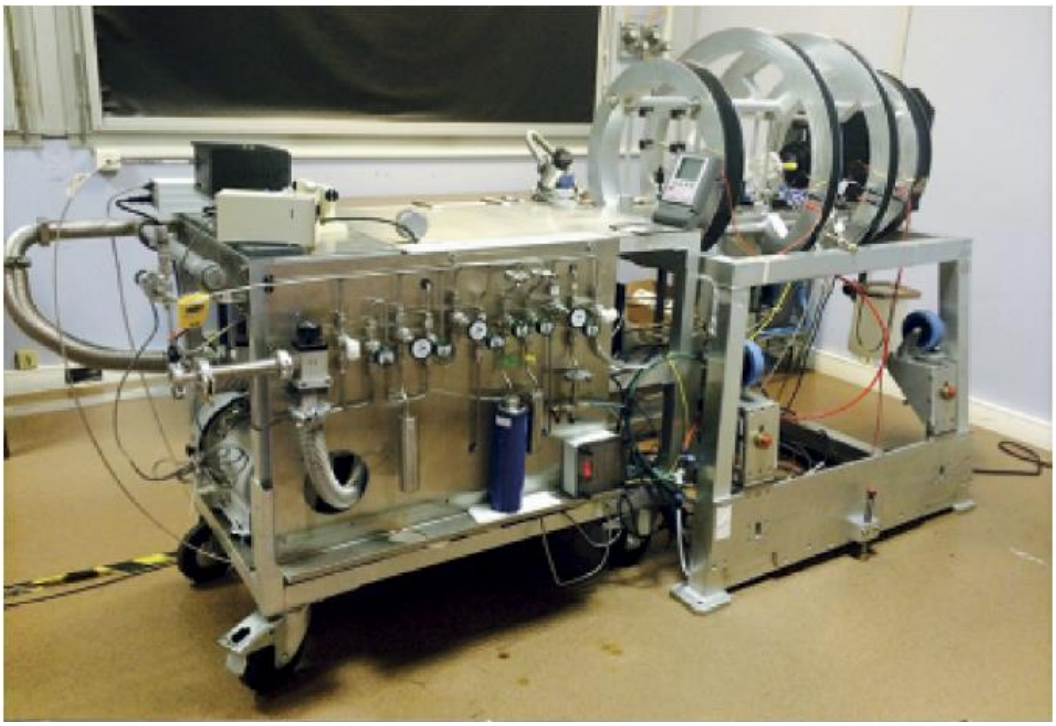

Figure 11: Equipment for hyperpolarizing xenon gas[46]

The first step is the optical pumping of rubidium.[47, 48] A chamber containing a mixture of rubidium steam, nitrogen and xenon preheated to 100 °C is illuminated by a laser beam at 794 nm. In the presence of a magnetic field, the only permitted electronic transition of rubidium is the one between the state spin -½ and the first excited state spin +½. Successive collisions between rubidium atoms will lead the populations in the excited states to return to the ground state (Figure 12). However, thanks to the excitation rate which is greater than the relaxation rate, a high concentration of rubidium at the state + ½ is obtained.

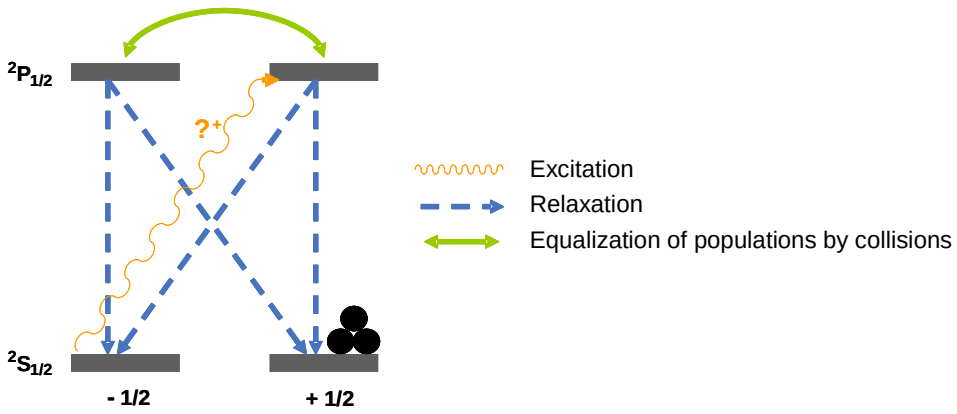

Figure 12: Electronic polarization of rubidium

The second step is the transfer of polarization to xenon nucleus. It involves multiple collisions between rubidium and xenon gas. These collisions will result in a dipolar coupling between electron spins of the metal and the nuclear spins of the gas (Figure 13). Thus, a high concentration in hyperpolarized xenon is obtained in a very short time.

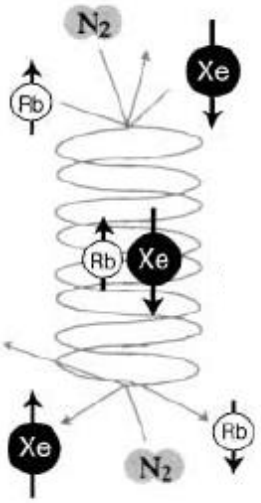

Figure 13: Transfer of polarization between rubidium and xenon

Hyperpolarized xenon is then separated by condensation and can be used for NMR experiments. This hyperpolarization of xenon results in a big difference of spin populations between two energy states and a strong increase in the sensitivity of NMR signals, which is about 10^4-10^5 times more intense (Figure 14).

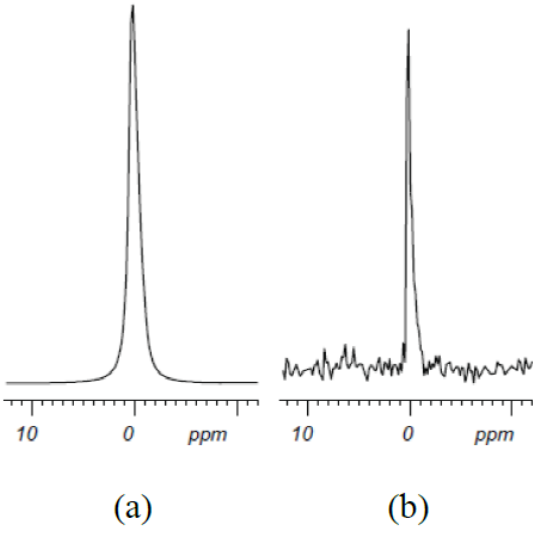

Figure 14[48]: Spectrums of ^{129}Xe NMR for a same sample (a) hyperpolarized (one scan) (b) non-hyperpolarized (15 h of acquisition)

c. *Encapsulating structures of xenon*

An important limitation for the application of xenon to *in vivo* molecular imaging is it does not enable to image a specific molecular target since it has no predictable specificity. To overcome this problem, it is therefore necessary to encapsulate the hyperpolarized xenon atom inside a biosensor.

A biosensor is a molecule composed of 1) a molecular cage used to encapsulate the gas with a particular chemical environment, 2) a linker, and 3) an antenna of recognition to target the molecule of biological interest (Figure 15). As xenon is extremely sensitive to its chemical environment, the chemical shifts in ^{129}Xe NMR is expected to be significantly different for free xenon gas, encapsulated xenon in a free biosensor and encapsulated xenon in a biosensor binding to its biological target.

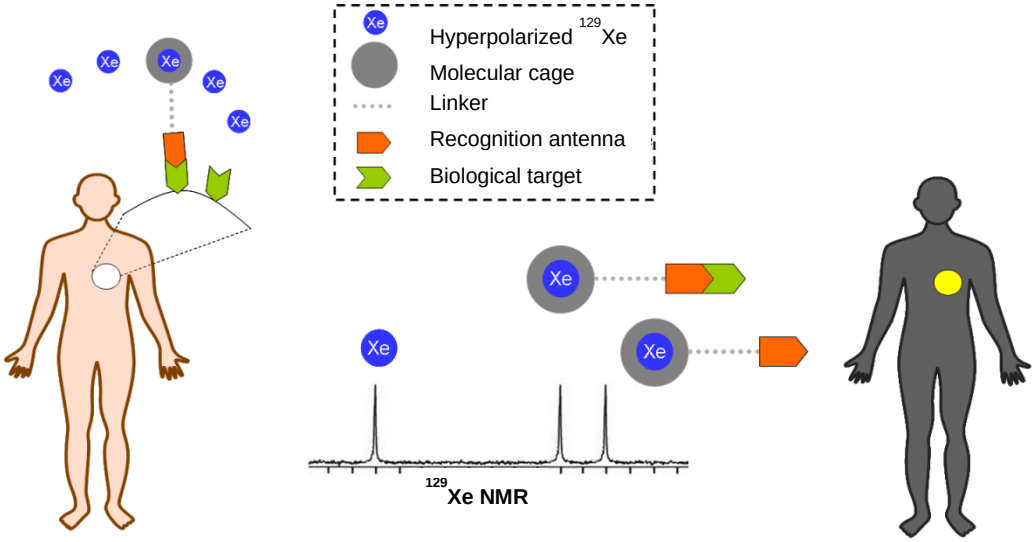

Figure 15: Concept of bio-sensors in ^{129}Xe MRI

i. The selection criteria

One of the main problems related to the design of xenon-based biosensors is the difficulty to encapsulate xenon with a sufficient affinity and a reasonable ability permitting xenon exchange in order to compensate the loss in sensitivity resulting from spontaneous xenon depolarization. The criteria required for an efficient molecular cage for xenon encapsulation are:

1. A good affinity for xenon quantified by the affinity constant K (M^{-1}), which is determined by the van der Waals interactions of xenon with the molecular cage.

2. An appropriate in/out exchanging rate, which should be slow enough to visualize the encapsulation of xenon in NMR, and fast enough to constantly enable the molecular cage to be refilled with freshly hyperpolarized xenon in order to overcome the lost in sensitivity due to time-dependent depolarization.
3. A NMR chemical shift for the encapsulated xenon which is significantly different from the free xenon.
4. A minimization of the relaxation of xenon inside the cage
5. A sufficient solubility of the molecular cage in aqueous milieu and an easy functionalization to allow *in vivo* applications.

In 1998, J. Rebek showed that there is an optimal ratio between the size of the guest molecule and the size of the host molecule, which is 0.55 ± 0.09.[49] As the van der Waals volume of xenon is 42 $Å^3$, the ideal van de Waals volume of the molecular cage should be 76 $Å^3$.

The hydrophobic character of the xenon makes it particularly sensitive to London forces,[50] caused by the dipole - dipole interactions. Consequently, the interaction between xenon and the atoms of the molecular cage is also a source of stabilization.[51]

In the literature, there are numerous molecules which satisfy more or less to the previous criteria.[52] Here below are given several relevant examples.

ii. Cyclodextrins

Cyclodextrins are cyclic oligosaccharides produced by enzymatic degradation of starch, formed by the assembling of 6 to 12 glucose units connected to each other by 1,4 α bonds (Figure 16). The cavity of the smallest cyclodextrin (α-cyclodextrin, consisting of 6 glucose units) has a volume between 140 $Å^3$ and 170 $Å^3$. Although it has been demonstrated that xenon readily enters this cage, the large volume of its cavity still causes a too fast in/out exchanging rate of xenon. Moreover, its very low affinity constant for xenon (about 20 M^{-1} at 298K) also limits its application for the design of biosensors.[53]

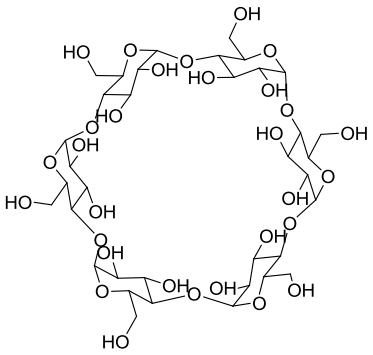

Figure 16: Structure of α-cyclodextrin

iii. Calixarenes

Calixarenes are macrocycles formed by n phenolic units (n = 4 to 20) which are connected to each other by methylene bridges in the *ortho* positions of the hydroxyl phenyl groups. These macrocycles are obtained by condensation of phenol with formaldehyde in a basic milieu. These molecules are amphiphiles with a hydrophilic region around the hydroxyl groups and a hydrophobic cavity between the aromatic rings. However, the in/out exchange rate of xenon in this kind of cage is still too fast. In addition, the affinity constant for xenon is generally too low. For example, the water-soluble Calix[4]arene STCAS (4-sulfothiacalix[4]arene sodium salt) presents an affinity constant of 14 M^{-1} at 298 K in water (Figure 17).[54]

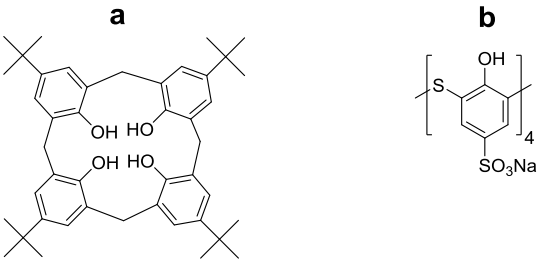

Figure 17: (a) calix[4]arene with *para-tert*-butyl substituents. (b) Structure of STCAS

iv. Hemicarcerands

Unlike carcerands which encapsulate a molecule without being able to let it out even at very high temperatures, the hemicarcerands are molecular cages allowing both the entry and the exit of the guest molecule at high-temperature, but forming a more or less robust complex at room temperature. They possess an exchange rate slow enough to visualize the difference between free xenon and encapsulated xenon by NMR. For example, the hemicarcerand obtained by J. Cram in 1991, which is composed of two aromatic tetramers linked by a

bridging chain, possesses a pretty good affinity constant of xenon of about 200 M^{-1} in chloroform at 22°C (Figure 18).[55]

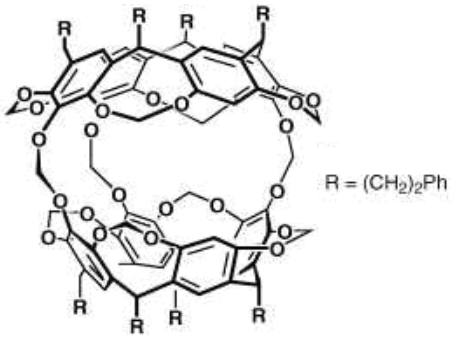

Figure 18: Structure of the hemicarcerand which can be used to encapsulate xenon

v. Cucurbiturils

The cucurbiturils are obtained by reaction of glycoluril with formaldehyde in acidic milieu. Their general structure is presented in Figure 17a. The cavity volume of the cucurbit[n]urils family (CB[n]) varies from 82 $Å^3$ to 870 $Å^3$ according to its size (n = 5, 6, 7, 8, 10). Theoretically, the smallest cucurbituril CB[5] was calculated to be the best candidate for encapsulating xenon. However, the rigidity of the molecule and the entrance gate defined by the oxygen in carbonyl groups are not favorable for the encapsulation of xenon.[56] Until now, the most-adapted cucurbituril for xenon encapsulation is the water-soluble CB*[6] synthesized by the group of K. Kim. It possesses a good affinity constant for xenon in the 3000 M^{-1} range (Figure 19).[57]

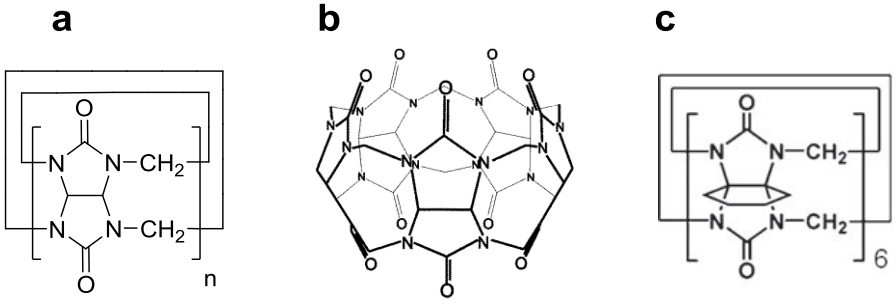

Figure 19: (a) General structure of cucurbit[n]urils (b) Structure of CB[5]. (c) Structure of CB*[6]

vi. Cryptophanes

Cryptophanes are composed of two units of cyclotriveratrylene (CTV) derivatives connected to each other through alkyldioxy bridges (Figure 20). The structure can vary

according to the length of the molecular bridges (l, m and n) as well as groups R1 and R2 on the aromatic rings. Their hydrophobic cavity is suitable for encapsulating little neutral molecules like xenon. As a consequence, they have the best affinity constant for xenon ever reported (29,000 M^{-1} for the water-soluble cryptophane[111][58]) and also exchange rates totally adapted to the experiment timescale.

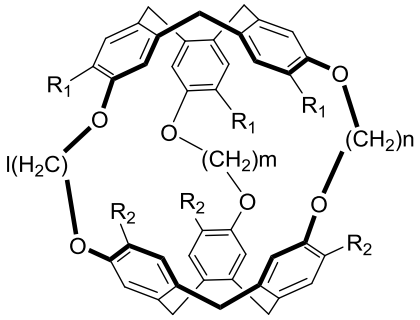

Figure 20: General structure of cryptophanes

According to the calculation of J. Rebek[49], the smallest cryptophane[111] approaches the optimal ratio of 0.55 between the volume of xenon and its cavity. This partly explains why cryptophane[111] has the best affinity for xenon, independently of the solvent used, either organic solvent tetrachloroethane (K = 10,000 M^{-1})[59] or water (29,000 M^{-1} for the water-soluble cryptophane[111][58]). In fact, the proximity of its aromatic rings with the xenon electronic cloud stabilizes the encapsulated gas.

Cyptophanes	[lmn]	R1, R2	Cavity ($Å^3$)	K (M^{-1})	*Ref.*
Organosolubles	[111]	H, H	81	10000	[59]
	[222]	OMe, OMe	95	3900	[60, 61]
	[223]	OMe, OMe	102	2800	[62]
	[233]	OMe, OMe	117	810	[62]
	[333]	OMe, OMe	121	5-10	[62]
Water-solubles	[111]	H + 6[Cp*Ru]$^+$	81	29000	[58]
	[222]	OCH_2COOH, OCH_2COOH	95	6800	[63]
	[223]	OCH_2COOH, OCH_2COOH	102	2200	[63]
	[233]	OCH_2COOH, OCH_2COOH	117	2200	[63]
	[333]	OCH_2COOH, OCH_2COOH	121	1000	[63]

Table 2: Volume of cavity and affinity constant to xenon of different cryptophanes

As shown in Table 2, for the organosoluble cryptophanes, the wider the cryptophane cavity (longer alkyldioxy bridges), the less the xenon is stabilized by the van der Waals force related

to aromatic rings, and therefore the worse the affinity for the xenon gas is.[61, 62, 63] When the cavity is large enough (e.g. like in cryptophane[333]) the molecule of solvent can also enter the cage and therefore competes with the solvent. This phenomenon can also explain the poor affinity of xenon for larger cages.

Table 2 also suggests that for cryptophanes with equivalent sizes, water-soluble molecules always display a better affinity for xenon than organosoluble ones. This is due to the hydrophobicity of the xenon gas which prefers the hydrophobic environment of the cryptophane cavity to the aqueous milieu.

The exchange rate is a very important factor for encaging hyperpolarized ^{129}Xe NMR. It directly affects the Xe NMR signal and is directly correlated to the width of peak at mid-height of the encapsulated xenon: wider is the peak, higher is the exchange rate.

As discussed previously, the exchange rate should be slow enough for visualizing the encapsulated xenon by NMR, suggesting that the difference in chemical shifts between free and encapsulated xenon should be large enough. Until now, this difference is larger than 112 ppm for all the reported cryptophanes (Table 3).

Cyptophanes	[lmn]	R1, R2	$\delta_{\text{encapsulated Xe}}$ (ppm)	$[\delta_{\text{free Xe}} - \delta_{\text{encapsulated Xe}}]$ (ppm)	*Ref.*
Organosolubles	[111]	H, H	31	194	59
	[222]	OMe, OMe	68	156	3
	[223]	OMe, OMe	60	164	62
	[233]	OMe, OMe	47	177	62
	[333]	OMe, OMe	30	186	62
Water-solubles	[111]	H + 6[Cp*Ru]$^+$	308	112	58
	[222]	OCH_2COOH, OCH_2COOH	64	133	63
	[223]	OCH_2COOH, OCH_2COOH	52	145	63
	[233]	OCH_2COOH, OCH_2COOH	42	155	63
	[333]	OCH_2COOH, OCH_2COOH	35	162	63

Table 3: Chemical shifts of encapsulated xenon in different cryptophanes

Concomitantly, the exchange rate should also be fast enough to enable the permanent refilling of the molecular cage with freshly hyperpolarized xenon. Generally, the exchange rate increases with the cage size. For example, cryptophane[111] has an exchange rate of 2.4

Hz[59], while cryptophane[222] with R1 = R2 = methoxy (also called cryptophane A) has a higher exchange rate of about two orders of magnitude.[60]

Another important criterion for an ideal xenon-encapsulating cage is the relaxation time of xenon inside the cage, which should be long enough to permit the acquisition in NMR or MRI. The main cause of relaxation of the encapsulated xenon is the xenon-proton dipolar coupling. According to the experimental measurement, relaxation times of xenon encapsulated in different cryptophanes vary from 5 s to 20 s.[61, 63, 66] These values meet well the specifications for signal acquisition by MRI.

Cryptophane has also demonstrated excellent characteristics in biological environments and thus a promising future for its application *in vivo*. The group of Dr. P. Berthault has realized hyperpolarized ^{129}Xe MRI of rat lungs and associated localized ^{129}Xe spectroscopy by introducing the cryptophane via instillation and then delivering hyperpolarized xenon gas via inhalation (Figure 21, unpublished results). The signal of xenon encapsulated in hydrophilic cryptophane which has crossed the lung epithelium unambiguously shows up at 60 ppm. A continuous exchange between the large reservoir of hyperpolarized xenon constituted by the lung (Xe_{gas}) and caged xenon has been highlighted, affording a further gain in sensitivity to the method.

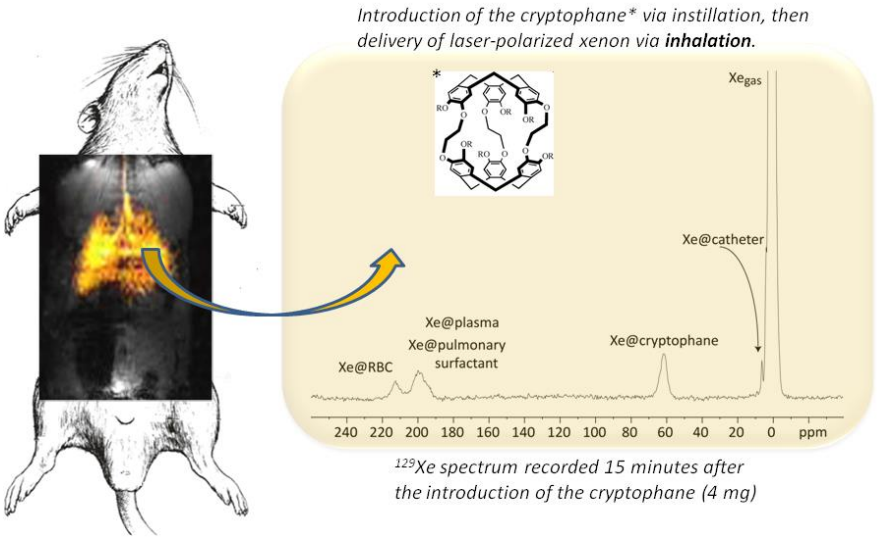

Figure 21: Hyperpolarized ^{129}Xe MRI of rat lungs and associated localized ^{129}Xe spectroscopy (Dr. P. Berthault, unpublished results)

In conclusion, cryptophanes seem to be the best molecular cages for the construction of biosensors usable by hyperpolarized MRI.

II. Cryptophanes: Structure, Synthesis and Applications

1. Structures – stereochemistry, symmetry and conformers

Developed by A. Collet in College de France in the 1980's,[2] cryptophanes belong to the family of hemicarcerands. As mentioned previously, they are composed of two cyclotriveratrylene (CTV) units connected one to each other by bridging chains whose species and length can be tuned. Considering that the systematic nomenclature of these molecules is particularly long and complex, a simplification was quickly adopted. The first elaborated cryptophanes were named "cryptophane A, B, C…". But for now, as a large diversity of structures in this family has been synthesized, this nomenclature fits no longer the new compounds. A new arbitrary nomenclature is often adopted, defining the number of carbon atoms in each bridging chains and the substituent groups on the aromatic rings. For example, the cryptophane A has been renamed cryptophane[222](OMe)$_6$ (Figure 22).

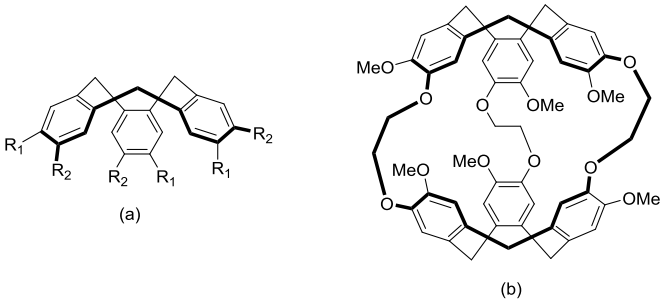

Figure 22: (a) General structure of CTVs. (b) Cryptophane A also called cryptophane[222](OMe)$_6$

a. Stereochemistry and symmetry

Stereomeric cryptophanes arise from the chirality of CTV units. When R_1 and R_2 are the identical groups, the CTV derivatives are achiral. And when they are different, the molecule presents a planar chirality with 2 enantiomers with C_3 symmetry (Figure 23).

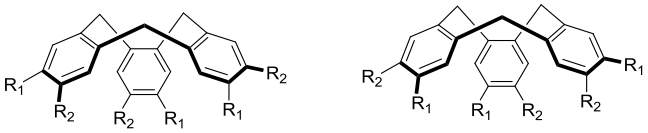

Figure 23: Two CTV enantiomers

Due to the different combinations of CTV units, 3 stereoisomers and 2 configurations are possible for the cryptophanes (Figure 24)[66, 67]. The cryptophane in *syn* configuration is obtained when the two CTV units possess different chiralities. It is achiral when R_1 and R_2 are identical and chiral when they are different. Two stereoisomers of *anti* cryptophane are obtained when the two CTV units possess the same chirality. No matter the R_1 and R_2 groups are different or not, the two stereoisomers are chiral and enantiomers to each other.[68]

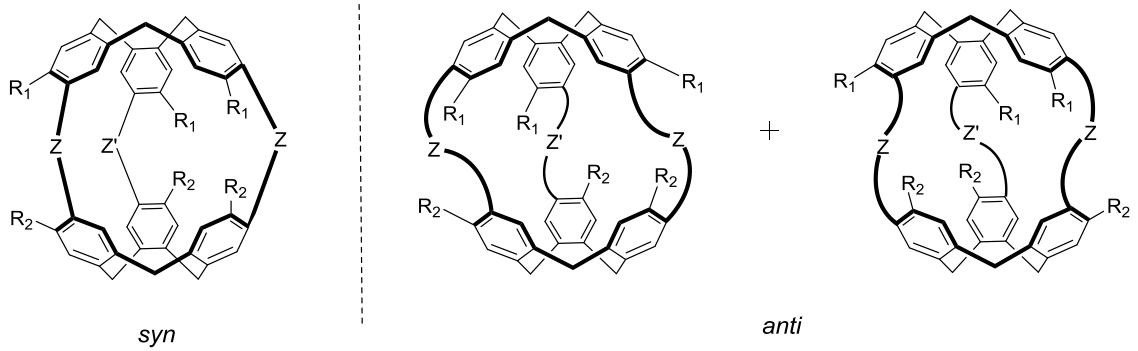

Figure 24: Configurations *syn* and *anti* of cryptophanes

Different bridging chains (Z and Z') and different substituent groups (R_1 and R_2) also induce different symmetries.

If $R_1 = R_2$ and Z = Z', cryptophane *syn* contains a C_3 rotation axis and σ_h plane of symmetry. Hence it belongs in the C_{3h} symmetry. On the other hand, cryptophane *anti* contains two C_2 axes perpendicular to the main rotation axis, the C_3 axis. Consequently it belongs in the D_3 symmetry.

If $R_1 \neq R_2$ and Z = Z', both of cryptophanes *syn* and *anti* contain only a C_3 axis of rotation. Hence they have the C_3 symmetry.

If $R_1 = R_2$ and Z ≠ Z', cryptophane *syn* only contains a mirror plane σ. Hence it has a C_s symmetry. On the other hand, cryptophane *anti* only contains a C_2 axis. Therefore it has the C_2 symmetry.

If $R_1 \neq R_2$ and Z ≠ Z', both of cryptophanes *syn* and *anti* possess no symmetry except for the identity operation and they thus have the C_1 symmetry.

b. Conformers

In solution, the CTV derivative exists in 3 different forms. Besides the most stable “crown” conformation, which is also the major form, there are also “saddle” and “twisted” conformations. Racemization of the enantiomerically pure CTV derivative through a “crown to crown” interconversion was observed (Figure 25). The intermediate “saddle” and “twisted” conformations, which are usually non-isolated, are less stable than “crown” because they induce repulsive interactions between a methylene group and its opposite aromatic ring.[68] It is possible to calculate the energy barrier for “crown to crown” inversion which has been evaluated to be about 110 kJ.mol^{-1}.[69, 70]

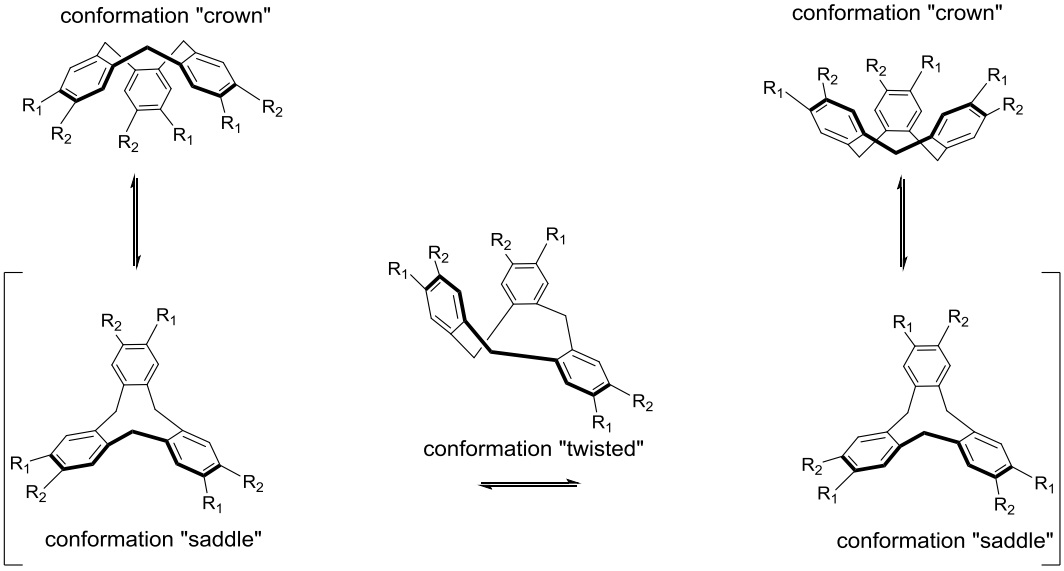

Figure 25: Different conformation of CTVs and their possible interconversions

As a consequence, cryptophanes, composed of two units of CTVs, also possess different conformations (Figure 26). Besides the major “out/out”conformation, the other three conformations, “in-out”, “in-in” and “out-saddle”, can be formed when there is no molecule inside of the cage. The imploded form (“in-out”) of cryptophane is preferred when the molecule of solvent does not penetrate easily into the cavity and its formation is discernable by a series of new specific signals in ^{1}H NMR.[63, 71, 72] In addition, longer is the bridging chain, more flexible is the cryptophane, leading to the formation of the imploded conformations.

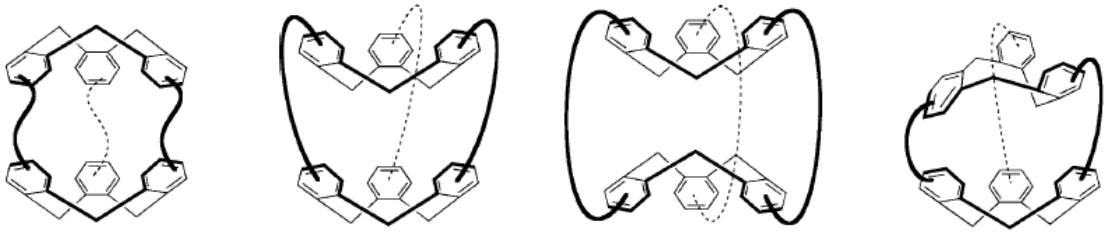

out/out *in/out* *in/in* *out/saddle*

Figure 26: Different conformations of cryptophanes

It is possible to interconvert “in-out”, “in-in” or “out-saddle” to “out/out” conformation by heating the molecules in a solution whose solvent molecule can enter inside the cage, or adding a gas which can be encapsulated by the cyptophane.

2. Synthesis

There are 3 strategies for synthesizing cryptophanes, all starting from benzylic alcohol derivatives (Figure 27). Each of them possesses different advantages and particular drawbacks.[66, 73]

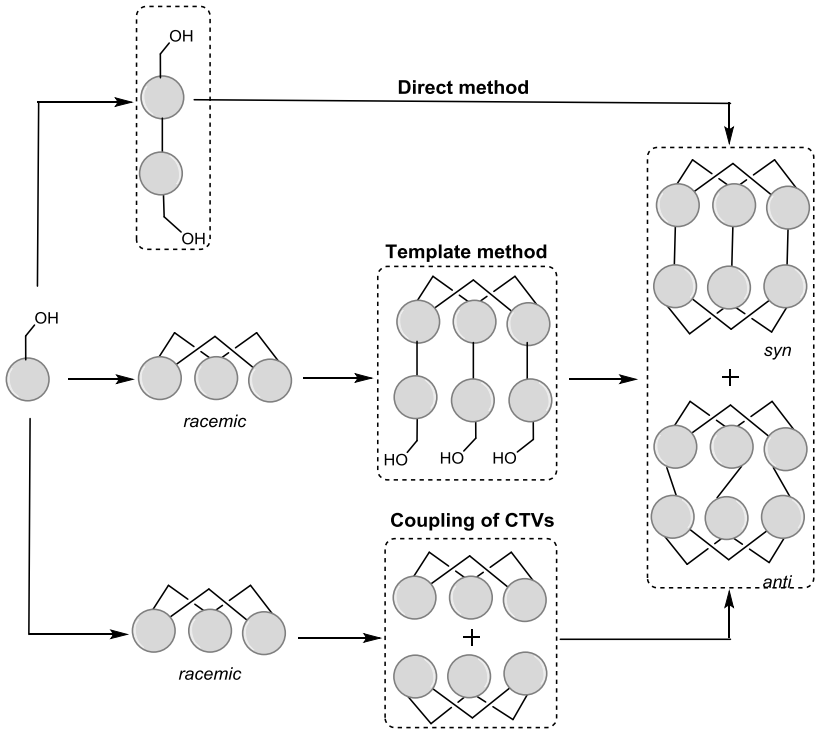

Figure 27: Three methods to synthesize cryptophanes

a. The "direct method"

In the "direct method", the benzyl alcohol is firstly converted to a "dimer" and then the dimer is used for cyclotrimerization to form the cryptophane (Figure 28). As the simplest and quickest method to synthesize cryptophanes, the poor yield (less than 5 % for small cryptophanes like cryptophane A, less than 20 % for the larger ones) and the limitation to synthesize only the cryptophanes of C_{3h} and D_3 symmetry jeopardize its further application. It is also interesting to notice that cryptophane *anti* is preferentially obtained in this method.[73]

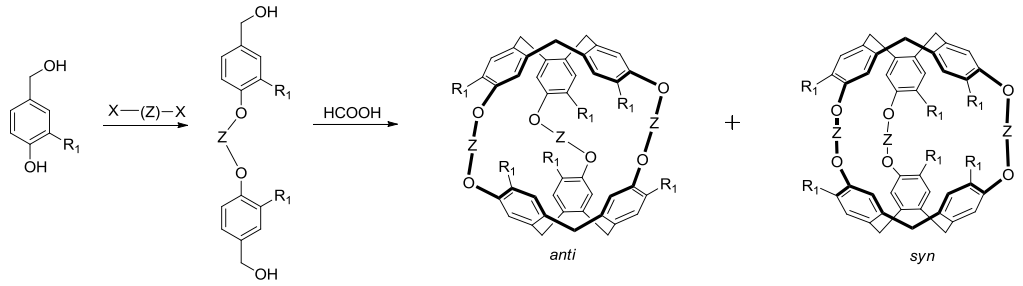

Figure 28: General synthesis of cryptophanes by the direct method

b. The "template method"

This approach is a multi-step synthesis which requires the formation of two cyclotriveratrylene units at different stages of the synthesis.

The "template method" starts with the synthesis of the first CTV which acts as a "template" here. In a general way, CTVs are obtained through cyclotrimerisation of benzyl alcohol derivatives. This reaction takes place in acidic milieu (Lewis acid or Brönsted acid). The choice of the acid depends on the substituent groups R_1 and R_2.

The proposed mechanism is shown in Figure 29. First, the carbocation is obtained from the benzyl alcohol derivative under acidic conditions. Two successive condensations of this carbocation lead to a dimer and then a linear trimer. The final cyclization affords the CTV.[68]

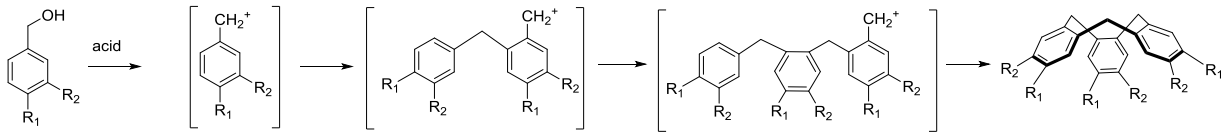

Figure 29: Proposed mechanism of cyclotrimerization to form CTVs

It is important to notice that this reaction needs an electron-donating group in position of R_2 of the benzylic alcohol in order to activate its nucleophilic *para* position on which an electrophilic Friedel-Crafts substitution takes place. The substituent group R_2 can be either -OR, -NRR′, or –SR. The methoxy group is mostly-used in the synthesis of CTVs. Furthermore, the R_1 position should be protected to avoid a secondary electrophilic substitution on this position.

After the first cylotrimerization, a deprotection step of the CTV **1** is necessary to obtain the free phenols. The generated CTV **2** is then functionalized with three substituted benzyl alcohol to obtain **4**, which is an already "pre-organized" intermediate to form the final cryptophane. Then the second cyclotrimerization is done according to the preformed "template" to obtain cryptophane *anti* **5** and/or *syn* **6** (Figure 30). The last step requires high dilution condition in the order of 10^{-3} M to promote the intramolecular reaction and reduce the formation of polymers.

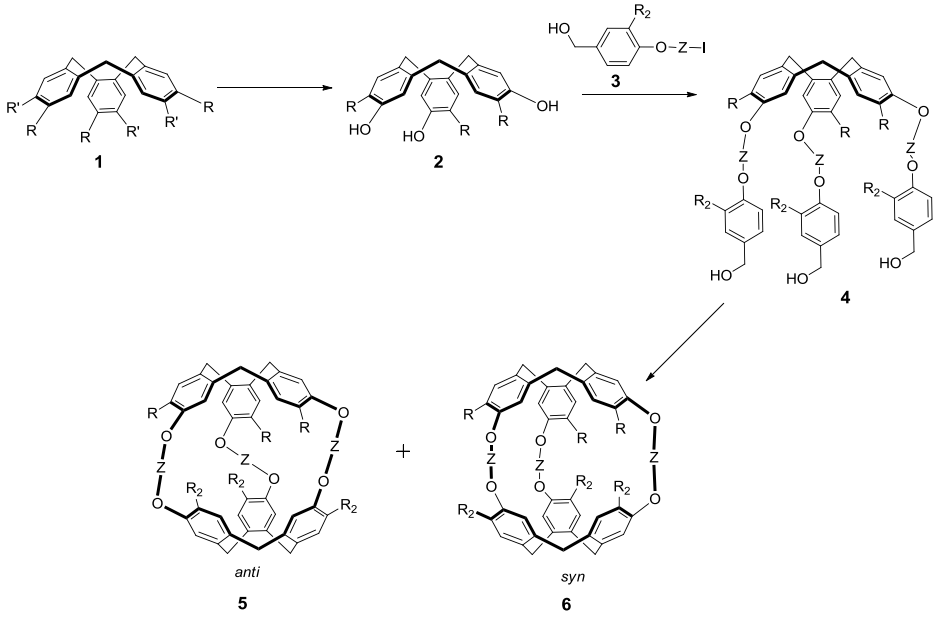

Figure 30: General synthesis of cryptophanes by template method

Regarding the distribution of *syn*- and *anti*-configurations, it is interesting to point out that the major configuration seems to depend on the number of carbons atoms on the bridging chain. When the number of carbon is even, cryptophane *anti* is obtained as major product (e.g. for cryptophane A, *syn*/*anti* = 0/80). When it is odd, the cryptophane *syn* is predominant (e.g. for cryptophane E, *syn*/*anti* = 50/21). In a general way, the parity of the number of carbons forming the bridge will determine the mode of cyclization (Figure 31).

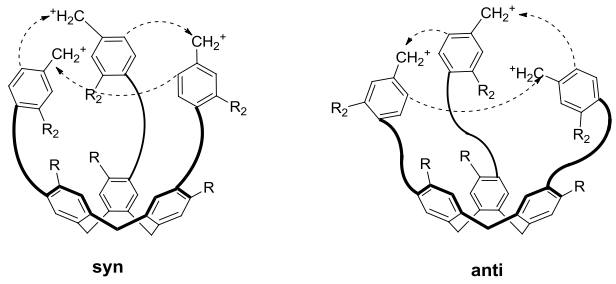

Figure 31: Probable intermediates for cryptophane *syn* and *anti* in the template method

Compared with the direct method, the template method displays advantages like significantly better yields and the possibility to synthesize cryptophanes with different symmetries. This is particularly important for its application in the construction of biosensors and it is also the reason why the template method is the most widely used strategy for synthesizing cryptophanes.

c. Coupling of CTVs

This method consists in synthesizing cryptophanes by coupling two CTV subunits. It was firstly reported by D. Cram for the preparation of cyptophanes with acetylene groups in the bridging chain.[74] This relatively direct strategy suffers from poor yield due to the formation of by-products like oligomers and polymers during the coupling reaction. Recently, this method was used for synthesizing the small-sized cryptophanes [111][59, 75] and [000][76] (Figure 32).

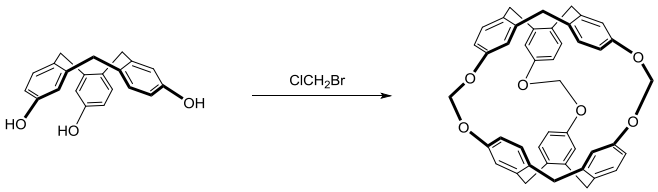

Figure 32: Synthesis of the cryptophane[111] by the coupling of CTVs

Our group has proven that it is also possible to introduce several different bridging chains. Cryptophane[112] and [122] were synthesized by the coupling of CTVs. A first coupling makes the two CTV units linked to each other by one or two bridging chains, which allows to introduce different bridging chains in the later reaction (Figure 33). Experiment shows that these two cryptophanes possess a good affinity for xenon and an unexpected high exchange rate.[77]

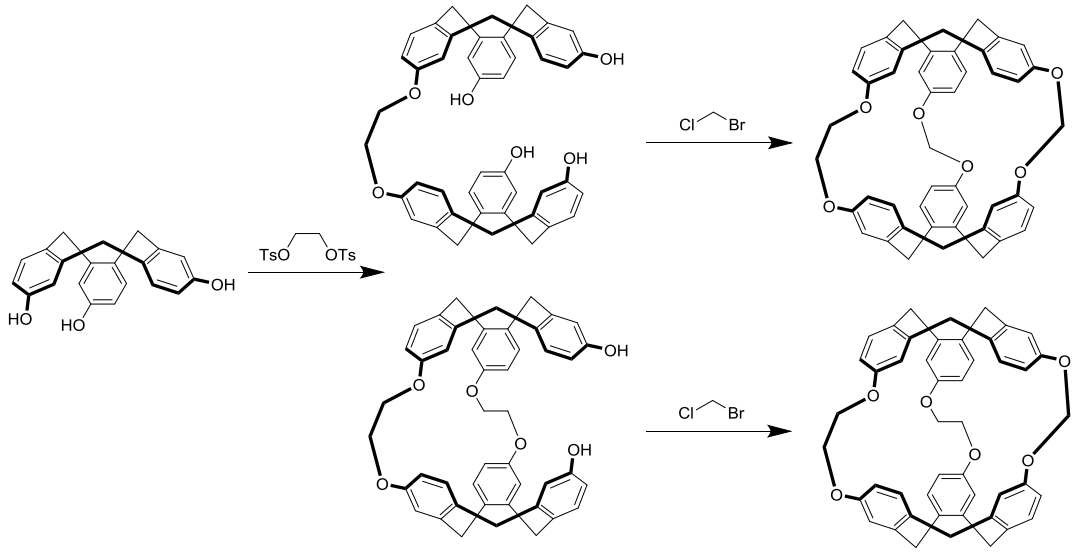

Figure 33: Synthesis of cryptophane[112] and [122] by coupling of CTVs

3. Strategies for the hydrosolubilization of cryptophanes

The design of biosensors usable for *in vivo* molecular imaging implies that the molecular platform has a good solubility in water. After more than 30 years development in cryptophane chemistry, a large number of different chemical functions can be introduced on the aromatic rings as well as the bridging chains. Although cryptophanes are still hydrophobic molecules, different functionalization can be used to improve their water-solubility.

The first strategy based on the introduction of carboxylic acid groups on the aromatic rings.[63] Starting from cryptophane A, the utilization of the lithium base PPh_2Li allows obtaining the expected cryptophane with six phenol moieties. Then the nucleophilic substitution with methyl bromoacetate leads to the formation of a cryptophane carrying six ester functions, which are finally hydrolyzed to give cryptophane[222] *hexa* carboxylic acid (Figure 34).

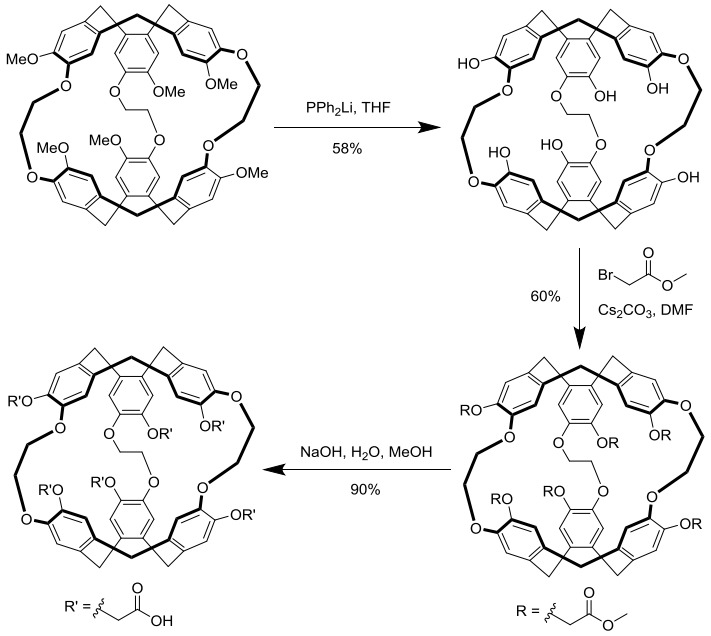

Figure 34: Hydrosolubilization of cryptophane A by introducing 6 carboxylic acid groups

With an excellent affinity for xenon, cryptophane[111] **7** is also a potential candidate for the development of *in vivo* biosensors. The first synthesis of its water-soluble derivative was achieved by the η^6 -coordination of the arene rings by cationic, electron-withdrawing [(η^5 -C_5Me_5)Ru^{II}] $^+$ moieties (hereafter [Cp*Ru]$^+$)[78], giving rise to the air stable chloride salt [(Cp*Ru)$_6$**7**]Cl_6, hereafter [**8**]Cl_6 (Figure 35). Unlike carboxylic acid derivatized cryptophanes, the water solubility of which is attributed to the deprotonation of the carboxyl groups, [**8**]Cl_6 is highly water-soluble at neutral pH (>30 mM, 293 K).[58] Moreover, this molecule has shown an affinity for xenon even better than **7** (10,000 for **7**, 29,000 for [**8**]Cl_6).

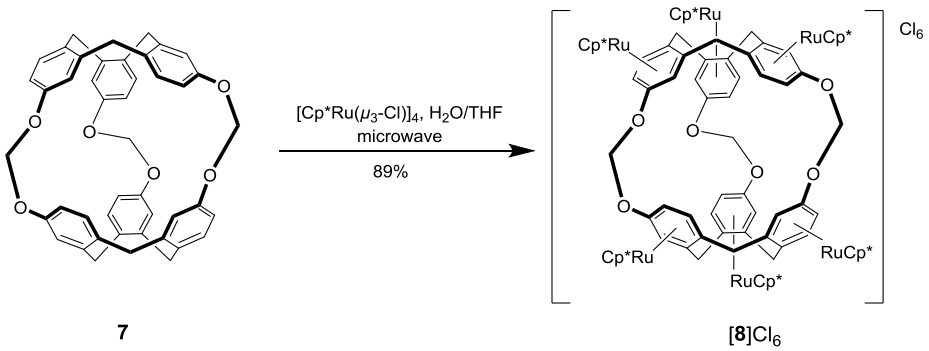

Figure 35: Hydrosolubilization of cryptophane[111] by cordination with 6[Cp*Ru]$^+$

Another effort aiming to hydrosolubilize cryptophane[222] was achieved by the group of I. Dmochowski.[79] By using the template method, the tripropargyl cryptophane was synthesized in 10 steps with 4 % overall yield. Then the reaction of cryptophane with 3 equivalents of 2-

azidoethylamine was carried out via copper(I)-mediated [3 + 2] Huisgen cycloadditions[80] to give the water-soluble tris-(triazole ethylamine) cryptophane (TTEC) (Figure 36). It was reported that the affinity constant for xenon of TTEC is as high as 42,000 M^{-1}. According to the author, the presence of different substituent groups on the two CTVs causes an axial dipole moment which complementally stabilizes the highly polarizable electron cloud of xenon.[81] However, the measurement of the affinity constant was carried out by isothermal titration calorimetry instead of NMR, thus limiting the comparison with other cryptophanes.

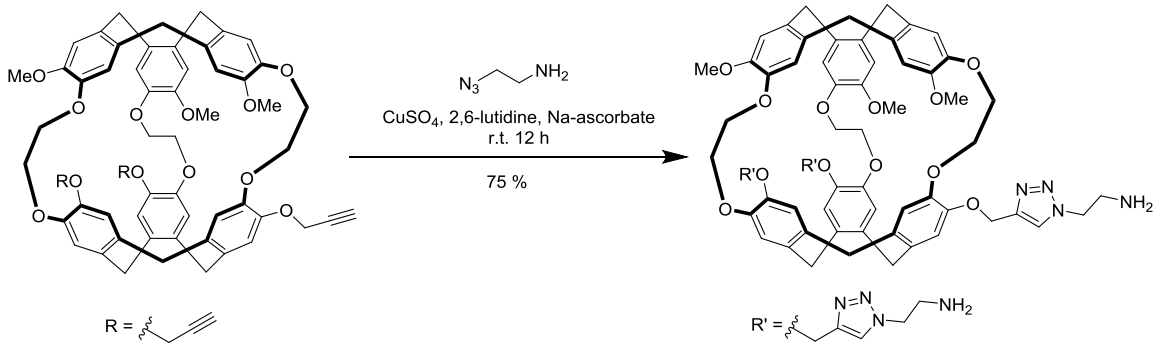

Figure 36: Hydrosolubization of cryptophane[222] by introducing triazole groups

The latest development in this field was made by the group of L. Schröder. Starting from cryptophane A diacid (CrA-da), which was commercially available, a straightforward synthesis of the dendronized cryptophanes was achieved with good yields (60 % for two steps).[82] Conjugation of CrA-da with polyglycerol dendrons by using the standard amide bond formation reaction conditions was followed by the subsequent deprotection under acidic conditions with TFA yielded the final dendronized cage molecules (Figure 37). According to xenon NMR experiments, the presence of dendrons on cryptophanes has no negative impact of the encapsulation of xenon gas.

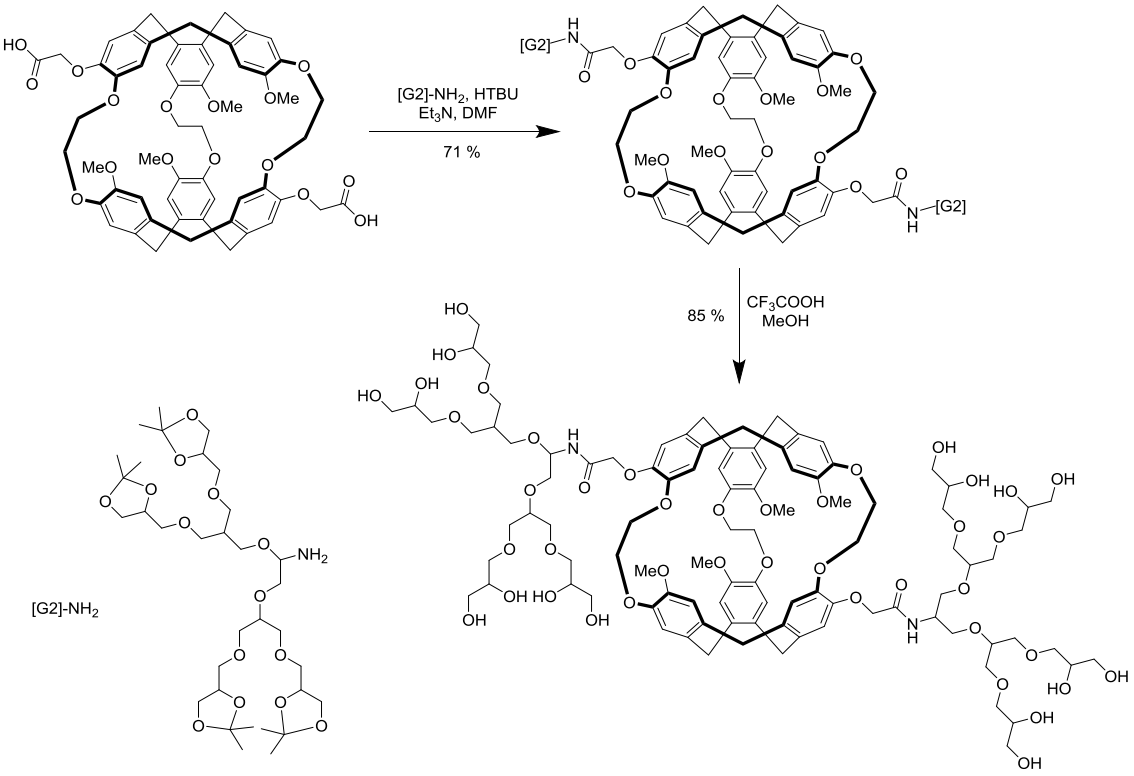

Figure 37: Hydrosolubization of cryptophane[222] by introducing dendrons

The synthesis of water-soluble cryptophanes was a major concern for our group. After several attempts, synthesis of water-soluble cryptophane [111] and [222] were successfully completed.

Based on a short, high-yielding, and scalable synthetic route of cryptophane[1.1.1] **7** (5 steps, 12 % overall yield)[83] which is also developed by our group, the functionalization leading to the first metal-free water-soluble cryptophane[111] was achieved. After a mono-bromination of the cryptophane[111] (this step will be discussed more in the part A-II-4), the lithiation of bromine **9** by *n*-BuLi followed by carboxylation with CO_2 afforded the carboxylic acid **10**. Then a Schotten–Baumann reaction was performed between cryptophane **10** and an amino acid-based poly-sulfonated linker **11** to give the desired water-soluble cryptophane **12** as a mixture of two racemic diastereomers (Figure 38).[84] As a metal-free cryptophane, **12** avoided the potential risk in its application *in vivo*, like a DNA-binding activity of some ruthenium–arene complexes.[85] Its solubility in water (about 1.0 mg/mL) is suitable for xenon NMR experiments.

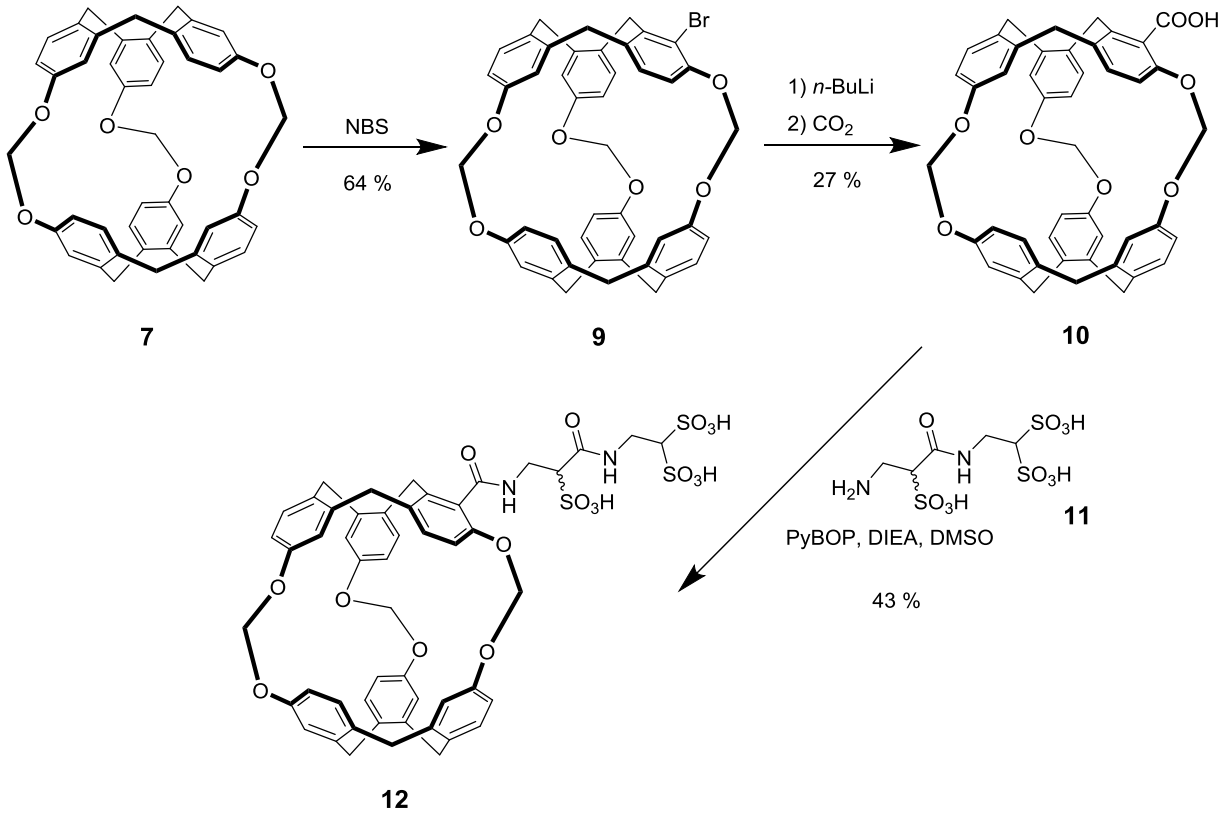

Figure 38: Hydrosolubilization of cryptophane[111] by introducing a trisulfonated linker

Alternatively, a completely different strategy was applied for synthesizing water-soluble cryptophane [111]. Inspired by the water solubility of cryptophane[222] bearing six carboxylic acid groups, a straightforward synthesis of cryptophane[111] hexacarboxylate **15** was designed (Figure 39). Starting from the cryptophane[1.1.1] **7**, a hexabromination with an excess of NBS was followed by a lithiation with *n*-BuLi. In this case, the lithium/bromine exchange occurred, but the lithiated cryptophanes were not efficiently trapped by CO_2. Conversely, using benzyl chloroformate as an electrophile led to hexa-benzyl ester compounds **14**, which was then deprotected by hydrogenolysis over Pd/C, to give cryptophane[111] hexacarboxylate **15** (18 % overall yield for three steps).[86] As expected, compound **15** is soluble in water at a concentration of 2.0 mg/mL.

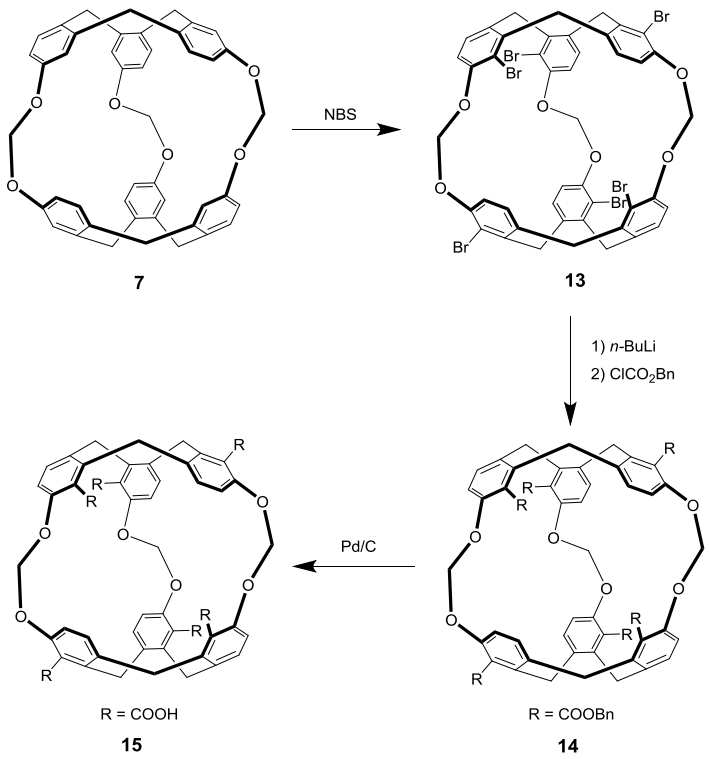

Figure 39: Hydrosolubilization of cryptophane[111] by introducing six carboxylic acid groups

As reported for the cryptophane[222], our group has developed the synthesis of a highly water-soluble cryptophane **24** which could be seen as a universal platform for the construction of ^{129}Xe MRI-based biosensors.[87] This platform contains a poly(ethylene glycol) (PEG) chain as water-soluble moiety: this choice will be discussed further in the part B-I-2. Unlike in the other strategies, the water-soluble moieties can be introduced at the early stage of the synthesis. This not only improves the solubility of the cryptophane intermediates and facilitates the synthesis and purification steps but also decreases the number of steps by avoiding successive protection and deprotection of the vanillyl alcohol. Thus the phenol group of **16** was substituted by the tosyl-functionalized PEG monomethyl ether **17** to give the PEGylated benzyl alcohol derivative **18**. After cyclotrimerization, product **19** was engaged in the demethylation with PPh_2Li. Then last two steps of the reaction were carried out following the classical template method, leading to PEGylated cryptophanes **23** and **24** with different substituent groups (Figure 40). These cryptophanes are soluble up to 50 mg/mL water in a physiologically relevant pH range (pH 5 to 8), which is the highest water solubility ever reported for cryptophane[222]. Moreover, the presence of three propargyl groups in cryptophane **24** makes possible further functionalization.

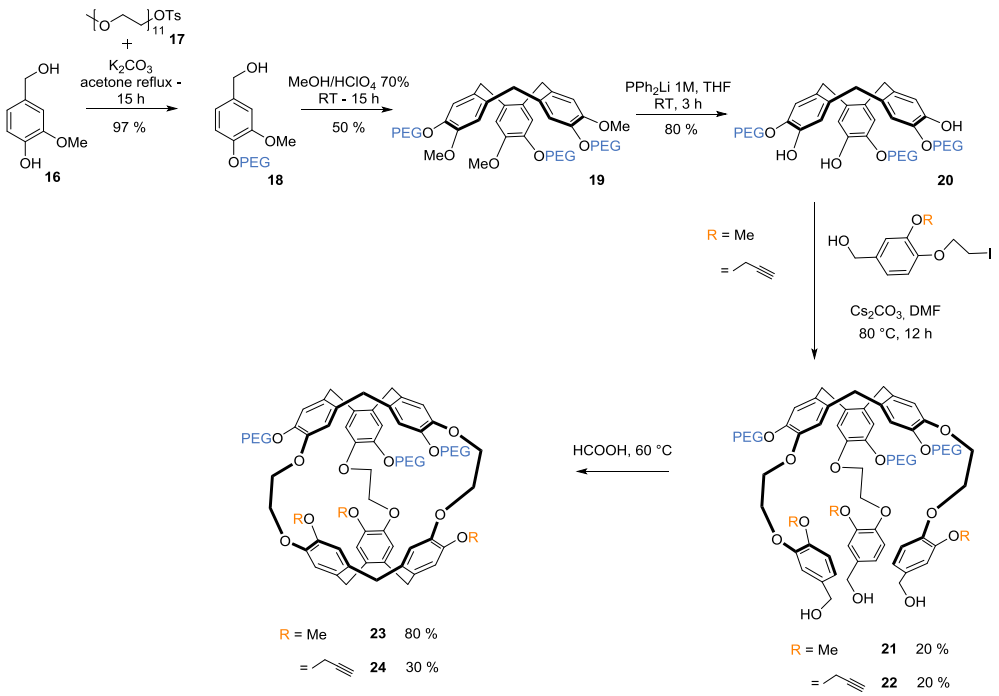

Figure 40: Synthesis of the water-soluble PEGylated cryptophanes

4. Strategies of mono-functionalization of cryptophanes

As underlined before most of the previously synthesized cryptophanes possess a high symmetry. In fact, this character can be an important drawback for the synthesis of biosensors for *in vivo* imaging. The high symmetry makes the control of the reactivity on a particular position difficult versus other equivalent sites. Usually, the cryptophanes used for synthesizing biosensors possess three (e.g. Figure 41)[88] or six (e.g. Figure 42)[89] functionalizable positions while only one is needed to react with the linker. Therefore a complex statistical mixture of different products is expected, complicating the purification steps. As a result, the optimization of yields is difficult and an efficient scale-up is then ruled out. Contradictorily, large quantities of desymmetrized cryptophane are required for the synthesis of biosensor which is often strenuous. Therefore, an optimization of the mono-functionalization of cryptophanes is crucial.

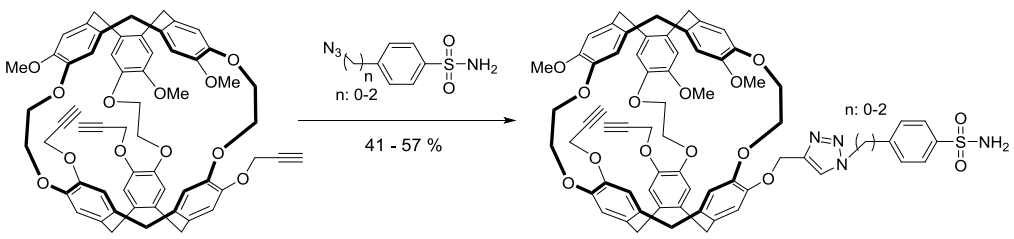

Figure 41: Cycloaddition with one of three propargyl groups on the cryptophane

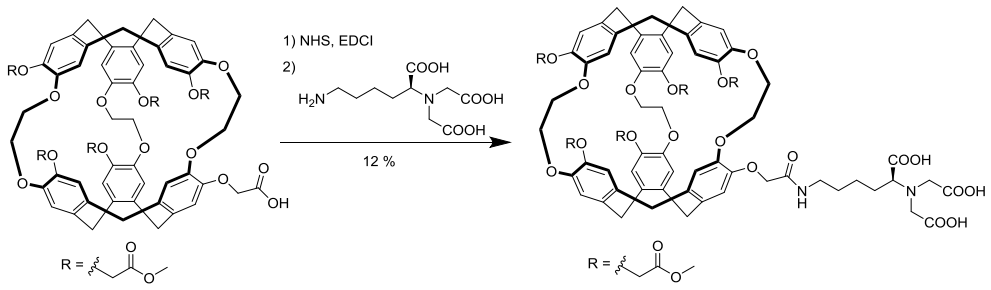

Figure 42: Peptide coupling with one of six carboxylic acid groups on the cryptophane

The earliest effort in this field focused on the synthesis of the monohydroxy cryptophanol **31**, which can be easily obtained through a deprotection from mono-protected cryptophane **30**. As an important intermediate in the synthesis of mono-functionalized cryptophanes, compound **30** can be synthesized using two alternative strategies. The first one, which is still the most widely-used to break the symmetry of cryptophanes, was developed by the group of T. Brotin and J. P. Dutasta.[90] This strategy is based on the mono-functionalization or the bis-functionalization of CTV **25**, which was treated successively with two different benzyl alcohol derivatives **26** and **28**. Through a disubstituted intermediate **27**, the cryptophane precursor **29** was obtained, latter transformed into the expected cryptophane **30** (Figure 43).[91] This synthesis significantly unlocked the development of cryptophanes usable for *in vivo* applications, and therefore numerous subsequent biosensors were obtained from this molecule.

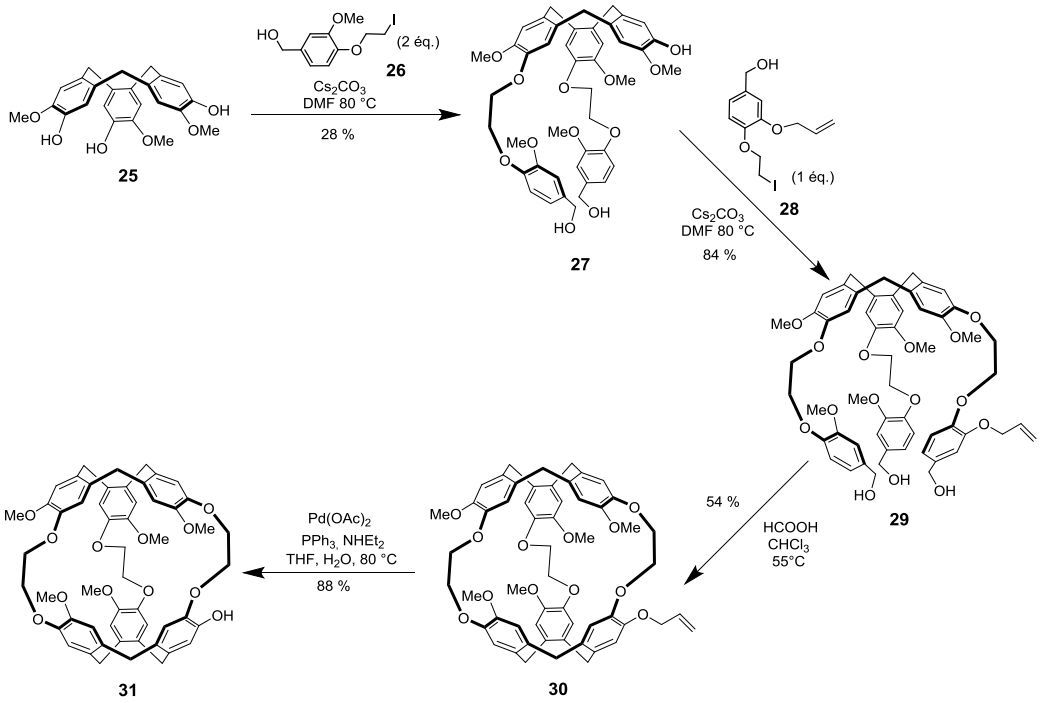

Figure 43: Synthesis of cryptophanol by the group of T. Brotin and J.P. Dutasta

Simultaneously, another strategy to synthesize cryptophane **30** was developed by the group of A. Pines.[92] It involves the selective deprotection of CTV **32** using $Pd[P(C_6H_5)_3]_4$ as a catalyst and Bu_3SnH.[83] The monoprotected CTV **33** was then allowed to react with protected vanillyl ether **34** to give the bis-functionalized CTV **35**. A second deprotection step followed by the condensation with the allylic containing derivative **37** provided the cryptophane precursor **38**. Finally, the last cyclization reaction was carried out in pure formic acid to yield cryptophane **30** (Figure 44).[3] Compared with the previous method, this synthetic route gives better yields but requires several additional steps.

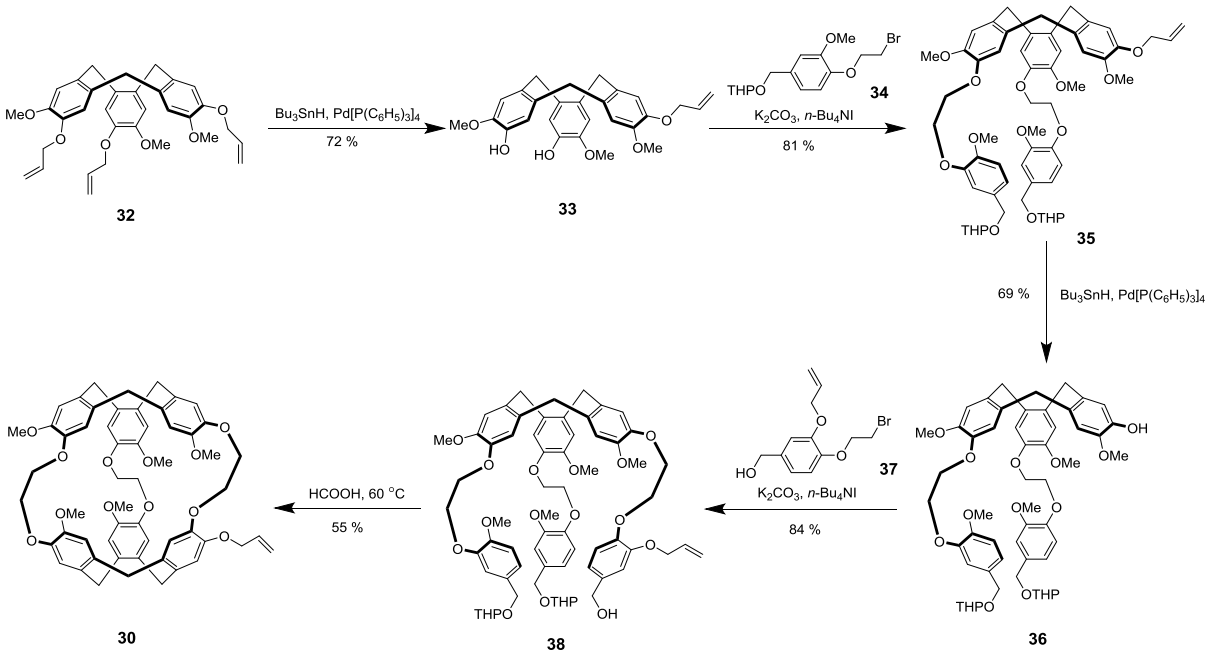

Figure 44: Synthesis of cryptophanol by the group of A. Pines

Afterwards, a more straightforward synthetic pathway to cryptophanol **31** was developed by the group of T. Brotin[94]. Removal of a single methyl group of cryptophane A was easily achieved by using iodotrimethylsilane, yielding cryptophanol **31** in 37 % yield as well as unreacted cryptophane A which could be reused in another cycle of reactions (Figure 45).

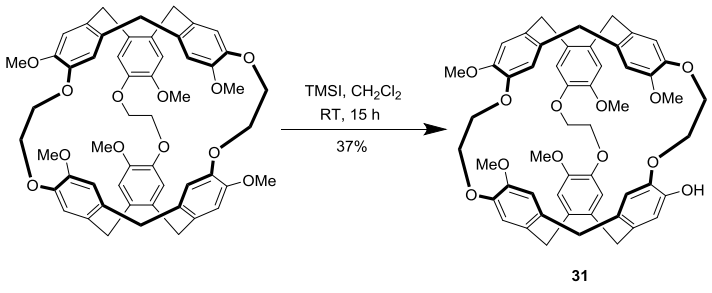

Figure 45: Mono-deprotection of cryptophane A

The newest development in this domain was also realized by the group of T. Brotin for the synthesis of cryptophane[223]. With large association constants[95] and appropriate exchange rates for xenon[91], these larger molecular cages could also be attractive candidates for xenon MRI. In addition, cryptophane[223] backbone offers the possibility of introducing a new functionality on the propylenedioxy linker which can be different from those attached on the benzene rings. This position is chosen because the presence of this new functional group does not introduce complexity in the structure. The central carbon bearing the alcohol function is not a stereogenic center if the two CTVs possess the same configuration.

Similar to the template method, the synthesis starts with the di-functionalization of the CTV **25**. After protection of the two alcohol groups of **27** with 3,4-dihydro-2*H*-pyran (DHP), the di-substituted CTV **36** reacted with oxirane **40** in the presence of 1,4-diazabicyclo[2.2.2]octane (DABCO) as a base to provide the cryptophane precursor **41**. The alcohol located on the central carbon of the bridge is then protected with an allyl group to avoid its undesired reaction with formic acid in the later cyclotrimerization step and leads to cryptophane **43** (Figure 46). In this approach, the generation of a statistical mixture is avoided when trying to selectively functionalize a symmetrical host molecule. And It enables the efficient large-scale production of new cryptophanes that can be used as chemical platforms for the preparation of xenon biosensors.[96]

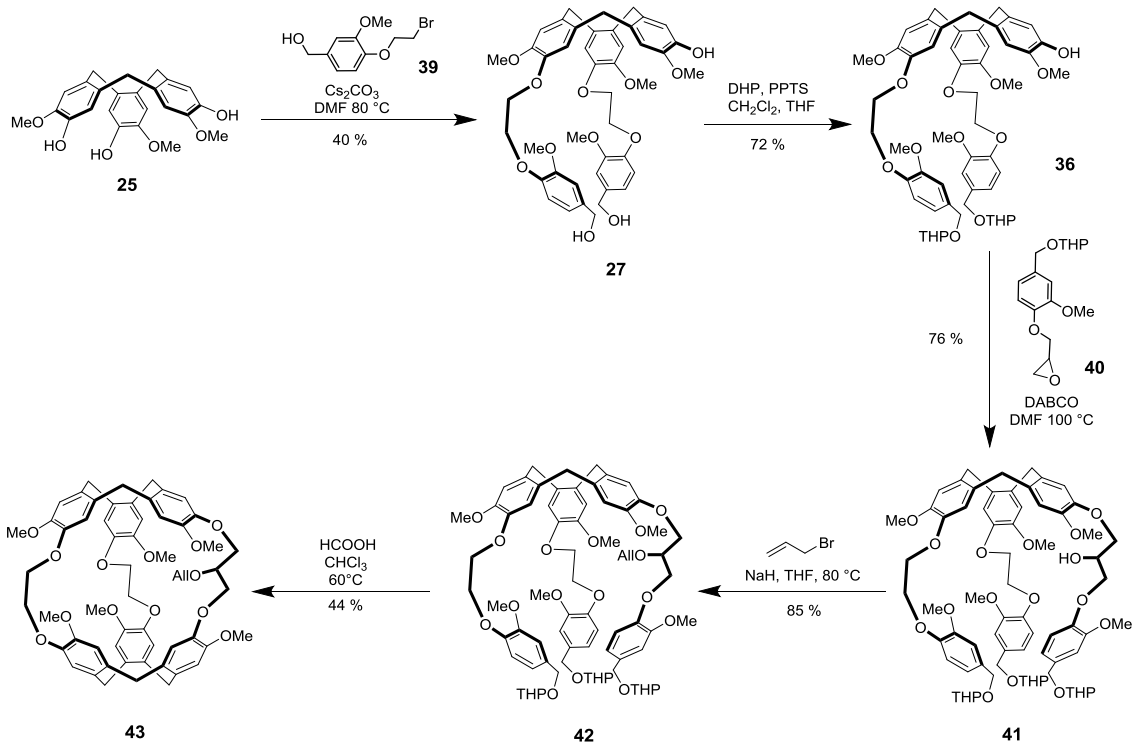

Figure 46: Synthesis of mono-functionalized cryptophane[223]

Our group has also reported the only existing approach to mono-functionalized cryptophane[111].[83] Limited by the lack of modifiable functional groups, the functionalization of cryptophane[111] was always difficult. However, since it is composed of phenoxy moieties, it is expected to be iodinated or brominated. After several attempts, the iodination was achieved by using (I_2, $C_6H_5I(OAc)_2$)[97], while the bromination was achieved with *N*-bromosuccinimide (NBS) (Figure 47). Starting from these halogenated compounds, a large number of chemical functions can be thus introduced using either organolithium or palladium chemistry, including the carboxylic acid and the trisulfonated linker as presented previously.

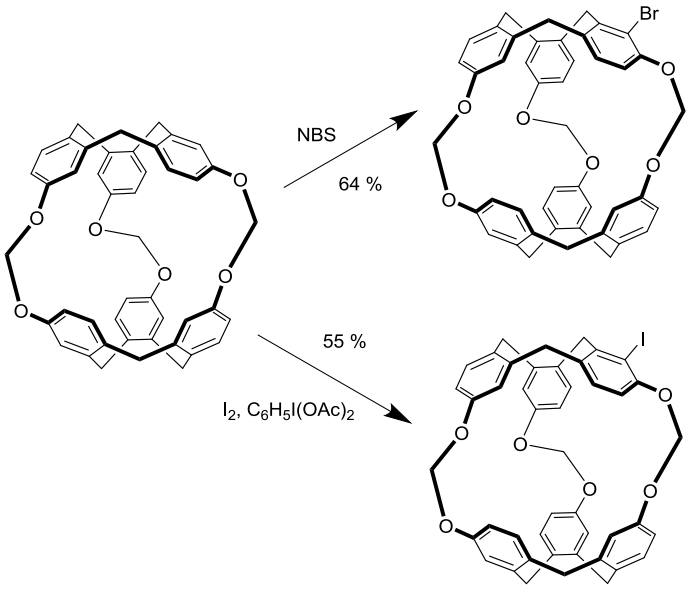

Figure 47: Mono-functionalization of cryptophane[111]

5. Cryptophane-based biosensors for ^{129}Xe MRI

The first cryptophane-based biosensor for ^{129}Xe NMR synthesized by the group of Pines in 2001 is capable to detect the formation of the complex biotin/avidin at micromolar concentrations.[3] This biosensor is composed of the hydrophobic core of cryptophane A (the black part), a water-soluble peptide linker (the green part) and an recognition antenna , containing a biotin motif (the blue part) which strongly binds to avidin (Figure 48).

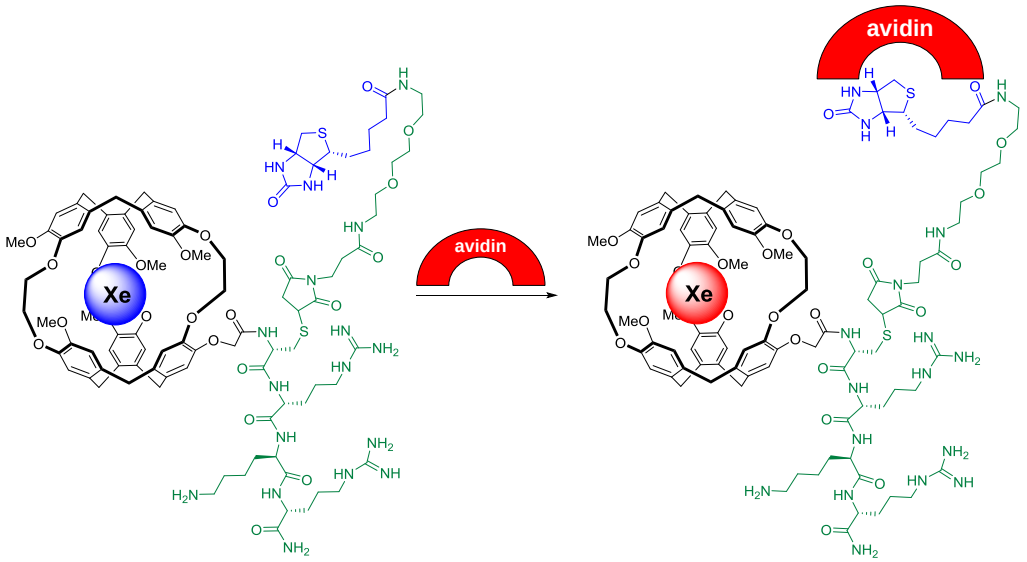

Figure 48: Structure and conception of the cryptophane-based biotin/avidin bio-sensor

Although this biosensor gave unsuitable complex NMR signals due to the presence of four diastereoisomers (there is one stereocenter in the linker and the cryptophane is used as a racemate)[92], it enables the detection of avidin when linked to the biosensor. Selective detection of the biotin/avidin complex is based on the changes in rotational and vibrational movements of the cryptophane causing deformation and distortion of the electron cloud of xenon when the bioprobe is bound to the large protein. In the NMR spectrum, this change was visualized by a shift from 72 ppm to 74 ppm (Figure 49). Afterward, this biosensor has been continuously optimized by changing the peptide linker between biotin and the cryptophane in order to improve the chemical shift difference.[98, 99]

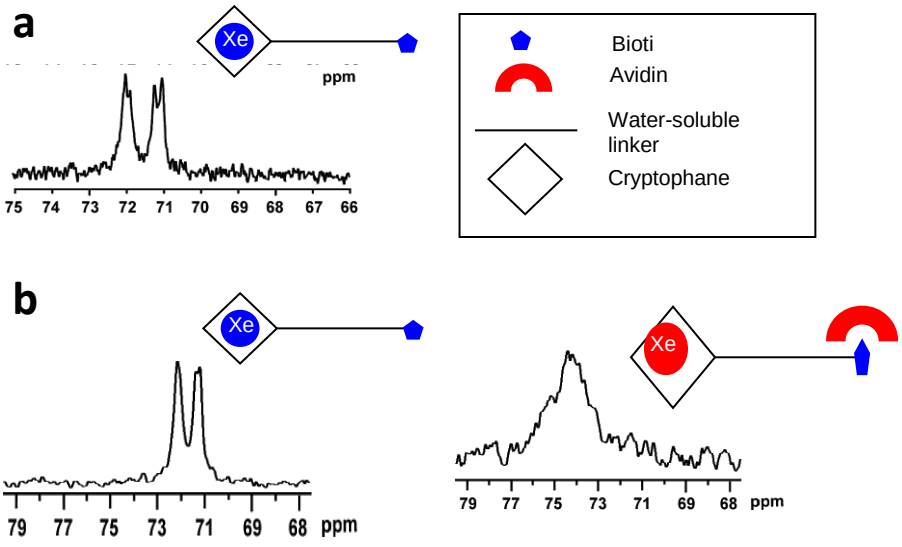

Figure 49: ^{129}Xe NMR spectrums of a) the biosensor without avidin in D_2O. b) a titration starting from biosensor without avidin (left) until with 1,2 equivalent of avidin (right)

Since then, numerous crytophane-based bio-sensors were developed, allowing to detect various biological parameters and phenomenon such as temperature[100], pH[101], complementarity binding to a DNA strand[102], proteolytic activity[88, 103, 104], glycoprotein[105], cations[89, 106, 107]… (Figure 50)

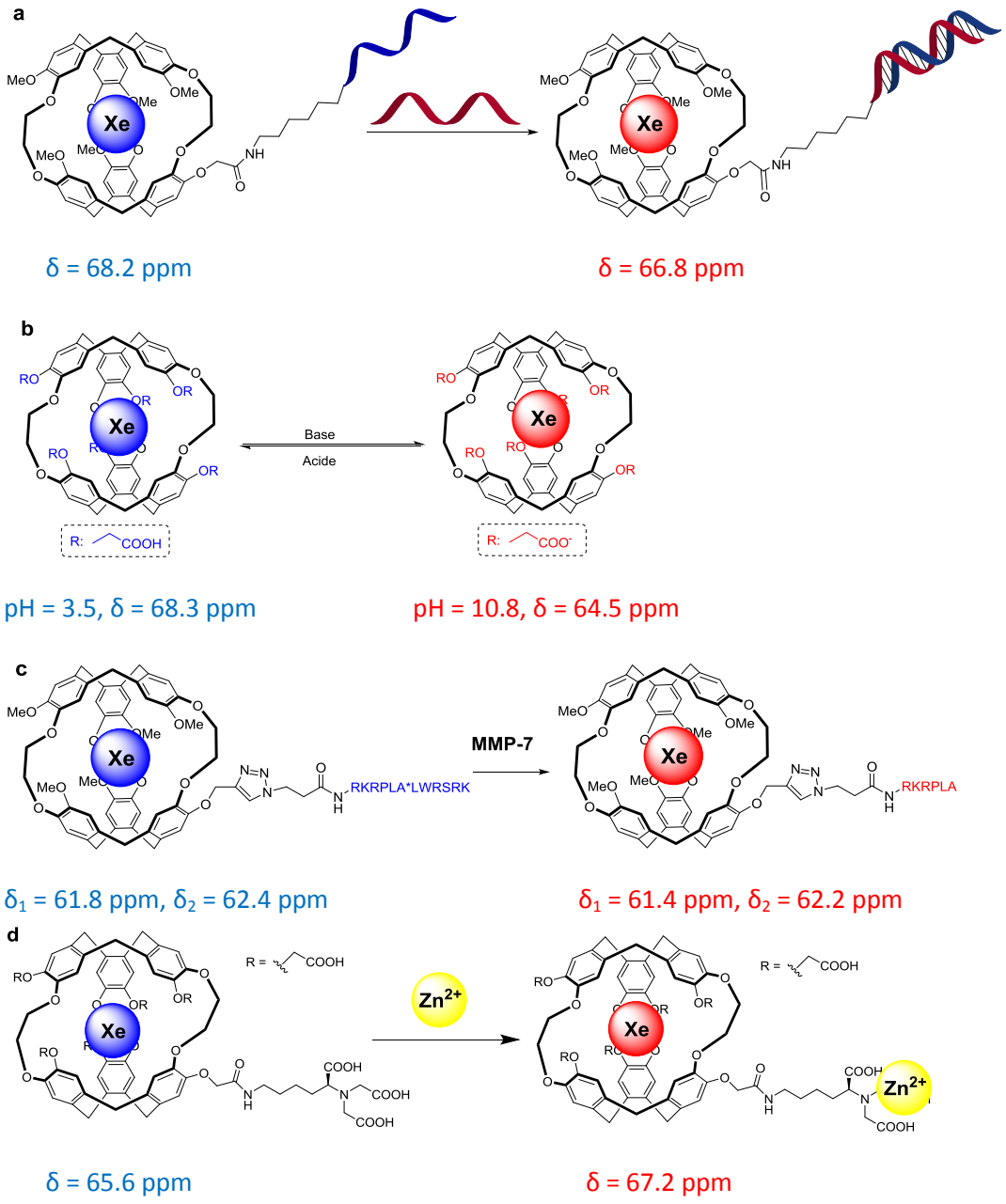

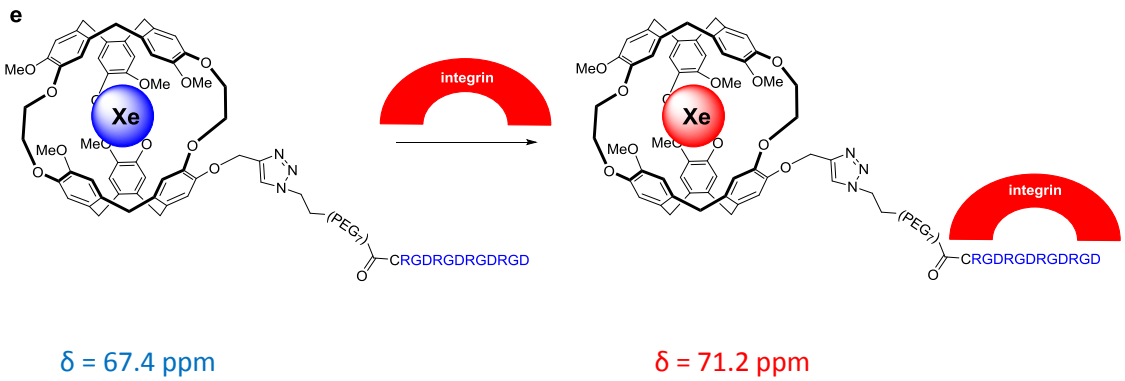

Figure 50: Structure, concept and the change of chemical shifts in ^{129}Xe NMR of cryptophane-based biosensor detecting a) DNA strands. b) pH. c) matrilysin. d) Zn^{2+}, Cd^{2+}, Pb^{2+}. e) integrin

However, to approach an application of the cryptophane-based MRI biosensors *in vivo*, the effort has turned to realize the study of bio-sensor inside the cells. Several important steps were made to realize this ambition.

The first system permitting to track the internalization of a cryptophane by ^{129}Xe NMR was developed in 2011.[94] It is made of a cryptophanol functionalized with a side chain carrying a pentafluorophenol group which allows to graft several cryptophane on the protein surface, thus potentially increasing the sensitivity of detection by ^{129}Xe NMR (Figure 51-a). This chemical group can be grafted onto the transferrin, which is a beta globulin protein synthesized by liver (Figure 51-b). The internalization of the protein carrying the biosensor by endocytosis is preliminarily proven by confocal microscopy, by localizing the fluorophores which are grafted on its surface beforehand (Figure 51-c and –d).

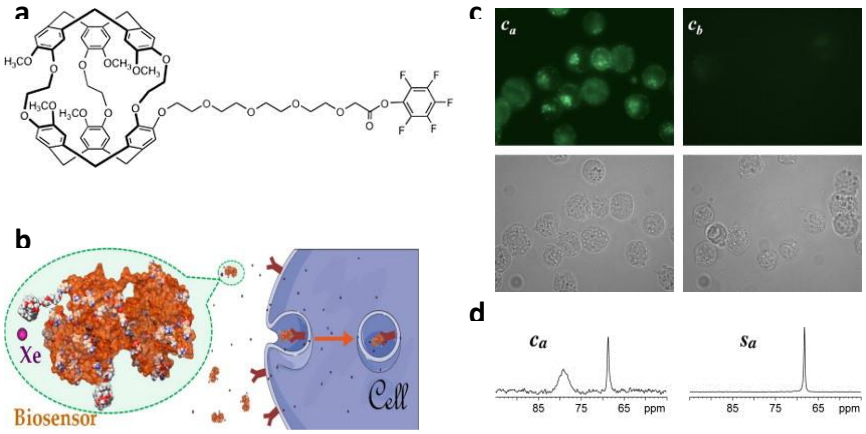

Figure 51: a) structure of the pentafluorophenol/transferrin biosensor. b) Internalization of the biosensor. c) Fluorescence (up) and bright field (down) images of cells incubated with biosensor, with (left) and without (right) pronase treatment. d) ^{129}Xe NMR spectrum of cells incubating biosensor (left) and corresponding supernatant (right)

The ^{129}Xe NMR experiments also confirm the recognition and the endocytosis of the biosensor, despite of the presence of an unexpected signal which corresponds to the non-specific interaction between the biosensor and the lipid membrane of the cells. This problem is undoubtedly due to hydrophobicity of the cryptophane moiety and could be solved by the introduction of the solubilizing groups on the molecular cage.

The first images of hyperpolarized ^{129}Xe MRI *in cellulo* were presented by the group of L. Schröder in 2014.[108] This biosensor, which is also based on the cryptophanol motif, bears a fluorescein moiety permitting to monitor its internalization by confocal microscopy (Figure 52-a). MRI experiments with the biosensor-labeled cells were done within a NMR compatible packed-bed bioreactor working under continuous perfusion with a hyperpolarized xenon-saturated milieu. The xenon gas is introduced into the culture medium within a bubbling chamber located upstream of the sample. The phantom was split into two compartments along the direction of media flow. Cells were immobilized by encapsulating them within solid alginate beads (Figure 52-b). One of the two compartments was filled with cells pre-incubated with the biosensor (the blue ones), and the other compartment was filled with the unlabeled cells (the red ones). Although the intracellular concentration of the bio-sensor is relatively low, the compartment bearing labeled cells could be clearly distinguished from the control compartment by Xe MRI after only 20 acquisitions (Figure 52-c).

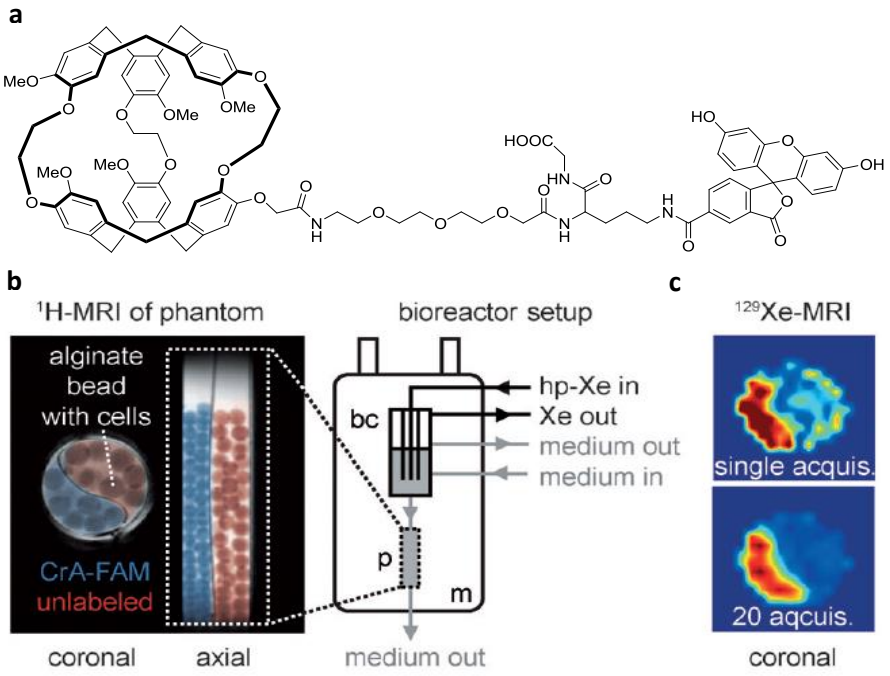

Figure 52: a) structure of the biosensor with a fluorescein moiety. b) Conception of the experiment. c) Images of the hyperpolarized Xe MRI

The development of the cryptophane-based hyperpolarized ^{129}Xe biosensors has highlighted the necessity to develop cryptophane chemistry for easy desymmetrization and water-solubilization of the cryptophane moiety. All the results encourage the researchers to continue the development of a cryptophane-based molecular imaging *in vivo*.

III. Objectives

As an efficient method to overcome the lack of sensitivity of MRI, the technique using ^{129}Xe as a hyperpolarized species has been developing fast since a few years. Benefiting from the development of cryptophane-based biosensors functionalized with different targeted groups, this technique shows great interest for molecular imaging. After numerous studies of this kind of biosensors in water, buffer solutions, human plasma and lipid environment, the actual advancements in imaging internalized biosensors by NMR of clearly open new prospects for *in vivo* applications.

In this context, the objective of this thesis is to design new cryptophanes which can be used as molecular platforms for constructing new ^{129}Xe MRI biosensors usable for *in vivo* MRI molecular imaging. To meet this demand, two main difficulties should be resolved.

First of all, the high symmetry of cryptophanes is proved to be an important drawback to control the reactivity of a particular position with respect to other equivalent sites. The *mono*-functionalization step is always inevitable and leads to a complex statistical mixture in all kinds of existing synthetic pathways to biosensors. This strategy complicates the purification steps and jeopardizes the production of large quantities of cryptophane derivatives required for the arduous synthesis of bioprobes. For this reason, there is a systematic discussion about cryptophanes symmetry breaking and different attempts were made to synthesize mono-functionalized molecular cages.

Secondly, the synthesized biosensors still suffer from the high hydrophobicity of the cryptophane poly-aromatic core. Even though the grafting of various water-soluble linkers increases the biosensor overall solubility, the high hydrophobicity of the cage itself in aqueous milieu confers amphiphilicity to the molecule which is prone to form self-organizing systems, promoting a non-specific interaction with the lipid bilayers and the subsequent embedding of the probe inside the cell membranes. To avoid this problem which is detrimental for the application of these biosensors *in vivo*, a new cryptophane cage designed to be fully water-soluble in different pH environments must be developed. In this thesis, the polyethylene glycol (PEG) group was therefore used to address efficiently the issue of cryptophane water-solubility.

In this thesis, the main effort focuses on the hydrosolubilization and the desymmetrization of cryptophane[222]. This molecular cage was chosen thanks to its good affinity and selectivity for xenon, as well as the suitable exchange rate that it can offer. Synthesis of different water-soluble mono-functionalized cryptophane[222] have been achieved (Figure 53). All the strategies and synthetic pathways will be discussed in the next chapter.

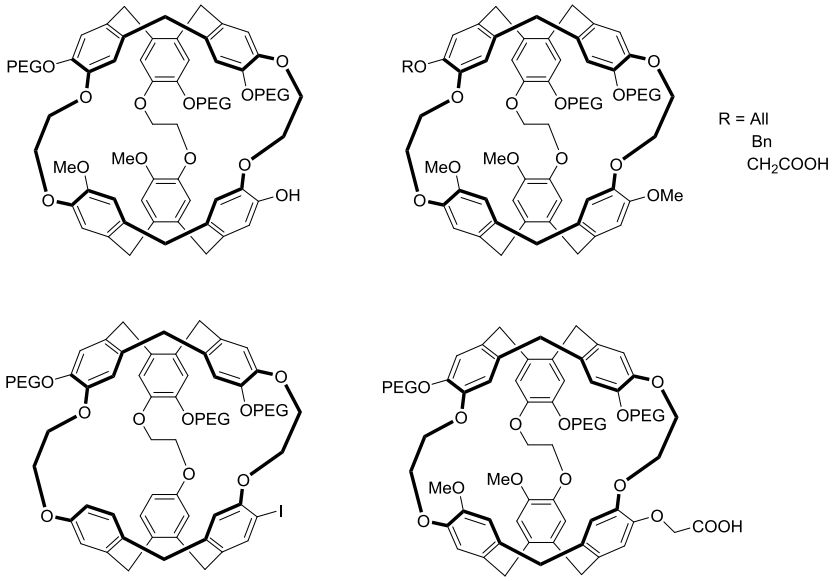

Figure 53: Different targeting water-soluble mono-functionalized cryptophane[222]

B. CONCEPTION AND SYNTHESIS OF WATER-SOLUBLE AND MONO-FUNCTIONALIZABLE CRYPTOPHANES

I. Water-Soluble and Mono-Functionalizable Cryptophanes – Why and How

1. Background and objective

This thesis is part of a bigger project in our laboratory which aims at developing and promoting a new technique for imaging non-small cell lung cancer (NSCLC). In France 37 000 new cases of lung cancer are diagnosed each year with a high mortality rate (28 700 death per year). Eighty percent of all cases are NSCLC, a type of cancer that remains the leading cause of cancer-related mortality. Despite numerous clinical trials, no major outbreak has been made in the treatment of the large majority of NSCLC during the last decades. The detection and biochemical characterization of growing lung tumors by molecular imaging is a prerequisite to an effective treatment. Therefore, a fine detection and monitoring of the response of tumor to therapy through imaging techniques is critically important for the treatment of NSCLC.

To date, most of NSCLC cases are detected either fortuitously (in particular during chest radiograph) or on the basis of characteristic symptoms (coughing, hemoptysis, shortness of breath etc.). Both situations need a confirmation by invasive techniques such as bronchoscopy and biopsy. The systematic detection of NSCLC is difficult due the absence of circulating biomarkers and the detection of large proportion of false positive cases. Moreover, scintigraphy techniques (SPECT and PET) using short-period radio-isotopes, which use gamma and positron emitters respectively, can be used to confirm strongly suspected lung cancer cases and to follow up treatment efficacy but not to screen a large at-risk population. As a consequence, NSCLC is frequently detected at late stages of development and is therefore difficult to cure. In this respect the development of an efficacious MRI technique for the detection and biological characterization of NSCLC is essential. In this project, we investigated the development of ^{129}Xe MRI-based biosensors for the diagnosis of NSCLC and follow up of treatment efficacy in an orthotopic tumor mice model.

The designed biosensors are composed of three conjugated parts which are assembled by a peptide linker (Figure 54).

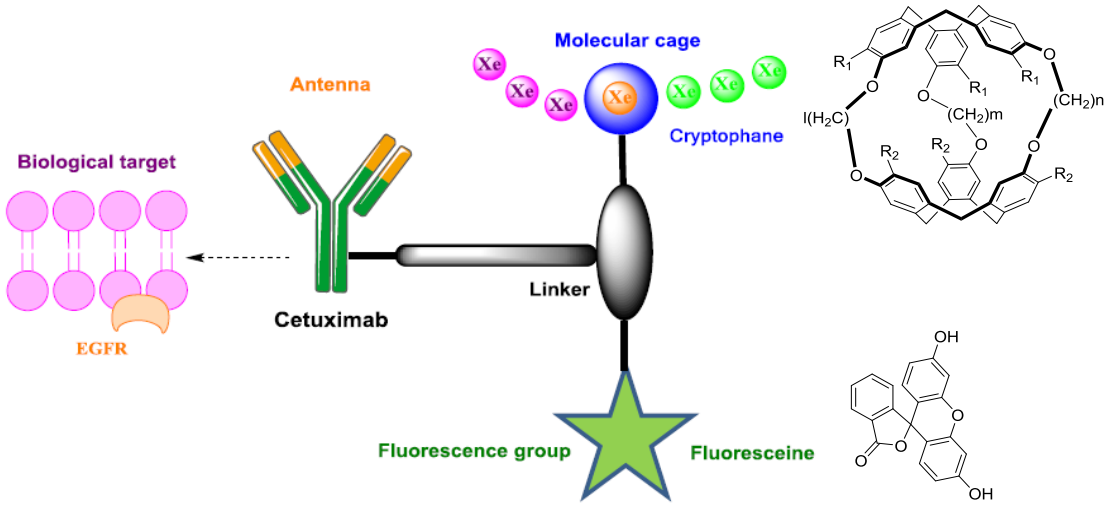

Figure 54: Conception of the cryptophane-based biosensor for lung cancer

1) The antibody Cetuximab as the recognition antenna to specifically bind to a NSCLC biomarker. Cetuximab is a chimeric monoclonal antibody with a high affinity (Kd = 0.28 nM)[109] for the epithelium growth factor receptor (EGFR), which is widely over-expressed on the surface of many cancer cells. It has been clinically approved for the therapeutic treatment of NSCLC. On top of its efficiency as anti-cancer agent, it exhibits a low toxicity at therapeutic concentrations (typical primary therapeutic dose of 400 mg/m^2 of body surface and no side-effect after injection of 1000 mg/m^2 of body surface in human).[110] The bio-conjugation of diverse chemical entities onto this antibody is well documented[111, 112] and bifunctional reagents are commercially available at a reasonable prize (1000 € / 500 mg).

2) A fluorescein moiety to allow the *in vitro* tracking of the biosensor by fluorescence confocal microscopy using the same probe, in order to make the proof of concept in cell cultures.

3) A cryptophane molecular cage encapsulating xenon which should be water-soluble, functionalizable and features an exchange rate adapted to the MRI experimental time scale. This part is also the focus of this thesis.

Cryptophane[222] *hexa*- carboxylic acid **48** was chosen as the molecular cage for constructing the biosensor. This compound was kindly provided by Dr. Thierry Brotin (ENS Lyon). With a well-developed synthetic route, cryptophane **48** can be obtained in several hundred milligrams in 1.4 %overall yield (Figure 55).[101]

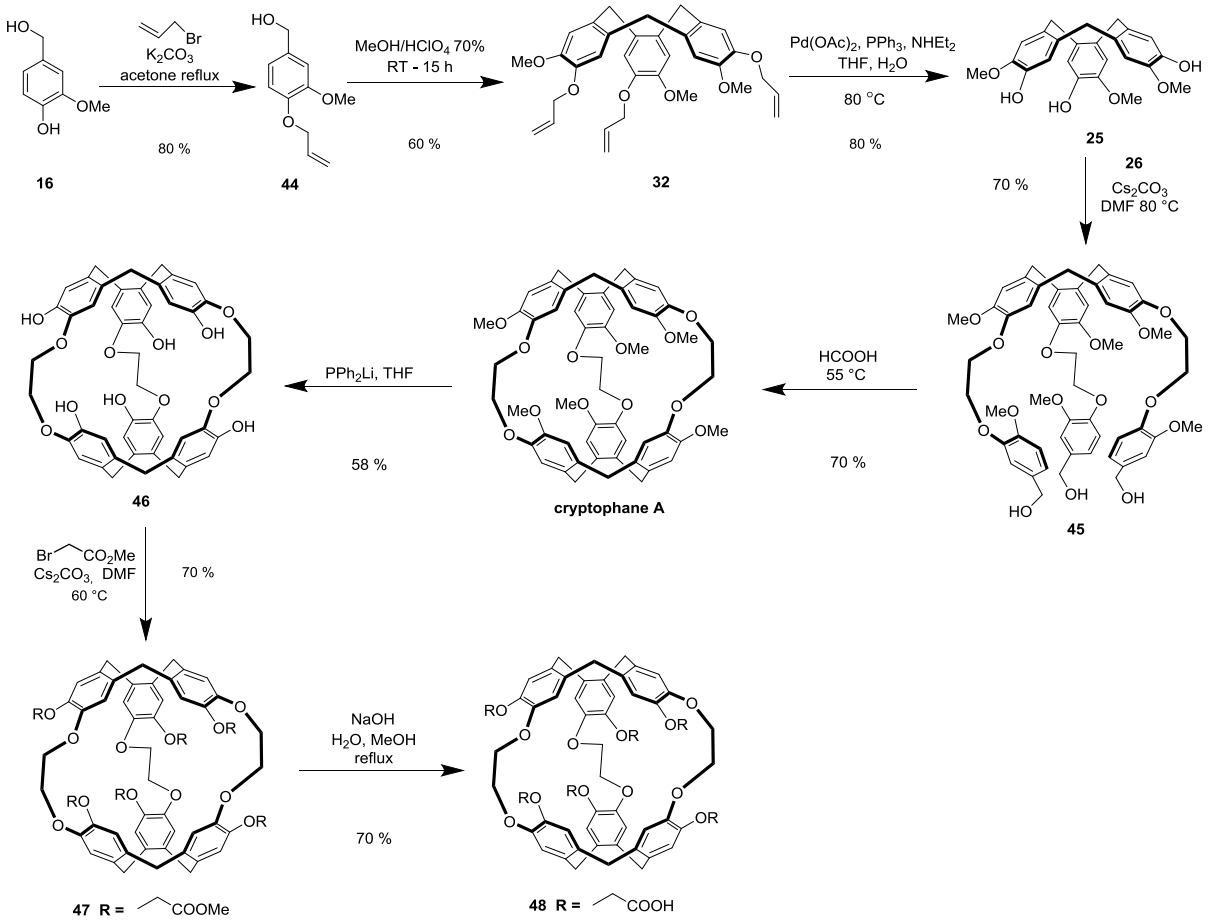

Figure 55: Synthesis of the cryptophane[222] *hexa*-acid carboxylic **48**

However, though this cryptophane has enabled recent advances in the development of bioprobes for ^{129}Xe NMR, it displays several drawbacks. First of all, its solubility in water (only when pH is lower than 5) is relatively low. Secondly, its synthesis is rather long and difficult. Moreover, the presence of six identical possible active positions for desymmetrization undoubtedly leads to a very poor yield when reacting with the linker with a maximum of 13 % after optimization (Figure 56). It should be mentioned that cryptophane **48** and the linker carrying a fluorescein moiety are both high value-added and thus expensive products which are only available in limited amounts.

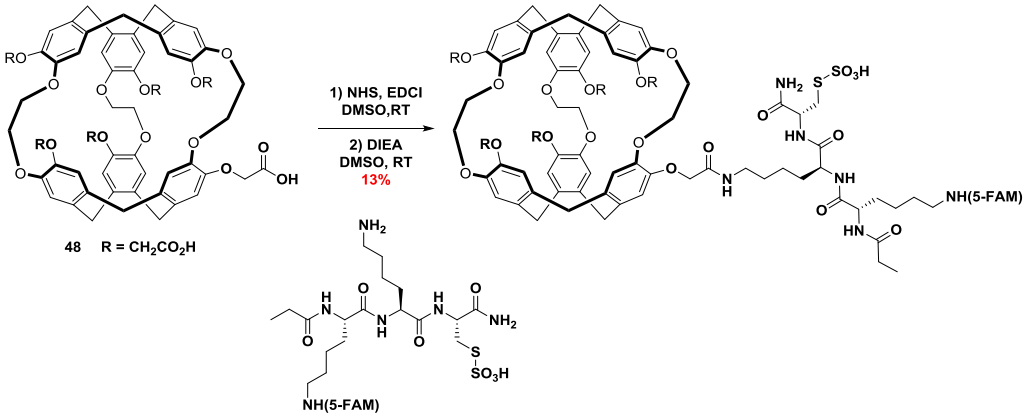

Figure 56: The step of *mono*-functionalization of cryptophane in the synthesis of the biosensor

In this context, it is necessary to develop a straightforward synthetic route leading to a water-soluble and mono-functionalizable cryptophane in good yield with the minimum waste of highly elaborated material.

In fact, this problem can be summarized by two interconnected issues: 1) how to break the symmetry of the system to make the cage mono-functionalizable and 2) how to efficiently solubilize the cryptophane moiety. In this thesis, different strategies to break the symmetry of cryptophane will be discussed in the latter parts. Regarding the problem of water-solubility, we focused our interest on the polyethylene glycol groups (PEG) which has been often used to augment the solubility of hydrophobic molecules in water.

2. Different strategies to synthesize asymmetric cryptophanes

The discussion of the strategy is based on the "template method" for synthesizing a cryptophane[222]. Cryptophane[222] is chosen because of 1) its good affinity and selectivity for xenon, 2) suitable exchange rates which are compatible with NMR experiments. Most of already reported cryptophane-based biosensors are built from a cryptophane[222] motif, including the previous PEGylated cage developed by our group.[87]

As the most widely-used method for synthesizing cryptophanes, the "template method" is selected thanks to its good yields and more noticeably, to the possibility of synthesizing cryptophanes with various symmetries. Compared with the "direct method" and the "coupling

of CTVs", it is clearly obvious that the "template method" offers much more possibilities to break the symmetry of the system (Figure 57).

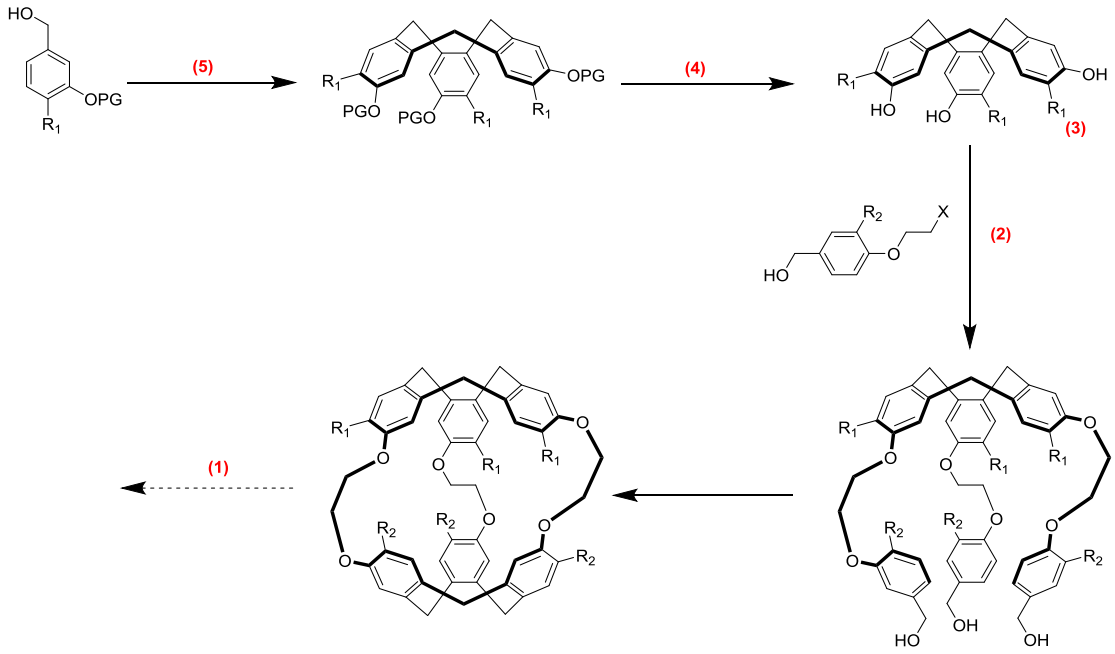

Figure 57: General pathway to synthesize a cryptophane[222] using the "template method" with the possible points to break its symmetry

In our point of view, there are five possible ways to break the symmetry of cryptophane:

(6) Desymmetrization (deprotection) of a symmetric cryptophane (part B-II).

(7) Functionalization of CTVs with different benzyl alcohol derivatives (part B-III-1).

(8) Mono-functionalization (e.g. mono-halogenation) of CTVs (part B-III-2).

(9) Selective hydrolysis of protected CTVs (part B-III-3).

(10) Cyclotrimerisation with different benzyl alcohol derivatives to form asymmetric CTVs (part B-IV).

3. Polyethylene glycol – our choice for hydrosolubilization

The PEG group was chosen to be used as the water-soluble group for several reasons[87]:

1) The alternance of hydrophilic and hydrophobic groups on the PEG confers a very good solubility in both organic milieu and aqueous milieu, which facilitates not only the hydrosolubilty of the biosensor *in vivo*, but also the dissolution in organic solvents and enables a large variety of treatments during the different steps of the synthesis.

2) It is inert to many chemical reactions such as oxidation, reduction, acids and bases.

3) It is stable at high temperature.

4) It is biocompatible and used in many pharmaceutical and biomedical applications.[113, 114]

We have chosen the methoxy-polyethylene glycol 550 (mPEG 550), a polydisperse PEG with the average molar mass of 550, which is made of the concatenation of about eleven ethylene glycol units. This PEG is long enough to solubilize the cryptophane and not too long to cause a steric hindrance jeopardizing the subsequent functionalization and encapsulation. According to the previous work done by our lab, the cryptophanes with three or six units of PEG moieties have satisfactory water-solubility (50 mg/mL) and possess very good abilities to encapsulate xenon gas (Figure 58).[87]

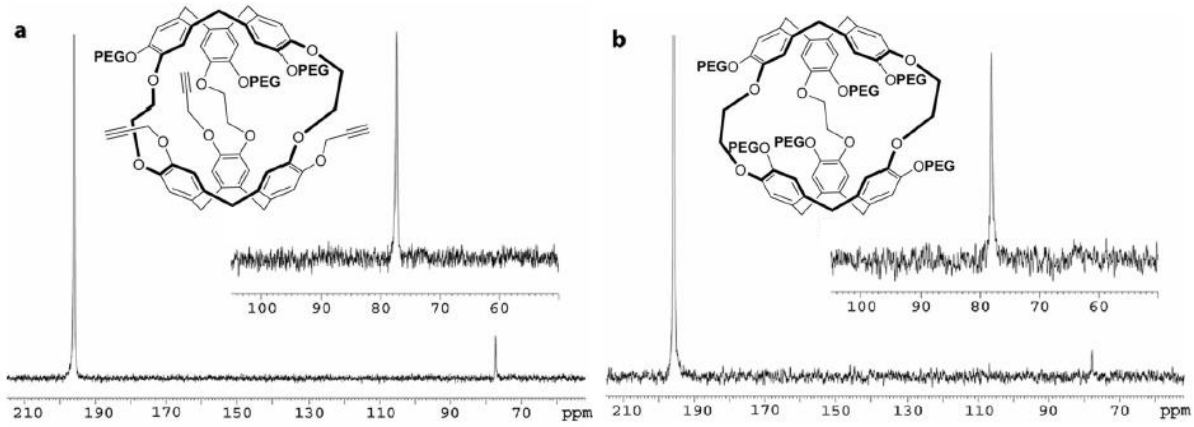

Figure 58: ^{129}Xe NMR spectrum of a) *tri*-PEGylated cryptophane. b) *hexa*-PEGylated cryptophane

Before being engaged in the synthesis, the mPEG 550 was firstly activated by 4-toluenesulfonyl chloride. Tosylate **17** was obtained quantitatively without necessity to be purified by chromatography (Figure 59).

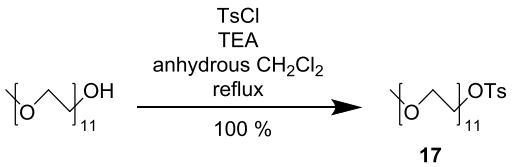

Figure 59: Activation of mPEG-550

II. Desymmetrization of Cryptophanes

The desymmetrisztion of a symmetric cryptophane was the more obvious and thus the first option attempted during my Ph.D. work. It does not require a complete revision of the synthetic pathways and only necessitates the addition of a selective desymmetrization step (Figure 60).

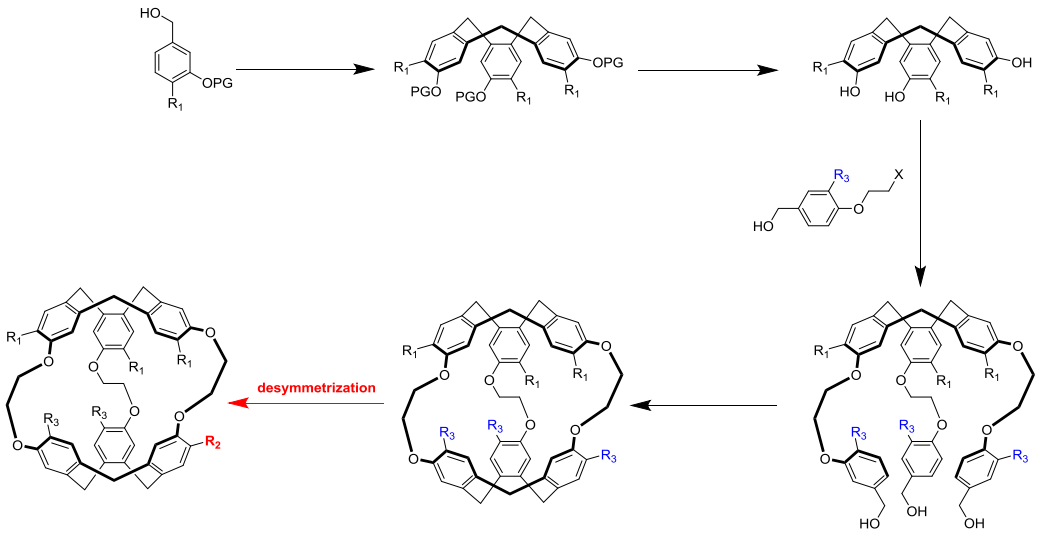

Figure 60: General description of the strategy "desymmetrization of a symmetric cryptophane". In this figure, R_2 represents the functionalizable group, R_3 represents the solubilizing group

1. Context

In 2013, Delacour et al. reported the synthesis of a general cryptophane platform which can be used to construct biosensors. By using a new strategy which introduces the PEG groups at the first step (Figure 61), the synthesis and purification steps are facilitated thanks to the improvement in the solubility of the intermediates. Moreover the synthesis is shortened by avoiding successive protection and deprotection of the vanillyl alcohol. The symmetric PEGylated cryptophanes are thus obtained, with three chains of PEG, three –OR substituent groups where R can be either methyl group (cryptophane **23**) or propargyl (cryptophane **24**). Cryptophane **24** was expected to be easily functionalized by click chemistry for a large diversity of applications. Cryptophane **23** is more especially interesting for selective mono-demethylation. Both cryptophanes possess the advantages of high water-solubility (50 mg/mL

at all relevant physiological pH), non-toxicity at concentrations used for Xe NMR, as well as a good encapsulation of xenon.

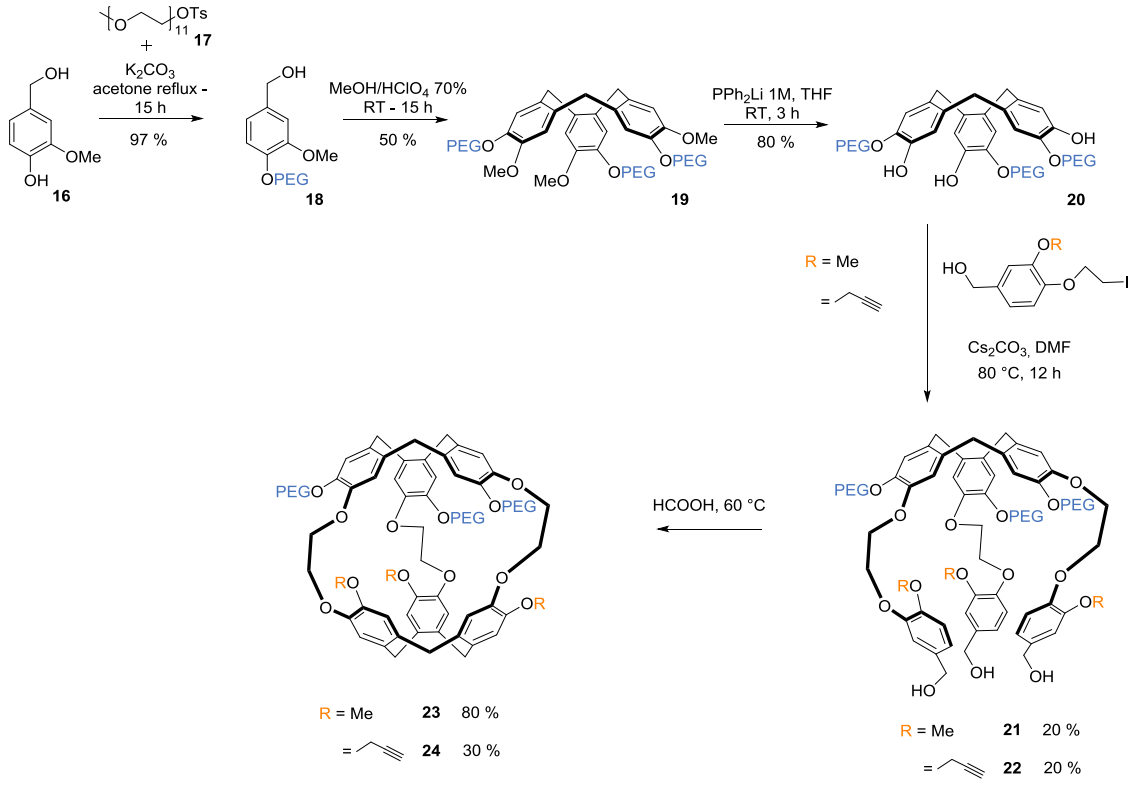

Figure 61: Synthesis of the PEGylated cryptophanes by L. Delacour

Although it is already a well-developed synthesis, several points remain to be optimized.

First of all, the total yields (6 % for the cryptophane **23** and 2 % for the cryptophane **24**) are limited, mainly due to the poor yield (20 %) obtained for the functionalization step of CTV **20**.

Secondly, the scale of this synthesis is limited to dozens of milligrams. These quantities are still far away from the need for the synthesis of reasonable amounts of biosensors (at least a dozen of miligrams of final compound for triplicate *in vitro* and *in vivo* experiments).

To date, mono-functionalization of the compounds **23** and **24** has not been achieved. The tri-propargyl cryptophane **24** leads to statistical mixtures after mono-functionalization and the presence of three PEG moieties is likely to make the purification even more difficult.

As reported for cryptophane **23**, Delacour et al. have tried to carry out a total demethylation in order to make the cryptophane functionalizable. According to the LC-MS analysis of the crude product, the formation of the targeted cryptophane **49** was observed,

together with partially demethylated cryptophanes **50** and **51,** even when a large excess of PPh_2Li was used (Figure 62). From her point of view, the small scale of this reaction made it difficult to secure a fine anhydrous environment which is necessary when the water-sensitive reagent PPh_2Li was employed.

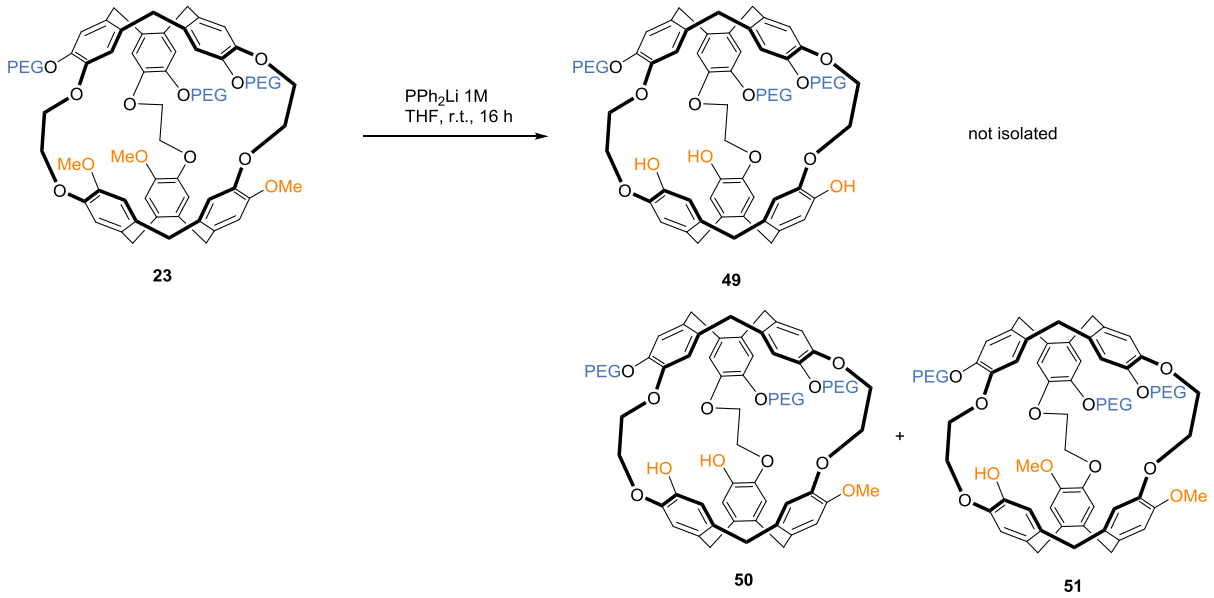

Figure 62: Attempts of Delacour to achieve the demethylation of the PEGylated cryptophane[87]

Although the total demethylation seems to be difficult, the presence of the mono-demethylated cryptophane **51** has demonstrated the validity of this approach.

Therefore our research plan was:

1) An optimization of the synthesis of cryptophane **23**, especially a yield improvement for the functionalization step of CTV **20**. Different reagents and reaction conditions will be tested to avoid the β-elimination of the leaving group X leading to the decrease of yield.
2) The scale-up of the synthesis for obtaining at least several hundred milligrams of cryptophane which can be used to synthesize biosensors.
3) To perform the desymmetrization, in particular a mono-demethylation of cryptophane **23** in order to obtain the water-soluble mono-functionalized cryptophane **51**.

2. Optimization and scale-up

As shown in Figure 57, the first step does not necessitate to be optimized since the PEGylated vanillyl alcohol **18** is obtained at the 10 g scale in 97% yield.

a. Optimization of the cyclotrimerization and the demethylation

The conditions of the first cyclotrimerization step and the subsequent demethylation are also well-optimized. Cyclotrimerization was performed in the classical conditions (perchloric acid/methanol 1:2). The crude product was purified by reversed-phase chromatography to give the PEGylated CTV **19** in 50 % yields. Demethylation of **19** was done using a freshly prepared solution of $LiPPh_2$ and was purified by silica gel chromatography in 80 % yield.

For these two steps, the necessity to purify the product by silica-gel chromatography was a strong limitation in terms of yields and quantities. Therefore, we plan to skip the purification step after the cyclotrimerization reaction and to purify the product at the end of the demethylation step. Successive liquid-liquid extraction was also proposed as an alternative to chromatography.

Thus, after cyclotrimerization, 4 g of obtained crude product was directly engaged in the next step.

After the demethylation, tests of solubility were carried out with the crude product and different deuterated solvents in order to find the best solution for product purification (Table 4). In most cases, a homogeneous solution was obtained, suggesting that the expected product and the impurity were both very soluble in these solvents. Conversely, none of them was soluble in cyclohexane. The best result was obtained with toluene, in which the impurity is more soluble than the targeted CTV **20**.

Solvent	Chloroform	MeOD	Acetone	Benzene	Acetonitrile
Result	Homogeneous solution	Homogeneous solution	Homogeneous solution	Homogeneous solution	Homogeneous solution

Solvent	DMF	Cyclohexane	Toluene	1,4-dioxane	D_2O
Result	Homogeneous solution	Not soluble	Partly soluble	Homogeneous solution	Homogeneous solution

Table 4: Result of the test of solubility

The crude product was solubilized in water and washed several times with toluene until the elimination of the impurity from the organic phase. Then the aqueous solution was extracted with dichloromethane, affording 3 g of very pure CTV **20**. This improvement enabled to increase the scale of purification by 15 times, leading to an optimization of the yield (2 steps) from 40 % to 85 %.

b. Optimization of the alkylation of CTV

As discussed previously, the alkylation of CTV **20** is a key problem which negatively affects yields putatively due to:

1) The chelation of Cs^+ by the PEG oxy groups forming bulky chelate which might sterically hinder the alkylation of CTV. Different bases (like NaH) will be tested to solve this problem.

2) The *β*-elimination of the benzyl alcohol derivatives during the CTV grafting (Figure 63), which was already observed by LC-MS analysis of the crude product.[87] Different quantities of benzyl alcohol derivatives with different leaving groups were tested.

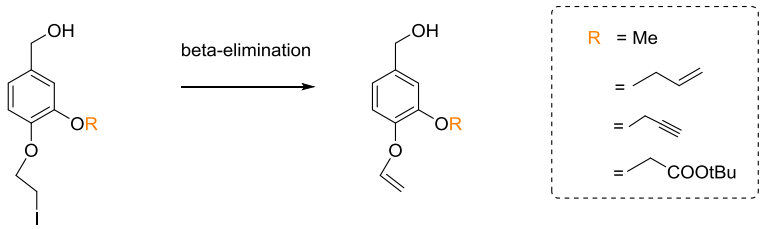

Figure 63: *β*-elimination of the benzyl alcohol derivatives

The synthesis of benzyl alcohol derivatives with different leaving groups depicted in Figure 64 was achieved as follows: starting from the vanillyl alcohol **16**, the derivative **39** was obtained in a single step in 60% yield, while the corresponding iodide (molecule **26**), tosylate (molecule **52**) and mesylate (molecule **53**) were obtained in two steps in respectively 59 %, 47 % and 40 % yields.

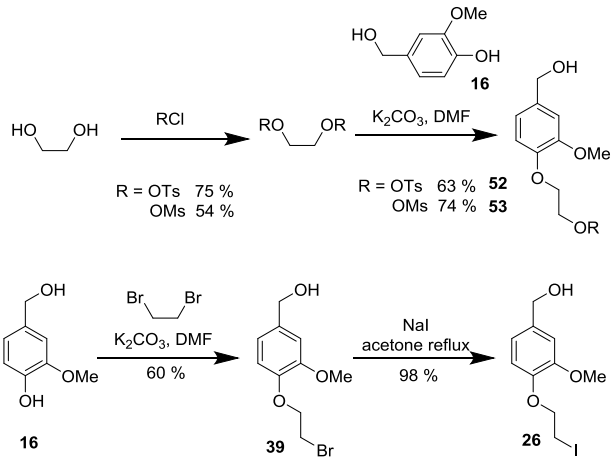

Figure 64: Synthesis of the benzyl alcohol derivative with different leaving groups

In the synthesis reported by Delacour et al., CTV **20** was heated overnight at 70 °C with 9 equivalents of derivative **26** and 6 equivalents of cesium carbonate in anhydrous DMF to yield 20 % of **21**. In order to optimize the reaction, different factors were tuned such as the quantity of benzyl alcohol derivative **54** and the nature of the leaving group and base (Figure 65).

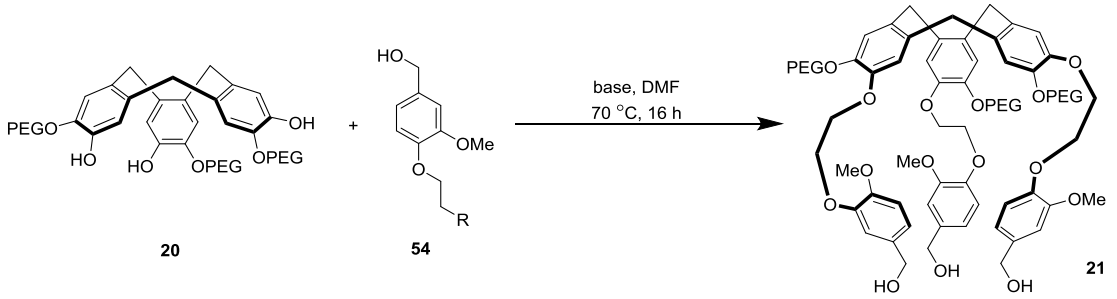

Figure 65: General image of the alkylation reaction of CTV

Firstly, we tested the reactions with –OTs as the leaving groups, Cs_2CO_3 as the base, and various quantities of the benzyl alcohol derivative **54** (Table 5).

	R	Base	Eq. of **54**	Eq. of base	Yield
1	-OTs	Cs_2CO_3	9	6	7 %
2	-OTs	Cs_2CO_3	4	6	28 %

Table 5: The influence of equivalent of benzyl alcohol on the reaction

As shown in Table 5, the less benzyl alcohol is used, the better yield is. This is probably caused by the side-reaction between the excess of **54** and targeted product **21** (Figure 66). With 4 equivalents of **52**, the obtained yield (28 %) was already improved relative to the original yield (20 %).

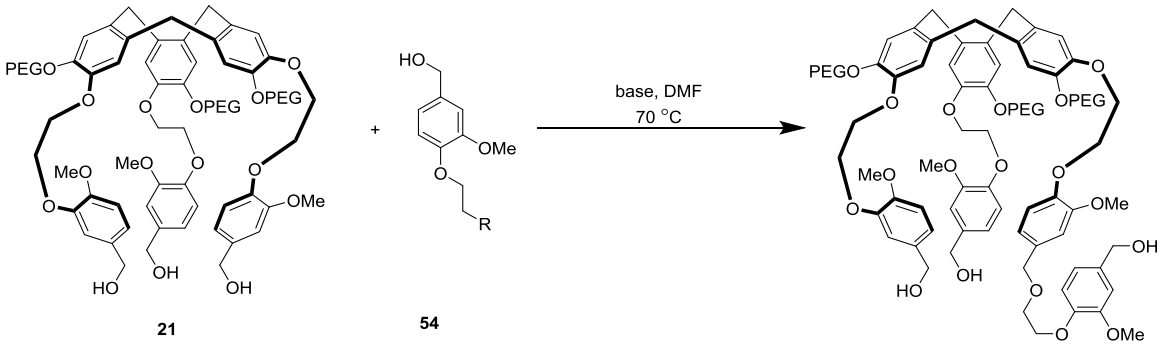

Figure 66: Possible side-reaction during the functionalization of CTV **20**

It should be noticed that the products in entry 1 and 2 were actually purified by reversed-phase chromatography and the real yields were calculated whereas in other cases, yields were evaluated according to the HPLC chromatogram using yields in entries 1 and 2 as the references.

	R	Base	Eq. of **54**	Eq. of base	yield
2	-OTs	Cs_2CO_3	4	6	28 %
3	-OMs	Cs_2CO_3	4	6	trace
4	-Br	Cs_2CO_3	4	6	36 %

Table 6: The influence of the leaving group on the reaction

For results reported in table 6, the quantity of benzyl alcohol derivative was fixed to 4 equivalents, while using Cs_2CO_3 as the base, and different leaving groups were tested. The best result was obtained with the benzyl bromide **39** (36 % yield, entry 4).

	R	Base	Eq. of **54**	Eq. of base	yield
4	-Br	Cs_2CO_3	4	6	36 %
5	-Br	K_2CO_3	4	6	22 %
6	-Br	NaH (60%)	9	3,5	24 %
7	-Br	NaH (95%)	9	3,5	31 %
8	-Br	NaH (95%)	5	3,5	57 %
9	-Br	NaH (95%)	4	3,5	33 %

Table 7: Influence of the base on the reaction yield

Results reported in table 7 highlight the influence of different bases on the reaction. It should be mentioned that the quantity of sodium hydride must be minimized (3.5 equivalents) because it can also react with the alcohol group of compound **39**. The purity of the sodium hydride suspension (60 % or 95 %) and the quantity of compound **39** were also important factors: the best result was obtained with NaH (95%) as the base and 5 equivalents of **39** (57 % yield, entry 8).

This product was purified by reversed-phase chromatography (water / acetonitrile = 100 : 0 → 0 : 100) because the CTV triol **21** is highly polar.

Therefore CTV **20** was functionalized with 5 equivalents of **39** in the presence of 3.5 equivalents of NaH 95 % as the base, to yield 200 mg of functionalized CTV **21** (yield 58 %).

Although all the factors in the condition of this reaction were investigated, the optimization was difficult due to limitations in our attempts for scaling up the reaction. In order to improve the efficiency of the purification in this step, the free alcohol group of derivative **39** was protected by tetrahydropyran group (THP). Thus, the corresponding functionalized CTV **55** was anticipated to be less polar and was expected to be purified by normal phase chromatography (Figure 67). In fact the THP motif was chosen among all the alcohol protecting groups because it can be easily cleaved concomitantly to cyclotrimerization in acidic conditions.

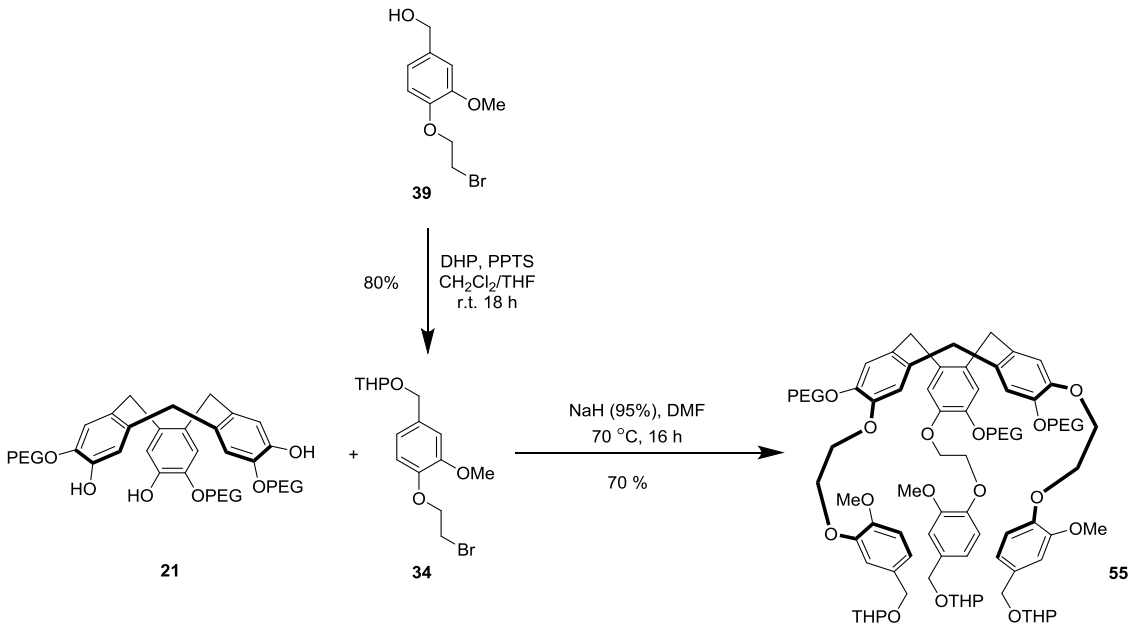

Figure 67: Alkylation of CTV with THP-protected benzyl alcohol

The protection of the alcohol group of compound **39** with THP was easily achieved in standard conditions. After several liquid/liquid extractions, the obtained product was already pure enough to be engaged in the next step without any additional purification. Several grams of **34** were isolated (yield 80 %).

The following functionalization of CTV **21** with protected benzyl alcohol derivative **34** was achieved in pretty good yield (70 %). As expected, the functionalized CTV **55** was

purified by normal-phase chromatography. Moreover, thanks to the protection of the benzyl alcohol, NaH could be used in excess. It should also be mentioned that this alkylation of CTV **21** was scaled up to 500 mg without decreasing the yield.

As previously mentioned, the THP groups were removed concomitantly to the cyclotrimerization step (Figure 68). Since a low concentration (about 1 mg/mL) of reaction milieu is necessary to promote the preferential intramolecular cyclization rather than intermolecular reactions, the scale-up of this step was limited by the size of available flasks. Even though, more than 500 mg PEGylated cryptophane **23** could be obtained in 80 % yield.

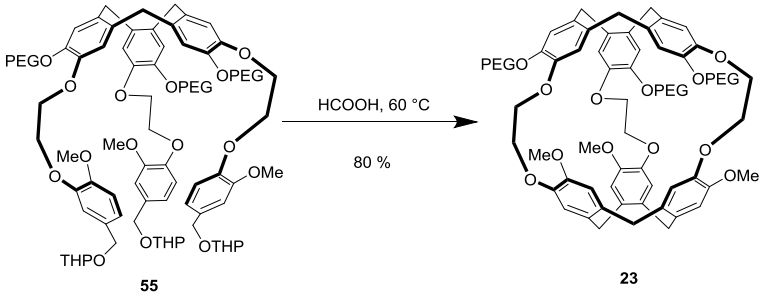

Figure 68: Cyclotrimerization of the THP-protected cryptophane precursor **55**

c. *Conclusion of the optimization and scale-up*

The total yield of the synthesis of PEGylated cryptophane **23** was improved from 5 % to 43 %, and the scale of the synthesis was raised from dozens of milligrams to several hundreds of milligrams.

3. Demethylation of symmetric cryptophane

After completing the synthesis of the symmetric PEGylated cryptophane **23**, the next challenge was the mono-demethylation step necessary for cryptophane desymmetrization (Figure 69).

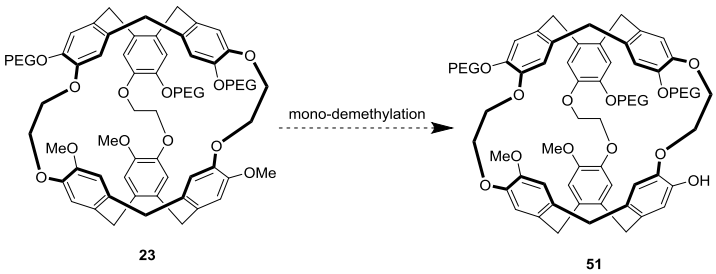

Figure 69: Mono-demethylation of the cryptophane **23**

In the literature, two methods for demethylation of cryptophanes have been reported. The use of a lithium diphenylphosphide (PPh_2Li) solution was firstly reported for the synthesis of cryptophane[222] *hexa*-carboxylic acid.[63] In order to secure the efficient demethylation, this PPh_2Li solution should be freshly prepared each time from lithium and cholorodiphenylphospine in a strictly anhydrous and anoxic environment and thus requires the use of a glove box (Figure 70).

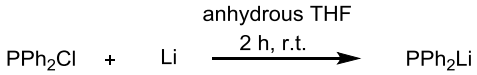

Figure 70: Synthesis of the PPh_2Li solution

This method, most widely used in demethylation of cryptophanes, has been proven to be efficient with the demethylation of PEGylated CTV **19** but has also several drawbacks:

(1) It is difficult to control the quality of the PPh_2Li solution and therefore arduous to precisely control the quantity of PPh_2Li in the demethylation reaction. This problem did not impact the demethylation of CTV **19** because a large excess of PPh_2Li was needed to cleave all the three methyl groups. Conversely, an inaccurate quantity of PPh_2Li was anticipated to jeopardize the reproducibility of the mono-demethylation step.

(2) Water potentially bound to PEG ethoxy chains through H bonding might unproductively hydrolyze PPh_2Li.

(3) As mentioned before, the diphenylphospine and diphenylphospine oxide generated in this reaction are very difficult to eliminate since they are soluble both in water and organic solvents, and thus contaminate all the fractions during the purification.

(4) On the safety point of view, the use of lithium is clearly not the perfect choice. It is difficult to manipulate due to its sensitivity for water and oxygen with an associated hazard related to explosion and inflammation.

The other demethylation procedure was achieved with trimethylsilyl iodide (TMSI), which was previously used in the synthesis of cryptophanol.[94] Compared with the above-mentioned method using $LiPPh_2$, this method has several advantages in particular a simpler manipulation, treatment and purification. Moreover, TMSI is a commercially available product which is relatively stable and can be directly engaged without a bias regarding the exact quantity necessary to perform mono-demethylation.

However, the demethylation of non-aromatic methoxy groups with TMSI has been reported,[115, 116] suggesting that the chemoselectivity might be insufficient for securing a mono-deprotection of the aromatic methoxy group (Figure 71). In contrast to the demethylation of cryptophane A in which the six methoxy groups are identical, the presence of methoxy groups at the end of the PEG chains in cryptophane **23** might lead to a mixture of two similar PEGylated cryptophanes which are presumably difficult to separate.

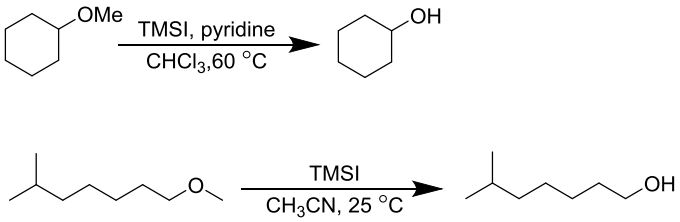

Figure 71: Examples of using TMSI in the dealkylation of aliphatic alkyl ethers[107, 108]

Anticipating a sufficient stability of the PEG chains, we decided to use TMSI in order to precisely control the quantity of reagent.

a. Demethylation of the PEGylated cryptophane with TMSI

Cryptophane **23** was demethylated with 1.1 equivalents of iodotrimethylsilane (Figure 72). Analysis of the crude product by LC-MS revealed that the product with a mass corresponding to cryptophane **51** was present in small quantity together with the starting cryptophane **23** which was still predominant. It should be noticed that the quantification of different products was difficult due to the polydispersity of the PEG and the predominance of the polarity of PEG moieties.

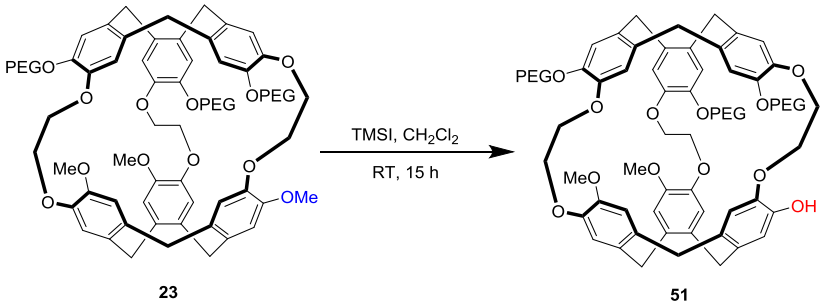

23 51

Figure 72: Mono-demethylation of PEGylated cryptophane **23** with TMSI

A particular effort was done to determine the quantity of TMSI necessary for selective mono-demethylation of product **51** starting form cryptophane **23**, while minimizing the formation of the undesired di-demethylated product **50** (Figure 73). This strategy was chosen

because the starting material **23** could be recycled for a new run of deprotection whereas the di-demethylated product **50** is useless. The result of this optimization is shown in the Table 8.

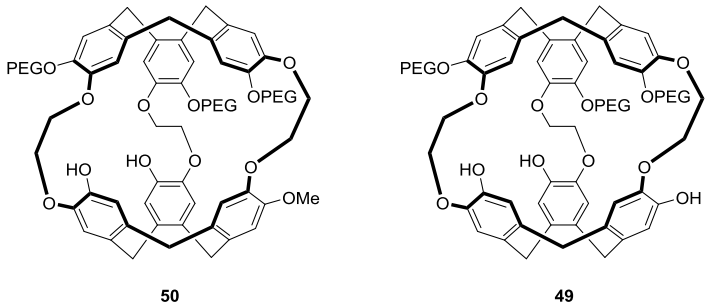

Figure 73: Structures of di-demethylated cryptophane **50** and tri-demethylated cryptophane **49**

	SM **23**	Mono **51**	Di **50**	Tri **49**	Tetra and more
1.1 eq.	++	+	-	-	-
1.5 eq.	++	+	-	-	-
2 eq.	++	+	+	-	-
3 eq.	++	++	+	+	-
6 eq.	+	++	++	+	+
12 eq.	-	-	-	-	+

Table 8: Optimization of the quantity of TMSI. In this table, "-" means no formation of this product; "+" means observation of the formation of this product; "++" means it is the major product of this reaction.

The formation of di-demethylated product **50** was detected when using at least 2 equivalents of TMSI. For 3 equivalents of TMSI and more, the quantity of **51** was almost equal to that of **23** with an unneglectable proportion of tri-demethylated product **49**. At 6 equivalents of TMSI, the mass of a tetra-demethylated product was detected by LC-MS analysis. This strongly suggests that at least one of the methoxy groups at the end of the PEG chains was cleaved. At 12 equivalents of TMSI, all the six methoxy groups (3 on the aromatic ring, 3 at the end of the PEG chain) were removed, as shown by the NMR spectrum of the crude product.

As one might dread, TMSI not only reacts with the methoxy groups on the aromatic rings but also with the ones at the end of PEG chains. Anticipating that the methoxy groups on the aromatic rings are more active than the PEG methoxy termini, the maximum quantity of TMSI was kept to 1.5 equivalents to favor the formation of product **51** without generating a mixture which was too complicated to purify.

Anyway, with 1.5 equivalents of TMSI, a mixture of starting cryptophane **23** and targeting crypotphane **51** was obtained. As mentioned before, these two products were very close in polarity but could be efficiently separated by HPLC in standard conditions. Surprisingly, two different adjacent fractions with the same mass corresponding to the targeted product **51** were obtained. Considering that demethylation of the methoxy groups at the end of the PEG chains can occur, the formation of mono-demethylated cryptophane **56** as the by product was anticipated (Figure 74).

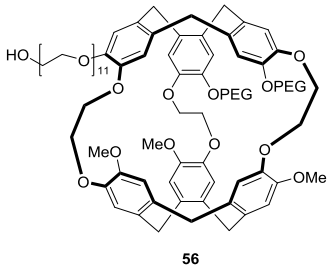

56

Figure 74: Possible by-product **56** in the demethylation with TMSI

Attempts were made to identify the components of these two fractions. The first one was the iron(III) chloride - pyridine test, which was designed to detect a phenol in a unknown sample (Figure 75). We observed the presence of phenol groups (possibly coming from the cryptophane **51**) in both of these two fractions.

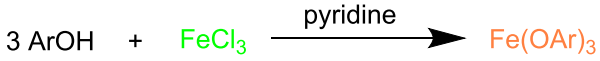

Figure 75: Iron(III) chloride - pyridine test for water-Insoluble phenols

In order to conclude about the formation of compound **51**, we treated the isolated product with MeI, considering that Cs_2CO_3 is not strong enough to deprotonate the alcohol group at the end of the deprotected PEG chains but should abstract the proton of the phenol group. Consequently only the cryptophane **51** was expected to lead to compound **23** (Figure 76).

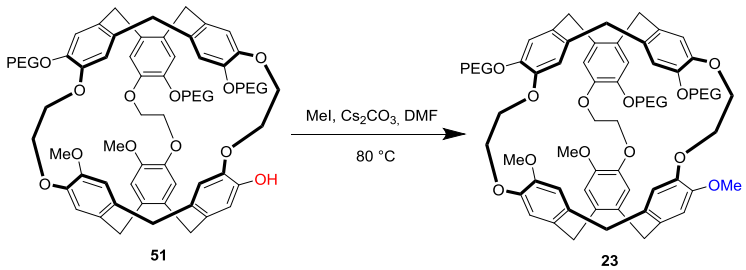

51 **23**

Figure 76: Methylation of the cryptophane **51**

Compound **51** was treated with a large excess of Cs_2CO_3 and MeI at 80 °C for three days in order to ensure a total methylation. LC-MS analysis of the crude product showed both the presence of cryptophane **23** and cryptophane **56** in each of these two fractions suggesting the cryptophane **51** and the cryptophane **56** exist simultaneously in both of these two adjacent fractions.

Molecules like PEGylated cryptophanes are not prone to be ionized easily in relatively soft conditions used for electrospray MS due to its lack of ionizable chemical groups. To solve this problem, MALDI-TOF analysis was performed and revealed the presence of the mass of cryptophanes **51**/**56.** Surprisingly, a mass corresponding to cryptophane **57** was also observed (Figure 77).

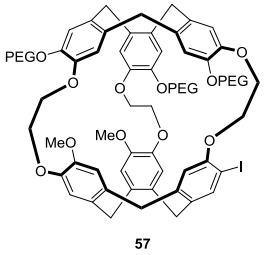

57

Figure 77: Possible by-product cryptophane **57** in the demethylation with TMSI.

This unexpected iodination can be explained by the particular mechanism of the demethylation reaction with TMSI (Figure 78). As a matter of fact, TMSI can cleave the C-O bond at both the two sides of the oxygen. Although cleavage of the methyl is preferential, the competitive formation of iodide by-products like cryptophane **57** has been already reported.[116]

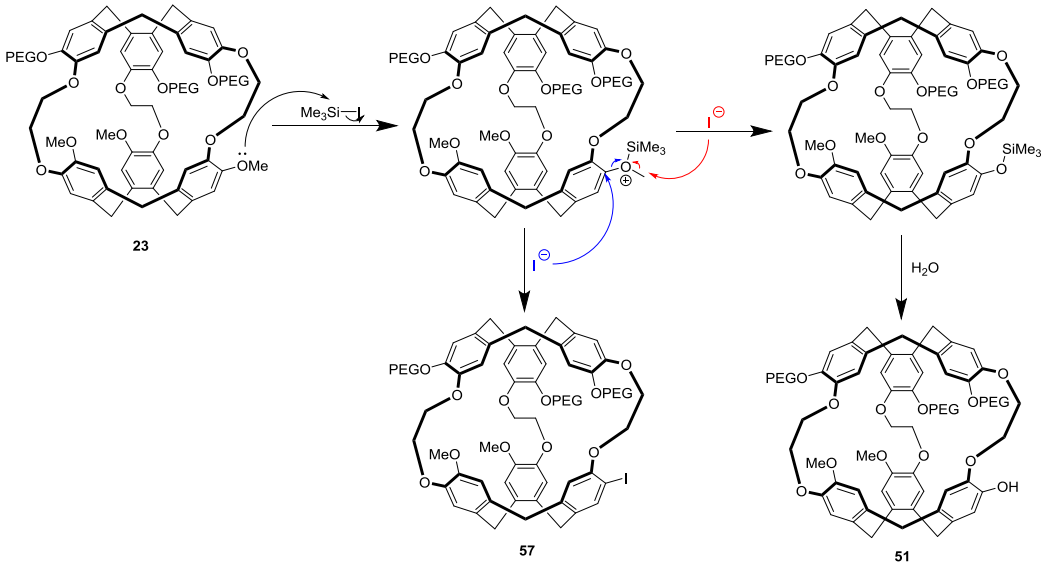

23 57 51

Figure 78: Mechanism of the formation of by-product **57**

Despite the interest of TMSI for deprotecting a single aryl methoxy group selectively, we observed that the fractions recovered are in fact a mixture of three cryptophanes **51**, **56**, **57**. As the long PEG chains predominantly determine the polarity of these molecules, it is difficult to separate them, even by HPLC. Consequently we turned back to the classical condition with $LiPPh_2$ which does not affect the methoxy group at the end of the PEG chains during demethylation of CTV **19**.

b. Demethylation of the PEGylated cryptophane by $LiPPh_2$

As mentioned before, it's difficult to ensure the quality of $LiPPh_2$ and thus to control an accurate quantity of $LiPPh_2$ necessary for a selective mono-demethylation. Therefore we needed to determine the precise concentration of the freshly-prepared $LiPPh_2$ solution using a titration test. After several attempts, the procedure using butanol and a solution of 1,10-phenanthroline in xylenes as the indicator revealed to be the most reliable.[117]

Optimization of the demethylation of compound **23** with $LiPPh_2$ was tricky. Progressive increase in $LiPPh_2$ from 1.1 equivalents to 6 equivalents had only a little effect, resulting in a mixture of cryoptophane **51** and majoritary **23**. This situation hardly changed with 30 equivalents of $LiPPh_2$ after 48 h. On the contrary, if we directly added 12 equivalents of $LiPPh_2$ at the beginning of the reaction, the mono-demethylated cryptophane **51** was already the major product after 3 hours, together with starting material **23** as well as a little amount of cryptophane **50** (Figure 79). The possible explanation for this phenomenon is that the formed $MePPh_2$ and its oxide may hinder the further reaction when we re-added the $LiPPh_2$ solution.

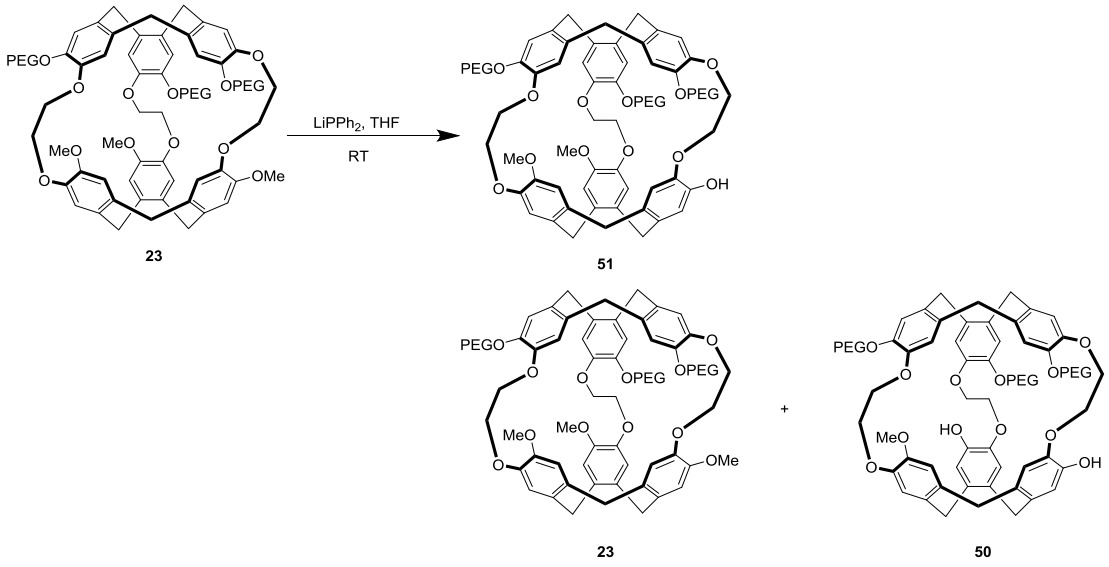

Figure 79: Mono-demethylation of PEGylated cryptophane with $LiPPh_2$

The same extraction method (water/toluene) previously used to eliminate the diphenylphospine and diphenylphosphine oxide formed during the demethylation of CTV **19** was also attempted for the treatment of the reaction. However, in the same condition, it was no longer possible to separate the phosphines from the desired compounds, probably due to the higher solubility of PEGylated cryptophanes **23**, **50**, **51** in toluene relative to the PEGylated CTV **19**.

After several other attempts, it was found that these phosphines can be eliminated by filtrating the product over a silica gel column with acetone/DMF = 50/50 as the solvent without separating cryptophanes **23**, **50**, **51**. The purification of these three cryptophanes by HPLC is still under investigation.

c. Scan of other reagents to perform the demethylation of cryptophane

As mentioned before, the other reagents were tested simultaneously in order to achieve the demethylation of cryptophane **23**.

In the literature, the most widely-used reagent for demethylation is boron tribromide.[118] However in our case, BBr_3 is clearly too reactive since it is expected to cleave not only the C-O bonds of the aryl methoxy groups, but also those located in the alkyldioxy bridges. The same problem can be observed with HBr and NaI, which has been proven to be an efficient method for the removal of methyl groups from aryl methyl ether in amino acids.[119]

Recently, the 1-decanethiol ($Et_2NCH_2CH_2SH.HCl$) has been shown to efficiently mono-deprotect an aryl methyl ether group when used simultaneously with of a base like NaO*t*Bu.[120] Unfortunately, this milder reagent seems to be not efficient enough to carry out the demethylation of cryptophane **23**. Even with a large excess of the reagents, the only product recovered was the starting material. A similar lack of reactivity was also observed with PhSH-(Catalytic) KF in *N*-Methyl-2-pyrrolidone (NMP), which has been reported as an efficient method for selective cleavage of aryl alkyl ethers under non-hydrolytic and neutral conditions.[121] We have also tried to realize the demethylation with magnesium iodide (MgI_2) in ionic liquid like [bmim]BF_4.[122] Once again, the starting material **23** was recovered after the reaction without trace of deprotected products.

Finally $LiPPh_2$ seems to give the best result for mono-deprotecting a methyloxy motif selectively despite several major drawbacks.

4. Conclusion and perspective

As the first attempted strategy to achieve the synthesis of a PEGylated mono-functionalizable cryptophane, this “desymmetrization of cryptophane” approach is based-on a two-step procedure including the synthesis of a symmetric PEGylated cryptophane, and the mono-deprotection of a single methoxy aryl group in order to break the symmetry.

The first step was achieved and optimized leading to the production of about 500 mg of the PEGylated symmetric cryptophane **23** synthesized in five steps with an overall yield of 43 %.

Desymmetrization of the cryptophane through mono-demethylation was attempted using several different methods. The best result was obtained with a solution of $LiPPh_2$, which generated a mixture of the targeted water-soluble mono-functionalized cryptophane **51** as majoritary product which was recovered along with two cryptophanes **23** and **50**. These last two cryptophanes are difficult to separate at the preparative scale by silica gel flash-chromatography but could be eliminated by HPLC. As underlined previously, the separation of different PEGylated cryptophanes is very difficult due to the predominant effect of the long PEG chains on the polarity of these molecules. To achieve an efficient synthesis which can meet the demand for large quantities of products in order to construct biosensors, the introduction of the PEG group might be done after the desymmetrization of the system. This approach was developed in the following strategies.

III. Desymmetrization of CTVs

In this chapter, we will describe the synthesis of a symmetric non-PEGylated CTV which will be used as a template for the step-by-step construction of a desymmetrized cryptophane with PEGylated moieties. These motifs will be introduced lately in order to avoid recurrent problems during purifications for separating structurally similar products. We anticipated that the introduction of only two PEG units should be sufficient to ensure the hydrosolubility of the final molecule.

Three different strategies to break the symmetry of CTV have been envisioned:

1) The functionalization of CTVs firstly with benzyl alcohol derivative linkers of series A and then with series B (Figure 80)

2) The mono-halogenation of CTVs (Part III-2)

3) The selective deprotection of protected CTVs (Part III-3).

1. Cryptophanes based on the functionalization of CTVs with different benzyl alcohol derivatives

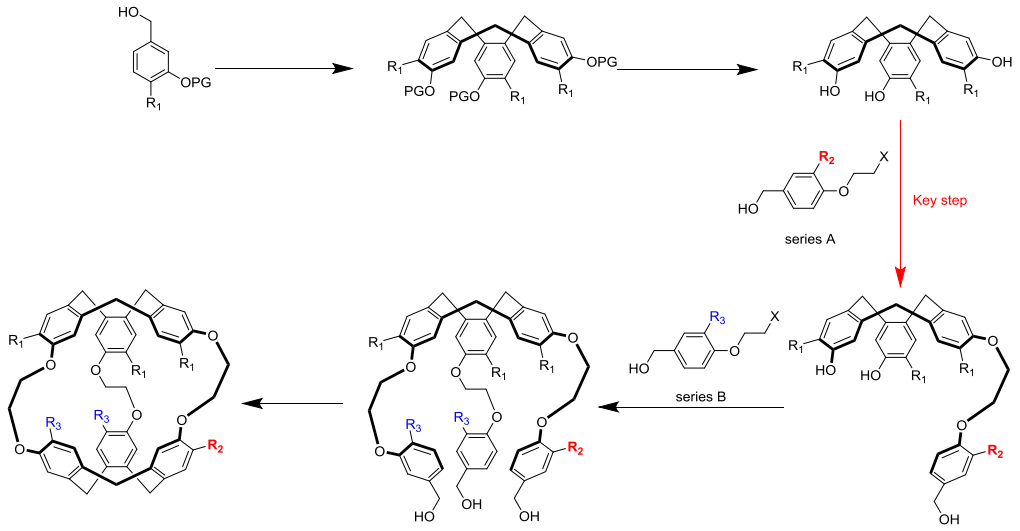

Figure 80: General description of the strategy "functionalization of CTVs with the different benzyl alcohol derivatives". In this figure, R_2 represents a functionalizable group and R_3 represents the solubilizing group

a. Conception and retrosynthetic analysis

This synthetic route is inspired by the classic synthesis of cryptophanol **31**.[90] The key step to achieve the desymmetrization is the functionalization of CTV **25** with different benzyl alcohol derivative linkers, including a PEGylated benzyl alcohol derivative **58**. Therefore the desymmetrization is achieved prior to the introduction of the PEG moieties.

The retrosynthesis is depicted in Figure 81:

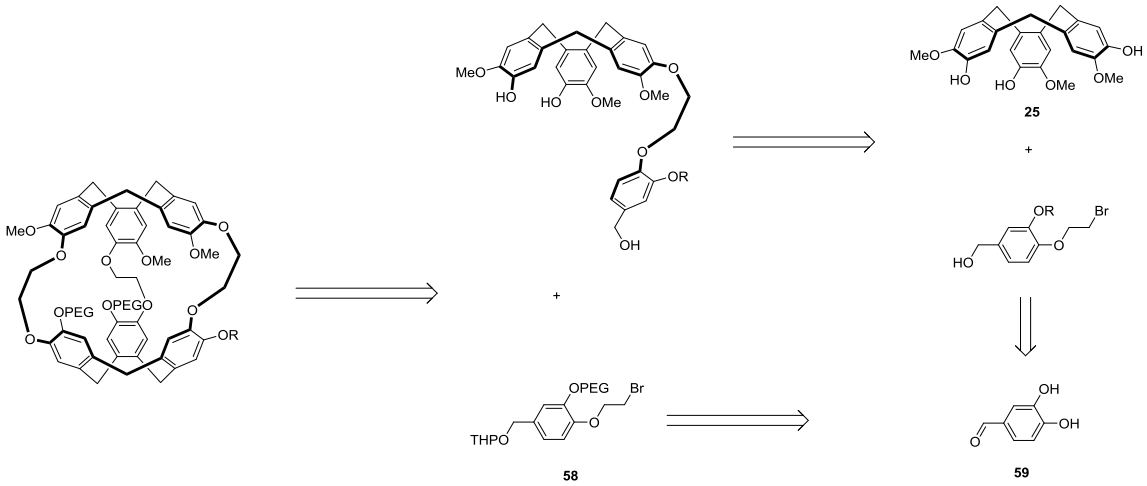

Figure 81: Retrosynthetic analysis of the mono-functionalized PEGylated cryptophane based on the mono-functinalization of CTV **25**

As we can see in the Figure 81, the asymmetric cryptophane is basically composed of three moieties: the CTV **25** and two different benzyl alcohol derivatives bearing either a PEG moiety (2 benzyl units) or a protected phenol moiety OR (1 benzyl unit) which can be used for mono-functionalization.

The synthesis of the CTV **25** is already well-described in the literature. Briefly, the phenol group of the commercially available vanillyl alcohol **16** was protected with an allyl group. Cyclotrimerization of this allylic vanillyl alcohol **14** led to the formation of CTV **32**. The allyl groups were subsequently deprotected with palladium acetate (Figure 82), the resulting CTV **25** could be obtained in three steps in 42 % overall yield (5 g scale).

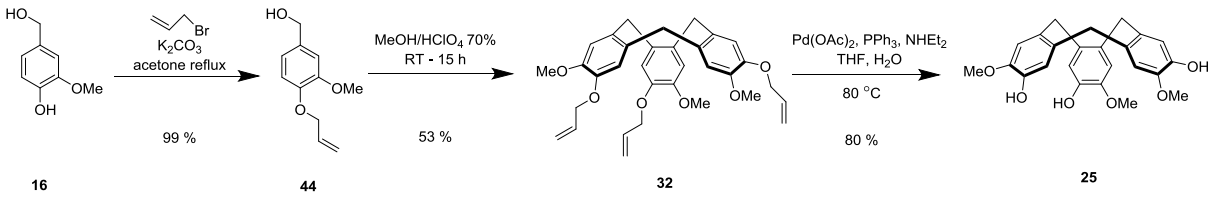

Figure 82: Synthesis of CTV **25**

The benzyl alcohol derivative linkers with various R groups can be synthesized from commercial 3,4-dihydroxybenzaldehyde **59**. Their synthesis will be introduced latter.

b. Synthesis towards a mono-allyl PEGylated cryptophane

The allyl group is the most widely used phenol protecting group in the chemistry of cryptophanes and therefore was chosen since it is easily cleaved by using a pallado-catalyzed reaction.

i. Synthesis of the allylic benzyl alcohol derivative **37**

A straightforward synthesis of the allylic benzyl alcohol derivative **37** is depicted in Figure 83.

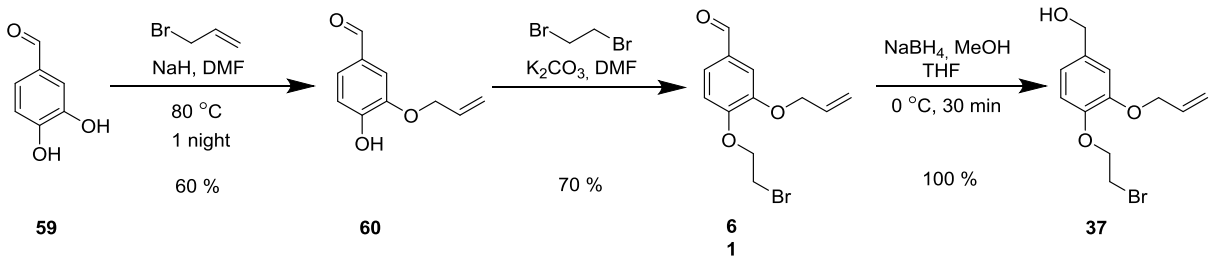

Figure 83: Synthesis of the benzyl alcohol derivative **37**

It should be noted that in the first step, the O-alkylation can take place on the two phenolic positions in molecule **59**. As a matter of fact, the chemoselectivity is controlled by the quantity of base used. If one equivalent of base is engaged, molecule **59** is predominantly O-alkylated at the 4-position to give O-allyl ether **63**. The phenoxide anion **62** is strongly stabilized by the *para*-aldehyde motif (Figure 84-a). Conversely, if molecule **59** is treated with two equivalents of sodium hydride, the vanillyl derivative **60** is formed as the major O-alkylation product. The predominant formation of **60** may be explained by the existence of dianion **64** in which negative charges are remote from each other, thus activating phenate in position 3. Compound **64** can undergo dialkylation to produce the unstable enol ether **65** which will give mono-allyl derivative **60** upon aqueous workup (Figure 84-b).[123] It should be mentioned that both products are useful in the subsequent synthesis.

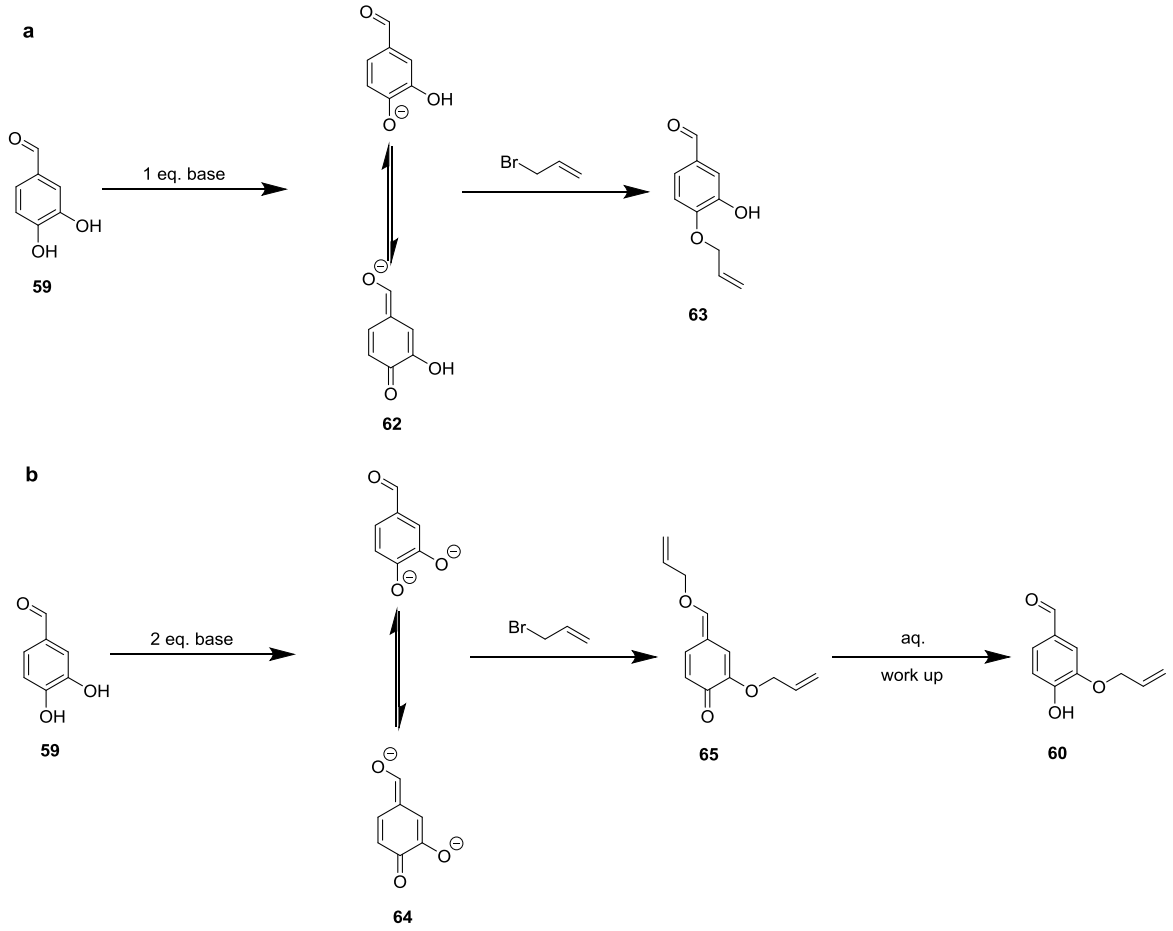

Figure 84: Explanation of the formation of different products in a) using 1 equivalent of base. b) using 2 equivalents of base

In the second step, the dibromoethane should be used in a large excess in order to minimize the formation of the by-product **66** (Figure 85).

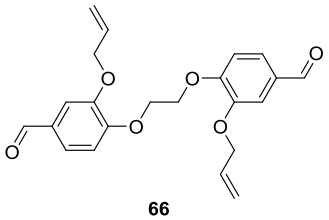

66

Figure 85: The possible by-product in the reaction between molecule **60** and dibromoethane.

Reduction of the aldehyde motif was easily achieved by using sodium borohydride ($NaBH_4$) in standard conditions. Pure compound **37** was obtained after several extractions without any further purification. It should be mentioned that the alcohol group in molecule **37** was kept unprotected to facilitate the purification in the next step.

To conclude, the allylic benzyl alcohol derivative **37** is obtained in three steps in 42 % overall yield (2 g scale).

ii. Synthesis of the PEGylated benzyl alcohol derivative **58**

In order to circumvent a possible lack of selectivity for the PEGylation of diphenol **59** which could give two position isomers presumably too difficult to separate, we firstly protected the phenol group on position 4 of the aromatic ring with an allyl group (Figure 86). This selective protection was achieved by reducing the quantity of NaH to 1.1 equivalents. An alternative would be also to recycle side-product **63** formed in the synthesis of **37**.

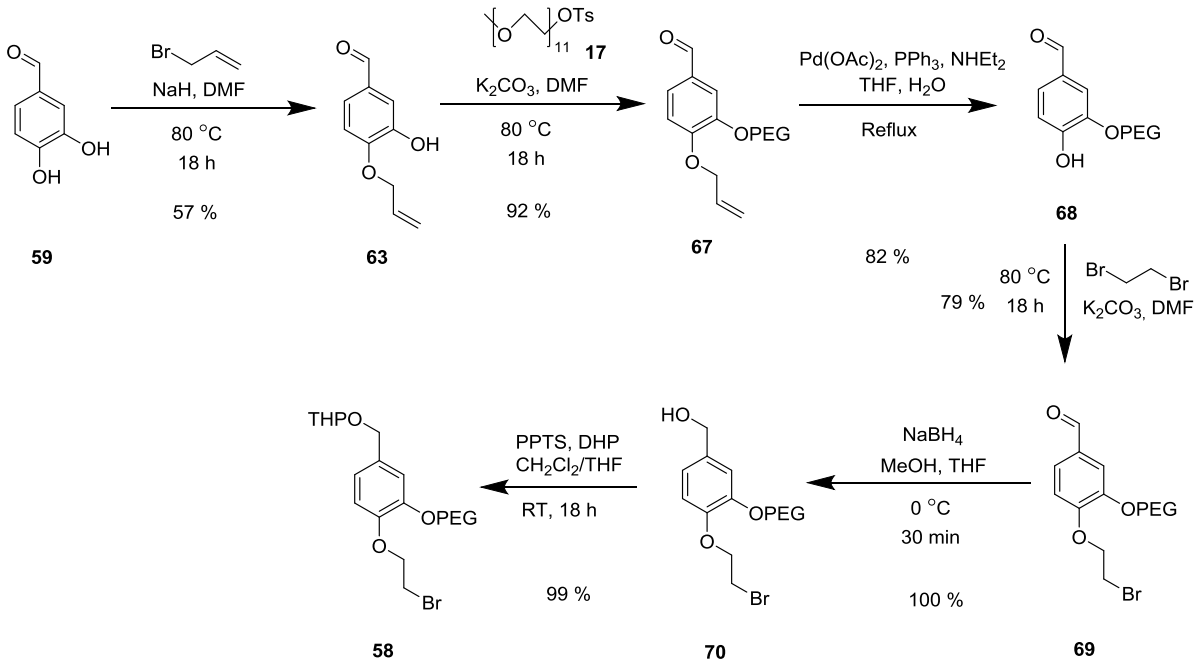

Figure 86: Synthesis of the PEGylated benzyl alcohol derivative **58**.

Then molecule **63** was PEGylated with the previously prepared mPEG-OTs **17**. In this step, compound **63** should be used in excess to ensure a complete conversion of mPEG-OTs and thus to eliminate difficulties in the purification of **67** due to similar polarities between compounds **17** and **67**.

The remaining of this synthesis was quite similar to the previous synthesis of **37**. However the alcohol group of derivative **70** was protected as a THP group in order to avoid the formation of a tri-alcohol which might be too polar for purification in the subsequent step.

To sum up, the PEGylated benzyl alcohol derivative **58** was synthesized in 6 steps in 34 % overall yield (3 g scale).

iii. Synthesis towards the mono-allylated PEGylated cryptophane

The synthetic route to the mono-allylated PEGylated cryptophane **73** implies the connection of benzyl alcohol **37** and **58** to CTV **25** as depicted in Figure 87.

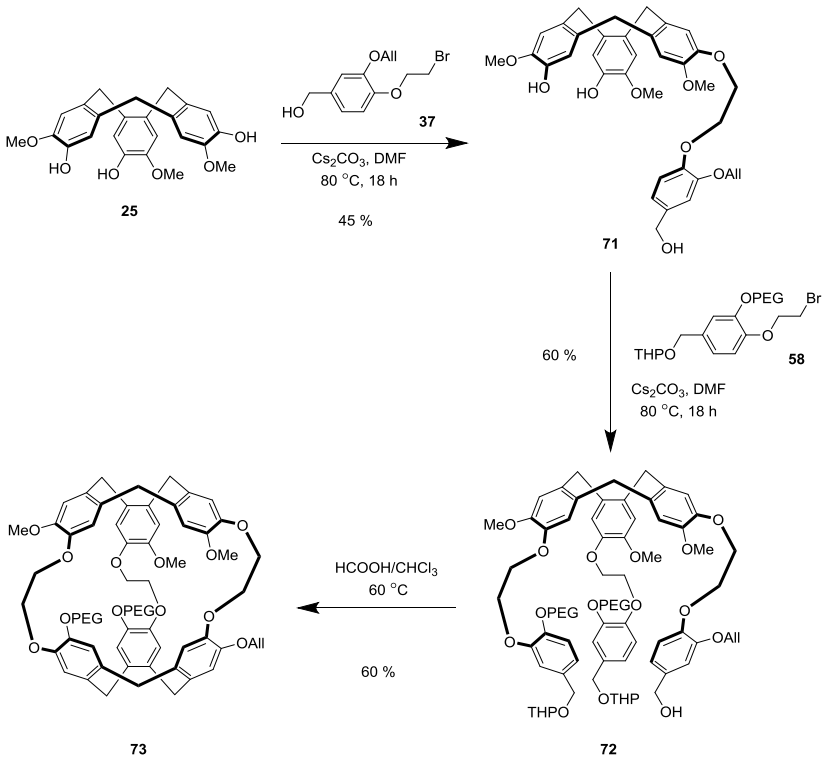

Figure 87: Synthesis towards the cryptophane **73**

Desymmetrization was achieved via the mono-functionalization of CTV **25** with the allylic linker **37**. With 1 equivalent of **37**, a mixture of the starting material **25**, mono-functionalized CTV **71** and di-functionalized CTV **74** was obtained (Figure 88). Products were easily separated thanks to the presence of the free alcohol in **37**. Consequently, chromatography over a silica column gave the targeted product **71** in 30 % yield. As the recycled CTV **25** could be reused in the next cycle of reaction, the yield based on the recovered starting material reached 39 %.

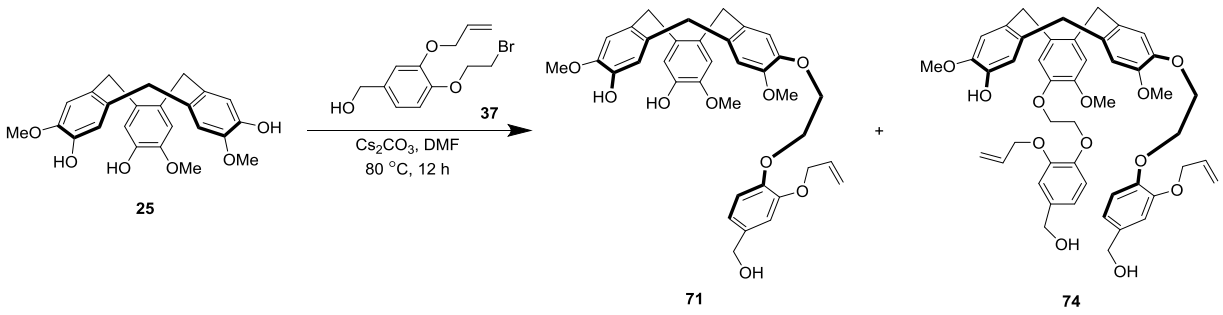

Figure 88: Mono-functionalization of CTV **25** with benzyl alcohol derivative **37**.

This reaction was optimized by changing the quantity of **37** in order to suppress the formation of CTV **74**. The best result was obtained with 0.5 equivalents of **37**, which yielded

37 % of **71** and the reaction yield based on recycling was 45 % (Table 9). No significant improvement was observed when reducing the quantity of **37** and the production of the targeted product became insignificant.

	CTV **25**	Mono **71**	Di **74**	Yield based on recycling
1 eq. of **37**	31 %	30 %	16 %	39 %
0.7 eq. of **37**	32 %	35 %	11 %	43 %
0.5 eq. of **37**	38 %	37 %	8 %	45 %

Table 9: Optimization of the mono-functinalization of CTV **25** with compound **37**

During the next step we grafted the PEGylated linker **58** onto CTV **71**. The purification step was facilitated by the presence of THP groups which avoided the formation of a too polar product. Normal-phase chromatography yielded 60 % of expected tri-functionalized CTV **72**.

As reported in the case of cyclotrimerization, the classic acidic conditions with pure formic acid were replaced by milder conditions using a mixture 50/50 of formic acid and chloroform in order to prevent hydrolysis of O-allyl groups.[90] However a Claisen rearrangement involving the allyl moiety was still observed in several attempts of this reaction (Figure 89).

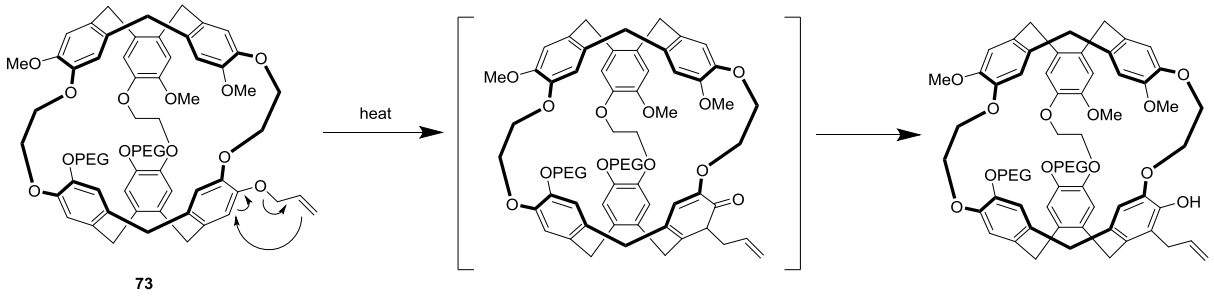

Figure 89: Possible Claisen rearrangement in the cyclotrimerization

After purification, cryptophane **73** was obtained in 60 % yield. Cyclotrimerization with scandium triflate $Sc(OTf)_3$ was also tested. This method was reported in the synthesis of calixarene leaving unreacted allyl groups.[124] According to the LC-MS of the crude product, the targeted cryptophane **73** was formed together with many impurities.

To conclude, the mono-allylated PEGylated cryptophane **73** was synthesized in six steps in 7 % overall yield (50 mg scale). This cryptophane was sufficiently soluble in water to be used for the synthesis of bioprobes (30 mg/mL). Considering that the synthesis of a water-soluble asymmetric cryptophane was already achieved, we investigated various possible chemical routes aiming at functionalizing the PEGylated cryptophane.

iv. Functionalization of the mono-allylated PEGylated cryptophane

We firstly planned to take full advantage of the O-allyl group already grafted onto cryptophane **73**. Consequently we tested an olefin metathesis reaction with hex-1-ene and Grubbs catalyst II (Figure 90). Although the formation of targeted product **75** was observed in the LC-MS analysis, the purification revealed to be so complicated that even HPLC was not capable to purify it. Different catalysts were tried (Grubbs I, Grubbs II, Hoveyda-Grubbs II), but the result remained unchanged.

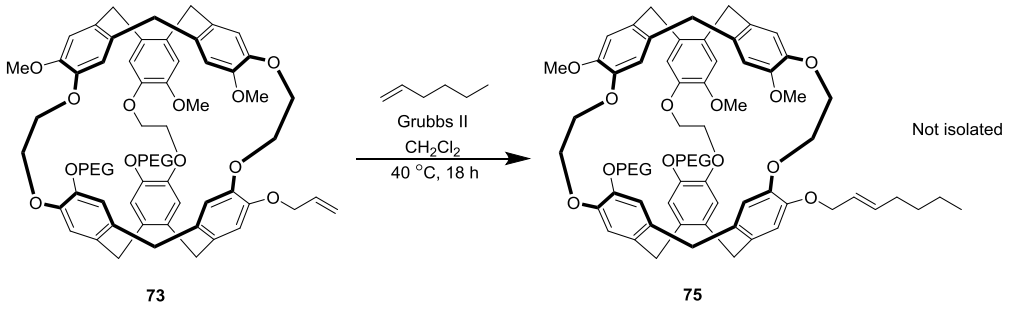

Figure 90: Attempts of metathesis reaction with cryptophane **73**.

Since the functionalization with the O-allyl group has been proven to be difficult, the deprotection of the allyl-protected phenol was therefore carried out on cryptophane **73** in order to release the free phenol group as a convenient access for the introduction of different functional groups.

v. Attempts to synthesize PEGylated cryptophanol

As mentioned in part B-I-1, the expected monofunctionalized cryptophane is supposed to be coupled with a peptide linker in order to approach the synthesis of biosensors. In this linker, a free amine group will be used for grafting onto the cryptophane through an amide coupling. Consequently the most straightforward strategy to access this biosensor was the conversion of cryptophane **73** into a mono-acid PEGylated cryptophane **76**. From this standpoint, PEGylated cryptophanol **78** is a very important intermediate (Figure 91).

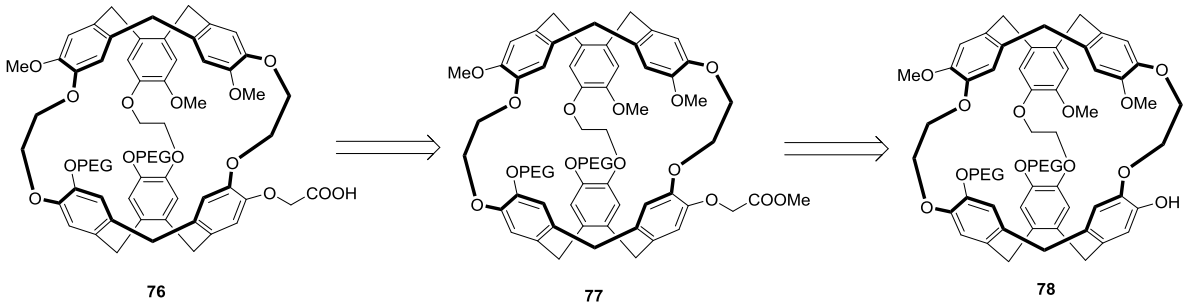

Figure 91: Retrosynthetic analysis of PEGylated mono-acid cryptophane **76**.

To achieve this goal, a deprotection of the O-allyl group in cryptophane **73** was attempted with $Pd(OAc)_2$ (Figure 92). This method proved to be efficient in the previously mentioned synthesis of CTV **25** and PEGylated linker **37**. According to the NMR spectrum of the obtained crude product, all the allylic protons disappeared. The formation of PEGylated cryptophanol **78** was observed by LC-MS, however this one could not be isolated from the mixture of several non-identifiable PEGylated impurities.

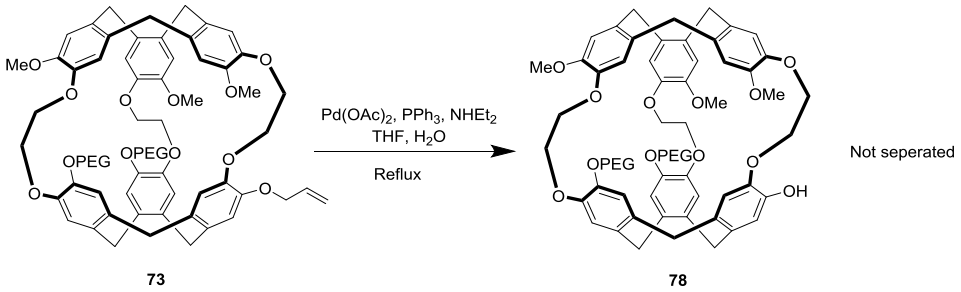

Figure 92: Attempt to synthesize PEGylated cryptophanol **78**.

Therefore another strategy was tried by deprotecting the allyl group before cyclotrimerization. The deprotection of tri-functionalized CTV **72** gave the tri-functionalized CTV **79** in 63 % yield (Figure 93).

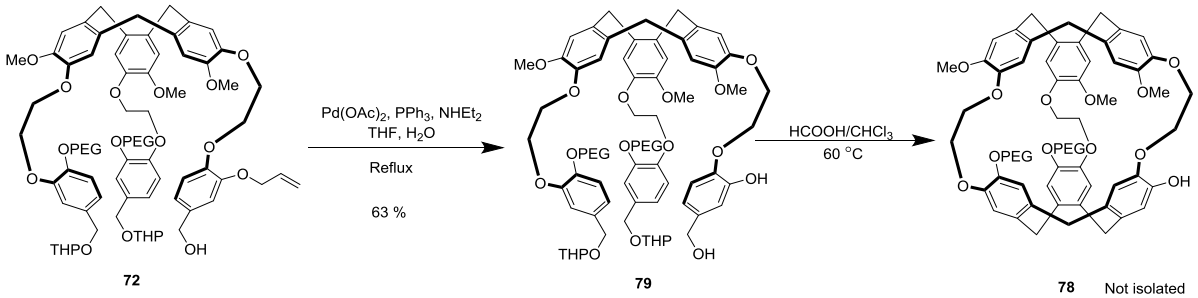

Figure 93: Deprotection of CTV **72** and its following cyclotrimerization

Although there are reports about the sensitivity of free phenol groups to the condition used for cyclotrimerization[2], the formation of PEGylated cryptophanol **78** was still observed by LC-MS analysis of the crude product after cyclotrimerization with a mixture of formic acid and chloroform 50/50. The apparent purity was improved compared to those observed in the deprotection of cryptophane **73**, but the existence of a PEGylated impurity jeopardized the purification once more. Additionally, the percentage of cryptophanol **78** in the obtained fraction was even worse after purification suggesting that the PEGylated cryptophanol **78** might be unstable during silica gel flash-chromatography purification.

vi. Conclusion

Mono-allylated PEGylated cryptophane **73** was synthesized in six steps in 7 % overall yield (50 mg scale). This cryptophane is enough soluble in water for being used to synthesize bioprobes in aqueous media. However, neither the functionalization of the double bond in this cryptophane nor the deprotection of the O-allyl group was successful.

The apparent lack of suitable reactivity of cryptophane **73** combined with the previously observed problem of Claisen rearrangement as well as potential isomerization of the double bond led us to conclude that the allyl group might not be the best choice as the protecting group in this strategy.

c. Synthesis towards a mono-benzylated PEGylated cryptophane

In order to overcome the above-mentioned problems encountered with the allyl protecting group, we focused our attention on the benzyl group for suitable phenol protection. Benzyl was expected to be stable in all the anticipated synthetic conditions used and its cleavage was anticipated to be easily archieved by hydrogenolyse. Moreover its applications as a protecting group in CTVs as well as cryptophanes were also reported (Figure 94).[83, 125]

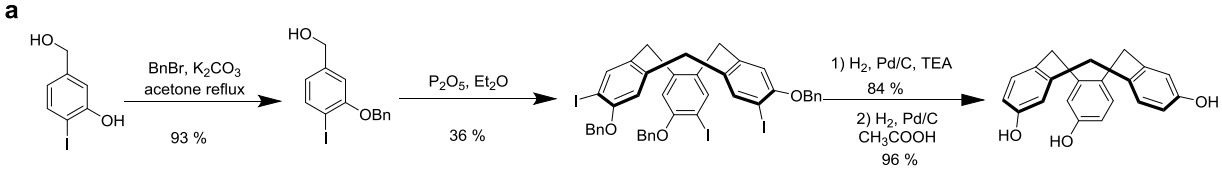

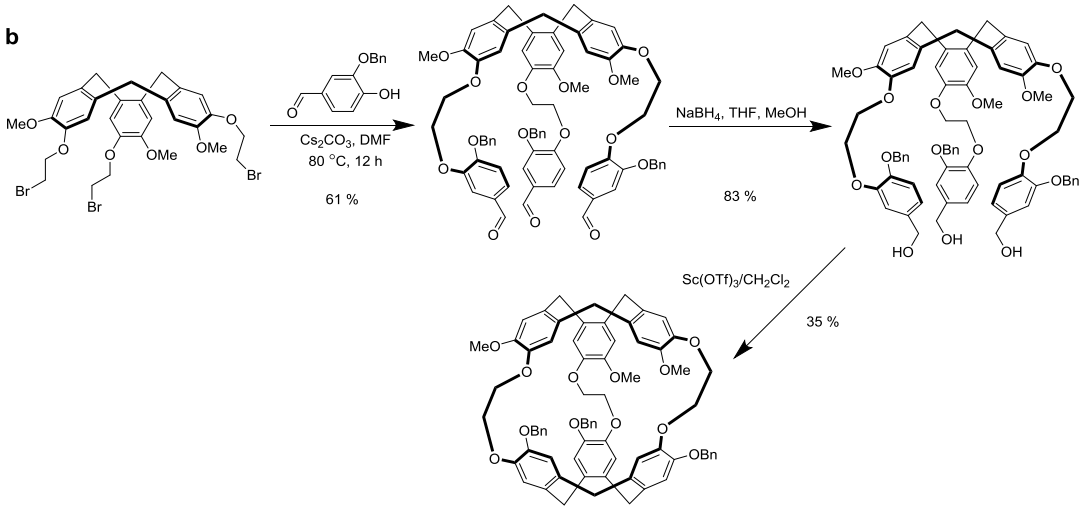

Figure 94: Utilization of benzyl as a protecting group in the chemistry of a) CTV[83]. b) cryptophane[125]

i. Synthesis to the mono-benzyl PEGylated cryptophane

The synthesis of benzylic linker **82** is similar to the one of the allylic linker **37** and was achieved as follows: commercial product 3,4-dihydroxybenzaldehyde **59** was O-benzylated with benzyl bromide. The chemoselectivity of this step was ensured by using two equivalents of NaH as the base. Then the O-benzylated product **80** was reacted with a large excess of dibromoethane to yield **81** and its aldehyde function was subsequently reduced with $NaBH_4$. Thus, benzylic ether **82** was obtained in three steps in 20 % yield (0.5 g scale) without any optimizations (Figure 95).

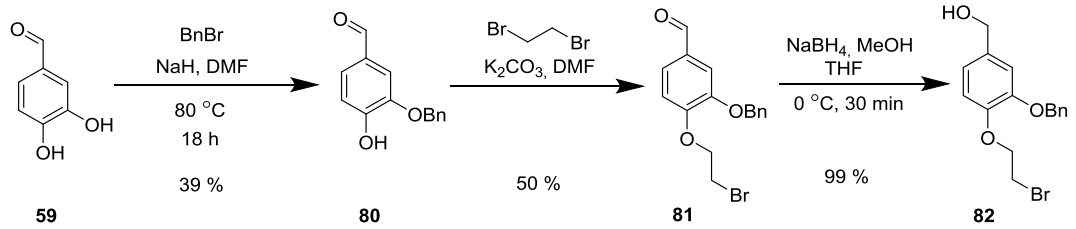

Figure 95: Synthesis of benzyl alcohol derivative **82**.

0.5 equivalents of **82** were then engaged in the mono-functionalization of CTV **25**, yielding mono-functionalized CTV **83** (43 % based on recycled starting material). The remaining two phenol groups available on the CTV scaffold were alkylated with an excess of PEGylated linker **58**, leading to the tri-functionalized CTV **84** in good yield (76 %). Finally, cyclotrimerization was performed in mild condition similar to that employed to synthesize the allylic precursor **72**. This method was successfully applied to the benzylic precursor **84** which provided the mono-benzyl PEGylated cryptophane **85** in 67 % yield (Figure 96).

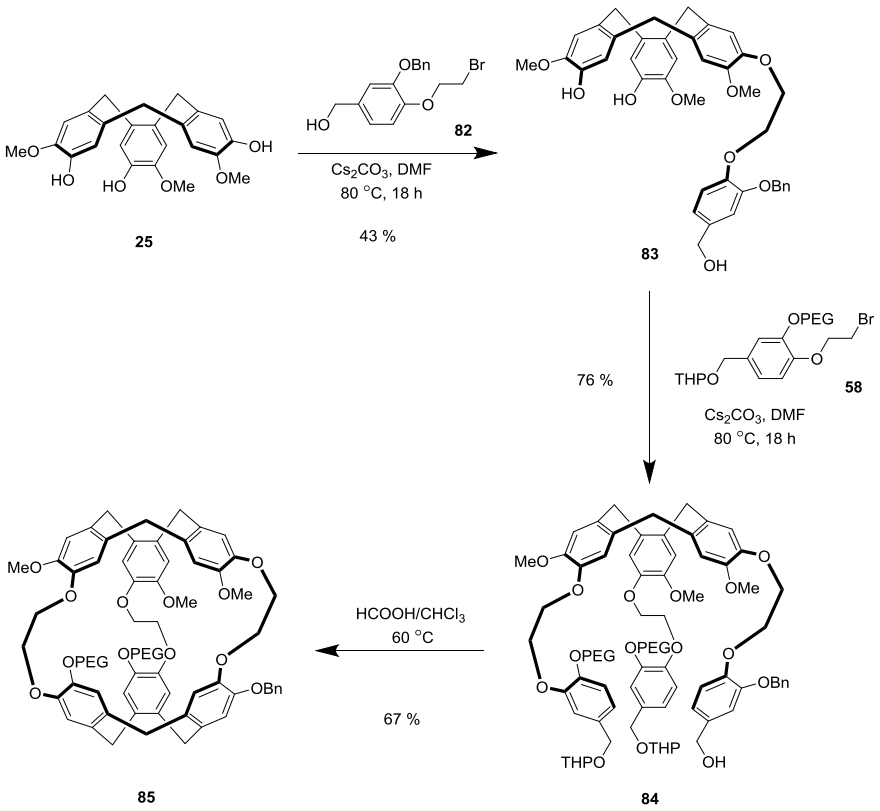

Figure 96: Synthesis towards cryptophane **85**

The mono-benzyl PEGylated cryptophane **85** was thus obtained in six steps in 9 % overall yield (50 mg scale). This cryptophane was sufficiently soluble in water to be used for the synthesis of bioprobes (30 mg/mL).

ii. Attempts to synthesize the PEGylated cryptophanol **78**

Cryptophane **85** is an asymmetric water-soluble cryptophane which is similar to the mono-allyl PEGylated cryptophane **73**. Unlike the O-allyl group, the lack of potentially reactive position in the O-benzyl group led us to deprotect the benzyl moiety to isolate the PEGylated cryptophanol **78** as starting material for the construction of biosensors.

The deprotection of benzyl group in cryptophane **85** was attempted by using 10% Pd/C in a methanolic solution of ammonium formate, as reported for the synthesis of a tri-benzylated cryptophane.[125] However, although the ^{1}H NMR spectrum of the debenzylated product strongly suggested that hydrogenolysis was completed, the expected cryptophanol **78** could not be identified by ES or MALDI-TOF mass spectrum analyses (Figure 97).

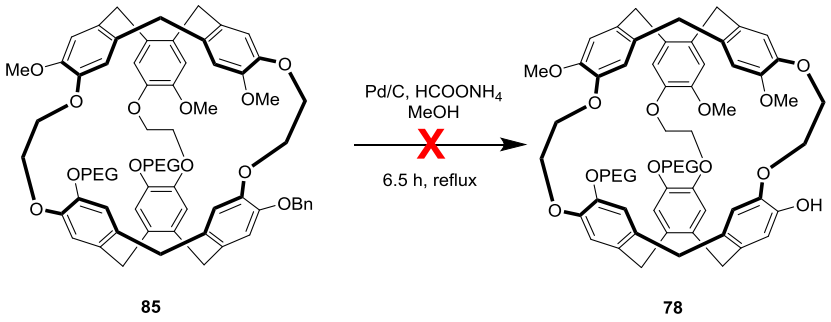

Figure 97: Attempts to hydrogenolyse the benzyl ether of cryptophane **85** with Pd/C and ammonium formate

Conversely, the same condition used to remove the benzyl group from the tri-functionalized CTV **84** gave the corresponding phenol **79** in 70% yield (Figure 98), suggesting that there was no problem with this reaction condition or the used reagents

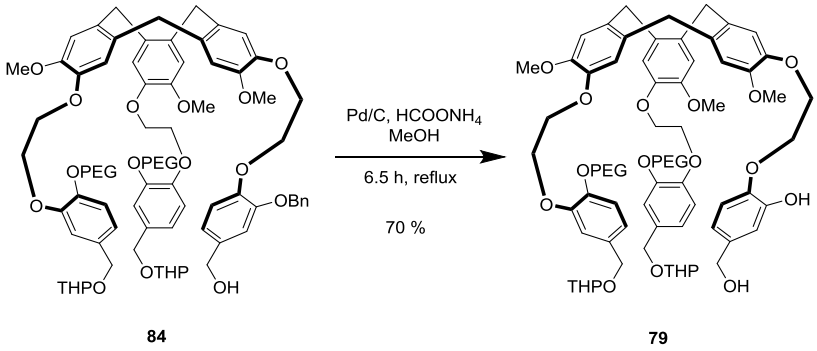

Figure 98: Attempts to hydrogenolyse the benzyl group of the cryptophane precursor **84** with Pd/C and ammonium formate

Therefore, we tried to deprotect the benzyl group of compound **85** with H_2, Pd/C and CH_3COOH (Figure 99), which was also reported as a well-working method in the debenzylation of CTV.[83] Unfortunately we did not succeed either though the starting compound disappeared. In order to better understand the fate of this reaction, we removed the acetic acid to slow down the kinetics. A follow-up by LC-MS analysis showed that after 18 h, the reaction milieu contained a mixture of targeted cryptophanol **78** and starting material **85**. After 24 h, the quantity of both the targeted product and the starting material decreased, while a new unidentified product began to form. After 40 h, the reaction was completed leading to the exclusive formation of the unexpected product, the mass of which was identical to that of the unidentifiable product obtained previously by debenzylation with ammonium formate and Pd/C.

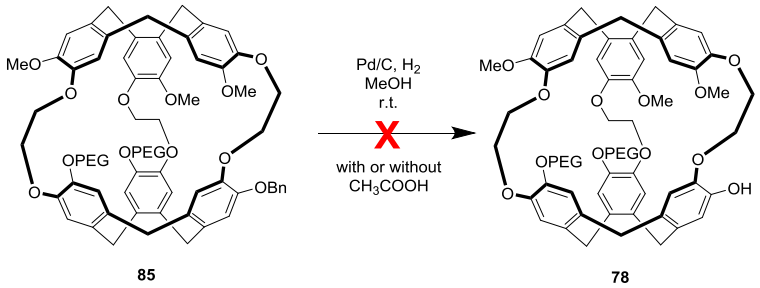

Figure 99: Attempts to debenzylate cryptophane **85** with Pd/C and H_2

^{1}H NMR analysis of this unexpected product ensured the total cleavage of benzyl group without giving more meaningful information due to the complexity and asymmetry of this molecule. The LC-MS and MALDI-TOF analyses showed that the mass of this product is $M_{unexpected} = M_{compound\ \mathbf{78}} + 6/50/94\ldots$ (because of the polydispersity of PEG). The only plausible explanation for $M_{unexpected}$ is the mass of cryptophane **86** (Figure 100) plus a sodium cation.

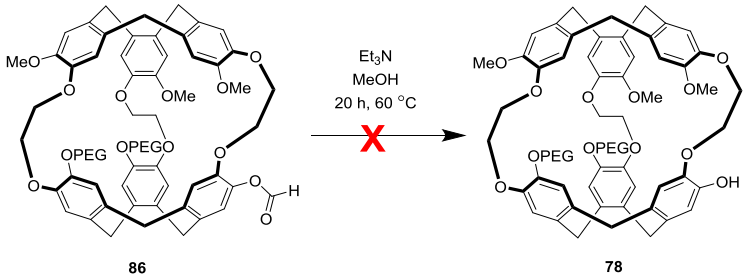

Figure 100: Attempts to prove the formation of cryptophane **86**

In order to check this hypothesis, a conversion of the phenyl formate to phenol group was attempted with this unexpected product (Figure 100).[126] No matter how long the reaction was kept, the LC-MS analysis of the crude product showed that the starting compound was not consumed. Therefore we still failed to determine the structure of this isolated compound.

Combined with the previous results obtained with the mono-allylated PEGylated cryptophane **73**, the hypothesis of a possible instability of PEGylated cryptophanol **78** might be evoked. This might be explained by a strong dissymmetry of the cryptophane structure induced by two long chains of PEG which could distort and then facilitate the breaking the structure of the cage. This hypothesis explained why cryptophanol **78** was observed but unexpectedly transformed into another product either during the reaction or the purification steps. However we could not produce any hypothetical structure accounting for this phenomenon.

d. Synthesis towards a mono-acid PEGylated cryptophane

According to the previous results discussed in parts III-1-b and III-1-c, it was necessary to develop an alternative strategy avoiding the use of the PEGylated cryptophanol **78** as an intermediate. Since a mono-acid PEGylated cryptophane was highly desirable to synthesize the biosensor, we decided to introduce a methyl acetate group on the tri-functionalized CTV **79** at an earlier stage of the synthesis (Figure 101).

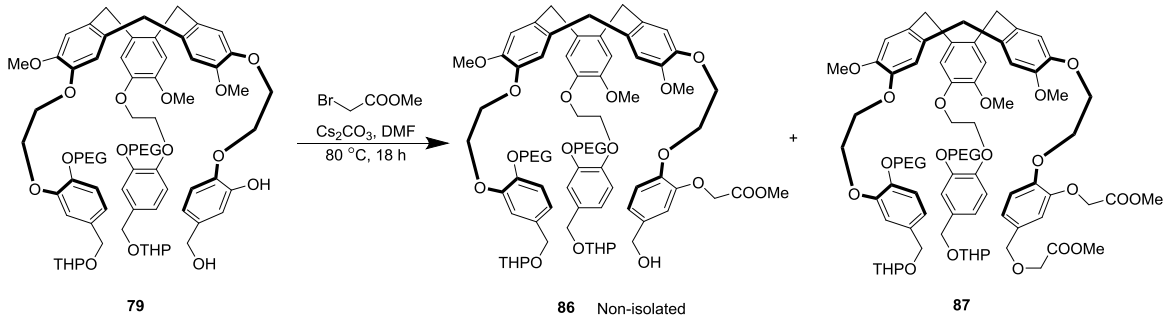

Figure 101: Attempt to synthesize the precursor of the mono-ester PEGylated cryptophane **86**.

Surprisingly, the targeted product **86** was obtained along with by-product **87**, suggesting that the central carbon atom of methyl bromoacetate was too electrophilic and thus reacted not only with the phenol group but also with the alcohol group, thus promoting a bis-alkylation (Figure 101). Once again, as the long chains of PEG were predominant for determining the polarity of these molecules, this by-product was impossible to be separated from compound **86**. Consequently we decided to introduce the methyl acetate group directly into the benzyl alcohol derivative linker.

i. The synthesis of the benzyl alcohol derivative with methyl acetate

The synthesis of methyl ester **90** is similar to that of allylic benzyl alcohol derivative **37**, with the replacement of allyl bromide with bromomethyl acetate (Figure 102).

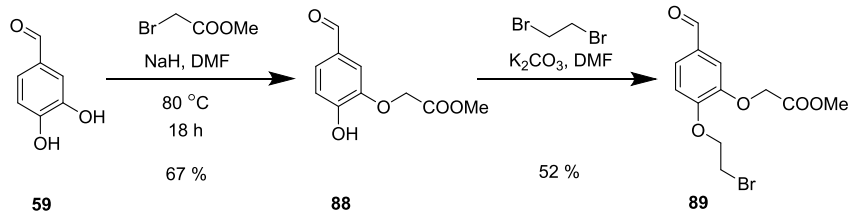

Figure 102: Synthesis of the benzyl alcohol derivative with methyl acetate

Selective O-alkylation of the phenol in position 3 of compound **59** with methyl bromoacetate and subsequent O-alkylation of position 4 with dibromoethane afforded compound **89** in 35% overall yield. Unfortunately, the reduction of the aldehyde with sodium borohydride as previously described clearly gave a mixture of two products which could be purified by chromatography to yield 59 % of the targeted product **90** and 28 % of the by-product **90'** containing an alcohol instead of the methyl ester (Figure 103).

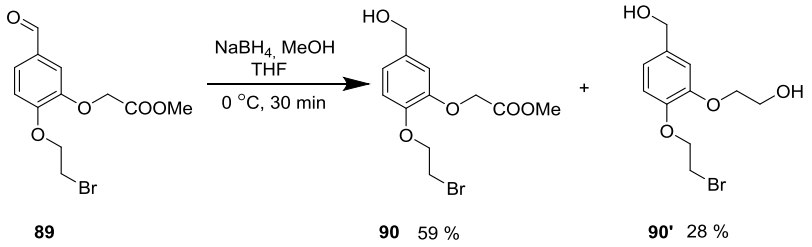

Figure 103: Reduction of **89** to give the expected benzyl alcohol derivative with methyl acetate **90** and by-product **90'**

In order to decrease the proportion of the bis-reduction reaction, we attempted to lower the reactivity of $NaBH_4$ by using a mixture of dichloromethane, ethanol and acetic acid (35:5:1) as a solvent (Figure 104), leading to the formation of sodium borohydride acetate $NaBH_m(OAc)_n$ (m + n = 4).[127, 128] This compound is a reducing agent which is much less drastic than $NaBH_4$ and selectively reduces carbonyl compounds.[129]

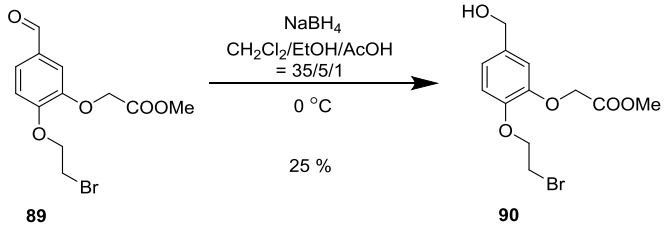

Figure 104: Reduction of **89** in milder conditions

In these conditions, no reduction of the ester group was observed but the yield was not enough satisfying. In fact, after purification by silica gel chromatography, only 25 % of targeted product **90** was obtained and 47 % of starting material **89** was recovered. Even though the obtained starting material could be reused in the next cycle of reaction, the yield based on recycling was only 37 %, which was much worse than the one obtained with the original conditions ($NaBH_4$, MeOH, THF). Moreover, prolongation of reaction time or reduction of the quantity of acetic acid did not efficiently improve the yield.

We had also vainly attempted other optimizations of the original reducing condition ($NaBH_4$, MeOH, THF) such as replacing methanol with ethanol or carrying out the reaction without any alcohol.

Finally, the best result was obtained by simply reducing the time of the reaction from 30 min to 10 min. yielding 77% of product **90** though by-product **91** was also obtained along in small quantity (Figure 105).

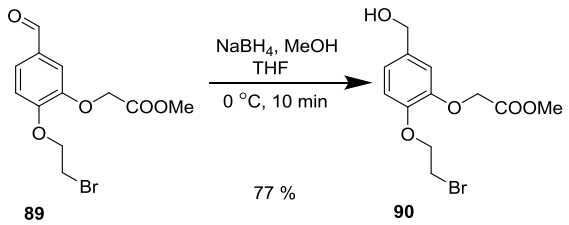

Figure 105: Optimization of the reduction by reducing the time of reaction.

In conclusion, the benzyl alcohol derivative **90** was obtained in three steps in 27 % overall yield (2.5 g scale).

ii. Synthesis to the mono-acid PEGylated cryptophane **76**

CTV **91** was obtained as previously described with CTV **25** and 0.5 equivalent of linker **90**, yielding 25 % of the mono-functionalized compound based on recovered starting material. This result was less attractive than that obtained with allyl or benzyl protecting groups, which was actually caused by the instability of the ester group. After purification, the hydrolyzed mono-functionalized CTV **93** was obtained in 29 % yield based on recycled starting material. The same problem was also observed in the subsequent functionalization of the CTV with the PEGylated linker **58**. Due to the presence of the grafted PEG groups on the benzyl moieties, it was complicated to separate the targeted product **92** from the hydrolyzed product **94**. Fortunately, as the ester group was expected to be converted into the corresponding acid at the end of the synthesis, we decided to work on the mixture, anticipating that the presence of the hydrolyzed product would not jeopardize the subsequent cyclotrimerization. It should be noticed that the 55 % yield for this step was calculated for both ester **92** and corresponding acid **94** (Figure 106).

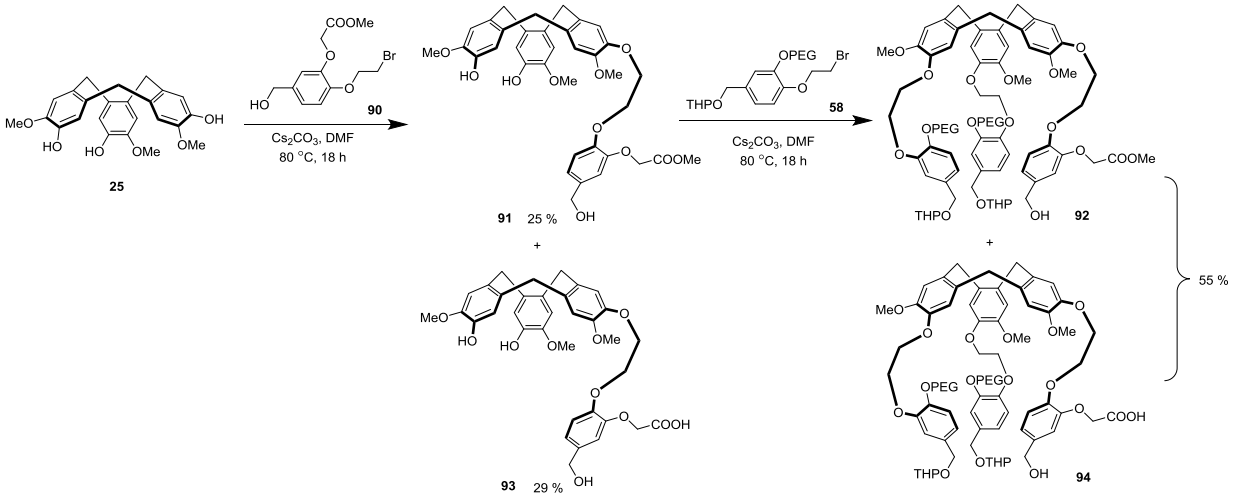

Figure 106: Functionalization of CTV **25** with the benzyl alcohol derivatives carrying methyl acetate groups and PEG groups

Cyclotrimerization was thus carried out with the mixture of **92** and **94** in formic acid/chloroform = 50/50. A mixture of PEGylated cryptophane **77** and **76** was obtained, respectively carrying a methyl acetate group and an acetate group. However, according to LC-MS analysis, an additional ester hydrolysis occurred during cyclotrimerization (Figure 107).

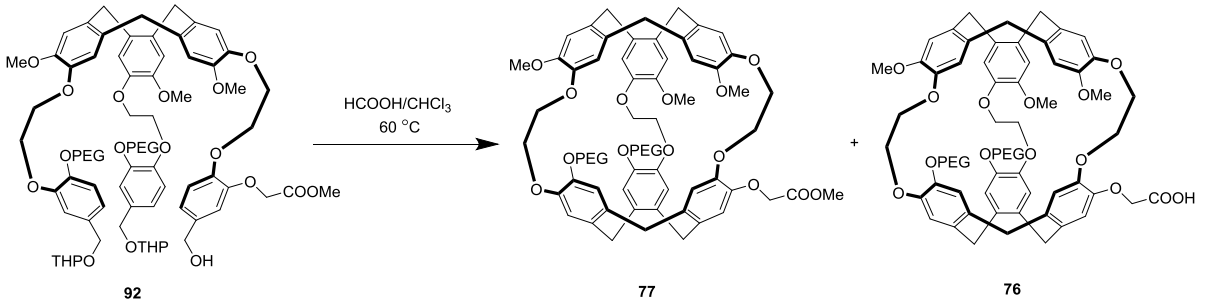

Figure 107: Cyclotrimerization to form the PEGylated cryptophanes carrying methyl acetate and carboxylic acid groups

We directly engaged the mixture of cryptophanes **76** and **77** in a saponification reaction with NaOH which was expected to lead to compound **76** exclusively. After the purification by chromatography, the pure PEGylated cryptophane **76** carrying a carboxylic acid was obtained in 74 % overall yield for 2 steps (Figure 108).

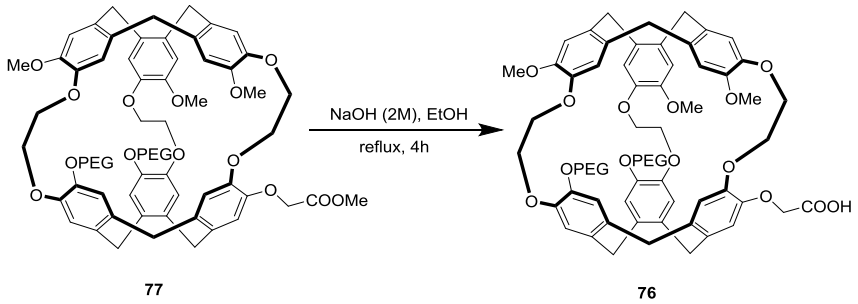

Figure 108: Saponification of the cryptophane **77**

We observed that as soon as the molecular cage was formed upon treatment with formic acid/chloroform = 50/50, two unexpected signals were detected by ^{1}H NMR spectrum respectively at 5.1 and 8.1 ppm (Figure 109). Based on our experience and according to related reports in the literature,[69, 70] the two unexpected peaks are likely to account for the encapsulation of a molecule of solvent (presumably chloroform in our case).

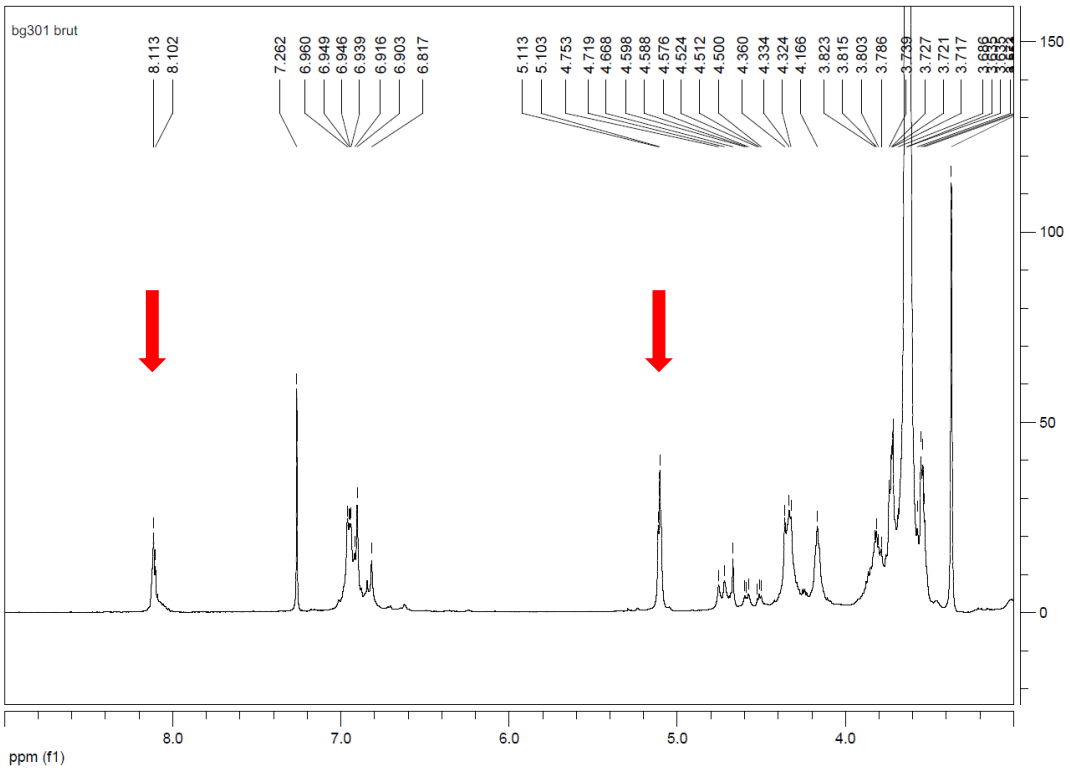

Figure 109: The two unexpected peaks in NMR spectrum after cyclotrimerization

To address this issue, several attempts were made such as heating the sample in different solvents or pumping xenon gas into it. Finally, we have succeeded by heating the cryptophane in refluxing methanol (Figure 110), suggesting that methanol molecules can enter into the cage to push out the previously hosted molecule.

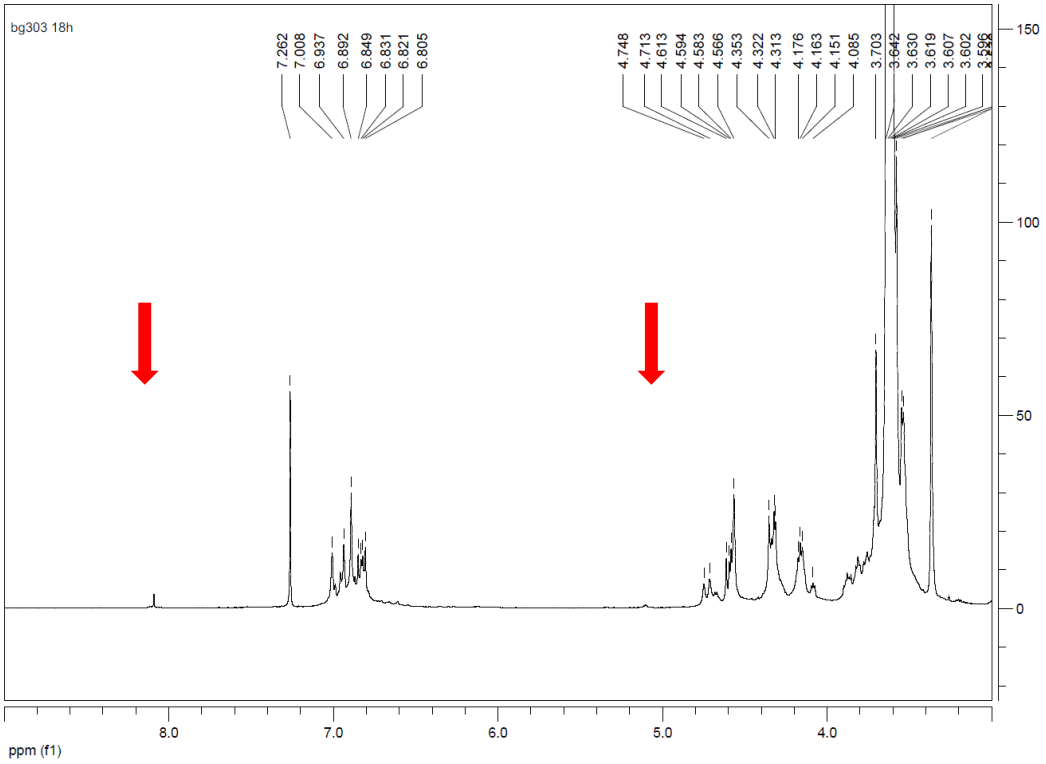

Figure 110: The disappearance of the two unexpected peaks by heating the cryptophane in MeOH

At the same time, the recovered mono-functionalized CTV **93** was also used to synthesize cryptophane **76** through the same chemical route as described above. Cryptophane **76** could be obtained in two steps in 24 % yield (Figure 111). This moderate yield probably results from the presence of the carboxylic acid group which complicates the purification process. The NMR spectrum of the product also displayed the two unexpected signals in ^{1}H NMR which disappeared upon reflux in methanol.

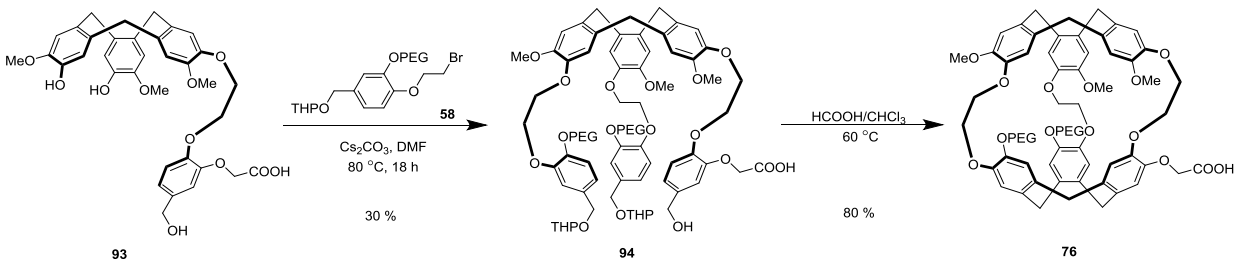

Figure 111: Synthesis of cryptophane **76** from mono-functionalized CTV **93**.

In conclusion, the PEGylated cryptophane carrying a carboxylic acid **76** was synthesized in seven steps in 4 % overall yield (50 mg scale). However, when including the recycling of mono-functionalized CTV **93**, the overall yield is improved to 7 % at the hundred mg scale.

As anticipated, we observed that cryptophane **76** displayed a satisfactory hydrosolubility (30 mg/mL).

iii. Encapsulation of xenon inside cryptophane **76**

Cryptophane **76** was dissolved in water and then tested via hyperpolarized ^{129}Xe NMR. The equipment for hyperpolarizing xenon has already been introduced in Part A-I-3-b and was used as described therein. Freshly hyperpolarized xenon is condensed in a tube submerged in liquid nitrogen. In the presence of an adapted magnetic field, the hyperpolarization of xenon in solid phase can be conserved for several hours.[130] The tube will be heated by putting into hot water which permits to turn xenon back to the gas phase.

Hyperpolarized xenon gas is introduced into the NMR tube through a three-way valve (Figure 112) Xenon gas contained inside the NMR tube is then frozen and remains in contact with the sample.

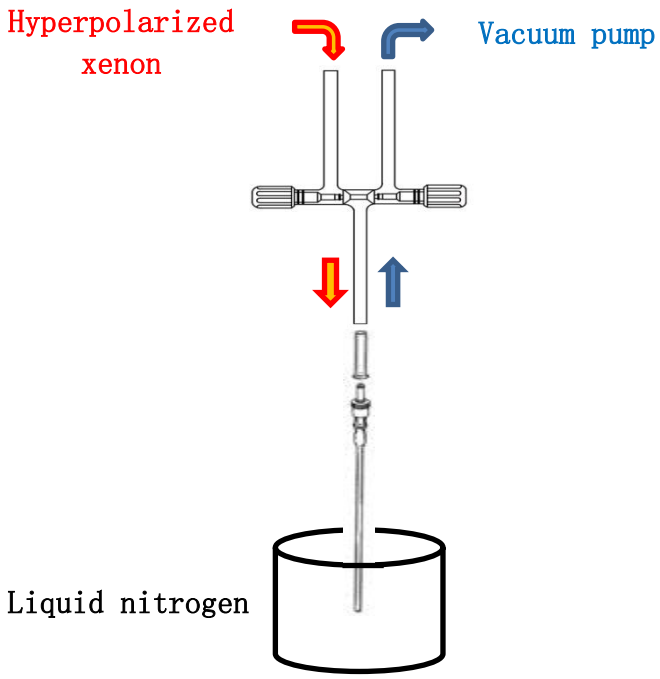

Figure 112: Introduction of hyperpolarized xenon into the NMR tube

Unexpectedly, no signal was observed, suggesting that there was no encapsulation of xenon gas at all. This was not in accordance with previous study carried out in our group with cryptophane[222](OMe)$_3$(OPEG)$_3$ **23** which encapsulated xenon efficiently. In order to explain the lack of xenon encapsulation, we might evoke a problem of solubility or the

aggregation of cryptophane **76** in water. Therefore, the same molecule was also tested in organic solvents like chloroform and methanol, however once again, no gas encapsulation was observed.

Another possible reason which might account for the non-encapsulation of xenon is that the cryptophane molecular cage is not properly closed. If a misconnection between the CTV scaffold and the benzyl motifs occurred, the cavity of the cage might be too large for xenon binding. Given the fact that the ^{1}H NMR spectra of PEGylated asymmetric cryptophanes are complex and unclosed precursors always show the mass of adducts lacking of –OH or –OTHP groups in LC-MS (the mass of which fortuitously corresponds to that of the corresponding cryptophanes), it is difficult to conclude whether the cage is well closed or not. It is possible that in the condition of cyclotrimerization, only the deprotection of THP group has occurred.

In order to conclude about this point, a simple deprotection of THP of the tri-functionalized CTV **92** was carried out (Figure 113). The corresponding ^{1}H NMR spectrum was compared with every spectrum recorded after cyclotrimerization of **92**. Detailed analysis showed that the cryptophane was effectively formed after cyclotrimerization, however we realized that the cage was reopened upon heating in refluxing methanol during our attempts to eliminate the two inexplicable signals in ^{1}H NMR.

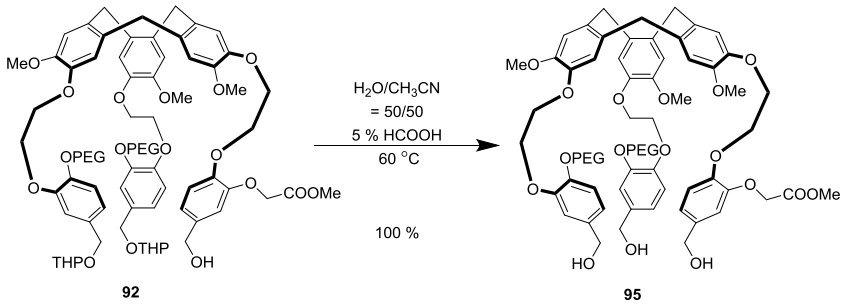

Figure 113: Deprotection of THP group in molecule **92**

Therefore, a genuine sample of cryptophane **76** (without being heated in methanol) was tested by ^{129}Xe NMR showing no encapsulation of xenon as well.

Then we focused our interest on the two unexpected peaks in ^{1}H NMR, which probably arises from a molecule who has got stuck in the cage and thus blocks the entrance of xenon. This process is only possible during the cyclotrimerization because once the cage is formed,

the molecules which can enter the cage should also be able to get out. During the cyclotrimerization step, only formic acid and chloroform are brought into contact with the product. Since formic acid has been largely used for the cyclotrimerization of cryptophane and even in the cyclotrimerization of PEGylated cryptophane[87] without being encapsulated, chloroform seems to be the only possibility. Consequently, the cyclotrimerization of molecule **94** was carried out in pure formic acid (Figure 114). The obtained cryptophane **76** was then tested by ^{1}H NMR, confirming the absence of the two unexpected peaks at around 5.1 and 8.1 ppm (Figure 115).

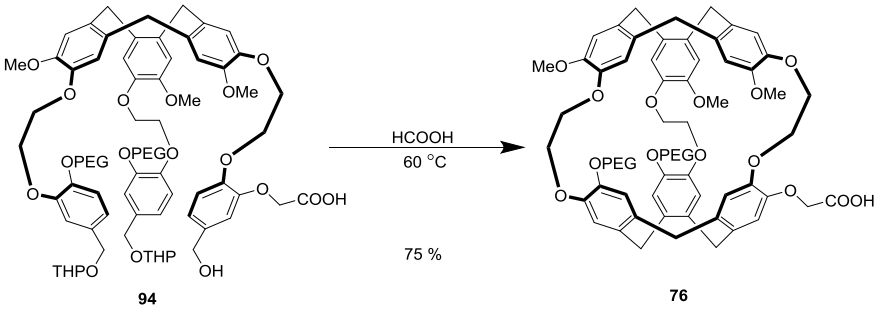

Figure 114: The cyclotrimerization of **94** with pure formic acid

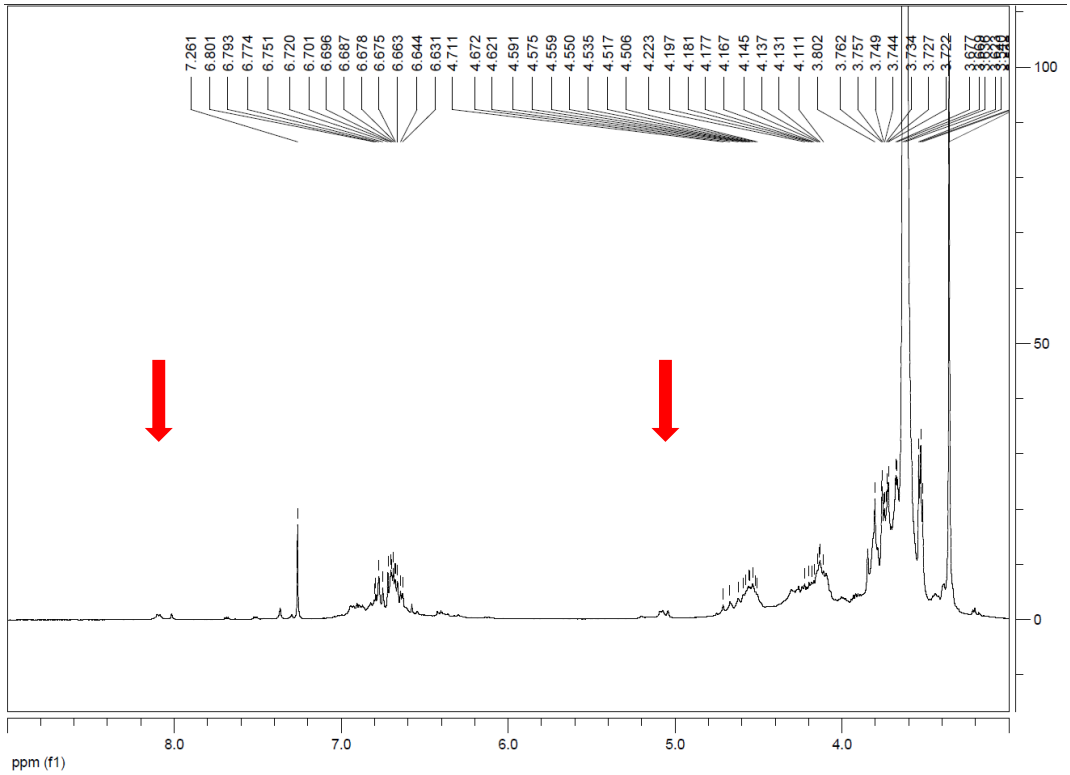

Figure 115: ^{1}H NMR spectrum of the cryptophane **76** cyclized with pure formic acid

Then the cryptophane was dissolved in water and tested by ^{129}Xe NMR, clearly showing an encapsulation of xenon as displayed by the NMR spectrum (Figure 116): In this spectrum, the signal of the free xenon in water is around 191 ppm and the signals of the xenon encapsulated inside cryptophane is around 70 ppm. All of these results demonstrated that the two unexpected peaks as well as the problem of encapsulation were caused by the presence of chloroform. Heating in refluxing methanol in order to remove chloroform from the cryptophane resulted in the opening of the molecular cage which was difficult to detect due to the complexity of large asymmetric structures.

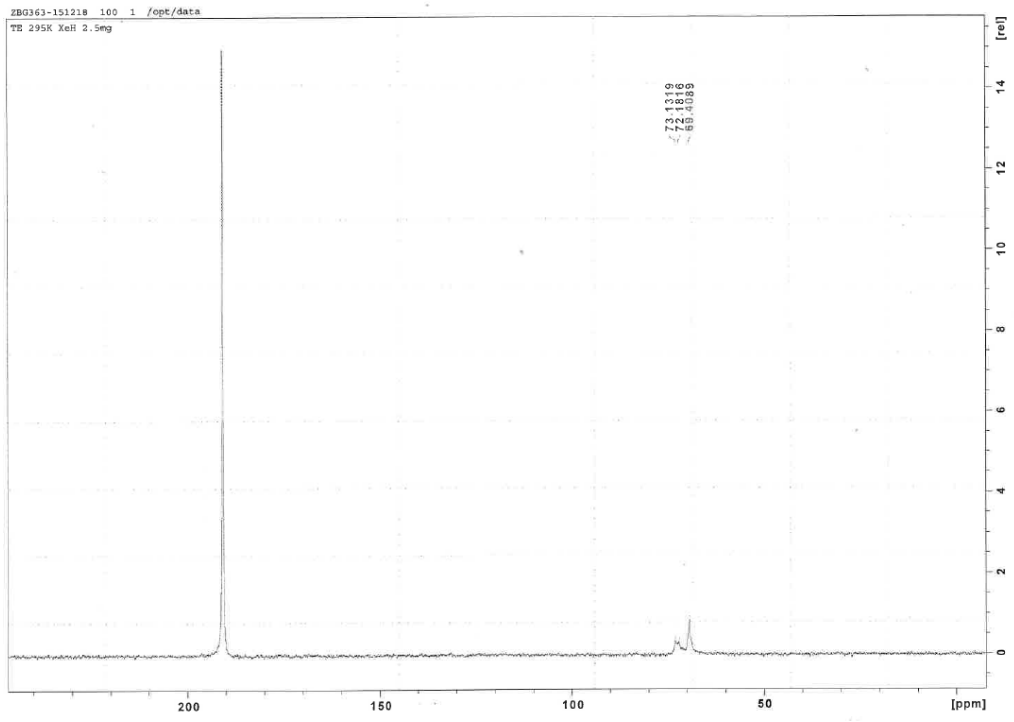

Figure 116: ^{129}Xe NMR spectrum of cryptophane **76** in water

The encapsulation of chloroform by cryptophane with different cavity sizes has been already reported.[131, 132, 133] Chloroform was currently used as a guest molecule in particular for the crystallization of cryptophane.[134, 135] It is anticipated that the affinity between these two molecules is mainly caused by Van de Waals interactions.[136] However, with an affinity constant which is by far lower than that of xenon, chloroform should not hamper the encapsulation of the gas. For example, the affinity constant between chloroform and cryptophane-A (which has more or less the same cavity size than cryptophane **76**) is 230 M^{-1},[137] while the affinity constant for xenon is 3900 M^{-1}.

Moreover, cyclotrimerization with a mixture of chloroform and formic acid has been widely used for synthesizing cryptophane carrying relatively sensitive substituent groups like allyl and no problem for xenon encapsulation has been reported. Therefore it seems highly probable that the PEG moieties have played a role in this unexpected phenomenon.

A possible explanation is that the presence of PEG has changed the cryptophane's affinity for chloroform, thus challenging the xenon encapsulation process. However the same sample of cryptophane **76** used for xenon NMR was previously dissolved in chloroform for proton NMR analysis without hampering the encapsulation of xenon in the latter experiments.

Another more plausible hypothesis might account for this phenomenon: when the cage is closed, an ethylene glycol motif might penetrate inside the cavity of cryptophane and then might block a molecule of chloroform inside the cage. Therefore the PEG moiety hampers the release of chloroform out of the cage, thus blocking the entrance of xenon molecule independently of the intrinsic affinity of xenon for cryptophanes (Figure 117).

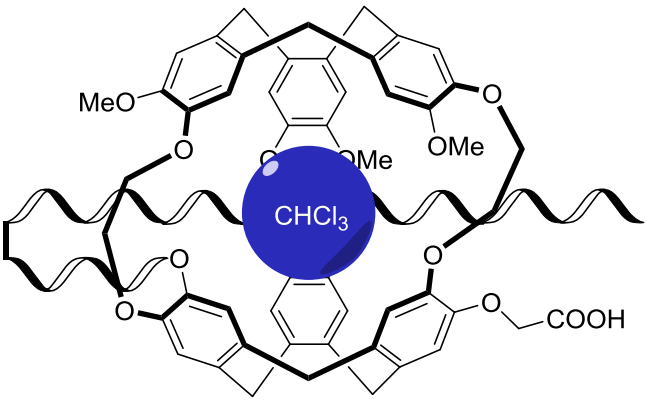

Figure 117: The simple conceptual drawing to explain the hypothesis that a part of the PEG chain, stuck inside the cryptophane cage, retained a molecule of chloroform inside the cryptophane.

This hypothesis might also account for the presence of the two unexpected signals in ^{1}H NMR. The peak around 5.1 ppm corresponds to protons of a partially encapsulated ethylene glycol motif and the other at around 8.1 ppm might be the signal of the encapsulated chloroform. Both signals are shifted for about 1 ppm related to their theoretical value because of interactions between the protons and the surrounding structure of cryptophane. Moreover, as the guest molecule inside the cage is so cumbersome, the cage itself has become more vulnerable and less stable than the free ones. This might explain propensity of the cage to

reopen upon heating in refluxing methanol, thus releasing both the PEG and the chloroform molecule as suggested by the vanishing unidentifiable signals in ^{1}H NMR.

iv. Hyperpolarized ^{129}Xe NMR analysis of cryptophane **76**

As shown in Figure 116, there is more than one signal corresponding to encapsulated xenon, suggesting that this multi-signal results from the coexistence of several distinct complexes in the tested sample.

As this product seemed already very pure in LC-MS (from the complicated ^{1}H NMR, it was difficult to estimate the purity of product), a purification by HPLC was carried out. Without discarding any obtained fraction, the original sample was separated into three adjacent fractions and each of them was retested by ^{129}Xe NMR (Figure 118).

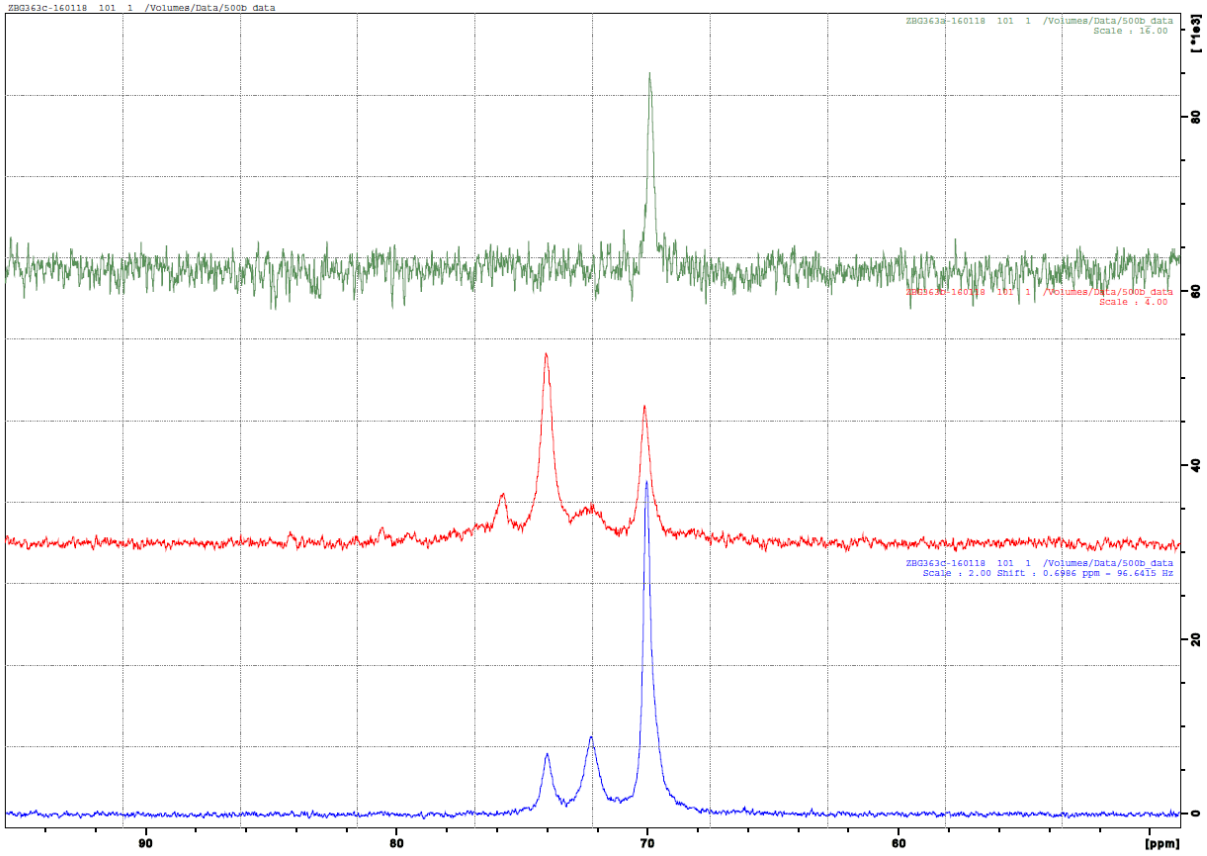

Figure 118: The ^{129}Xe NMR result for the three fractions after HPLC. Each spectum represents one of the fractions

Each fraction collected after HPLC separation was analyzed by xenon NMR as previously reported. The first fraction (20%, green spectrum), shows a single signal around 70 ppm. The second fraction (25 %, shown in red) and the third fraction (55 % in blue) also displayed the

same signal around 70 ppm, but also several other peaks nearby. The major fraction was separated in order to discriminate between the different constituents. The corresponding 3 collected fractions gave the same ^{129}Xe NMR spectrum than that observed from the third fraction, thus suggesting either the presence of *syn*-/*anti*- isomers, the chelation of cations by the PEG chains, the formation of aggregates etc. This question is presently under investigation.

v. Conclusions and perspectives

Cryptophane **76** was synthesized in seven steps in a non-optimized 1.4 % yield (if only the green fraction in Figure 115 was considered as the good product). This cryptophane displayed a good water-solubility (30 mg/mL) thanks to the presence of two PEG chains and is mono-functionalized with one carboxylic acid group. Moreover, it has shown a satisfactory capacity to encapsulate xenon. Consequently cryptophane **76** is a good candidate for the construction of ^{129}Xe NMR biosensors for *in vivo* applications.

Optimizations of yields and scale-up attempts are undergoing, leading us to explore the reasons accounting for the multi-signal problem in ^{129}Xe NMR. On the other hand, the coupling reaction between cryptophane **76** and a peptide linker is actually being investigated (Figure 119). The protected thiol group (underlined in red in Figure 119) in the targeted cryptophane-linker will be subsequently activated and used to bind the Cetuximab antibody through a classical thiol/maleimide addition, thus completing the construction of the biosensor for NSCLC.

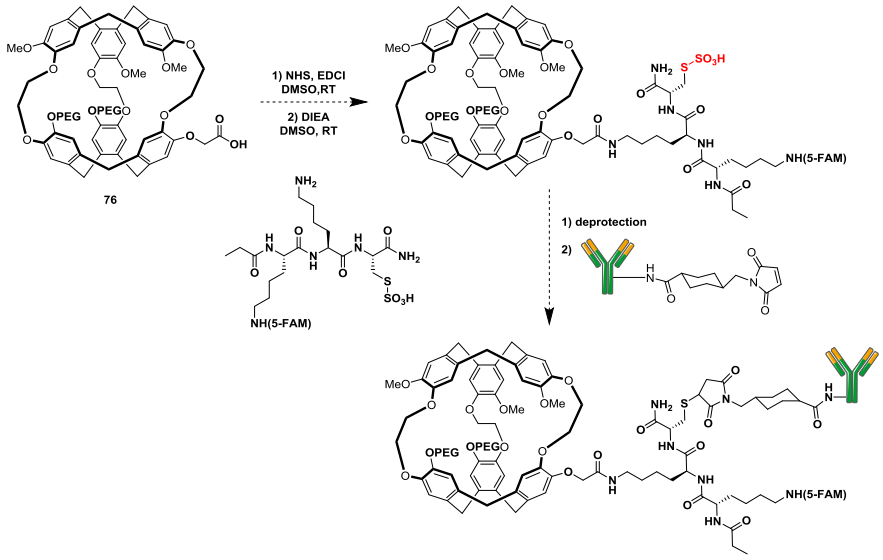

Figure 119: Perspectives of cryptophane **76** on its application for constructing biosensors

2. Cryptophanes based on mono-halogenation of CTVs

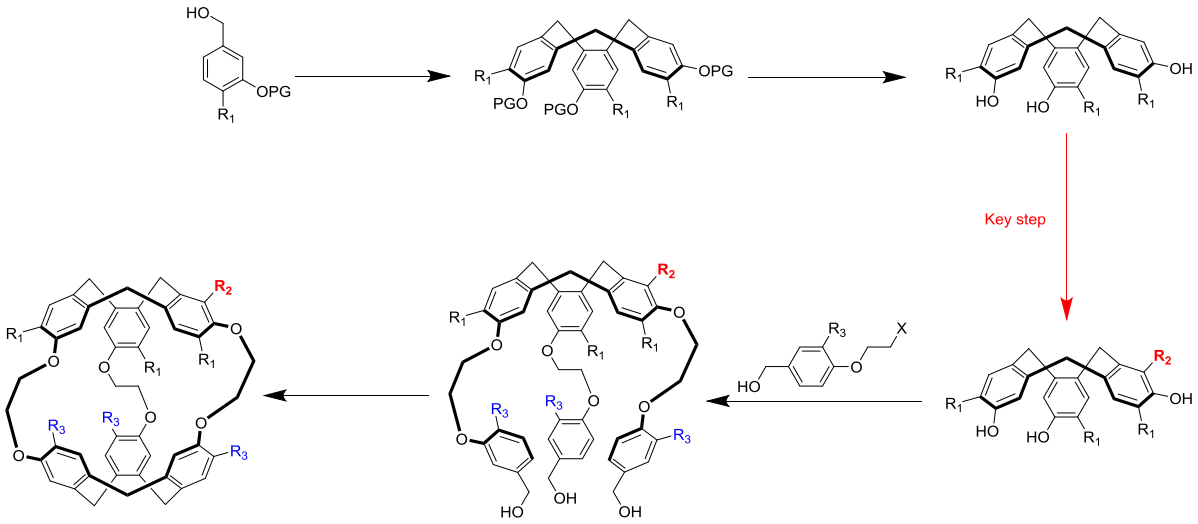

Figure 120: General description of the strategy "synthesis of PEGylated mono-functionalized cryptophane based on mono-halogenated CTVs". In this figure, R_2 represents a functionalizable group and R_3 represents the solubilizing group

An alternative to the desymmetrization of cryptophane by successive grafting of different benzyl moieties is the mono-halogenation of the CTVs followed by the subsequent conjugation of identical benzyl motif and cyclotrimerization. In the literature, halogenation reactions of phenoxy functions have been extensively described.[138] The presence of multiple chemically equivalent phenoxy functions in cryptophanes offers the possibility to achieve this kind of functionalization.

Several successful attempts of the halogenation of cryptophanes have been already achieved by our group. For the cryptophanes lacking of reactive positions (like cryptophane[111] **7**), this is the only reported method to achieve its functionalization.[83, 84, 86] The halogen atoms in cryptophanes **9** and **96** can be used for halogen-metal exchange reactions[139] or palladium-catalyzed coupling reactions[140] (Figure 121). Thus, the water-soluble moieties[84, 86] and different linkers[83, 84] can be added in view of applications to the development of biosensors.

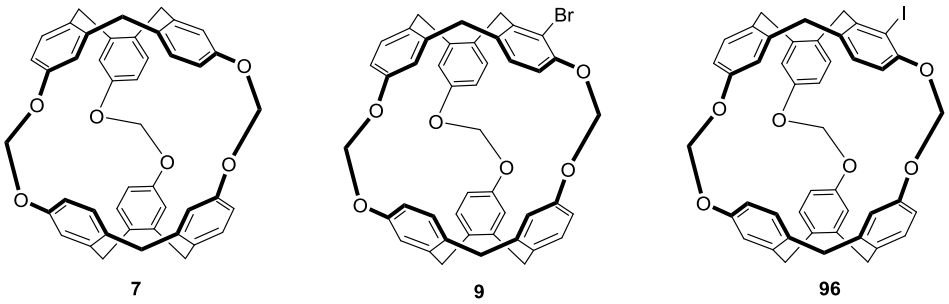

Figure 121: Structure of cryptophane[111] **7** and its halogenated product cryptophane **9** and **96**.

However, all previous halogenation reactions of cryptophane have been achieved in the cryptophane[111] series and no halogenation of cryptophane[222] was reported to date.

As shown by our previous attempts, the monohalogenation of PEGylated cryptophane is challenging: the remains of unreacted cryptophane and the formation of poly-halogenated cryptophanes will undoubtedly give a mixture of different PEGylated products which are presumably difficult to separate at the preparative scale. Therefore, we planned to break the symmetry of the CTV scaffold through mono-halogenation and to functionalize this asymmetric CTV with PEGylated linkers (Figure 122).

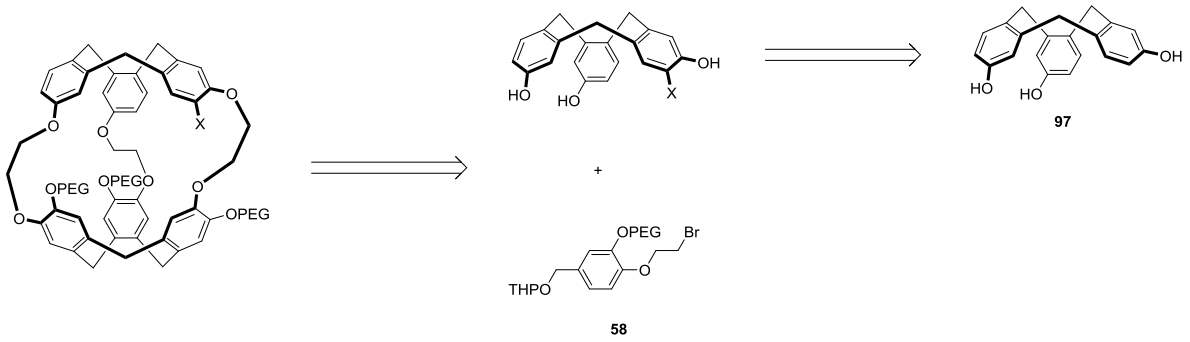

Figure 122: Retrosynthetic analysis of the PEGylated mono-halogenated cryptophanes.

a. Synthesis of mono-halogenated CTV

i. Synthesis of the symmetric CTV **97**

CTV **97** was chosen to be the platform for preliminary attempts of mono-halogenation because all the previous halogenation reactions were achieved on cryptophane[111] **7** which is obtained by coupling two units of CTV **97**.[59, 83]

To the best of our knowledge, there are three existing methods for synthesizing CTV **97**.[83, 141, 142] In our case, we chose the synthetic route developed by T. Traoré in our group thanks to its simplicity, inexpensiveness and the potentially easy scale-up (Figure 123).[143]

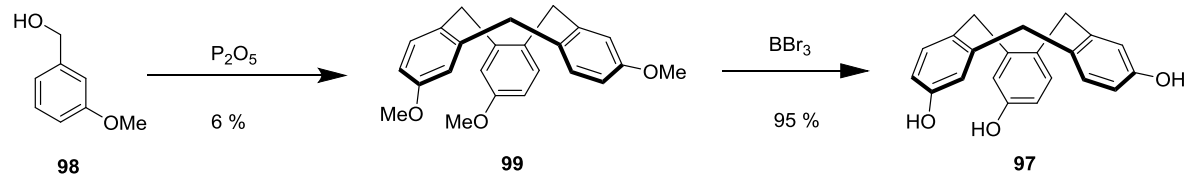

Figure 123: Scalable synthesis of CTV **97** developed by T. Traoré

Thus, CTV **97** can be easily synthesized in two steps in 6 % overall yield at the scale of 40 g within 3 days).

ii. Mono-halogenation of CTV **97**

This work was done by G. Milanole in our group.

Mono-iodation of CTV **97** was achieved by treatment with *N*-iodosuccinimide (NIS) in acetonitrile which gave a mixture of mono-iodinated CTV **100** along with di-iodinated CTV **101** and unreacted cyclotriphenolene **97** (Figure 124). Purification by silica gel flash-chromatography provided the desired mono-iodinated CTV **100** in a 72% isolated yield (yield based on done starting material CTV **97** which was easily recovered).

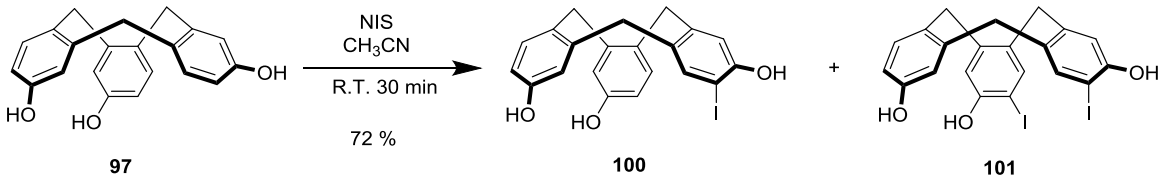

Figure 124: Mono-iodation of CTV **97**.

Iodination took place regioselectively: the ^{1}H NMR spectrum of CTV **100** clearly showed that iodination occurred at the *ortho* position of a phenoxy ring (Figure 124). The two singlets in the aromatic area at 7.74 and 6.99 ppm represented the two protons in *para* position at the iodinated aromatic ring (Figure 125).

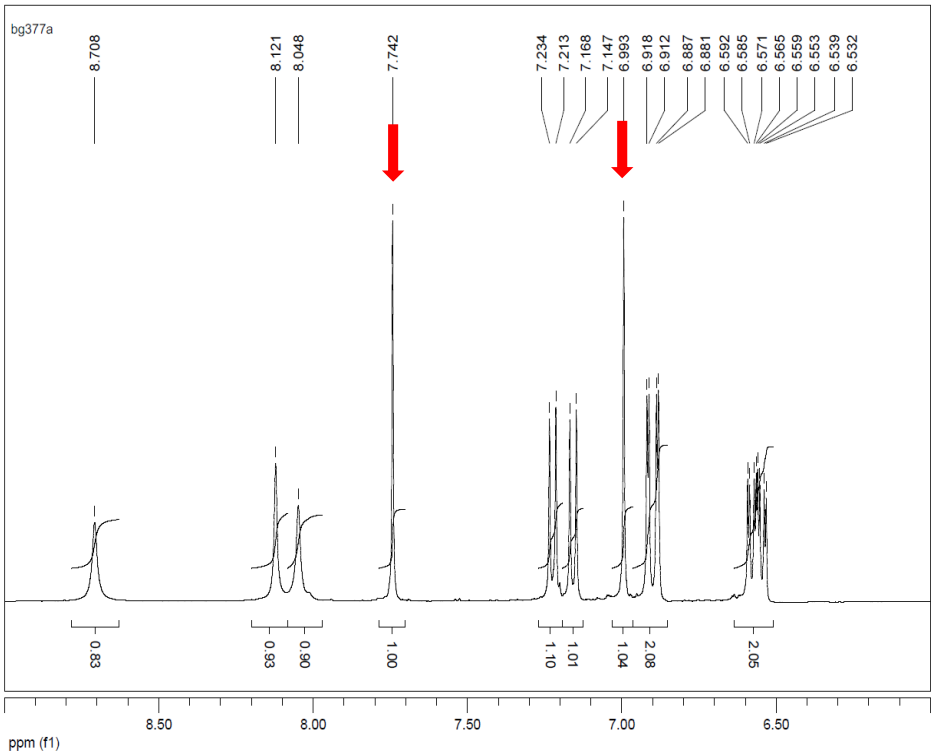

Figure 125: The aromatic area of the ^{1}H NMR spectrum of the mono-iodinated CTV **100**.

Similarly, mono-bromination of CTV **97** was achieved using *N*-bromosuccinimide (Figure 126). Surprisingly, a mixture of two regioisomers was obtained. Both compounds were easily separated by chromatography on silica gel to afford compounds **102** and **103** in 81% overall yield. Di-brominated CTV **104** was also observed and recovered (22 %).

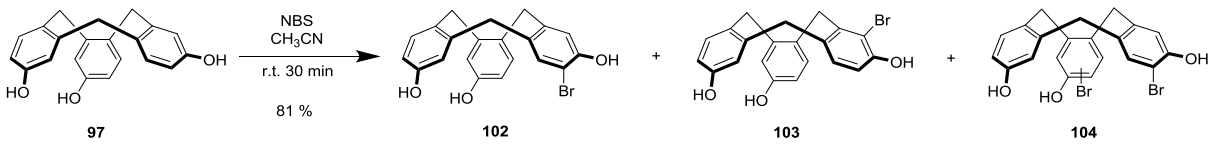

Figure 126: Mono-bromination of CTV **97**.

Desymmetrization of the CTV through mono-iodination/bromination offers new opportunities for the synthesis of functionalized cryptophanes. Subsequent discussion about the synthesis of PEGylated cryptophanes refers to the mono-iodinated CTV **100**.

b. Synthesis of a PEGylated mono-iodinated cryptophane

The synthesis was performed according to the classic "template method" (Figure 127). Deprotonation of CTV **100** with Cs_2CO_3, followed by treatment with the previously synthesized PEGylated linker **58** in DMF led to the *tris*-functionalized CTV **105** in 74% yield. Subsequent cyclotrimerization of this preorganized precursor with formic acid gave cryptophane **106** in a satisfying 41% yield. To conclude, from CTV **97**, the PEGylated mono-iodinated cryptophane **106** could be obtained in three steps in 22 % overall yield (1.3 % for five steps when starting from the commercially available product (3-methoxyphenyl)methanol **98**).

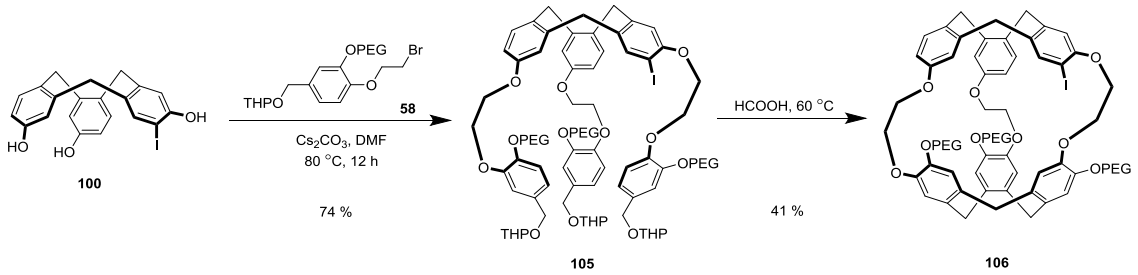

Figure 127: Synthesis of cryptophane **106** from CTV **100**.

i. The analysis of cryptophane **106** by ^{129}Xe NMR

The obtained cryptophane **106** was dissolved in water and then tested by ^{129}Xe NMR (Figure 128). Beside the large signal at about 197 ppm which corresponds to free xenon in water (Figure 128a), the signal related to the cryptophane-encapsulated xenon corresponds to 2 sharp signals at 70 and 56 ppm and a broad peak around 66 ppm (Figure 128-b).

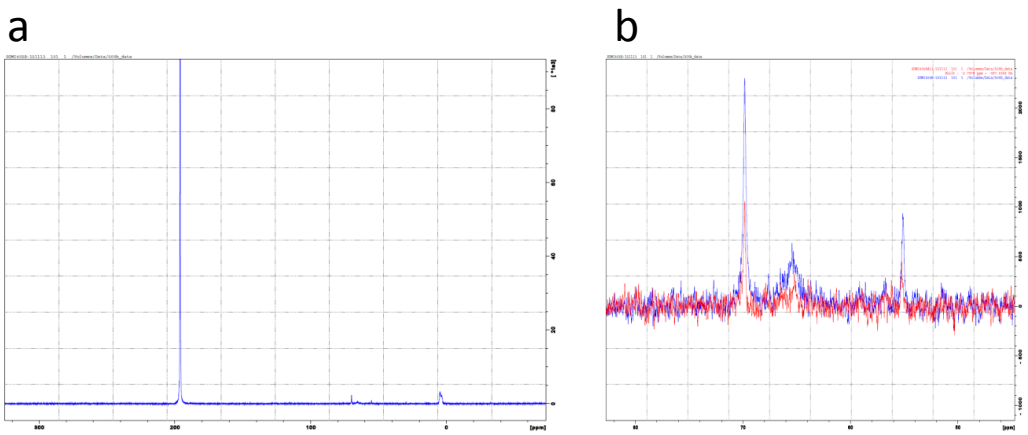

Figure 128: The ^{129}Xe NMR spectrum of a) the full range. b) the zoomed-in region between 50 ppm and 80 ppm.

In order to decide on the purity of the product, HPLC repurification of the original sample of cryptophane gave two different fractions with identical LC-MS profiles and ^{1}H NMR spectra. Both of the two fractions (which were called fractions A and B) were also analyzed by MALDI-TOF MS analysis in order to decrease the potential risk that the PEGylated cryptophane was not well-ionized in electrospray. Surprisingly, these two fractions revealed to be fully similar (Figure 129). In both fractions, the minor mass distribution corresponded to the correct mass of cryptophane **106** (M = 2383 +/- 44) and the major distribution corresponded the mass of cryptophane **106** plus a sodium cation (M + [Na^{+}] = 2406 +/- 44).

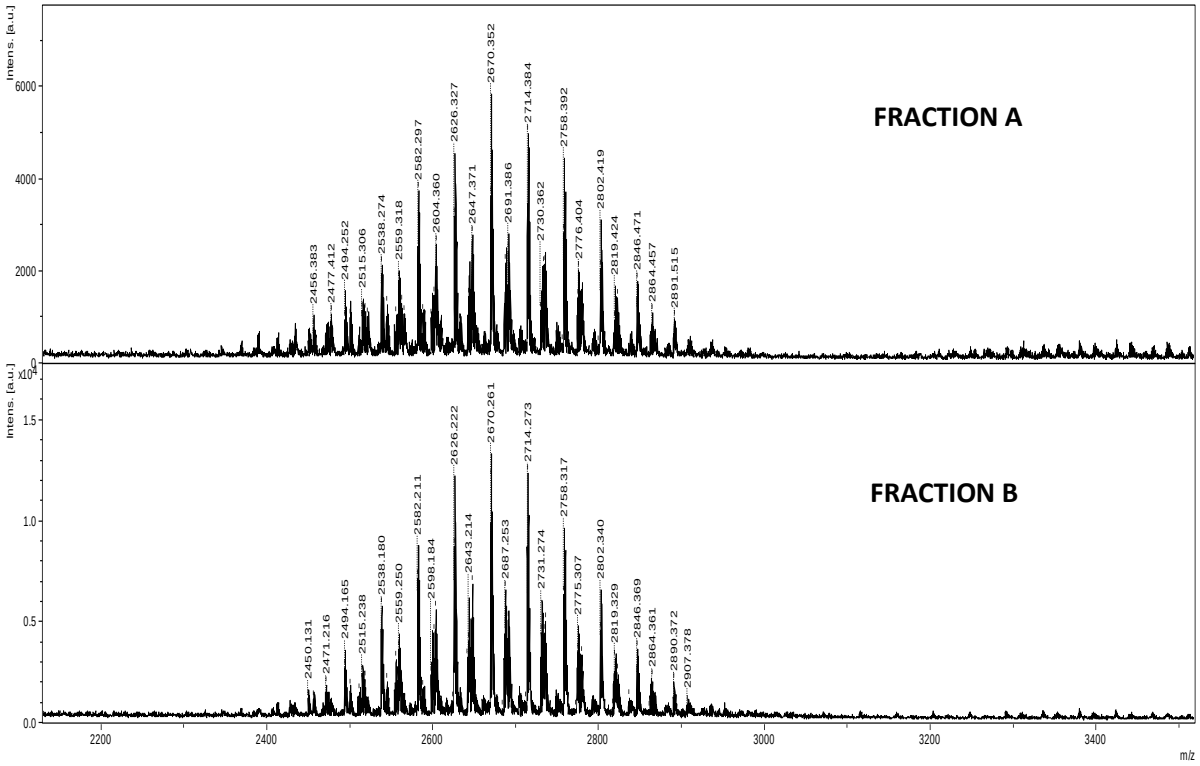

Figure 129: Result of MALDI-TOFMS analysis of fractions A and B. The samples were solubilized in a mixture 50/50 of water and methanol with 0.1 % of TFA.

Fractions A and B were retested by ^{129}Xe NMR. The resulting spectra displayed in Figure 127 exhibits large differences: fraction A shows two sharp peaks at 70 and 56 ppm (Figure 130-a) whereas fraction B shows a broad peak at 70 ppm (Figure 130-b). If the spectra of these two fractions were overlapped with the one from the sample before purification, it was obvious that these two sharp peaks in fraction A and the “crude” sample were well overlapped. On the other hand, the broad peak in fraction B was shifted about 5 ppm and had turned even more broad (Figure 130-c).

a) Fraction A

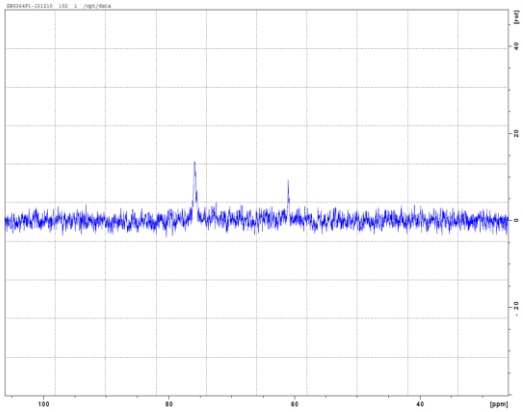

b) Fraction B

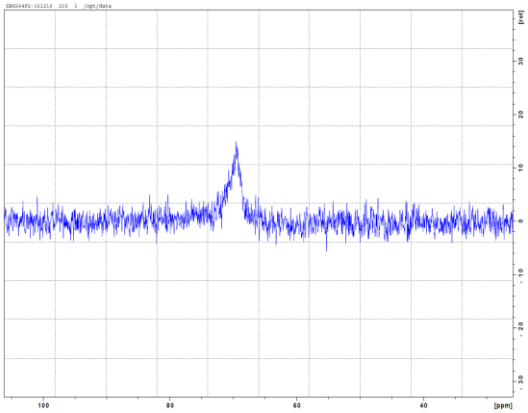

c)

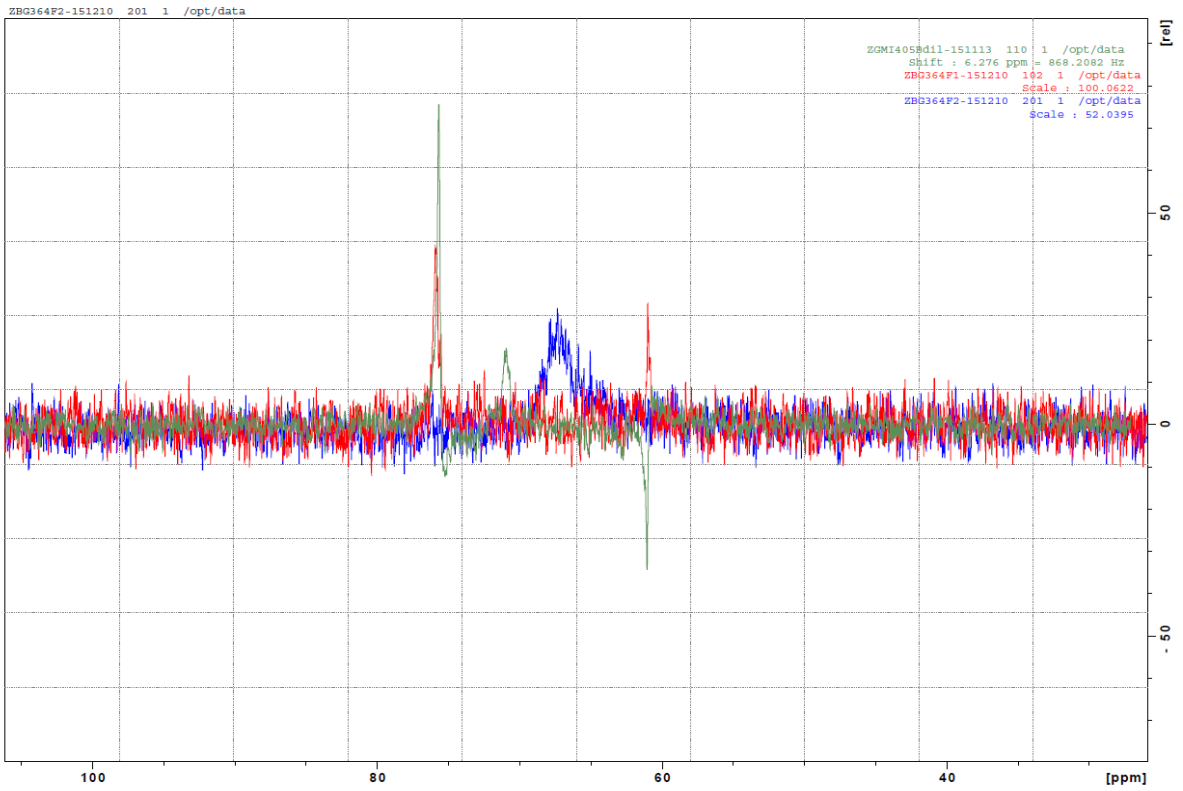

Figure 130: ^{129}Xe NMR spectra of a) fraction A. b) fraction B. c) spectra overlapped with the one obtained from the sample before purification of HPLC, in which the red curve represents the fraction A, the blue curve represents the fraction B, and the green curve represents the "crude" product

Considering the 5 ppm shift of fraction B relative to the mixture of A and B, we hypothesized that PEGylated cryptophane aggregates of various morphologies could form in water. With a hydrophobic cage and three hydrophilic PEG chains, the amphiphilic cryptophanes were assembled together to leave their hydrophilic parts outside and therefore form aggregates in aqueous solution.

In this way, several kinds and size of aggregates might coexist in solution, resulting in multi-peaks and broad signal in ^{129}Xe NMR. Changes in concentration and additives in solution (e.g. presence of salts) are anticipated to cause different distributions of aggregates, thus accounting for the shift and the change of widths of the broad peak.

In order to check the formation of aggregates, fraction A and fraction B were tested by dynamic light scattering (DLS) at the same concentration as the xenon NMR samples. DLS is a technique used to determine the size distribution profile of small particles in solution. A monochromatic light source, usually a laser beam, is transmitted to the sample through a polarizer. The hit particles scatter the light and thereby imprint information about their motion. Analysis of the fluctuation of the scattered light thus yields information about the particles. A diffusion coefficient can be calculated and the radius of the particles (which is related to this coefficient) can be thus determined.[143, 144]

DLS results are shown in Figure 131. The quantitative distribution of the sizes of particles (particles percentage in number) showed a distribution from 20 nm to 200 nm with the majority of size at about 40 nm, showing the presence of particles that are by far much larger than a single molecule of cryptophane **106**.

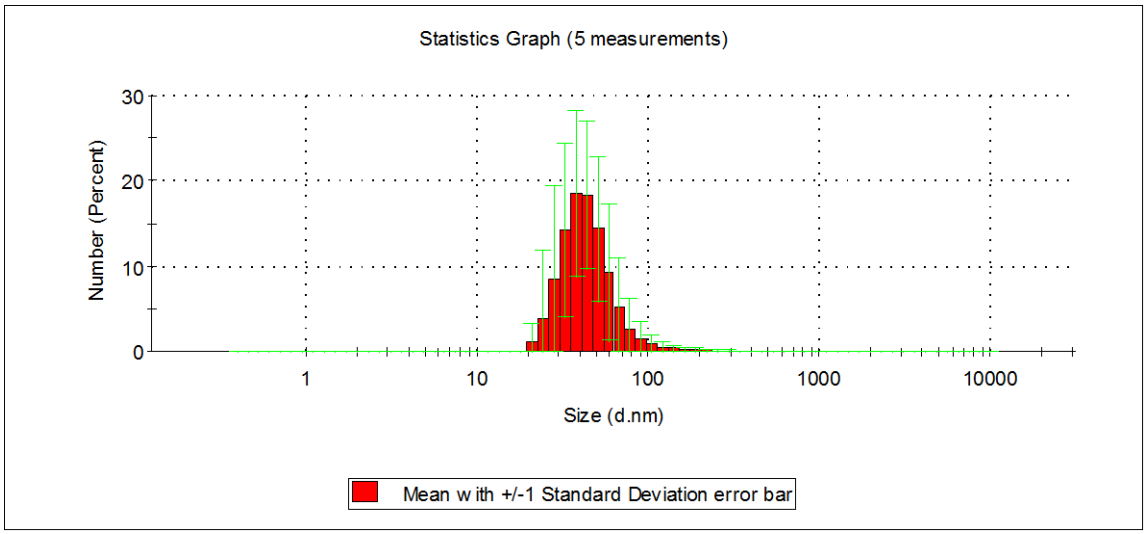

Figure 131: The results of DLS of fraction B

The same test performed with the fraction A demonstrated also the existence of big particles, and their sizes were even larger than the ones presented in fraction B (Figure 132).

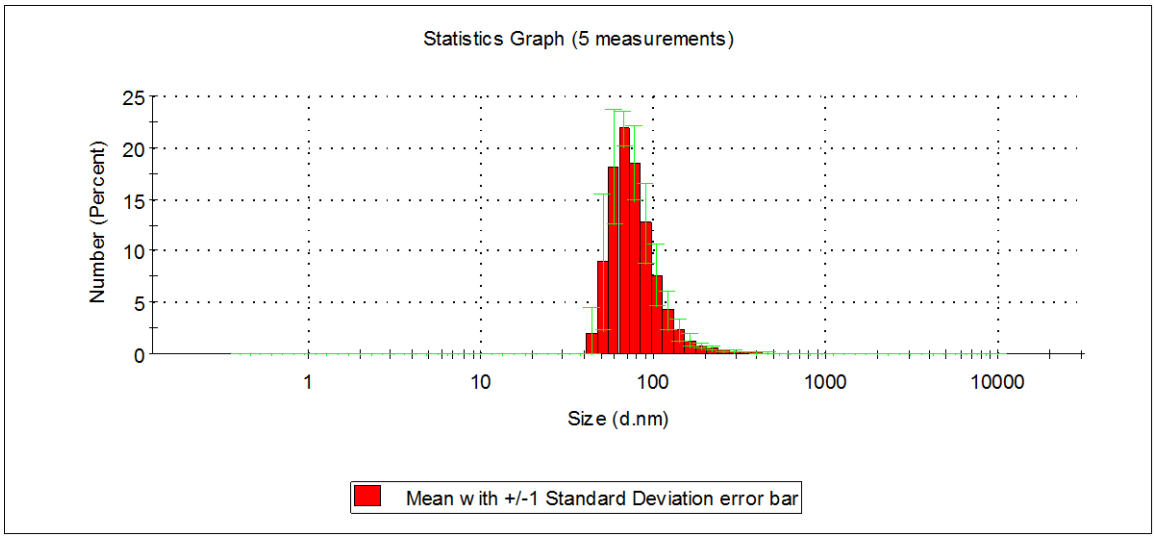

Figure 132: The results of DLS of fraction A

To confirm or invalidate this hypothesis, we performed a test of ^{129}Xe NMR in organic solvent in order to minimize the formation of aggregates. The two fractions were solubilized in tetrachloroethane since this bulky solvent is not expected to compete with xenon for encapsulation inside the molecular cage. However, except for the regular shifting caused by the change of solvent, there was no difference observed between the signals in water and in organic solvents (Figure 133). This result suggested that the multi-peak problem was caused neither by the formation of aggregations, nor the chelation between cations and PEG moieties.

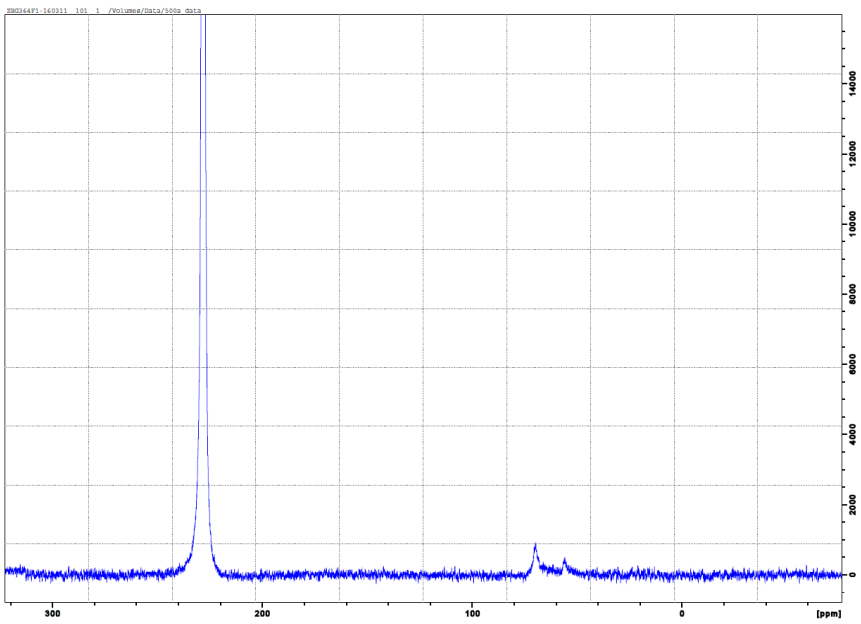

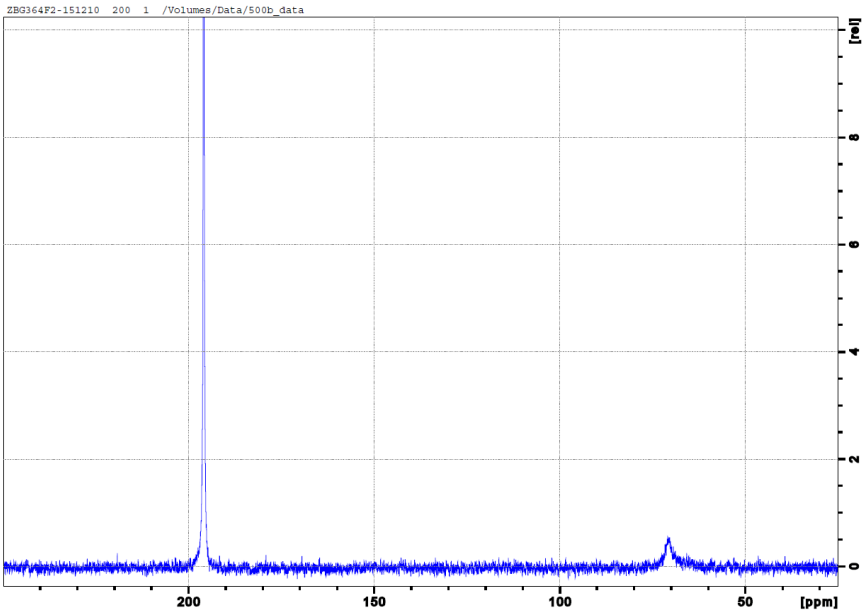

Figure 133: ^{129}Xe NMR results of fraction A (up) and fraction B (down) in tetrachloroethane

ii. Study of *anti*-/*syn*- isomers

Another possible reason for the multi-peak problem in ^{129}Xe NMR was the formation of *syn*-/*anti*- isomers of cryptophanes (Figure 134). For cryptophane[222], the formation of *syn*-isomers is reported[141, 145] but very disfavored because cryptophanes with an even number of carbon atoms in the bridges preferentially adopts *anti*-conformation. In fact, in our previous research on the tri-PEGylated cryptophanes **23** and **24**, the formation of *syn*-isomer was never observed.[87] However, in the case of cryptophane **106**, the presence of iodine might weaken the preference for the *anti*-conformation versus the *syn*-conformation.

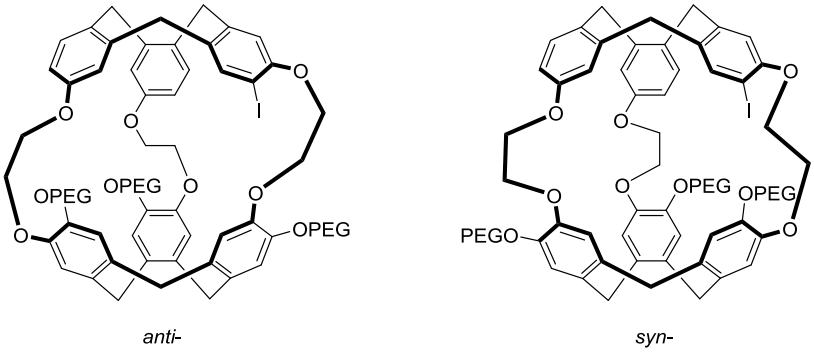

Figure 134: The possible *anti*-/*syn*- isomers of cryptophane **106**

Normally, the *syn*-/*anti*-isomers of cryptophane[222] could be easily separated by chromatography thanks to their clear difference in polarity,[146, 147] however the three long PEG

chains should engross the difference in polarity and consequently render the separation more challenging .

In order to study the influence of iodine atom on the *syn*-/*anti* preference, we decided to synthesize a mono-iodinated cryptophane without PEG moieties and to separate the two possible isomers (Figure 135).

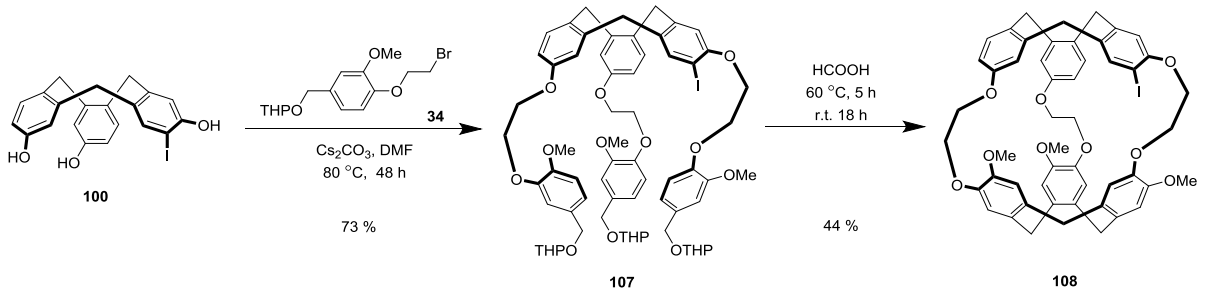

Figure 135: Synthesis of cryptophane **108** from mono-iodinated CTV **100**.

The synthesis of cryptophane **108** from mono-iodinated CTV **100** was roughly equivalent to that of cryptophane **106** by simply replacing the PEGylated linker **58** by molecule **34**. It should be mentioned that, in a general way this synthesis needed a longer reaction time compared with the synthesis of PEGylated cryptophanes possibly due to the poorer solubility of the intermediates and thus the functionalization of CTV **100** was carried out for 48 h. During cyclotrimerization, the reaction was heated to 60 °C for 5 h and then kept at room temperature overnight instead of being heated for 3 h at 60 °C as described for cryptophane **106**. After purification by chromatography, another adjacent fraction was also recovered besides the targeted product **108**, the LC-MS chromatogram of which showed two signals with a mass value corresponding to cryptophane **108** (Figure 136).

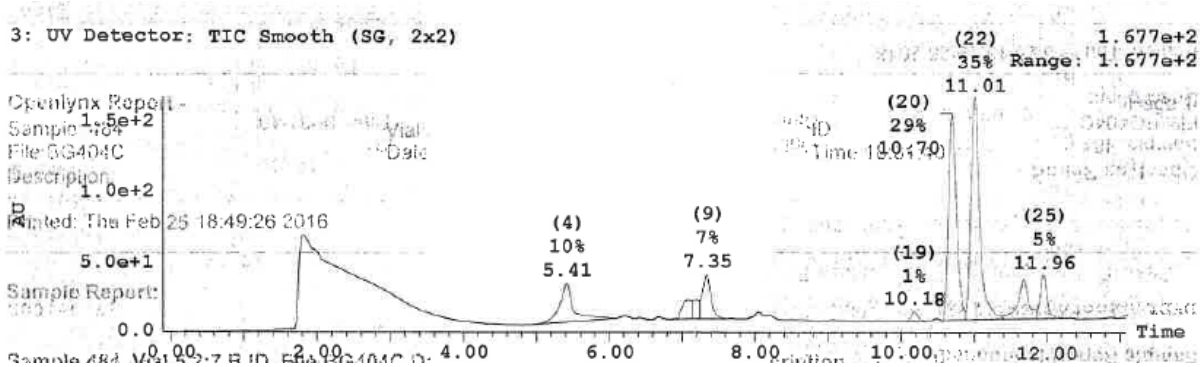

Figure 136: LC-MS chromatogram of two peaks (t=10.70 and 11.01) showing the same mass of cryptophane **108**

The presence of two different products in this fraction was also proven by thin layer chromatography (TLC) (Figure 137). With dichloromethane/ethyl acetate = 9/1 as the elution solvent, there was just one spot under UV. For the same sample with chloroform/ethyl acetate = 9/1 as the eluting solvent, the original spot was divided into two spots.

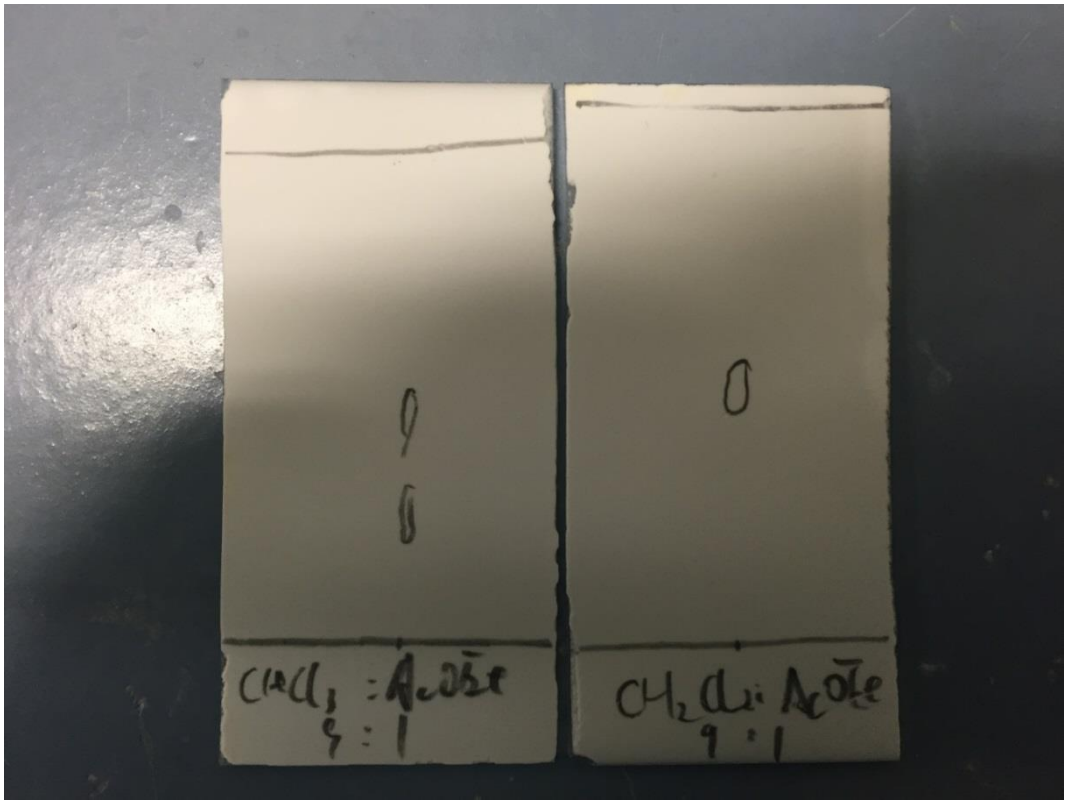

Figure 137: TLC result of the previously discussed fraction. On the left, the sample was eluted with chloroform/ethyl acetate = 9/1, and on the right with dichloromethane/ethyl acetate = 9/1

In order to separate these two products, a purification by preparative TLC was carried out using a mixture of chloroform/ethyl acetate = 9/1 as the eluent. The two products isolated, characterized with NMR and LC-MS, exhibit the same mass with different retention time in LC-MS and totally different spectrums in NMR. Therefore, this strongly suggests the formation of *syn*-isomer upon cyclotrimerization.

The two isomers of cryptophane **108** were also tested by ^{129}Xe NMR for comparison with the results obtained with PEGylated cryptophane **106**. The **108**-*anti* showed a nice single peak at about 74 ppm as expected (Figure 138). On the other hand, the encapsulation of xenon by **108**-*syn* was difficult to observe after only one scan, but the subsequent selective impulsion at the relative region revealed its signal at about 78 ppm (Figure 139).

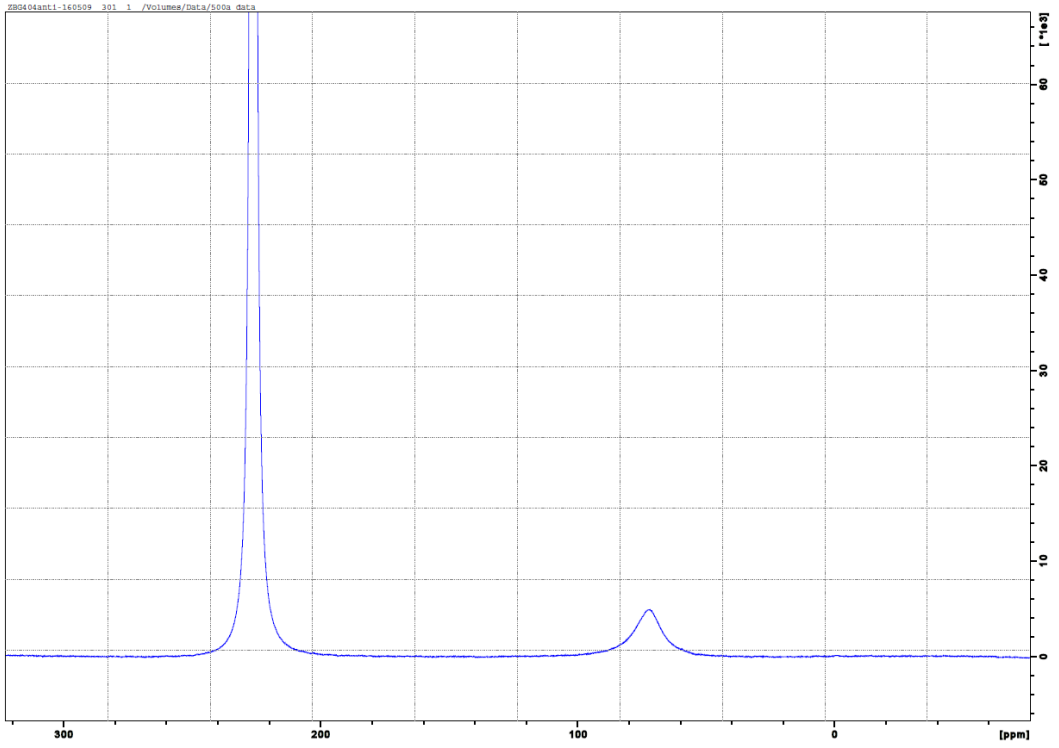

Figure 138: The ^{129}Xe NMR spectrum of the *anti*-isomer of cryptophane **108**

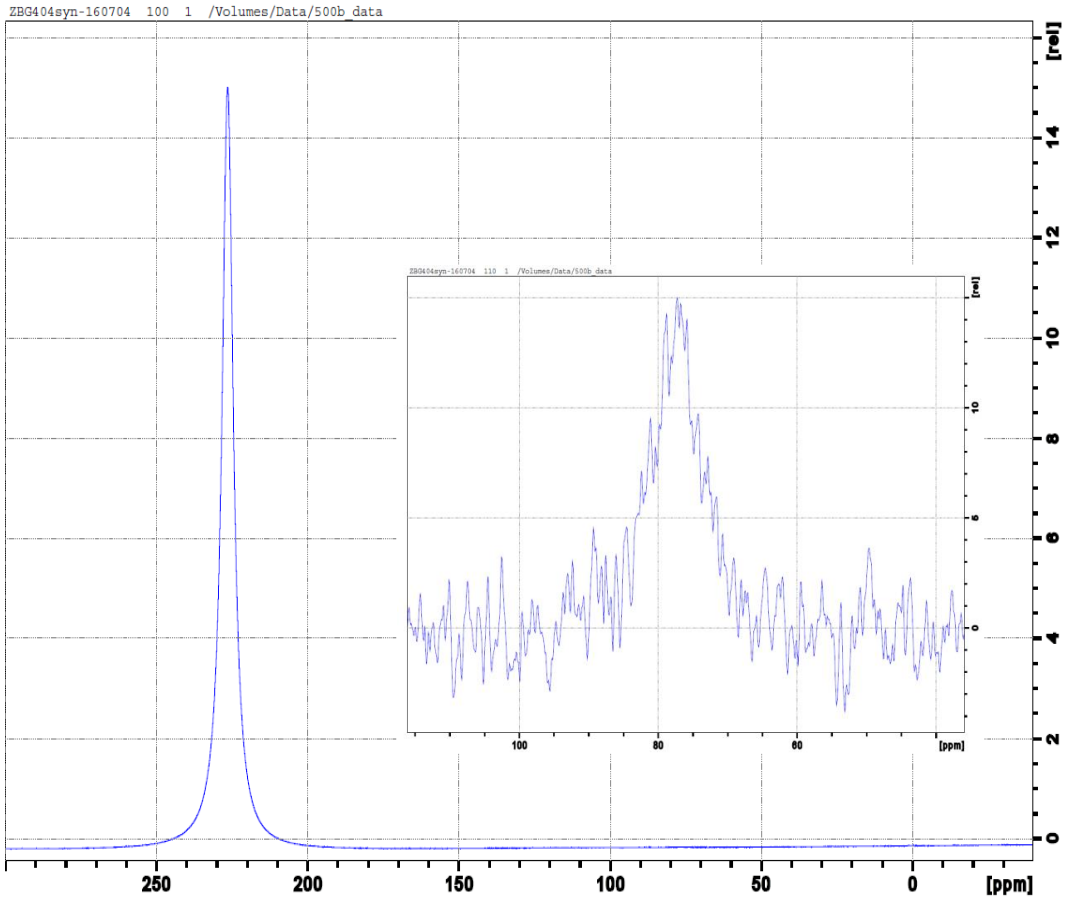

Figure 139: The ^{129}Xe spectrum of the *syn*-isomer of cryptophane **108**

This study of cryptophane **108** confirmed the formation of *anti*- and *syn*- isomers in the synthesis of mono-iodinated cryptophane[222], suggesting that a similar problem is very likely with cryptophane **106**. Since the PEGylated *anti*- and *syn*- isomers of cryptophane **106** were unlikely to be separated by chromatography, they coexisted in fraction A where they loom up as two sharp signals at 70 ppm and 56 ppm (Figure 130).

Unfortunately, there was no reliable explanation accounting for the broad signal in fraction B of **106**. However, fraction B was a separable minor fraction (less than 20 %) which is not a concern for the synthesis and applications of cryptophane **106**.

c. Synthesis towards a mono-ester PEGylated cryptophane

In the study carried out by G. Milanole, the mono-iodinated CTV **100** was tested towards different reagents to take full advantage of the presence of a suitably positioned iodine which is anticipated to be used for grafting a variety of chemical functions. Among them, the organolithium reagents have drawn a particular attention since the CTV could be easily functionalized with an electron-withdrawing group such as an ester which was useful for the conjugation of a peptide linker.

Thus, a synthetic route leading to the mono-ester PEGylated cryptophane **109** was designed as depicted in figure 140:

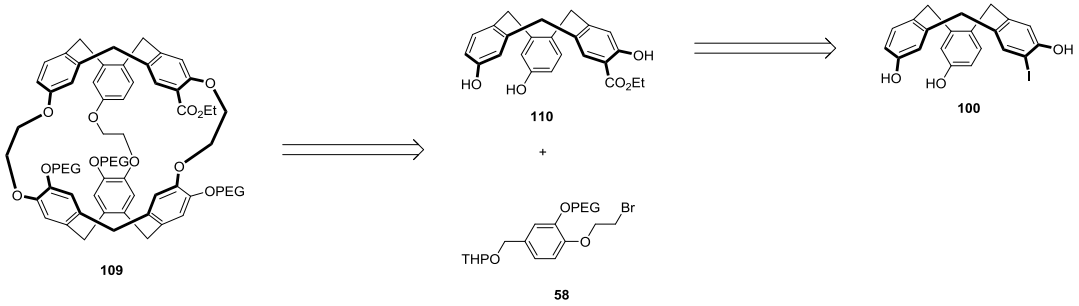

Figure 140: Retrosynthetic analysis of cryptophane **109**

Iodine-lithium exchange reaction on CTV **100** required the benzylation of phenolic moieties in order to mask the alcohol and to improve the solubility of mono-iodinated CTV in THF. Treatment of CTV **100** with benzyl bromide, K_2CO_3 and catalytic amount of tetrabutylammonium iodide (TBAI) led to the protected CTV **111** in excellent yield (Figure 141).

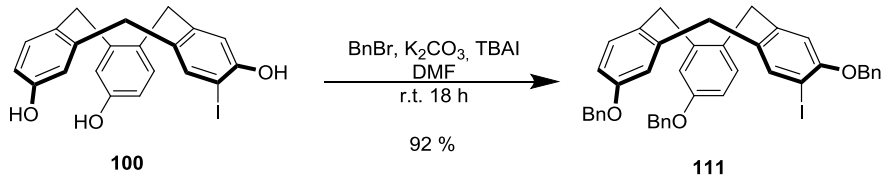

Figure 141: Protection of the phenol groups in CTV **100**

Subsequently, a halogen-metal exchange with *n*-BuLi at low temperature, followed by addition of ethyl chloroformate, converted the CTV **111** to the corresponding ester **112** (Figure 142).

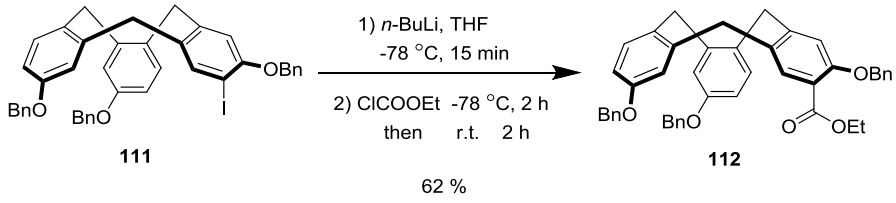

Figure 142: Halogen-metal exchange reaction of CTV **111**

Then, removal of the benzyl protecting groups by hydrogenolysis over Pd/C in EtOAc gave CTV **110** quantitatively (Figure 143).

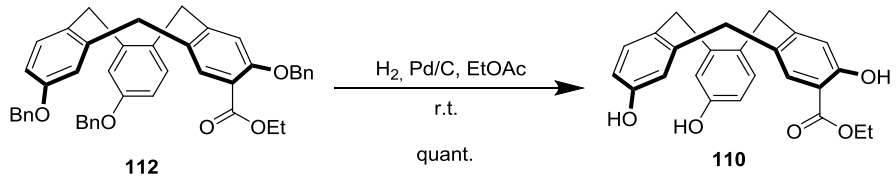

Figure 143: Removal of the benzyl groups in CTV **122**

Surprisingly, the time needed for this reaction was much longer than expected. The reaction was monitored by LC-MS to track the evolution of different intermediates. According to the result of the test (Table 10), the conversion was not totally completed after 96 h of reaction. During a long period of reaction, the major product was a mono-benzylated CTV. This very interesting observation suggests that it is possible to selectively deprotect a CTV and might be a simple and straightforward strategy for breaking the symmetry of the cryptophanes which will be discussed in part III-3.

	CTV **112**	Di-benzylated CTV	Mono-benzylated CTV	CTV **110**
0 h	100 %	0 %	0 %	0 %
24 h	75 %	4 %	17 %	4 %
48 h	31 %	9 %	43 %	17 %
72 h	2 %	15 %	16 %	67 %
96 h	0 %	0 %	0 %	100 %

Table 10: Evolution of different intermediates during the debenzylation. Percentages were calculated according to the chromatograms of LC-MS

The rest of the synthesis was performed according to the classical "template method" (Figure 144). The functionalization of CTV **110** with the PEGylated linker **58** was achieved in 51 % yield. The subsequent cyclotrimerisation was carried out in pure formic acid. The targeted cryptophane **109** was formed as the major product. Its purification by HPLC is presently under investigation.

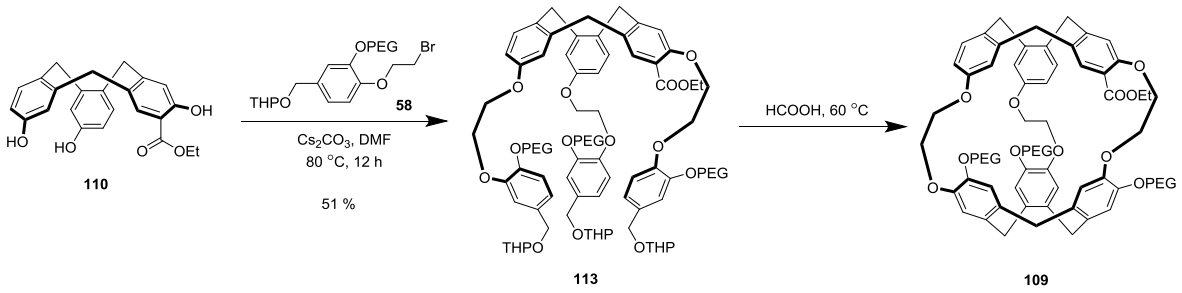

Figure 144: Synthesis to the mono-ester PEGylated cryptophane **109**

d. Conclusion and perspectives

Based on the mono-iodination reaction of CTV **97**, a PEGylated mono-functionalized cryptophane **106** was synthesized. This cryptophane could be obtained as a mixture of *syn*-/*anti*- isomers in three steps in 18 % overall yield (1.1 % for five steps when starting from the commercially available product **98**).

In order to study the formation of *syn*-/*anti*- isomers, a non-PEGylated mono-iodinated cryptophane **108** was also synthesized in three steps from CTV **97** (non-optimized 23 % overall yield). To the best of our knowledge, this is the first report of the synthesis of a mono-halogenated cryptophane[222]. The *syn*-/*anti*- isomers of cryptophane **108** were discriminated and separated by preparative TLC and their properties for encapsulating xenon were tested.

In order to hydrosolubilize cryptophane **108**, a demethylation reaction needs to be carried out. The resulting three free phenol groups can be used to introduce PEG moieties. However, considering the stability of the iodine group in the conditions used for demethylation (possibly with $LiPPh_2$), the iodine should be firstly removed to introduce a more stable and easily functionalizable group through a Sonogashira coupling reaction (Figure 145).

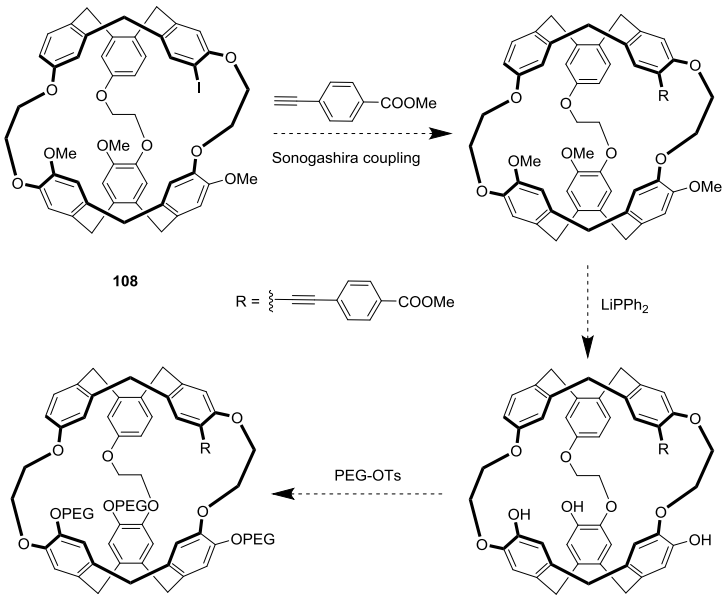

Figure 145: Perspective on the hydrosolubilization of cryptophane **108**

On the other hand, the synthesis of the PEGylated mono-ester cryptophane **109** was also attempted (Figure 144). The formation of **109** was well observed and its purification was under investigation.

3. Cryptophanes based on mono-protected CTVs

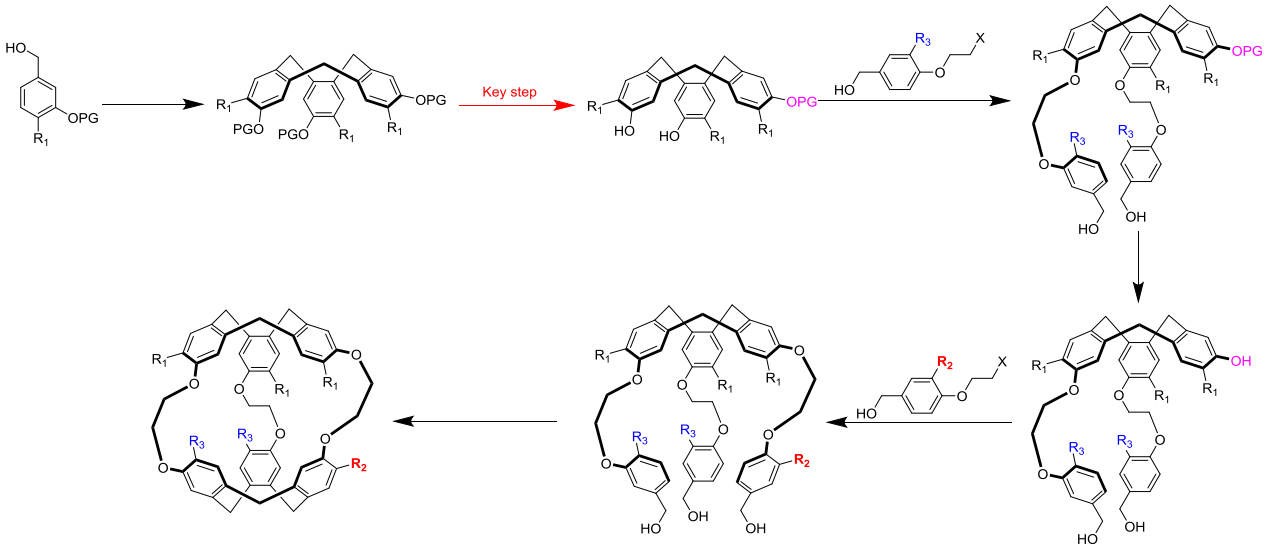

Figure 146: General description of the strategy "synthesis of PEGylated mono-functionalized cryptophane based on mono-protected CTVs". In this figure, R_2 represents a functionalizable group and R_3 represents the solubilizing group

This synthetic route is inspired by the synthesis of cryptophanol **31** published by A. Pines.[92] The key step to achieve the desymmetrization is the selective deprotection of CTVs and then different benzyl alcohol derivative linkers, including the PEGylated linker **58**, can be grafted.

In 2004, the group of A. Pines has reported a synthesis of cryptophanol **31** based on a mono-protected CTV **33** which was prepared through a selective deprotection of the tri-allylic CTV **32** using $Pd[P(C_6H_5)_3]_4$ as catalyst and Bu_3SnH (Figure 147).[92]

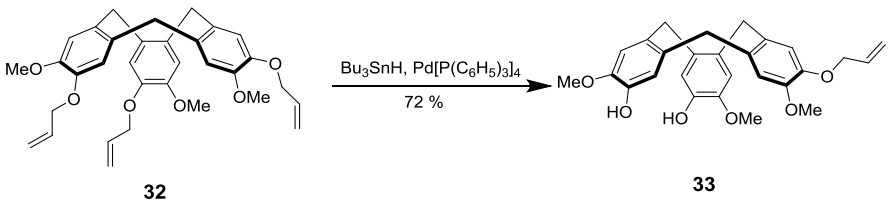

32 **33**

Figure 147: Selective deprotection of the allyl groups in CTV **32**.

The unquestionable advantage of this method is that the mono-protected CTV permits to use the benzyl alcohol derivative linkers in large excess in order to functionalize the desymmetrized CTV in better yields.

Taking advantage of our previous experience with the debenzylation of CTV **112**, we investigated the synthesis of mono-benzylated CTV **115** in order to functionalize it with an excess of PEGylated linker **58** as a precursor of desymmetrized cryptophanes. According to this synthetic route, the obtained di-functionalized CTV **114** should be successively debenzylated, functionalized with an excess of another benzyl alcohol derivative linker carrying a R group. The resulting grafted CTV can be finally cyclized to yield the targeted PEGylated mono-functionalized cryptophane (Figure 148).

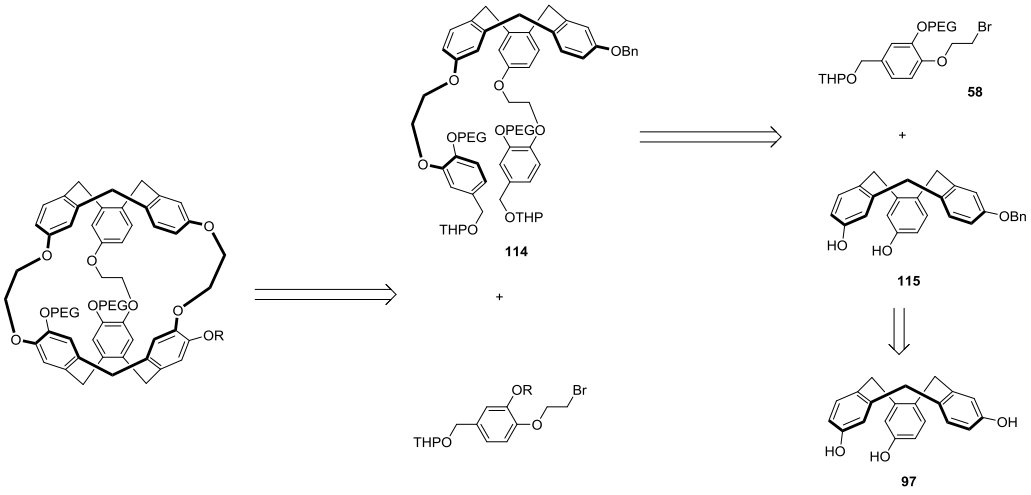

Figure 148: Retrosynthetic analysis of the strategy based on the use of the mono-protected CTV **115**.

Theoretically, the key step to implement this strategy is the synthesis of mono-protected CTV **115** from the corresponding tri-benzyl ether. For this purpose, treatment of CTV **97** with benzyl bromide, K_2CO_3 and a catalytic amount of tetrabutylammonium iodide (TBAI) as reported for CTV **100** was attempted (Figure 149). Surprisingly, in the absence of iodine, the kinetics of the benzylation was much slower and, after one night of reaction at room temperature, the major product obtained was the mono-benzylated product **115** in 55 % yield after purification (non-optimized). Therefore, this lower reactivity of the CTV revealed to be extremely interesting for the one-step early desymmetrization of cryptophanes.

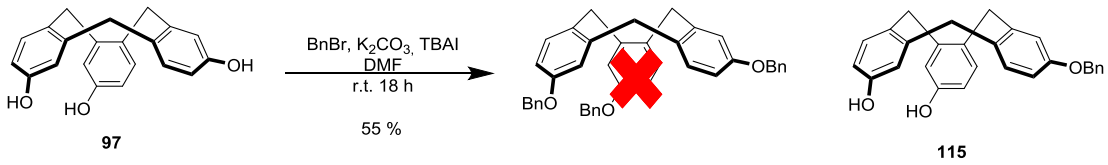

Figure 149: The benzylation of CTV **97**

The subsequent functionalization of CTV **115** with PEGylated linker **58** was easily achieved in classical conditions in 96 % yield. Unfortunately, the debenzylation reaction could not be achieved through hydrogenolysis with Pd/C or $Pd(OH)_2/C$ in the presence of acetic acid and therefore, we unfortunately failed to get product **116** (Figure 150).

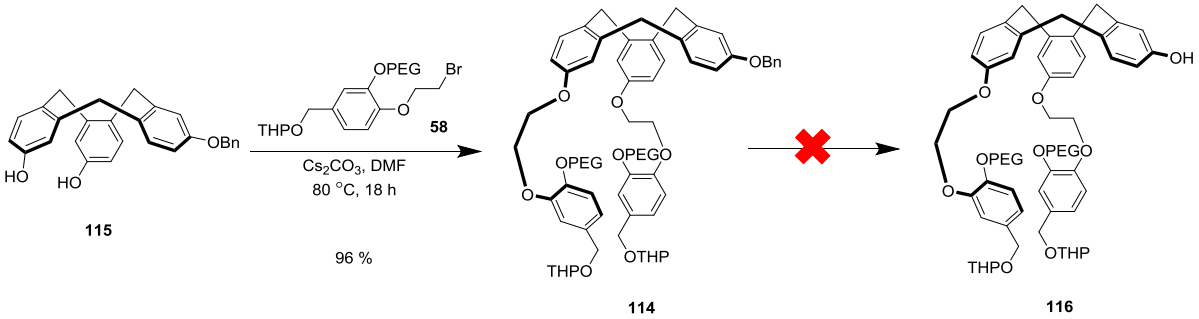

Figure 150: Functionalization of CTV **115** and subsequent debenzylation

Other conditions of debenzylation are being scanned and tested to achieve this reaction, including using other hydrogen donors such as triethylsilane[148] or ammonium formate[125]. Another option for the cleavage could be proposed such as using ozone[149] or 2,3-dichloro-5,6-dicyano-*p*-benzoquinone (DDQ)[150] to oxidize the benzyl ether to benzoate which allows for the subsequent hydrolysis of the resulting ester under basic conditions. There are also reports about using strong Lewis acid like boron trichloride (BCl_3)[151, 152] or using HBr in ionic liquid[153] to achieve this deprotection.

IV Synthesis of Asymmetric CTVs

Our previous attempts to break cryptophane symmetry suggest that the strategy is difficult to implement efficiently and is often marred by the uncontrollable formation of non-recyclable side-products and a large proportion of remaining starting material. Therefore, our experience suggests that the earlier the symmetry is broken, the more efficient the strategy is. For the "template method", the earliest possible point to break the symmetry of the system could be the first cyclotrimerization reaction leading to the formation of asymmetrical CTVs (Figure 151).

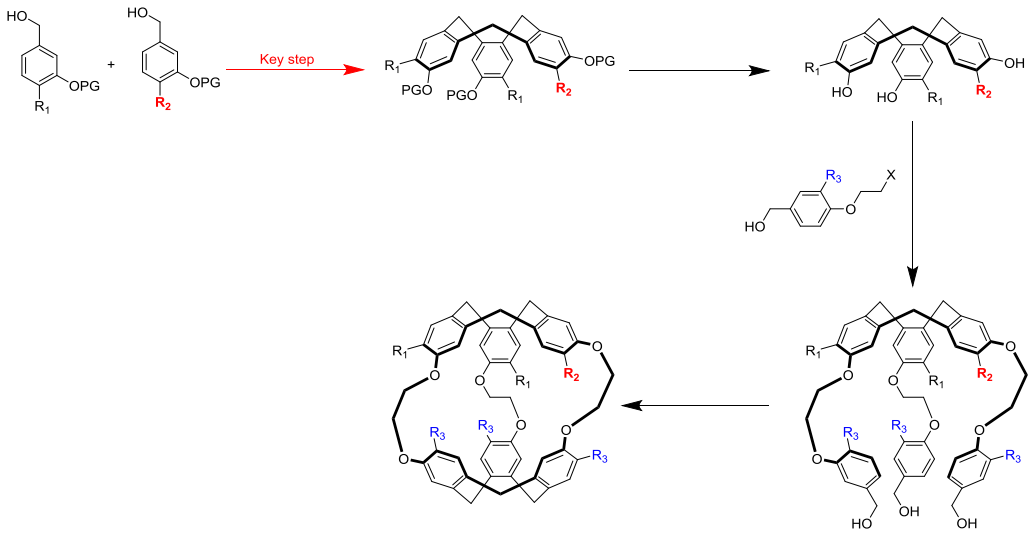

Figure 151: General description of the strategy "synthesis of PEGylated mono-functionalized cryptophane based on the synthesis of asymmetric CTVs". In this figure, R_2 represents a functionalizable group and R_3 represents the solubilizing group

Therefore we focused our interest on strategies based on the synthesis of an asymmetrized CTV scaffold and then using it as a universal precursor for the construction of unsymmetrical cryptophanes.

1. Design and retrosynthetic analyse

Symmetrical CTVs are usually formed by cyclotrimerization of three identical monomers. In part B-III, we have overall discussed how to break the symmetry of symmetrical CTVs. An alternative to this strategy could be to cyclize a mixture of two different monomers in order to form directly an asymmetric CTV which avoids the further desymmetrization of the molecule. Then the asymmetrical CTV is used as a scaffold for synthesizing mono-functionalized PEGylated cryptophanes through the standard "template method" procedure.

Ideally, the PEG groups should be born by the monomers in order to meet simultaneously the demand for hydrosolubility and for asymmetry. Therefore grafting a bis-PEG CTV with molecule **34** followed by a subsequent cyclotrimerization is expected to give a desymmetrized cryptophane (Figure 152).

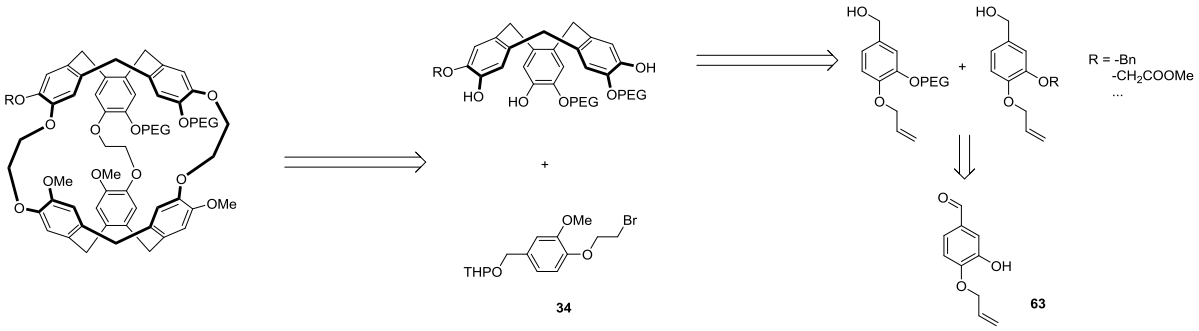

Figure 152: One possible retrosynthetic analysis of the mono-functionalized PEGylated cryptophanes based on the asymmetric CTV

An inverse (but equivalent) strategy involves the preliminary construction of a non-PEGylated asymmetric CTV and then its functionalization with the PEGylated linker **58**. The main advantage of this alternative is that potential difficulties in the purification of different CTVs related to the presence of the PEG motifs are avoided (Figure 153).

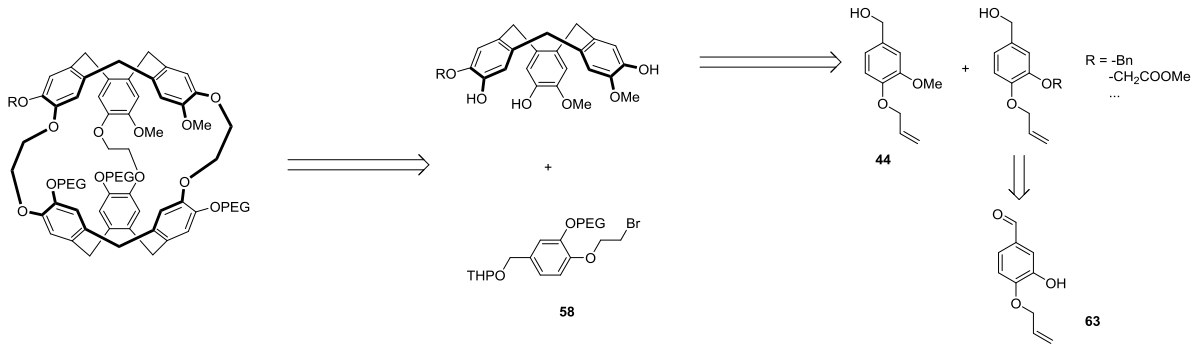

Figure 153: The other possible retrosynthetic analysis of the mono-functionalized PEGylated cryptophanes based on the asymmetric CTV.

As a matter of fact, we investigated both strategies which were evaluated for the simple and straightforward synthesis of asymmetric CTVs.

2. Synthesis of the benzyl alcohol derivatives

The preparation of the methylated monomer **44** (Figure 154) has already been presented in the synthesis of CTV **25** (Figure 82) One step of allylation from vanillyl alcohol gave quantitatively monomer **44**.

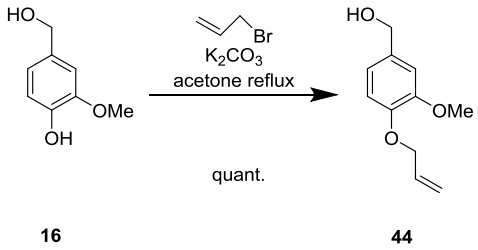

Figure 154: Synthesis of methylated monomer **44**

Other monomers can all be obtained in two steps from the previously synthesized allyl ether **63** (Figure 155). The main difficulty for synthesizing monomer **121** is that the reaction time of the reduction of the aldehyde moiety needs to be controlled after 10 min in order to avoid the simultaneous reduction of the methyl ether. Anyway, the yield of this reduction step is lower than that of the similar reduction of molecules **67** and **118**.

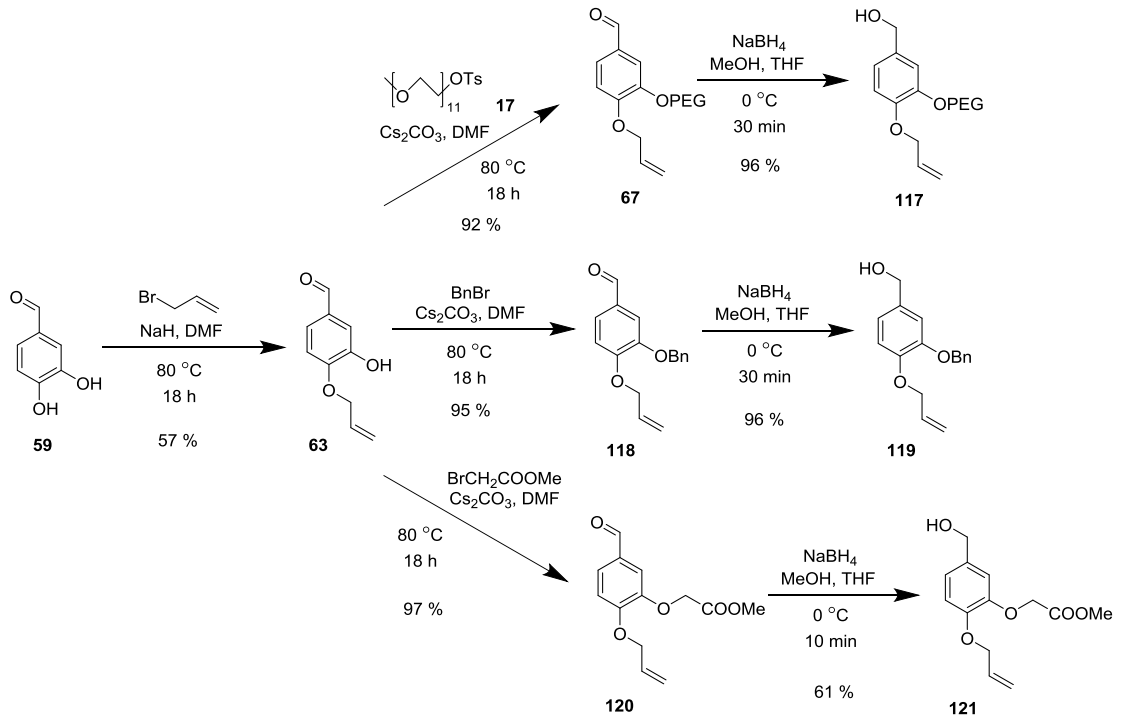

Figure 155: Synthesis of different substituted monomers

Finally all three monomers can be synthesized in three steps from the commercial 3,4-dihydroxybenzaldehyde **59** yielding 700 mg of the PEGylated benzylic alcohol **117** (50 % overall yield), 300 mg of the benzylated monomer **119** (52 % overall yield) and 1.2 g of the benzylic alcohol carrying methyl acetate **121** (34 % overall yield).

3. Synthesis of asymmetric CTVs by cyclotrimerization with different monomers

The first attempted cyclotrimerisation was performed with 2 equivalents of PEGylated monomer **117** and 1 equivalent of benzylated monomer **119**, aiming to generate CTV **122** bearing two PEG groups and one benzyl group usable for the further functionalization of the molecule (Figure 156). Unfortunately, the crude product revealed to be a complex mixture, the LC-MS analysis of which could not permit to detect the formation of the desired product. We anticipated that a polymerization occurred instead of the expected cyclotrimerization, leading to a mixture of unidentified oligomers. In this respect, cyclotrimerization of benzyl derivatives bearing side chains too different in size (-OPEG and –OBn) might favor the formation of bigger oligomers or polymers instead of the expected trimer. However it is difficult to draw a general tendency from this result since only one condition was tested for cyclotrimerization.

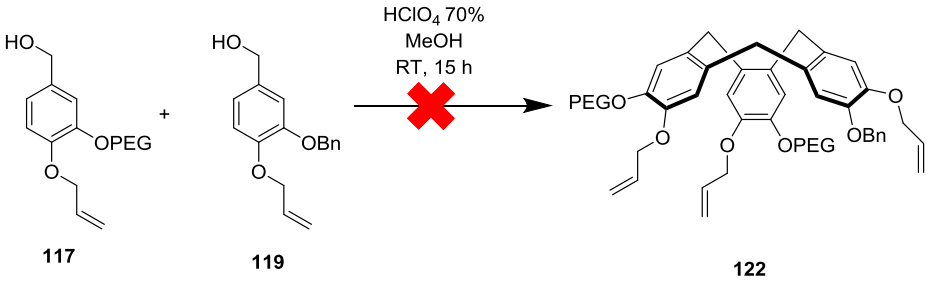

Figure 156: Cyclotrimerization between monomer **117** and **119**

Therefore, the synthesis of asymmetric non-PEGylated CTVs was investigated. Firstly, cyclotrimerization of a mixture of 2 equivalents of methylated monomer **44** and 1 equivalent of benzylated monomer **119** yielded the targeted CTV **123** along with CTV **32** (which comes from the homo-cyclotrimerization of 3 monomers **44**) (Figure 157).

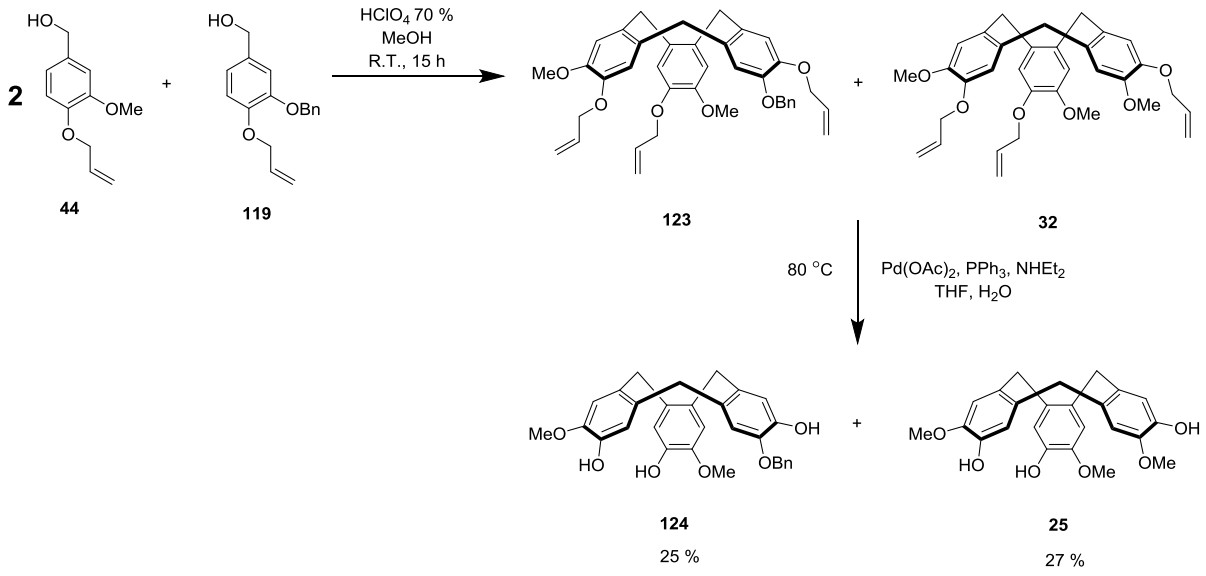

Figure 157: Cyclotrimerization between monomer **44** and **119** and the subsequent deprotection

Purification of these two CTVs by chromatography failed and therefore, the mixture was directly engaged in the next step. As a matter of fact, deprotection of compounds **124** and **25** is supposed to lead to the corresponding di and tri-phenol compounds which are expected to be more easily separable than their parent molecules. The three allyl groups of CTV **123** and **32** were cleaved by using palladium acetate, triphenyl phosphine and diethyl amine. The mixture of the deprotected CTV **124** and **25** were obtained. As anticipated, the separation of these two CTVs by silica gel chromatography was successful, giving the asymmetric CTV **124** in 25 % overall yield for two steps. CTV **25** was also recovered in 27 % overall yield and can be reused for other synthesis since it is an important intermediate in the syntheses of different cryptophanes (Figure 157).

A second attempt was performed with 2 equivalents of monomer **44** and 1 equivalent of monomer **121** which enabled the direct introduction of a methyl acetate group already available for functionalization. After cyclotrimerization, a mixture of three different CTVs was obtained as depicted in Figure 158.

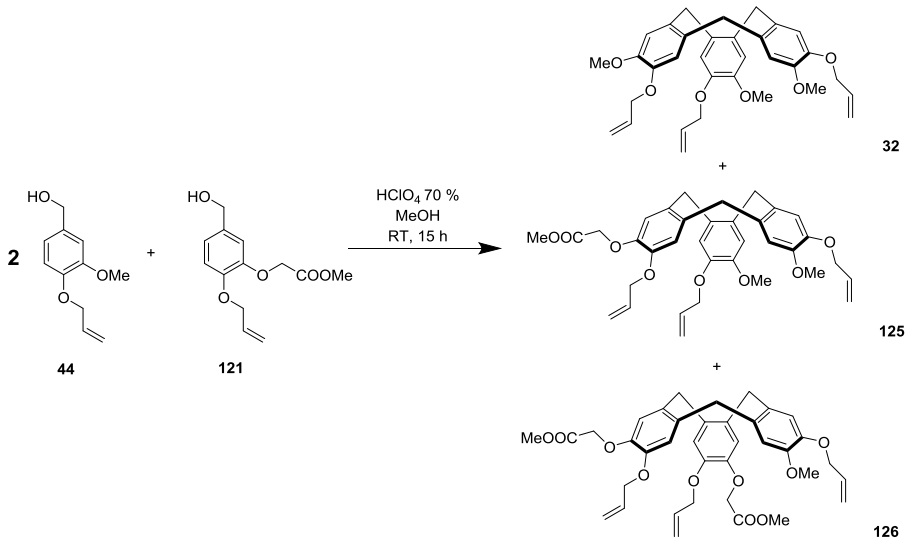

Figure 158: Hetero-cyclotrimerisation of monomers **44** and **121**

Unfortunately, the polarity of CTV **32**, **125** and **126** revealed to be less different than that of CTV **32** and **123**, rendering the purification step more difficult to achieve. Two different strategies were evaluated for separating the 3 CTVs.

The first one was the same strategy which had been used for the purification of CTV **123**. The mixture of three CTVs was engaged in the deallylation: besides the expected CTV **25**, carboxylic acid derivatives **127** and **128** were obtained by hydrolysis of the corresponding esters (respectively **125** and **126**). The crude mixture was treated by liquid/liquid extraction: CTV **25** remained in the organic phase whereas CTV **127** and **128** were essentially distributed in the aqueous phase (Figure 159).

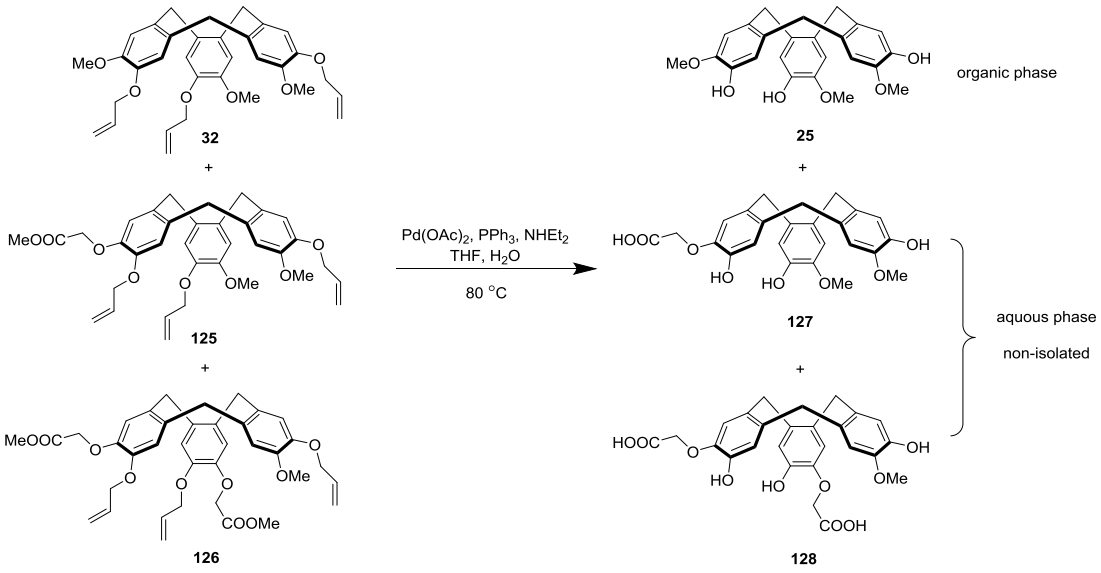

Figure 159: Deallylation of the CTV **32**, **125** and **126**

Since CTV **25** was already eliminated, we focused our interest on the separation of CTV **127** and **128**. Unfortunately, these products could not be separated either by normal-phase or reversed-phase chromatography.

Therefore, the cyclotrimerization reaction was reconsidered in order to favor CTV **32** and **125** and minimize the formation of CTV **126**. Different ratios between monomer **44** and **121** were tested. On the basis of the LC-MS analysis of the different crude products, we observed that the proportion of CTV **126** in the crude mixture was reduced to 2% when the **44**:**121** ratio was larger than 6/1 (Table 11).

Ratio **44** : **121**	2 : 1	3 : 1	4 : 1	5 : 1	6 : 1	8 : 1
CTV **32**	50 %	57 %	62 %	66 %	68 %	71 %
CTV **125**	35 %	32 %	30 %	30 %	32 %	27 %
CTV **126**	15 %	11 %	8 %	4 %	2 %	2 %

Table 11: Results of cyclotrimerization with different ratios of monomer **44**:**121** engaged. All the percentages were calculated according to their LC-MS chromatograms

The cleavage of the allyl ether was performed on the mixture of CTV **32** and **125** and, after liquid/liquid extraction, CTV **25** distributed into the organic phase whereas the targeted CTV **127** was essentially dissolved into the aqueous phase. CTV **127** was then purified by chromatography in order to eliminate a few oligomers, giving the pure asymmetric CTV **127** carrying one carboxylic group in 14 % overall yield (two steps without optimization).

The main advantage of this strategy was the easy elimination of CTV **25** (the main side-product) by simple liquid-liquid extraction. Moreover, the unexpected acidification permits to save one step for the whole synthesis. Nevertheless, to carry out this synthesis successfully, the ratio of the two monomers should be fixed to 6 : 1 or even more and optimization of the relatively poor yield seems illusive.

In order to solve this problem, an alternative strategy was investigated. This strategy implies the saponification of the mixture of CTV **32**, **125** and **126** with NaOH which do not affect CTV **32** (Figure 160). Therefore it is possible to discriminate between CTV **129** (mono-acid) and CTV **130** (di-acid) which display significantly different polarities. Thus, the

asymmetric CTV **129** was purified to yield 14 % for two steps without any optimization. Although this yield was relatively low, it might be optimized by increasinging the quantity of monomer **121** used for the cyclotrimerization in order to favor the formation of CTV **125** versus CTV **32**. Tuning the **44**:**121** ratio (Figure 157) for this purpose is currently under investigation.

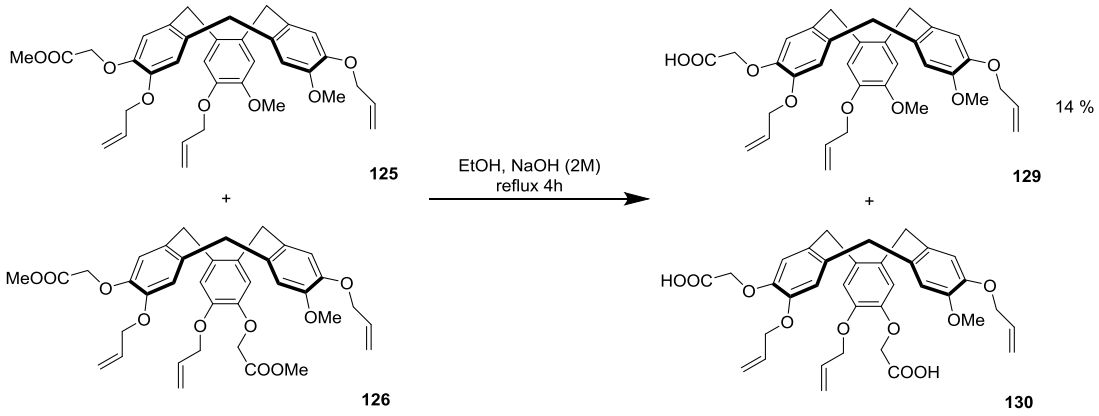

Figure 159: Saponification of the mixture of CTV **125** and **126**.

Then the O-allyl groups of CTV **129** were cleaved in standard conditions (Figure 160). The crude product was relatively pure and thus was directly engaged in the subsequent functionalization with the PEGylated linker **58** (49 % overall yield for two steps, presented in the next part).

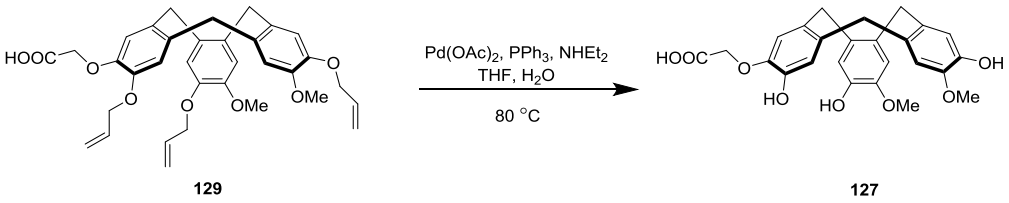

Figure 160: Cleavage of the O-allyl groups in the CTV **129**.

Asymmetric CTVs **124** and **127** are very interesting intermediates which can be directly used for the synthesis of water-soluble mono-functionalized cryptophanes.

4. Synthesis of a mono-acid PEGylated cryptophane

As mentioned above, the crude product of CTV **127** can be directly engaged in the functionalization by O-alkylation with the PEGylated linker **58**. Synthesis of the functionalized CTV **131** was performed in 49 % overall yield (two steps together) (Figure 161).

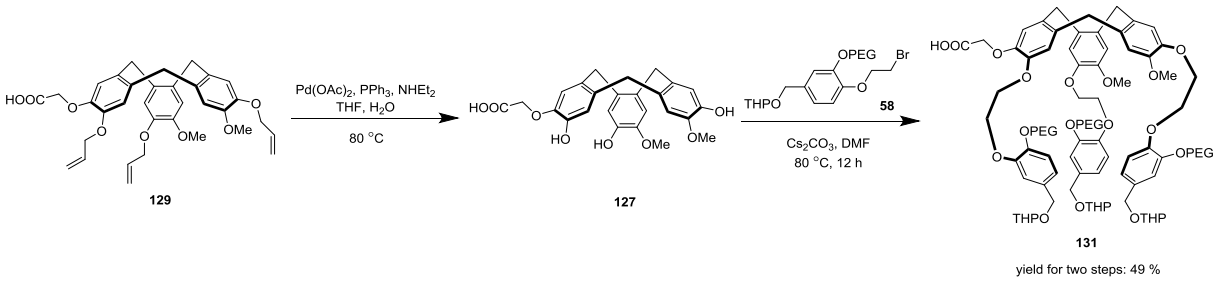

Figure 161: Deprotection of CTV **129** and the subsequent functionalization with **58**.

Then CTV **131** was cyclized in pure formic acid (Figure 162) to give cryptophane **132** which was isolated in 65 % yield after purification. This CTV showed to be water-soluble with three PEG chains and is mono-functionalized with one free carboxylic acid.

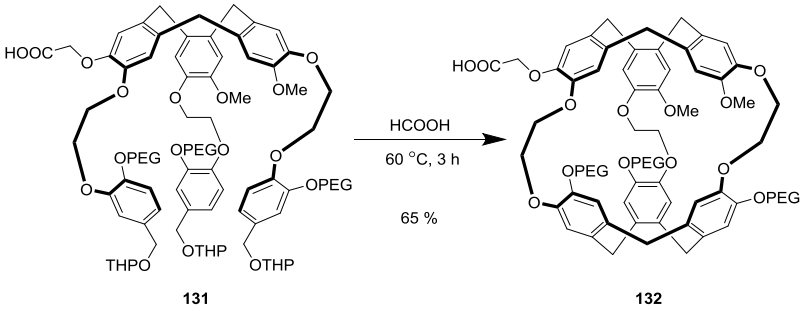

Figure 162: Cyclotrimerisation of functionalized CTV **131**.

As a conclusion, the PEGylated mono-functionalized cryptophane **132** was performed in seven or eight steps (depending on the strategy for obtaining CTV **125**) from the commercial 3,4-dihydroxybenzaldehyde **59**. This synthetic route enables to isolate compound **132** at a scale of 30 mg in a non-optimized 1.5 % overall yield. There is no doubt that the yields can be improved in particular by augmenting the proportion of monomer **121** used in the cyclotrimerization step (Figure 157). Before this research is undertaken, we are presently investigating the xenon-encapsulation properties of cryptophane **132** in order to evaluate its response in xenon NMR.

GENERAL CONCLUSIONS AND PERSPECTIVES

The objective of this Ph.D. work was to design and synthesize new cryptophanes usable for the construction of ^{129}Xe NMR biosensors. These cryptophanes should satisfy three criteria: a satisfactory affinity and exchange rate for xenon gas compatible with *in vivo* ^{129}Xe MRI experiments, a good solubility in water, and the capacity to be specifically bio-conjugated in order to be inserted inside a bio-probe. We selected cryptophane [2,2,2] as the molecular cage since it displays both a good affinity and an exchange rate which enables xenon renewal with a sufficient turnover. The intrinsic poor hydrosolubility of cryptophanes was overcome by the grafting polyethylene glycol (PEG) moieties although the presence of bulky and polydisperse moieties raises specific synthetic issues. Different strategies were envisioned to synthesize PEGylated mono-functionalized cryptophanes and their development was the core of this PhD work.

After an overall analysis of the classic "template method" of synthesizing cryptophane[222], five possible strategies to achieve the mono-functionalization of the molecular cage were investigated. The resulting conclusions and corresponding perspectives will be summarized sequentially.

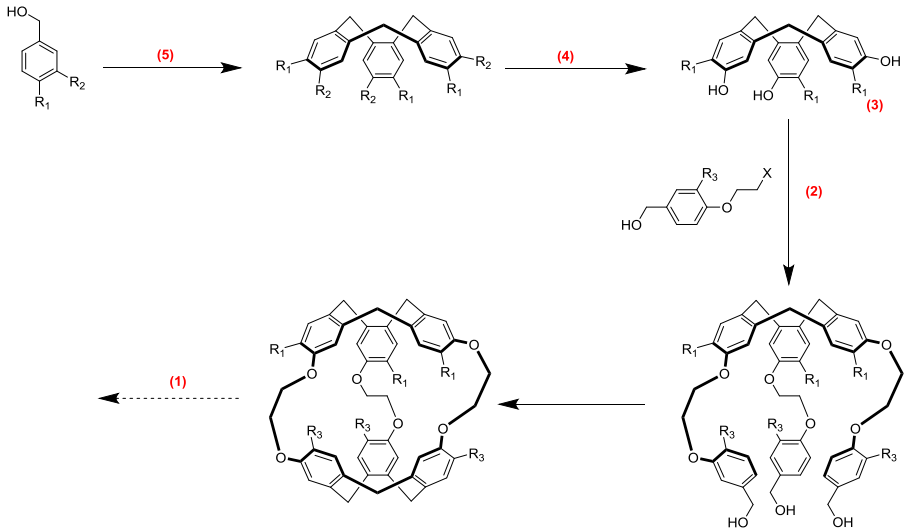

1) Mono-deprotection of a PEGylated C_3 symmetric cryptophane

In this strategy, based on a previous synthesis developed by L. Delacour, a PEGylated symmetric cryptophane **23** was synthesized in 5 steps. After several trials for optimizing and scaling up the synthesis, we improved the overall yield from 5 % to 43 %, and the scale of the synthesis was raised from dozens of milligrams to several hundreds of milligrams.

The mono-deprotection was tricky due to the presence of the PEG moieties which predominantly influence the polarity of products and thus complicate the purification steps. After we have tested numerous deprotection conditions, the majority formation of the target molecule **51** was observed however its purification remains to be improved.

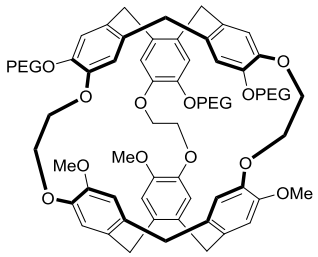

23

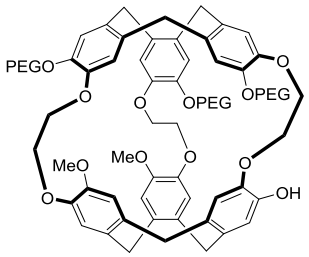

51

2) Functionalization of CTVs with different benzylic alcohol linkers

Following this strategy, 3 different PEGylated asymmetric cryptophanes were synthesized at the scale of 50 mg. Cryptophane **73** was synthesized in six steps in 7 % overall yield, cryptophane **85** was prepared in six steps in 9 % overall yield; cryptophane **76** was obtained in seven steps in 1.4 % yield (non-optimized). All of these 3 cryptophanes bearing two PEG moieties display sufficient solubility (30 mg/mL).

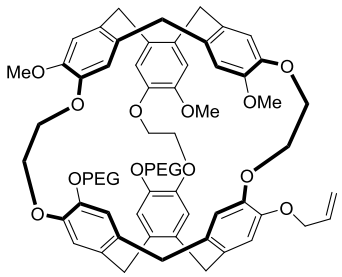

73

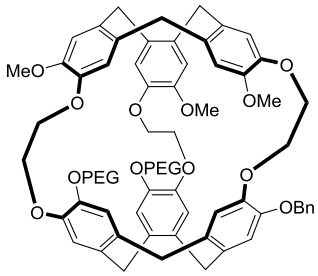

85

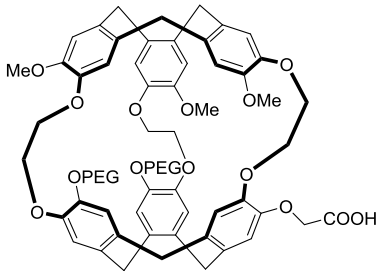

76

Cryptophane **73** and **85** need one more deprotection step to be used for grafting. Unfortunately, the corresponding deprotections of allyl or benzyl groups could not be achieved successfully despite numerous attempts, suggesting that the PEGylated cryptophanol **78** might be unstable.

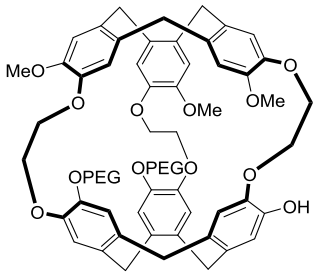

78

With a carboxylic acid group, cryptophane **76** can be directly bio-conjugated for the construction of bio-probes. Its capacity to encapsulate and exchange xenon was studied but the analysis was marred by a multi-signal problem which suggests the formation of aggregates, the encapsulation of cations or a putative *syn*-/*anti*- isomerism. Therefore the yield and production scale of this compound still needs being optimized by avoiding the issues mentioned above.

3) Mono-halogenation of CTVs

A PEGylated mono-iodinated cryptophane **106** was synthesized in three steps in 18 % overall yield. This cryptophane has shown satisfying solubility in water (30 mg/mL) as well as good properties for xenon encapsulation. Unfortunately, it was obtained as a mixture of *syn*-/*anti*- isomers which are impossible to be separated.

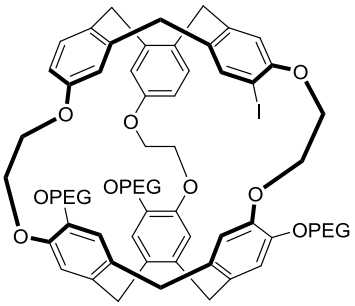

anti-**106**

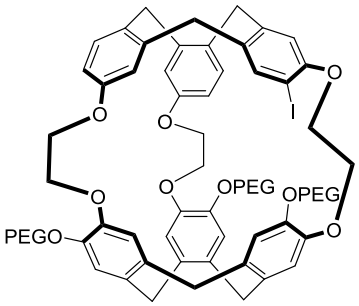

syn-**106**

Alternatively, a non-PEGylated mono-iodinated cryptophane **108** was also synthesized in three steps in 23 % overall yield (non-optimized). To the best of our knowledge, this is the first report regarding the synthesis of a mono-halogenated cryptophane[222]. The *syn*- and *anti*- isomers of cryptophane **108** were separately obtained and their properties for encapsulating xenon were evaluated.

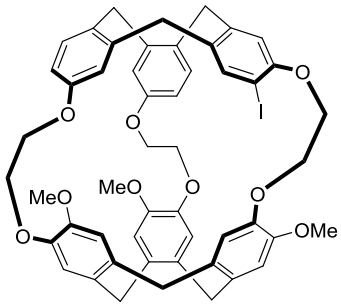

anti-**108**

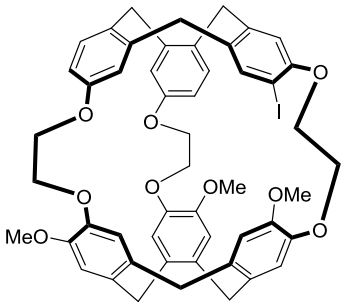

syn-**108**

For this synthesis, optimizations need to be carried out in order to improve the overall yield as well as the production scale. Now the efforts are focused on the hydrosolubilization of this compound by introducing PEG moieties.

Applying the same strategy to the CTV, the tri-functionalized CTV **113** was synthesized in 5 steps in 21 % overall yield. The cyclotrimerization step leading to the corresponding cryptophane **109** as the major product was carried out however the purification stage revealed to be challenging once again.

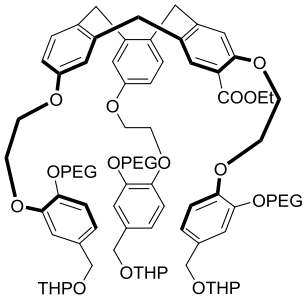

113

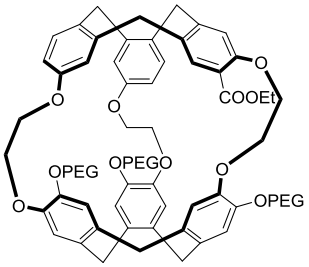

109

In contrast to the previous startegies, the symmetry of the cryptophane motif can be broken at the early stage, either by mono-depotecting a symmetric CTV (strategy 4) or by directly constructing an asymmetric CTV with different monomers (strategy 5).

4) Selective deprotection of CTVs

The selective mono-deprotection of CTVs was an alternative to the previouslty exposed strategy. The PEGylated mono-protected CTV **114**, which is an important and interesting intermediate in the synthesis of water-soluble mono-functionalized cryptophane, was obtained in two steps in 53 % non-optimized yield. However removal of the benzyl ether is difficult and therefore currently locks this synthetic pathway. Additional deprotection conditions have to be scanned in order to achieve the construction of the corresponding cryptophanes.

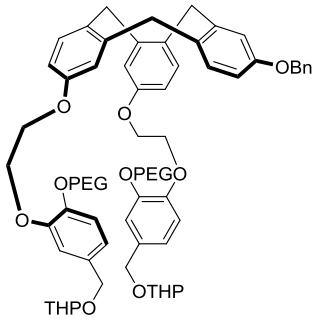

114

5) Synthesis of asymmetric CTVs through the cyclotrimerizations with different monomers

By implementing this strategy, two asymmetric CTVs were synthesized in two steps (25% overall yield for CTV **124**, 14 % yield for CTV **127**, non-optimized). CTV **127** was then engaged in the synthesis of the PEGylated mono-functionalized cryptophane **132**. This synthetic route enabled to isolate compound **132** in 7 steps in 1.5 % overall yield which has to be optimized. We are presently investigating the xenon-encapsulation properties of this cryptophane and preliminary results suggest that its capacity to encapsulate and exchange xenon complies with the specifications determined by the development of bio-probes usable for xenon MRI.

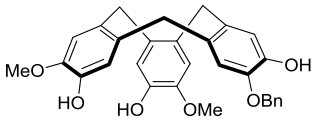

124

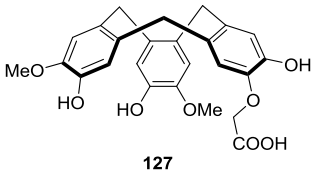

127

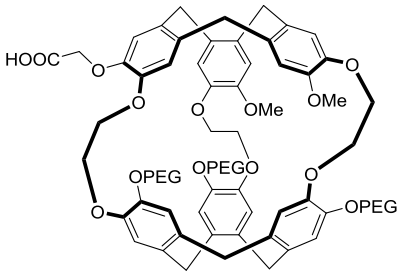

132

This work demonstrates that the solubilization of cryptophane by grafting polyethylene glycol moieties which is a prerequisite to the development of bio-probes recurrently complicates the purification of intermediates and final compounds which only slightly differ in polarity. Therefore, desymmetrization at the late stage of the synthesis is challenging. Moreover, as a bulky group, PEG moities can trap water or ions, which may jeopardize further chemical modification of the cryptophanes. Presently, the most promising synthetic routes imply the early desymmetrization of the CTV unit and the subsequent introduction of three benzyl-PEG adducts which are finally cyclotrimerized. After optimization and scale-up of the synthesis, cryptophanes **79** and **132** will be conjugated to a lysine-containing peptide

bearing a fluoresceine moiety in order to produce a dual imaging (fluorescence/^{129}Xe MRI) bio-probe in sufficient quantities for *in vivo* experiments on NSCLC mice models.

REFERENCES

[1] G. Li, H. Xie, H. Ning, D. Citrin, A. Kaushal, K. Camphausen, R. W. Miller, *J. Appl. Clin. Med. Phys.*, **2011**, *12*, 1

[2] J. Gabard, A. Collet, *J. Chem. Soc., Chem. Commun.*, **1981**, 1137

[3] M. M. Spence, S. M. Rubin, I. E. Dimitrov, E. J. Ruiz, D. E. Wemmer, A. Pines, S. Q. Yaoi, F. Tiani, P. G. Schultzi, *PNAS*, **2001**, *98*, 10654

[4] L. Emsley, Cours M1 RMN Structurale

[5] S. Pirot, *Neuropsychiatrie : Tendances et Débats* **2008**, *33*, 37

[6] S. R. Meikle, F. J. Beekman, S. E. Rose, *Drug Discovery Today : Technologies*, **2006**, *3*, 187

[7] Journal du CNRS n°260-261, septembre-octobre **2011**

[8] J.L. Barnhart, N. Kuhnert, D.A. Bakan, R.N. Berk, *Magn. Reson. Imag.*, **1987**, *5*, 221

[9] A. J. L. Villaraza, A. Bumb, M. W. Brechbiel, *Chem. Rev.*, **2010**, *110*, 2921

[10] S. Laurent, D. Forge, M. Port, A. Roch, C. Robic, L. Vander Elst, R. N. Muller, *Chem. Rev.* **2008**, *108*, 2064.

[11] D. Canet, C. Aroulanda, P. Mutzenhardt, S. Aime, R. Gobetto, F. Reineri, *Magn. Reson.*, **2006**, *28A*, 321.

[12] M. Goldman, H. Johannesson, O. Axelsson, M. Karlsson, *Magn. Reson. Imaging.*, **2005**, *23* , 153.

[13] S. B. Duckett, N. J. Wood, *Coord. Chem. Rev.* **2008**, *252*, 2278.

[14] S. B. Duckett, R. E. Mewis, *Acc. Chem. Res.*, **2012**, *45*, 1247.

[15] A. M. S. Albert, G. D. Cates, B. Driehuys, W. Happer, B. Saam, C. S. Springer, A. Whishnia, *Nature*, **1994**, *370*, 199

[16] L. L. Walkup, J. C. Woods, *NMR. Biomed.*, **2014**, *27*, 1429

[17] J. Kurhanewicz, D. B. Vigneron, K. Brindle, E. Y. Checkmenev, A. Comment, C. H. Cunningham, R. J. DeBerardinis, G. G. Green, M. O. Leach, S. S. Rajan, R. R. Rizi, B. D. Ross, W. S. Warren, C. R. Malloy, *Neoplasia*, *13*, 81

[18] P. Nikolaou, B. M. Goodson, E. Y. Checkmenev, *Chem. Eur. J.*, **2015**, *21*, 3165

[19] M. E. Merritt, C. Harrison, C. Storey, F. M. Jeffery, A. D. Sherry, C. L. Malloy, *PNAS*, **2011**, *65*, 557

[20] A. Viale, S. Aime, *Current Opinion in Chemical Biology*, **2009**, *14*, 1

[21] K. Golman, R. Zandt, M. Lerche, R. Perhson, H. Ardenkjaer-Larsen, *Cancer Res.*, **2006**, *66*, 10855

[22] S. E. Day, M. I. Kettunen, M. K. Cherukuri, J.B. Mitchell, M. J. Lizak, H. D. Morris, S. Matsumoto, A. P. Koretsky, K. Brindle, *Magn. Reson. Med.*, **2011**, *65*, 557

[23] M. R. Clatworthy, M. I. Kettunen, D. Hu, R. J. Mathews, T. H. Witney, B. W. Kennedy, S. E. Bohndiek, F. A. Gallagher, B. L. Jarvis, K. G. C. Smith, K. Brindle, *PNAS*, **2012**, *109*, 13374

[24] K. Kawakami, *Ann. Nucl. Med.*, **1997**, *11*, 67

[25] R. Sriram, J. Kurhanewicz, D. B. Vigneron, *Magn. Res.*, **2014**, *3*, 1

[26] N. Colloc'h, J. Sopkova-de Oliveira Santos, P. Retailleau, D. Vivarès, F. Bonneté, B. Langlois d'Estainto, B. Gallois, A. Brisson, J. J. Risso, M. Lemaire, T. Prangé, J.H. Abraini, *Biophys. J.*, **2007**, *92*, 217

[27] J. P. Mugler, T. A. Altes, *J. Magn. Reson. Imag.*, **2013**, *37*, 313

[28] S. D. Swanson, M. S. Rosen, B. W. Agranoff, K. P. Coulter, R. C. Welsh, T. E. Chupp, *Magn. Reson. Med.* **1997**, *38*, 695

[29] G. Duhamel, P. Choquet, E. Grillon, L. Lamalle, J.-L. Leviel, A. Ziegler, A. Constantinesco, *Magn. Reson. Med.*, **2001**, *46*, 208

[30] B. M. Goodson, Y. Q. Song, R. E. Taylor, V. D. Schepkin, K. M. Brennan, G. C. Chingas, T. F. Budinger, G. Navon, A. Pines , *PNAS*, **1997**, *94*, 14725

[31] J. G. Riess, *Chem. Rev.*, **2001**, *101*, 2797

[32] A. K. Venkatesh, L. Zhao, D. Balamore, F. A. Jolesz, M. S. Albert, *NMR Biomed.*, **2000**, *13*, 245

[33] J. Wolber, I. J. Rowland, M. O. Leach, A. Bifone, *Magn. Reson. Med.* **1999**, *41*, 442

[34] G. Duhamel, P. Choquet, E. Grillon, J.-L. Leviel, A. Ziegler, A. Constantinesco, *C.R. Acad. Sci. Paris*, **2001**, *4*, 789

[35] B. M. Goodson, Journal of Magnetic Resonance, **2002**, *155*, 157

[36] T. Pietrass, H. C. Gaede, *Adv. Mat.*,**1995**, *7*, 826

[37] C. Boutin, H. Desvaux, M. Carrière, F. Leteurtre, N. Jamin, Y. Boulard, P. Berthault, *NMR Biomed.*, **2011**, *24*, 1264

[38] J. Wolber, F. Ellner, B. Fridlund, A. Gram, H. Jóhannesson, G. Hansson, L. H. Hansson, M. H. Lerche, S. Mansson, R. Servin, M. Thaning, K. Golman, J. H. Ardenkjaer-Larsen, *Nucl. Instrum. Methods A*, **2004**, *526*, 173

[39] E. Terreno, D. Delli Castelli, A. Viale, S. Aime, *Chem. Rev.*, **2010**, *110*, 3019

[40] R. Eisenberg, *Acc. Chem. Res.*, **1991**, *24*, 110

[41] C. R. Bowers, D. P. Weitekamp, *J. Am. Chem. Soc.*, **1987**, *109*, 5541

[42] J. Natterer, J. Bargon, *Prog. Nuc. Mag. Res.*, **1997**, *31*, 29

[43] D. Blazina. et al., *Dalton Trans.*, **2004**, *17*, 2601

[44] A. J. Kastler, *Phys. Radium*, **1950**, *11*, 225

[45] M. A. Bouchiat, T. R. Carver, C. M. Varnum, *Phys. Rev. Lett.*, **1960**, *5*, 373

[46] C. Chauvin, L. Liagre, C. Boutin, E. Mari, E. Léonce, G. Carret, B. Coltrinari, P. Berthault, *Rev. Sci. Instrum*. **2016**, *87*, 016105

[47] B. M. Goodson, *Journal of Magnetic Resonance*, **2002**, *155*, 157

[48] P. Berthault, G. Hubert, H. Desvaux, *Progress in Nuclear Magnetic Resonance Spectroscopy*, **2009**, *55*, 35

[49] S. Mecozzi, J. Rebek Jr., *Chem. Eur. J.*, **1998**, *4*, 1016

[50] F. London, *Z. Phys.*, **1930**, *60*, 491.

[51] J.Černý, P. Hobza, *Phys. Chem. Chem. Phys.*, **2007**, *9*, 5291

[52] D.M. Rudkevich, *Angew. Chem. Int. Ed.*, **2004**, *43*, 558

[53] K. Bartik, M. Luhmer, S.J. Heyes, R. Ottinger, J. Reisse, *J. Magn. Reson.* B, **1995**, *109*, 164

[54] J. Fukotomi, Y. Adachi, A. Kaneko, A. Kimura, H. Fujiwara, *J. Incl. Phenom. Macrocycl. Chem.*, **2007**, *58*, 115

[55] D. J. Cram, M. E. Tanner, C. B. Knobler, *J. Am. Chem. Soc.*, **1991**, *113*, 7717

[56] Y. Miyahara, K. Abe, T. Inazu, *Angew. Chem. Int. Ed.*, **2002**, *41*, 3020

[57] B.S. Kim, Y.H. Ko, Y. Kim, H.J. Lee, N. Selvapalam, H.C. Lee, K. Kim, *Chem Commun* , **2008**, 2756

[58] R. M. Fairchild, A. I. Joseph, K. Travis Holman, H. A. Fogarty, T. Brotin, J.-P. Dutasta, C. Boutin, G. Huber, P. Berthault, *J. Am. Chem. Soc.*, **2010**, *132*, 15505

[59] H. Fogarty, P. Berthault, T. Brotin, G. Huber, H. Desvaux, J.-P. Dutasta, *J. Am. Chem. Soc*., **2007**, *129*, 10332

[60] K. Bartik, M. Luhmer,J. P. Dutasta, A. Collet, J. Reisse, *J. Am. Chem. Soc.*, **1998**, *120*, 784

[61] G. Huber, L. Beguin, H. Desvaux, T. Brotin, H. Fogarty, J.-P. Dutasta, P. Berthault, *J. Phys. Chem. A*, **2008**, *112*, 11363

[62] T. Brotin, J.-P. Dutasta, *Eur. J. Org. Chem.*, **2003**, 973

[63] G. Huber, T. Brotin, L. Dubois, H. Desvaux, J.-P. Dutasta, P. Berthault, *J. Am. Chem. Soc*., **2006**, *128*, 6239

[64] H. Desvaux, G. Huber, T. Brotin, J.-P. Dutasta, P. Berthault, *Chem. Phys. Chem.*, **2003**, *4*, 384

[65] M. Luhmer, B.M. Goodson, Y.-Q. Song, D.D. Laws, L. Kaiser, M.C. Cyrier, A. Pines, *J. Am. Chem. Soc.*, **1999**, *121*, 3502

[66] T. Brotin, J-P. Dutasta, *Chem. Rev.*, **2009**, *109*, 88

[67] K. T. Holman, *Encyclopedia of Supramolecular Chemistry*, **2004**

[68] A. Collet, *Tetrahedron*, **1987**, *43*, 5725

[69] A. Collet, J. Gabard, *J. Org. Chem.*, **1980**, *45*, 5400

[70] H. Zimmermann, P. Tolstoy, H. H. Limbach, R. Poupko, Z. Luz, *J. Phys.Chem. B*, **2004**, *108*, 18772

[71] G. Haberhauer, S. Woitschetzki, H. Bandlann, *Nat. Commun.* , **2014**, 5

[72] S. T. Mough, I. C. Goeltz, K. T. Holman, *Angew. Chem. Int. Ed.*, **2004**, *43*, 5631

[73] A. Collet, J-P. Dutasta, B. Lozach, J. Canceill, *Topics in Current Chemistry*, **1993**, *165*

[74] D. Cram, M. Tanner, S. Keipert, C. Knobler, *J. Am. Chem. Soc.*, **1991**, *113*, 8909

[75] A. I. Joseph, G. El-Ayle, C. Boutin, E, Leonce, P. Berthault, K. T. Holman, *Chem Commun* , **2014**, *50*, 15905

[76] M. A. Little, J. Donkin, J. Fisher, M. A. Helcrow, J. Loder, M. J. Hardie, *Angew. Chem. Int. Ed.*, **2012**, *51*, 764

[77] N. Kotera, L. Delacour, T. Traoré, N. Tassali, P. Berthault, D. A. Buisson, J. P. Dognon, B. Rousseau, *Org. Lett*., **2011**, *13*, 2153

[78] R. M. Fairchild, K. T. Holman, *J. Am. Chem. Soc*. **2005**, *127*, 16364

[79] D. R. Jacobson, N. S. Khan, R. Collé, R. Fitzgerald , L. Laureano-Pérez , Y. Bai, I. J. Dmochowski, *PNAS*, **2011**, *108*, 10969

[80] C. W. Tornoe, C. Christensen, M. Meldal, *J. Org. Chem*., **2002**, *67*, 3057

[81] P. A. Hill, Q. Wei, T. Troxler, I. J. Dmochowski **,** *J. Am. Chem. Soc.*, **2009**, *131*, 3069

[82] R. Tyagi, C. Witte, R. Haag, L. Schröder, *Org. Lett*., **2014**, *16*, 4436

[83] T. Traoré, L. Delacour, S. Garcia-Argote, P. Berthault, J.-C. Cintrat, B. Rousseau, *Org. Lett*., **2010**, *12*, 960

[84] T. Traoré, G. Clavé, L. Delacour, N. Kotera, P.-Y. Renard, A. Romieu, P. Berthault, C. Boutin, N. Tassali, B. Rousseau, *Chem. Commun.,* **2011**, *47*, 9702

[85] (a) S. K. Singh, S. Joshi, A. R. Singh, J. K. Saxena, D. S. Pandey, *Inorg. Chem*., **2007**, *46*, 10869; (b) K. Gkionis, J. A. Platts, J. G. Hill, *Inorg. Chem*., **2008**, *47*, 3893

[86] E. Dubost, N. Kotera, S. Garcia-Argote, Y. Boulard, E. Léonce, C. Boutin, P. Berthault, C.Dugave, B. Rousseau, *Org. Lett*., **2013**, *15*, 2866

[87] L. Delacour, N. Kotera, T. Traoré, S. Garcia-Argote, C Puente, F Leteurtre, E. Gravel, N. Tassali, C. Boutin, E. Léonce, Y. Boulard, P. Berthault, B. Rousseau, *Chem. Eur. J*., **2013**, *19*, 6089

[88] J. M. Chambers, P. A. Hill, J. A. Aaron, Z. Han, D. W. Christianson, N. N. Kuzma, I. J. Dmochowski, *J. Am. Chem. Soc.,* **2009**, *131*, 563

[89] N. Kotera, N. Tassali, E. Léonce, C. Boutin, P. Berthault, T. Brotin, J-P. Dutasta, L. Delacour, T. Traoré, D. A. Buisson, F. Taran, S. Coudert, B. Rousseau, *Angew. Chem. Int. Ed.*, **2012**, *51*, 4100

[90] M. Darzac, T. Brotin, D. Bouchu, J.-P. Dutasta, *Chem. Commun,*. **2002**, 48

[91] M. Darzac, T. Brotin, L. Rousset-Arzel, D. Bouchu, J.-P. Dutasta, *New J. Chem.*, **2004**, *28*, 502

[92] M. M. Spence, E. J. Ruiz, S. M. Rubin, T. J. Lowery, N. Winssinger, P. G. Schultz, D. E. Wemmer, A. Pines, *J. Am. Chem. Soc.*, **2004**, *126*, 15287

[93] H. X. Zang, F. Guibé, G. Balavoine, *Tetrahedron Lett.*, **1988**, *29*, 619

[94] C. Boutin, A. Stopin, F. Lenda, T. Brotin, J.-P. Dutasta, N. Jamin, A. Sanson, Y. Boulard, F. Leteurtre, G. Huber, A. Bogaert-Buchmann, N. Tassali, H. Desvaux, M. Carrière, P. Berthault, *Bioorg. Med. Chem.*, **2011**, *19*, 4135

[95] A. Bouchet, T. Brotin, M. Linares, D. Cavagnat, T. Buffeteau, *J. Org. Chem*. **2011**, *76*, 7816−7825

[96] L.-L. Chapellet, J. R. Cochrane, E. Mari, C. Boutin, P. Berthault, T. Brotin, *J. Org. Chem*., **2015**, *80*, 6143

[97] H. Togo, G. Nogami, M. Yokoyama, *Synlett.* **1998**, 534

[98] C. Hilty, T. J. Lowery, D. E. Wemmer, A. Pines, *Angew. Chem. Int. Ed.*, **2006**, *118*, 76

[99] T. J. Lowery, S. Garcia, L. Chavez, E. J. Ruiz, T. Wu, T. Brotin, J-P. Dutasta, D. S. King, P. G. Schultz, A. Pines, D. E. Wemmer, *ChemBioChem*, **2006**, *7*, 65

[100] F. Schillings, L. Schröder, K. K. Palaniappan, S. Zapf, D. E. Wemmer, A. Pines, *ChemPhysChem*, **2010**, *11*, 3529

[101] P. Berthault, H. Desvaux, T. Wendlinger, M. Gyejacquot, A. Stopin, T. Brotin, J-P. Dutasta, Y. Boulard, *Chem. Eur. J.*, **2010**, *16*, 12941

[102] V. Roy, T. Brotin, J-P. Dutasta, M-H.Charles, T. Delair, F. Mallet, G. Huber, H. Desvaux, Y. Boulard, P. Berthault, *ChemPhysChem*, **2007**, *8*, 2082

[103] Q. Wei, G. K. Seward, P. A. Hill, B. Patton, I. E. Dimitrov, N. N. Kuzma, I. J. Dmochowski, *J. Am. Chem. Soc.*, **2006**, *128*, 13274

[104] J. A. Aaron, J. M. Chambers, K. M. Jude, L. Di Costanzo, I. J. Dmochowski, D. W. Christianson *J. Am. Chem. Soc.*, **2008**, *130*, 6942

[105] G. K. Seward, Y. Bai, N. S. Khan, I. J. Dmochowski, *Chem. Sci.*, **2011**

[106] N. Tassali, N. Kotera, C. Boutin, E. Léonce, Y. Boulard, B. Rousseau, E. Dubost, F. Taran, T. Brotin, J-P. Dutasta, P. Berthault, *Anal. Chem.*, **2014**, *86*, 1783

[107]P. D. Garimella, T. Meldrum, L. S. Witus, M. Smith, V. S. Bajaj, D. E. Wemmer, M. B. Francis, I. J. Dmochowski, *J. Am. Chem. Soc.*, **2014**, *136*, 164

[108] S. Klippel, J. Döpfert, J. Jayapaul, M. Kunth, F. Rossella, M. Schnurr, C. Witte, C. Freund, L. Schröder, *Angew. Chem. Int. Ed.*, **2014**, *53*, 493

[109] (a) F. Ciardello, G. Tortora, *Eur. J. Cancer*., **2003**, *39*, 1348; (b) M. Zimmerman, A. Zouhair, D. Azria, M. Ozsahin, *Radiation Oncol*,. **2006**, *1*, 11 (c) D. E. Milenic, K. J. Wong, K. E. Baidoo, G. L. Ray, K. Garmestani, M. Williams, M. W. Brechbiel, *Cancer Biother. Radiopharm*., **2008**, *23*, 619.

[110] Cetuximab monography (Erbitux) Bristol-Myers Squibb Canada, Montreal **2012**

[111] J. Lee, Y. Choi, K. Kim, S. Hong, H-Y. Park, T. Lee, G. J. Cheon, R. Song, *Bioconjugate Chem*. **2010**, *21*, 940.

[112] N. K. Devaraj, R. Upadhyay, J. B. Haun, S. A. Hilderbrand, R. Weissleder, *Angew. Chem. Int. Ed*. **2009**, *48*, 7013.

[113] S. Corneillie, P. N. Lan, E. Schacht, M. Davies, A. Shard, R. Green, S. Denyer, M. Wassall, H. Whitfield, S. Choong, *Polym. Int*., **1998**, *46*, 251

[114] V. G. Kadajji, G. V. Betageri, *Polymers*, **2011**, *3*, 1972

[115] M. E. Jung, M. A. Lyster, *Org. Synth.* **1979**, *59*, 35

[116] M. E. Jung, M. A. Lyster, *J. Org. Chem.* **1977**, *42*, 3761

[117] J. A. Mccall, M. J. Hintze, *Patent*, WO 2009102481 A1

[118] J. F. W. McOmie, M. L. Watts, D. E. West, *Tetrahedron*, **1968**, *24*, 2289

[119] G. LI, D. Patel, V. J. Hruby, *Tetrahydron lett*. **1993**, *34*, 5393

[120] B. Kale, A. Shinde, S. Sonar, B. Shingate, S. Kumar, S. Ghosh, S. Venugopal, M. Shingare, *Tetrahedron Lett.* **2010**, *51*, 3075

[121] A. K. Chakraborti, L. Sharma, M. K. Nayak, *J. Org. Chem.* **2002,** *67*, 2541

[122] K. S. Lee, K. D. Kim, *Bull. Korean Chem. Soc.* **2010**, *31*, 3842

[123]A. Reitz, M. A. Avery, M. S. Verlander, M. Goodman, *J. Org. Chem*., **1981**, *46*, 4859

[124] H. Konishi, H. Sakakibara, K. Kobayashi, O. Morikawa, *J. Chem. Soc., Perkin Trans.*, **1999**, 2583.

[125] O. Taratula, P. A. Hill, Y. Bai, N. S. Khan, I. J. Dmochowski, *Org. lett.* **2011,** *13*, 1414

[126] T. Fujihara, T. Hosoki, Y. Katafuchi, T. Iwai, J. Terao, Y. Tsuji, *Chem. Commun.*, **2012**,*48*, 8012

[127] A. F. Abdel-Magid, K. G. Carson, B. D. Harris, C. A. Maryanoff, R. D. Shah, *J. Org. Chem.*, **1996**, *61*, 3849

[128] A. F. Abdel-Magid, S. J. Mehrman, *Org. Process Res. Dev.*, **2006**, *10*, 971

[129] J. Ni, D. A. Auston, D. A. Freilich, S. Muralidharan, E. A. Sobie, J. P. Y. Kao, *J. Am. Chem. Soc.*, **2007**, *129*, 5316

[130] *Hyperpolarized xenon-129 magnetic resonance : concepts, production, techniques and applications*, Cambridge, Royal Society of Chemistry: Cambridge, 2015

[131] K. E. Chaffeea , M. Marjanskab , B. M. Goodson, *Solid State Nucl. Mag.*, **2006**, *29*, 104

[132] Y. Shi, X. Li, J. Yang, F. Gao, C. Tao, *J. Fluoresc*., **2011**, *21*, 531

[133] J. Lang, J. J. Dechter, M. Effemey, J. Kowalewski, *J. Am. Chem. Soc.*, **2001**, *123*, 7852

[134]O. Taratula, I. J. Dmochowski, P. A. Hill P. J. Carroll, *Protocol Exchange*, **2011**

[135] E. Steiner, R. Mathew, I. Zimmermann, T. Brotin, M. Edéna, J. Kowalewski, *Magn. Reson. Chem.*, **2015**, *53*, 596

[136] D. Cavagnat, T. Brotin, J-L. Bruneel, J-P. Dutasta, A. Thozet, M. Perrin, F. Guillaume, *J. Phys. Chem. B* , **2004**, *108*, 5572

[137] O. Taratula, P. A. Hill, N. S. Khan, P. J. Carroll, I. J. Dmochowski, *Nat. Commun*., **2010**, *1*, 148

[138] H. Togo, G. Nogami, M. Yokoyama, *Synlett*, **1998**, 534.

[139] K. Menzel, L. Dimichele, P. Mills, D. E. Frantz, T. D. Nelson, M. H. Kress, *Synlett*, **2006**, 1948

[140] N. Miyaura, A. Suzuki, *Chem. Rev.*, **1995**, *95*,2457

[141] T. Brotin, V. Roy, J-P. Dutasta, *J. Org. Chem.*, **2005**, *70*, 6187.

[142] T. Traoré, L. Delacour, N. Kotera, G. Merer, D.-A. Buisson, C. Dupont, B. Rousseau, *Org. Process Res. Dev.* **2011**, *15*, 435.

[143] B. Chu, *Annu. Rev. Phys. Chem*., **1970**, *21*, 145.

[144] R. Pecora, *J. Chem. Phys*., **1964**, *40*, 1604.

[145] J. Canceill, L. Lacombe, A. Collet, *C. R. Acad. Sci. Paris, Sér. II*, **1984**, *298*, 39.

[146] D. Humiliere, Doctorat thesis, Ecole Normale Superieure de Lyon, France, **2002**.

[147] P. Soulard, P. Asselin, A. Cuisset, J. R. Aviles Moreno, T. R. Huet, D. Petitprez, J. Demaison, T. B. Freedman, X. Cao, L. A. Nafie, J. Crassous, *Phys. Chem. Chem. Phys*. **2006**, *8*, 79.

[148] P. K. Mandal, J. S. McMurray, *J. Org. Chem.*, **2007**, *72*, 6599

[149] P. Angibeaud, J. Defaye, A. Gadelle, J.-P. Utille, *Synthesis*, **1985**, 1123

[150] M. A. Rahim, S. Matsumura, K. Toshima, *Tetrahedron Lett.*, **2005**, *46*, 7307

[151] M. S. Congreve, E. C. Davison, M. A. M. Fuhry, A. B. Holmes, A. N. Payne, R. A. Robinson, S. E. Ward, *Synlett*, **1993**, 663

[152] K. Okano, K. Okuyama, T. Fukuyama, H. Tokuyama, *Synlett*, **2008**, 1977

[153] S. K. Boovanahalli, D. W. Kim, D. Y. Chi, *J. Org. Chem.*, **2004**, *69*, 3340

EXPERIMENTAL PART

Solvents and reagents

Anhydrous solvents are obtained by distillation under nitrogen atmosphere in the presence of drying agents: calcium hydride for dichloromethane and sodium (and benzophenone) for tetrahydrofuran.

The commercial reagents are directly used without purification.

Purification and analysis

Purifications by chromatography on silica gel column are carried out either by gravity or under pressure of nitrogen or air using Merck silica (particle size 40-63 μm). The eluent mixture is specified for each purification.

The automatic purifications by CombiFlash® were performed on a RediSep apparatus (Serlabo Technologies, Teledyn ISCO) using cartridges "pre-packaged" with SiO_2 for normal phase and C_{18} for reversed phase.

Analytical thin layer chromatography (TLC) was performed on silica plates Merck 60 F254 on glass substrate.

Products are revealed either by ultraviolet illumination at 254 nm, or by reaction in the presence of iodine vapor, an aqueous solution of potassium permanganate and potassium carbonate or a phosphomolybdic acid solution of 5% by weight in ethanol.

Nuclear magnetic resonance spectra (NMR) ^{1}H, ^{13}C and the additional experiments were recorded on a Bruker DPX 400 MHz equipped with a forward calculator. Resonance frequencies of the nuclei are equal to 400.13 MHz for the proton and 100.61 MHz for the ^{13}C.

Chemical shifts δ are expressed in parts per million (ppm) and coupling constants *J* in Hertz (Hz). The references used are: chloroform proton respectively (δ = 7.26 ppm) or tetramethylsilane (δ = 0.00 ppm) in ^{1}H NMR and carbon 13 deuterated chloroform (δ = 77.00 ppm) in ^{13}C. In the description of the spectra, signal multiplicities are abbreviated as follows: s (singlet), d (doublet), t (triplet), q (quartet), quint (quintet), dd (doublet of doublets), m (multiplet of indeterminate nature or massif resulting from the superposition of different signals). Other abbreviations used include the shape or the nature of the cores to which they correspond: bs (broad singlet).

The infrared absorption (IR) spectra were recorded on a Perkin Elmer System 2000 FT-IR. Solid compounds are included in a KBr pellet. Wave numbers of the absorption bands corresponding to different vibrations are given in cm^{-1}, at their maximum intensities.

Mass spectra (MS) were obtained by electrospray on an ESI TOF spectrometer MARINER. In the description of the spectra, "M" represents the molar mass of the analyzed molecule. High resolution mass spectra (HRMS) are realized in the Natural Substances Chemistry Institute (INSC) in Gif-sur-Yvette.

Compound 17

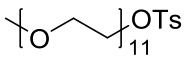

17

$C_{30}H_{54}O_{14}S$

Mw = 670.81

- Experimental protocol for the synthesis of methoxy-polyethylene glycol 550 (5g scale)

Methoxy-polyethyene glycol 550 (5 g, 9.7 mmol) and tosyl chloride (18.5 g, 96.8 mmol) were dissolved in 100 mL of anhydrous DCM. Then triethylamine (9.5 mL, 70 mmol) was added dropwise under nitrogen atmosphere. The reaction was heated to reflux of dichloromethane overnight. The solvent were evaporated and then an extraction water / dichloromethane was carried out. The organic phase was dried over $MgSO_4$ and dichloromethane was evaporated. Purification by chromatography on silica gel (dichloromethane / methanol 100 : 0 → 90 : 10) yielded quantitatively the compound **17** (6.4 g).

- Experimental protocol for the synthesis of methoxy-polyethylene glycol 550 (20g scale)

Methoxy-polyethyene glycol 550 (20 g, 39 mmol) and tosyl chloride (74 g, 387 mmol) were dissolved in 400 mL of anhydrous dichloromethane. Then triethylamine (37.8 mL, 271.1 mmol) was added dropwise under nitrogen atmosphere. The reaction was heated to reflux of dichloromethane overnight. The solvent was evaporated and the residue was taken up in diethyl ether and washed twice with water. The aqueous phase was then recovered and extracted with dichloromethane. Finally the organic phase was dried over $MgSO_4$ and the solvent was evaporated. The compound **17** was obtained in 60 % yield (15.7 g).

Yellow oil

^{1}H NMR (400 MHz, $CDCl_3$, δ in ppm): 2.44 (s, 3H), 3.37 (s, 3H), 3.54 – 3.69 (m, 42H), 4.15 (t, *J* = 4.7 Hz, 2H), 7.33 (d, *J* = 8.1 Hz, 2H), 7.78 (d, *J* = 8.3 Hz, 2H)

^{13}C NMR (100 MHz, $CDCl_3$, δ in ppm): 21.55, 58.91, 68.57, 69.18, 70.45, 70.63, 71.83, 127.87, 129.74, 132.93, 144.70

MS (ESI-TOF) *m/z*: distribution centered at 715.5 ± 44, $[M+H]^+$

Compound 18

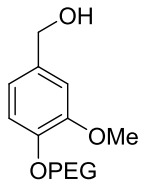

$C_{31}H_{56}O_{14}$

Mw = 652.78

18

Vanillyl alcohol (2.6 g, 16.8 mmol) was dissolved in 20 mL of acetone. Compound **17** (7.5 g, 11.2 mmol) and potassium carbonate (2.6 g, 19 mmol) were then added in the reaction milieu with stirring. The reaction was heated to reflux of acetone, under inert atmosphere overnight. Acetone was evaporated and then an extraction using water / dichloromethane was carried out. The organic phase was washed twice with an aqueous solution of potassium carbonate (pH = 11) and twice with water. It was finally dried over $MgSO_4$ and dichloromethane was evaporated. Compound **18** was obtained without purification in 98 % yield (6.0 g).

Pale yellow oil

^{1}H NMR (400 MHz, $CDCl_3$, δ in ppm): 3.37 (s, 3H), 3.54 – 3.72 (m, 40H), 3.86 (s, 3H), 3.88 (t, *J* = 5.2 Hz, 2H), 4.17 (t, *J* = 5.2 Hz, 2H), 4.61 (s, 2H), 6.84 – 6.92 (m, 3H)

^{13}C NMR (100 MHz, $CDCl_3$, δ in ppm): 55.84, 58.95, 65.08, 68.64, 69.61, 70.50, 70.77, 71.86, 110.95, 113.80, 119.28, 134.38, 147.73, 149.70

HRMS-ESI (m/z) : distribution centered at 675.3597 ± 44, $(M+Na)^+$

Compound 19

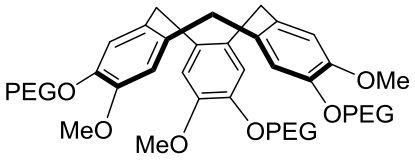

19

$C_{93}H_{162}O_{39}$

Mw = 1904.28

To a solution of **18** (4.05 g, 6.15 mmol) in 40 mL of MeOH was slowly added 20 mL of perchloric acid 70 % at 0 °C under nitrogen atmosphere. The reaction mixture was then warmed to room temperature and stirred for 24 hours. The mixture was diluted in dichloromethane and neutralized with a solution of NaOH 1N at 0 °C. The recovered organic phase was washed successively with water, brine and was finally dried over $MgSO_4$ and dichloromethane was evaporated. The obtained residue was directly engaged in the next step.

To realize the characterization of **132**, a purification by reversed-phase chromatography (water / acetonitrile 80 : 20 → 20 : 80) allowed the obtention of compound **19** in 50% yield (1.95 g).

Transparent oil

^{1}H NMR (400 MHz, $CDCl_3$, δ in ppm): 3.38 (s, 9H), 3.50 (d, *J* = 13.7 Hz, 3H), 3.54 – 3.70 (m, 120H), 3.81 (s, 9 H), 3.80 – 3.90 (m, 6H), 4.11 – 4.20 (m, 6H), 4.71 (d, *J* = 13,7 Hz, 3H), 6.81 (s, 3H), 6.89 (s, 3H)

^{13}C NMR (100 MHz, $CDCl_3$, δ in ppm): 36.44, 56.26, 58.99, 68.83, 69.61, 70.51, 70.72, 71.88, 113.87, 116.08, 131.77, 132.61, 146.89, 148,37

MS (MALDI-TOF) *m/z*: distribution centered at 1705.9 ± 44 ($[M+Na]^+$)

Compound 20

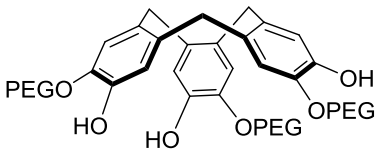

$C_{90}H_{156}O_{39}$

Mw = 1860.20

20

To a solution of **19** (3.6 g, 1.8 mmol) in 27 mL of anhydrous THF was added slowly 12.3 mL of a freshly-prepared solution of 1M PPh_2Li (12.3 mmol) under inert atmosphere. The reaction was stirred at room temperature for 3 hours. Then it was quenched with water and neutralized with a solution of HCl 1N. The organic phase was extracted with dichloromethane, then washed with a solution of saturated NaCl. The organic solution was finally dried over $MgSO_4$, filtered and concentrated *in vacuo*. A purification with silica gel chromatography (dichloromethane / methanol 99 : 1 → 90 : 10) allowed the production of compound **20** in 80 % yield (2.7 g).

Transparent oil

^{1}H NMR (400 MHz, $CDCl_3$, δ in ppm): 3.36 (s, 9H), 3.44 (d, *J* = 13.7 Hz, 3H), 3.54 – 3.75 (m, 126H), 4.08 – 4.29 (m, 6H), 4.61 (d, *J* = 13.7 Hz, 3H), 6.84 (1s, 3H), 6.85 (1s, 3H)

^{13}C NMR (100 MHz, $CDCl_3$, δ in ppm): 36.13, 58.98, 69.48, 70.37, 70.49, 71.86, 116.51, 117.64, 130.87, 134.41, 144.50, 146.14

MS (MALDI-TOF) *m/z*: distribution centered at 1707.9 ± 44 ($[M+Na]^+$)

Compound 39[103]

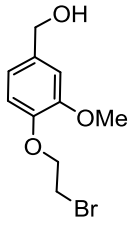

39

$C_{10}H_{13}BrO_3$

Mw = 261.12

Vanillyl alcohol (10 g, 74.9 mmol) was dissolved in DMF (120 mL) then K_2CO_3 (45 g, 0.3 mol) and 1,2-dibromoethane (50 mL, 0.7 mol) were added into the solution. The reaction was heated with stirring to 60 °C for 16 hours. After, the mixture was poured into water (800 mL) and extracted with ethyl acetate (3 x 400 mL). The organic phases were collected and concentrated to about 500 mL and washed successively with a solution of NaOH 1N (2 x 400 mL), water (500 mL) and brine (2 x 500 mL). The organic phase was dried and the solvent was evaporated under vacuum. Compound **39** was obtained in 60 % yield (11.7 g).

White solid

^{1}H NMR (400 MHz, $CDCl_3$, δ in ppm): 3.65 (t, *J* = 6.7 Hz, 2H), 3.89 (s, 3H), 4.33 (t, *J* = 6.7 Hz, 2H), 4.64 (s, 2H), 6.89 – 6.97 (m, 3H)

Compound 26[103]

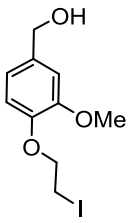

$C_{10}H_{13}IO_3$

Mw = 308.12

26

Compound **39** (8.87 g, 34.1 mmol) was dissolved in acetone (60 mL) and then NaI (22 g, 0.15 mol) was added, the mixture was stirred at 50 °C for 8 hours. Acetone was evaporated and the residue was dissolved in dichloromethane (400 mL) and washed with a saturated solution of sodium thiosulfate (2 x 400 mL), water (400 mL) and brine (400 mL). The organic phase was dried over $MgSO_4$ and concentrated. Compound **26** was quantitatively obtained without purification (10.5 g).

White Solid

^{1}H NMR (400 MHz, $CDCl_3$, δ in ppm): 3.40 (t, *J* = 6.7 Hz, 2H), 3.86 (s, 3H), 4.27 (t, *J* = 6.7 Hz, 2H), 4.61 (s, 2H), 6.86 – 6.94 (m, 3H)

Ethane-1,2-diyl bis(4-methylbenzenesulfonate)

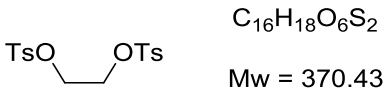

Over 30 min, small portions of TsCl (95 g, 0.5 mol) were slowly added to a solution of ethylene glycol (11.2 mL, 0.2 mol) in pyridine (325 mL) under nitrogen at 0 °C. After it was continuously stirred at room temperature under nitrogen overnight, the solution was poured onto crushed ice. The white precipitate formed was filtered and washed with cold water and methanol. Then it was dried for 48 h in vacuum to yield 55 g of Ethane-1,2-diyl bis(4-methylbenzenesulfonate) 75% yield (55.6 g).

White powder

^{1}H NMR (400 MHz, $CDCl_3$, δ in ppm): 7.71 (d, 4H, *J* = 6.6 Hz), 7.32 (d, 4H, *J* = 8.0 Hz), 4.17 (s, 4H), 2.43 (s, 6H)

^{13}C NMR (100 MHz, $CDCl_3$, δ in ppm): δ 145.25, 132.23, 129.92, 127.91, 66.67, 21.65

MS (ESI-TOF) *m/z*: 370.9, $[M+H]^+$

Compound 52

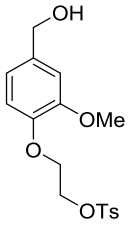

$C_{17}H_{20}O_6S$

Mw = 352.40

52

Vanillyl alcohol (1 g, 6.5 mmol) was dissolved in DMF (30 mL) then K_2CO_3 (4.5 g, 30 mmol) and ethylene ditosylate (12 g, 32.5 mmol) were added into the solution. The reaction was stirred at 60 °C for 16 hours. After, the mixture was poured into water (200 mL) and extracted with ethyl acetate (3 x 300 mL). The organic phases were collected and concentrated to about 200 mL and washed successively with a solution of NaOH 1N (2 x 200 mL), water (200 mL) and brine (2 x 200 mL). The organic phase was dried and the solvent was evaporated under vacuum. Compound **39** was obtained in 63 % yield (1.4 g).

Brownish oil

^{1}H NMR (400 MHz, $CDCl_3$, δ in ppm): 2.44 (s, 3H), 3.84 (s, 3H), 4.21 (t, *J* = 4.6 Hz, 2H), 4.36 (t, *J* = 4.6 Hz, 2H), 4.62 (s, 2H), 6.78 – 6.92 (m, 3H), 7.33 (d, *J* = 8.7 Hz, 2H), 7.82 (d, *J* = 8.7 Hz, 2H)

^{13}C NMR (100 MHz, $CDCl_3$, δ in ppm): 21.62, 55.86, 67.02, 68.05, 71.71, 111.88, 114.65, 120.36, 127.96, 129.81, 132.37, 132.72, 144.87, 146.98, 149.84

MS (ESI-TOF) *m/z*: 335.0, $[M+H-H_2O]^+$

Ethane-1,2-diyl dimethanesulfonate

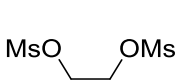

$C_4H_{10}O_6S_2$

Mw = 218.24

A solution of MsCl (2.55 mL, 33 mmol) in anhydrous dichloromethane (5 mL) was drop by drop added to the mixture of ethylene glycol (0.84 mL, 15 mmol) and trimethylamine (5.44 mL, 39 mmol) dissolved in 30 mL of dichloromethane under nitrogen at 0 °C. Then it was stirred at room temperature under nitrogen for 2 hours. A solution of 5 % HCl was added until the reaction milieu turned to a limpid solution. The organic phase was collected and washed successively with a saturated solution of $NaHCO_3$, water and brine. Then it was dried over $MgSO_4$ and the solvent was evaporated. After a recrystallization in methanol, the targeting product was obtained in 54 % yield (1.8 g).

White powder

^{1}H NMR (400 MHz, $CDCl_3$, δ in ppm): 3.09 (s, 6H), 4.74 (s, 6H)

^{13}C NMR (100 MHz, $CDCl_3$, δ in ppm): 33.75, 66.69

MS (ESI-TOF) *m/z*: 219.0, $[M+H]^+$

Compound 53

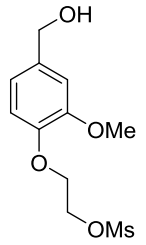

$C_{11}H_{16}O_6S$

Mw = 276.30

53

Vanillyl alcohol (0.25 g, 1.6 mmol) was dissolved in DMF (10 mL) then K_2CO_3 (1 g, 6.7 mmol) and ethylene dimesylate (1.73 g, 7.9 mmol) were added into the solution. The reaction was heated with stirring at 60 °C for 16 hours. After, the mixture was poured into water (50 mL) and extracted with ethyl acetate (3 x 100 mL). The organic phases were collected and concentrated to about 100 mL and washed successively with a solution of NaOH 1N (2 x 100 mL), water (100 mL) and brine (2 x 100 mL). The organic phase was dried and the solvent was evaporated under vacuum. After a purification using silica gel chromatography (dichloromethane / methanol 100 : 0 → 95 : 5) compound **53** was obtained in 74 % yield (0.33 g).

Yellow oil

^{1}H NMR (400 MHz, $CDCl_3$, δ in ppm): 3.14 (s, 3H), 3.85 (s, 3H), 4.27 (t, *J* = 4.5 Hz, 2H), 4.60 (t, *J* = 4.5 Hz, 2H), 4.64 (s, 2H), 6.87 (s, 2H), 6.957 (s, 1H)

^{13}C NMR (100 MHz, $CDCl_3$, δ in ppm): 37.72, 55.74, 67.22, 68.45, 71.76, 111.75, 114.09, 120.37, 132.43, 146.94, 149.72

MS (ESI-TOF) *m/z*: 277.2, $[M+H]^+$

Compound 21

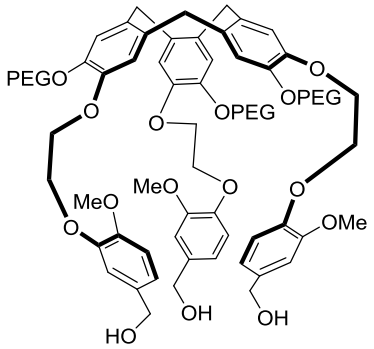

21

$C_{120}H_{192}O_{48}$

Mw = 2402.81

NaH 95 % (9 mg, 0.35 mmol) was added to a solution of **20** (183 mg, 0.1 mmol,) in 20 mL of anhydrous DMF. After one hour of stirring at 70 °C, **39** (131 mg, 0.5 mmol) was added in the solution and this mixture was heated at 70 °C overnight. DMF was evaporated and then an extraction water / dichloromethane, followed by washing with brine was carried out. The organic solution was finally dried over $MgSO_4$ and the dichloromethane was evaporated. A purification on reversed-phase column (water / acetonitrile 70 : 30 → 45 : 55) allowed the production of compound **21** in 58 % yield (139 mg).

Pale yellow oil

^{1}H NMR (400 MHz, $CDCl_3$, δ in ppm): 3.36 (s, 9H), 3.47 (d, *J* = 13.7 Hz, 3H), 3.24 – 3.68 (m, 126H), 3.77 (s, 9H), 3.95 – 4.05 (m, 6H), 4.32 (sl, 12H), 4.58 (s, 6H), 4.67 (d, *J* = 13.7 Hz, 3H), 6.82 – 6.95 (m, 15H)

^{13}C NMR (100 MHz, $CDCl_3$, δ in ppm): 36.31, 55.74, 58.99, 64.84, 67.96, 68.57, 69.19, 69.62, 70.48, 71.86, 110.98, 113.92, 116.73, 117.57, 119.28, 132.73, 133.10, 134.97, 147.36, 147.51, 147.79, 149.62

MS (MALDI-TOF) *m/z*: distribution centered at 2293.2 ± 44 ($[M+Na]^+$)

Compound 34

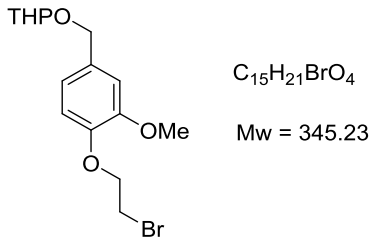

34

$C_{15}H_{21}BrO_4$

Mw = 345.23

A solution of PPTS (0.33 g, 1.3 mmol) in dichloromethane (5 mL) was added in one portion to a mixture of **39** (3.4 g, 13 mmol) and dihydropyran (1.64 g, 20 mmol) in THF (40 mL). The solution was stirred overnight at room temperature under argon. The solvent was stripped off to leave a residue, which was extracted with diethyl ether. The combined organic layers were washed twice with brine, dried over $MgSO_4$ and evaporated to give an oily residue. Chromatography on silica gel (diethyl ether / pentane 40 / 60) yielded compound **34** (3.6 g, 80 %)

Colorless oil

^{1}H NMR (400 MHz, $CDCl_3$, δ in ppm): 6.91 - 6.87 (m, 3H), 4.70 (d, *J* = 11.8 Hz, 1H), 4.65 (m, 1H), 4.42 (d, *J* = 11.8 Hz, 1H), 4.30 (t, *J* = 7.0 Hz, 2H), 3.90 (m, 1H), 3.86 (s, 3H), 3.62 (t, *J* = 7. 0 Hz , 2H), 3.55 (m, 1H), 1.90 - 1.40 (m, 6 H)

^{13}C NMR (100 MHz, $CDCl_3$, δ in ppm): 149.75, 146.81, 132.34, 120.45, 114.60, 112.09, 97.61, 69.25, 68.63, 62.26, 55.94, 30.56, 28.84, 25.41, 19.44

MS (ESI-TOF) *m/z*: 345.6, $[M+H]^+$

Compound 55

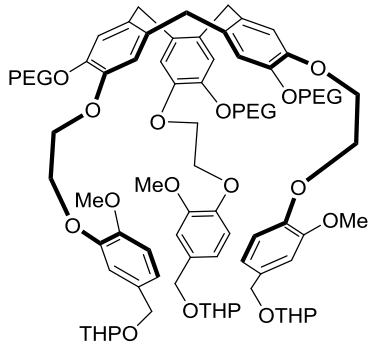

55

$C_{135}H_{216}O_{51}$

Mw = 2655.16

NaH 95 % (123 mg, 5.1 mmol) was added to a solution of **20** (1.59 g, 0.85 mmol,) in anhydrous DMF (175 mL). After one hour of stirring at 70 °C, **34** (1.76 g, 5.1 mmol) was added in the solution and this mixture was stirred at 70 °C overnight. DMF was evaporated and then an extraction water / dichloromethane, followed by washing with brine were carried out. The organic solution was finally dried over $MgSO_4$ and dichloromethane was evaporated. A purification on silica gel column (dichloromethane / methanol 100 : 0 → 90 : 10) allowed the obtention of compound **21** in 70 % yield (1.58 g).

Yellow oil

^{1}H NMR (400 MHz, $CDCl_3$, δ in ppm): 1.47 – 1.92 (m, 18 H), 3.36 (s, 9H), 3.47 (d, *J* = 13.7 Hz, 3H), 3.24 – 3.68 (m, 126H), 3.77 (s, 9H), 3.95 – 4.05 (m, 6H), 4.32 (sl, 12H), 4.58 (s, 6H), 4,67 (d, *J* = 13.7 Hz, 3H), 6.82 – 6.95 (m, 15H)

^{13}C NMR (100 MHz, $CDCl_3$, δ in ppm): 20.32, 25.34, 30.40, 36.36, 55.79, 59.06, 63.28, 68.01, 68.65, 69.29, 69.68, 70.53, 71.46, 71.96, 111.04, 113.99, 114.53, 116.78, 117.60, 119.33, 132.78, 133.14, 135.00, 147.41, 147.58, 147.84, 149.66

MS (ESI-TOF) *m/z*: distribution centered at 1175.3 ± 22, $[(M+2H-3THPOH)/2]^+$, irregular mass caused by an ionisation problem

Compound 23

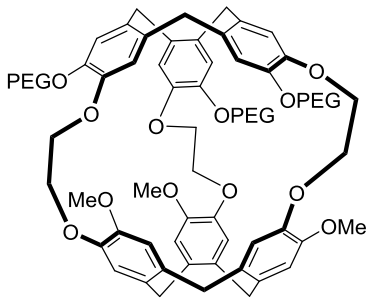

$C_{120}H_{186}O_{45}$

Mw = 2348.76

23

Compound **55** (0.75 g, 0.32 mmol) was dissolved in a minimum of chloroform, and then formic acid (750 mL) was added to the solution. The mixture was heated at 60 °C for 3 h. The reaction mixture was evaporated to afford a crude material, which was then purified by silica gel chromatography (dichloromethane / methanol 100 : 0 → 90 : 10) to afford compound **23** in 80 % yield (0.60 g).

Yellow oil

^{1}H NMR (400 MHz, $CDCl_3$, δ in ppm): 3.34 (d, *J* = 13,3 Hz, 3H), 3.36 (s, 9H), 3.40 (d, *J* = 13.3 Hz, 3H), 3.52 – 3.93 (m, 138H), 3.93 – 3.98 (m, 3H), 4.12 – 4.22 (m, 15H), 4.52 (d, *J* = 13.3 Hz, 3H), 4.55 (d, *J* = 13.3 Hz, 3H), 6.67 (s, 3H), 6.69 (s, 3H), 6.71 (s, 3H), 6.76 (s, 3H)

^{13}C NMR (100 MHz, $CDCl_3$, δ in ppm): 36.12, 36.15, 56.03, 59.00, 68.58, 69.23, 69.61, 69.82, 70.51, 70.80, 71.87, 114.36, 116.73, 120.39, 122.37, 131.61, 132.38, 133.94, 134.24, 146.65, 147.14, 148.96, 149.63

MS (MALDI-TOF) *m/z*: distribution centered at 2371.2 ± 44 ($[M+Na]^+$)

Compound 14

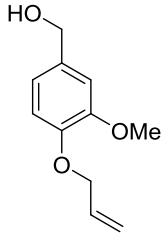

$C_{11}H_{14}O_3$

Mw = 194.23

14

A mixture of vanillyl alcohol (10 g, 0.065 mol), allyl bromide (6.3 mL, 0.073 mol), and potassium carbonate (9 g, 0.065 mol) in 15 mL of acetone was refluxed for 4 h with magnetic stirring. Then, after most of the solvent was stripped off, water was added and the organic material was extracted with dichloromethane, yielding 12.5 g (99%) of crude **14**. This product was recrystallized from 25 mL of diisopropyl ether, affording 10 g (80%) of pure **14**.

White powder

^{1}H NMR (400 MHz, $CDCl_3$, δ in ppm): 3.89 (s, 3H), 4.59-4.65 (m, 4H), 5.28 (dd, *J1* = 10.5 Hz, *J2* = 1.2 Hz, 1H) 5.8-6.3 (dd, J1 = 17.3 Hz, J2 = 1.4 Hz, 1H), 6.02-6.14 (m, 1H) 6.86 (s, 2H) and 6.94 (s, 1H)

^{13}C NMR (100 MHz, $CDCl_3$, δ in ppm): 55.6, 64.6, 147.1, 113.2, 118.9

MS (ESI-TOF) *m/z*: 195.1, $[M+H]^+$

Compound 32

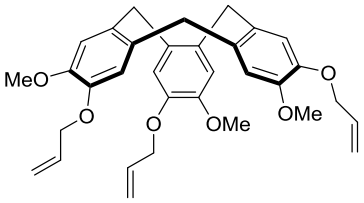

$C_{33}H_{36}O_6$

Mw = 528.65

32

To a solution of phenolprotected vanillyl alcohol **14** (10 g, 52 mmol) in methanol (60 mL), cooled in an ice bath and magnetically stirred, was added dropwise 30 mL of 70 % perchloric acid, and the resulting pink solution was stirred under nitrogen at room temperature for 18 h. The formed precipitate was dissolved by adding dichloromethane and the organic phase was thoroughly washed with water until neutral pH. The dichloromethane solution was dried over magnesium sulfate and evaporated under vacuum, affording a crystalline residue, which was washed by 20 mL of diethyl ether and finally isolated by suction filtration, yield 4.8 g of CTV **32** (53%)

^{1}H NMR (400 MHz, $CDCl_3$, δ in ppm): 3.51 (d, *J* = 13.6 Hz, 3H), 3.84 (s, 9H), 4.53 – 4.65 (m, 6H), 4.74 (d, *J* = 13.6 Hz, 3H), 5.25 (dd, *J1* = 1.4 Hz, *J2* = 10.4 Hz, 3H), 5.37 (dd, *J1* = 1.4 Hz, *J2* = 17.3 Hz, 3H), 6.00-6.12 (m, 3H), 6.79 (s, 3H), 6.85 (s, 3H)

^{13}C NMR (100 MHz, $CDCl_3$, δ in ppm): 36.3, 55.9, 70.0, 113.5, 115.5, 117.2, 131.6, 132.2, 133.6, 146.6, 148.1

MS (ESI-TOF) *m/z*: 529.1, $[M+H]^+$

Compound 25

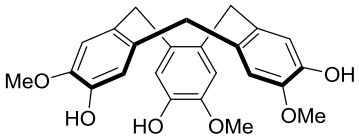

$C_{24}H_{24}O_6$

Mw = 408.45

25

A solution of **32** (4.4 g, 8.2 mmol), palladium acetate (122 mg, 0.56 mmol), triphenylphosphine (0.42 g, 1.6 mmol), diethylamine (40 mL), THF (100 mL), and H_2O (20 mL) was stirred at 80 °C under an argon atmosphere for about three hours. The dark solution was then stripped off under reduced pressure and the product was extracted with ethyl acetate. The organic layer was washed with water followed by filtration with filter paper to remove insoluble material. The combined organic layers were washed three times with brine and then dried over $MgSO_4$. Evaporation of the solvent under reduced pressure left a yellow solid, which was filtered and washed three times with diethyl ether to yield **25** (1.15 g, 67 %).

White solid

^{1}H NMR (400 MHz, acetone-D_6, δ in ppm): 6.99 (s, 3H), 6.92 (s, 3H), 4.73 (d, *J* = 13.5 Hz, 3H), 3.79 (s, 3 H), 3.43 (d, *J* = 13.5 Hz, 3H)

^{13}C NMR (100 MHz, acetone-D_6, δ in ppm): 145.2, 144.1, 132.4, 131.2, 115.4, 112.2, 55.0, 36.3

MS (ESI-TOF) *m/z*: 426.2, $[M+H+H_2O]^+$

Compound 60

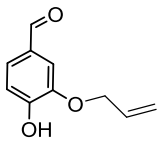

$C_{10}H_{10}O_3$

Mw = 178.19

60

To a suspension of NaH 95 % (1.93 g, 76.3 mmol) in anhydrous DMF (17 mL), it was slowly added at 0 °C a solution of 3,4-dihydroxybenzaldehyde (5 g, 36.2 mmol) in anhydrous DMF (17 mL). After 30 min of stirring, a solution of allyl bromide (3.1 mL, 36.2 mmol) in anhydrous DMF (17 mL) was added. The reaction was kept at room temperature with stirring for 18 hours. The reaction was quenched with water and a solution of HCl 1N was added until reaching pH 2. An extraction water / EtOAc was carried out and the organic phase was dried over $MgSO_4$ and concentrated under vacuum. A purification by chromatography on silica gel (cyclohexane / ethyl acetate 90 : 10 → 70 : 30) afforded the product **60** in 60 % yield (3.87 g).

White Solid

^{1}H NMR (400 MHz, $CDCl_3$, δ in ppm): 4.68 (d, *J* = 5.5 Hz, 2H), 5.38 (dd, *J1* = 10.5 Hz, *J2* = 1.2 Hz, 1H), 5.46 (dd, *J1* = 17.3 Hz, *J2* = 1.2 Hz, 1H), 6.08 – 6.18 (m, 1H), 6.26 (s, 1H), 7.05 (d, *J* = 7.8 Hz, 1H), 7.42 (s, 1H), 7.44 (d, *J* = 7.8 Hz, 1H), 9.82 (s, 1H)

^{13}C NMR (100 MHz, $CDCl_3$, δ in ppm): 69.89, 110.16, 114.55, 119.06, 127.45, 129.76, 131.93, 146.00, 151.78, 190.78

MS (ESI-TOF) *m/z*: 178.9, $[M+H]^+$

Compound 61

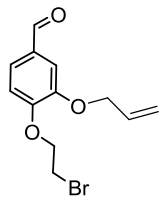

$C_{12}H_{13}BrO_3$

Mw = 285.14

61

Compound **60** (1.7 g, 9.7 mmol) was dissolved in DMF (15 mL) and then K_2CO_3 (1.6 g, 11.7 mmol) and 1,2-dibromoethane (3.3 mL, 39 mmol) were added into the solution. The reaction was heated at 80 °C with stirring for 16 hours. After cooling, diethyl ether was added and it was washed with a solution of HCl 1N. The organic phase was dried over $MgSO_4$ and concentrated under vacuum. A purification by chromatography on silica gel (cyclohexane / ethyl acetate 80 : 20 → 50 : 50) afforded product **61** in 70 % yield (1.9 g).

White Solid

^{1}H NMR (400 MHz, $CDCl_3$, δ in ppm): 3.68 (t, *J* = 6.6 Hz, 2H), 4,40 (t, *J* = 6.6 Hz, 2H), 4.65 (d, *J* = 5.5 Hz, 2H), 5.30 (dd, *J1* = 10.5 Hz, *J2*= 1.2 Hz, 1H), 5.44 (dd, *J1* = 17.3 Hz, *J2* = 1.2 Hz, 1H), 6.07 – 6.18 (m, 1H), 6.99 (d, *J* = 7.8 Hz, 1H), 7.44 (s, 1H), 7.46 (d, *J* = 7.8 Hz, 1H), 9.85 (s, 1H)

^{13}C NMR (100 MHz, $CDCl_3$, δ in ppm): 28.26, 68.81, 69.81, 112.16, 112.99, 118.10, 126.34, 130.80, 132.50, 148.95, 153.31, 190.71

MS (ESI-TOF) *m/z*: 285.1, $[M+H]^+$

Compound 37

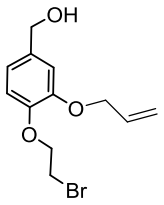

$C_{12}H_{15}BrO_3$

Mw = 287.15

37

Compound **61** (2 g, 8.5 mmol) was dissolved in THF (19 mL). The solution was cooled to 0 °C with an ice bath and then $NaBH_4$ (0.3 g, 8.5 mmol) and methanol (2.3 mL) were added. The reaction was kept at 0 °C with stirring for 30 minutes and then it was quenched with a solution of HCl 1N and extracted with dichloromethane. The organic phase was dried over $MgSO_4$ and concentrated under vacuum. Product **37** was obtained quantitatively (2 g).

White solid

^{1}H NMR (400 MHz, $CDCl_3$, δ in ppm): 3.65 (t, *J* = 6.6 Hz, 2H), 4.33 (t, *J* = 6.6 Hz, 2H), 4.55 – 4.65 (m, 4H), 5.30 (dd, *J1*= 10.5 Hz, *J*2= 1.2 Hz, 1H), 5.44 (dd, *J1* = 17.3 Hz, *J2* = 1.2 Hz, 1H), 6.07 – 6.18 (m, 1H), 6.89 – 6.96 (m, 3H)

^{13}C NMR (100 MHz, $CDCl_3$, δ in ppm): 29.09, 65.05, 69.59, 69.96, 113.59, 115.69, 117.65, 119.89, 133.17, 135.22, 147.45, 149.07

MS (ESI-TOF) *m/z*: 287.1, $[M+H]^+$

Compound 63.

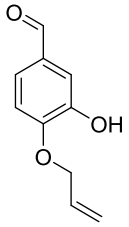

$C_{10}H_{10}O_3$

Mw = 178.19

63

To a suspension of NaH 95 % (1.05 g, 43.8 mmol) in anhydrous DMF (17 mL), it was slowly added at 0 °C a solution of 3,4-dihydroxybenzaldehyde (5 g, 36.2 mmol) in anhydrous DMF (17 mL). After 30 min of stirring, a solution of allyl bromide (3.1 mL, 36.2 mmol) in anhydrous DMF (17 mL) was added. The reaction was kept at room temperature with stirring for 18 hours. After, the reaction was quenched with water and a solution of HCl 1N was added until reaching pH 2. An extraction water / ethyl acetate was carried out and the organic phase was dried over $MgSO_4$ and concentrated under vacuum. A purification by chromatography on silica gel (cyclohexane / ethyl acetate 90 : 10 → 70 : 30) afforded the product **63** in 57 % yield (3.68 g).

White Solid

^{1}H NMR (400 MHz, $CDCl_3$, δ in ppm): 4.70 (d, *J* = 5.4 Hz, 2H), 5.37 (d, *J* = 10.3 Hz, 1H), 5.43 (dd, *J* = 17.2 Hz, 1H), 5.84 (s, 1H), 6.01 – 6.12 (m, 1H), 6.96 (d, *J* = 8.3 Hz, 1H), 7.40 (dd, *J1* = 8.3 Hz, *J2* = 1.7 Hz, 1H), 7.45 (d, *J* = 1.7 Hz, 1H), 9.84 (s, 1H)

^{13}C NMR (100 MHz, $CDCl_3$, δ in ppm): 69.91, 111.37, 114.34, 119.24, 124.29, 130.71, 131.76, 146.22, 150.69, 190.98

MS (ESI-TOF) *m/z*: 178.9, $[M+H]^+$

Compound 67

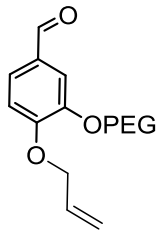

$C_{33}H_{56}O_{14}$

Mw = 676.80

67

Compound **63** (3.36 g, 18.9 mmol) was dissolved in DMF (35 mL) and then K_2CO_3 (3.04 g, 22.0 mmol) and compound **17** (3,3 mL, 39 mmol) were added into the solution. The reaction was heated to 80 °C with stirring for 16 hours. The solvent was evaporated and an extraction dichloromethane / water was carried out. The organic was washed twice with a solution of K_2CO_3 pH = 11 and twice with water, then was dried over $MgSO_4$ and concentrated under vacuum. A purification by chromatography on silica gel (dichloromethane / methanol 100 : 0 → 90 : 10) afforded product **67** in 92 % yield (11.8 g).

Pale yellow oil

^{1}H NMR (400 MHz, $CDCl_3$, δ in ppm): 3.36 (s, 3H), 3.50 – 3.76 (m, 40H), 3.89 (t, *J* = 4.9 Hz, 2H), 4.22 (t, *J* = 4.9 Hz, 2H), 4.66 (d, *J* = 5.9 Hz, 2H), 5.30 (dd, *J1* = 10.8 Hz, *J2*= 1.3 Hz, 1H), 5.42 (dd, *J1* = 17.2 Hz, *J2* = 1.3 Hz, 1H), 5.99 – 6.10 (m, 1H), 6.95 (d, *J* = 8.8 Hz, 1H), 7.38 – 7.45 (m, 2H), 9.81 (s, 1H)

^{13}C NMR (100 MHz, $CDCl_3$, δ in ppm): 30.90, 53.41, 59.00, 68.68, 69.47, 69.64, 70.52, 70.89, 71.88, 111.69, 112.45, 118.15, 126.52, 130.10, 132.38, 149.13, 153.93, 190.80

MS (ESI-TOF) *m/z*: distribution centered at 809.6 ± 44, $[M+H]^+$

Compound 68

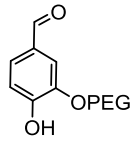

$C_{30}H_{52}O_{14}$

Mw = 636.73

68

A solution of **67** (7.7 g, 11.4 mmol), palladium acetate (180 mg, 0.8 mmol), triphenylphosphine (0.3 g, 1.16 mmol), diethylamine (60 mL), THF (150 mL), and H_2O (30 mL) was stirred at 80 °C under a nitrogen atmosphere for 3 h. The dark solution was then stripped off under reduced pressure and the product was extracted with ethyl acetate. The organic layer was washed once with water followed by filtration with filter paper to remove insoluble dark material. The combined organic layers were washed three times with brine and then dried over Mg_2SO_4. A purification by chromatography on silica gel (dichloromethane / methanol 100 : 0 → 90 : 10) afforded product **68** in 82 % yield (5.9 g).

Pale yellow oil

^{1}H NMR (400 MHz, $CDCl_3$, δ in ppm): 3.37 (s, 3H), 3.50 – 3.76 (m, 40H), 3.86 (t, *J* = 4.7 Hz, 2H), 4.22 (t, *J* = 4.7 Hz, 2H), 7.00 (d, *J* = 8.9 Hz, 1H), 7.39 – 7.46 (m, 2H), 9.79 (s, 1H)

^{13}C NMR (100 MHz, $CDCl_3$, δ in ppm): 58.99, 68.22, 69.26, 70.17, 70.29, 70.36, 70.51, 71.88, 111.34, 115.84, 128.00, 129.06, 146.94, 153.77, 190.79

MS (ESI-TOF) *m/z*: distribution centered at 769.7 ± 44, $[M+H]^+$

Compound 69

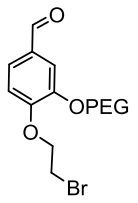

$C_{32}H_{55}BrO_{14}$

Mw = 743.68

69

Compound **68** (5.19 g, 8.15 mmol) was dissolved in DMF (15 mL) and then K_2CO_3 (1.35 g, 9.78 mmol) and 1,2-dibromoethane (2.8 mL, 33 mmol) were added into the solution. The reaction was heated at 80 °C with stirring for 16 hours. After cooling, diethyl ether was added and it was washed with a solution of HCl 1N. The organic phase was dried over $MgSO_4$ and concentrated under vacuum. A purification by chromatography on silica gel (dichloromethane / methanol 100 : 0 → 90 : 10) afforded product **69** in 79 % yield (4.8 g).

Pale yellow oil

^{1}H NMR (400 MHz, $CDCl_3$, δ in ppm): 3.37 (s, 3H), 3.50 – 3.78 (m, 42H), 3.90 (t, *J* = 4.8 Hz, 2H), 4.23 (t, *J* = 4.8 Hz, 2H), 4.40 (t, *J* = 6.4 Hz, 2H), 6.98 (d, *J* = 9.0 Hz, 1H), 7.41 – 7.47 (m, 2H), 9.84 (s, 1H)

^{13}C NMR (100 MHz, $CDCl_3$, δ in ppm): 28.58, 53.41, 59.00, 68.97, 69.46, 70.52, 70.66, 70.94, 71.89, 112.27, 113.42, 126.35, 130.87, 149.36, 153.35, 190.75

MS (ESI-TOF) *m/z*: distribution centered at 877.6 ± 44, $[M+H]^+$

Compound 70

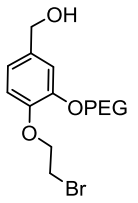

$C_{32}H_{57}BrO_{14}$

Mw = 745.7

70

Compound **68** (3.25 g, 4.37 mmol) was dissolved in THF (15 mL). The solution was cooled to 0 °C with an ice bath and then $NaBH_4$ (165 mg, 4.37 mmol) and methanol (1.8 mL, 43.7 mmol) were added. The reaction was kept at 0 °C with stirring for 30 minutes and then it was quenched with a solution of HCl 1N and extracted with dichloromethane. The organic phase was dried over $MgSO_4$ and concentrated under vacuum. Product **70** was obtained quantitatively (3.26 g).

Transparent oil

^{1}H NMR (400 MHz, $CDCl_3$, δ in ppm): 3.37 (s, 3H), 3.50 – 3.76 (m, 42H), 3.86 (t, *J* = 4.9 Hz, 2H), 4.19 (t, *J* = 4.9 Hz, 2H), 4.31 (t, *J* = 6.6 Hz, 2H), 4.59 (d, *J* = 5.4 Hz, 2H), 6.84 – 6.92 (m, 2H), 7.01 (d, *J* = 1.1 Hz, 1H)

^{13}C NMR (100 MHz, $CDCl_3$, δ in ppm): 29.42, 59.01, 64.84, 68.92, 69.75, 69.84, 70.52, 70.66, 70.80, 70.89, 113.95, 116.17, 120.01, 135.73, 147.44, 149.41

MS (ESI-TOF) *m/z*: distribution centered at 879.7 ± 44, $[M+H]^+$

Compound 58

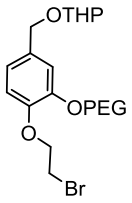

$C_{37}H_{65}BrO_{15}$

Mw = 829.82

58

A solution of PPTS (103 mg, 0.41 mmol) in CH_2Cl_2 (1.8 mL) was added in one portion to a mixture of **39** (3.1 g, 4.1 mmol) and dihydropyran (0.56 mL, 6.2 mmol) in THF (15 mL). The solution was stirred overnight at room temperature under nitrogen. The solvent was stripped off and the residue was extracted with diethyl ether. The combined organic layers were washed twice with brine, dried over Mg_2SO_4 and evaporated to leave an oily residue. A purification by chromatography on silica gel (dichloromethane / methanol 100 : 0 → 90 : 10) afforded product **58** in 99 % yield (3.35 g).

Transparent oil

^{1}H NMR (400 MHz, $CDCl_3$, δ in ppm): 1.48 – 1.66 (m, 4H), 1.67 – 1.77 (m, 1H), 1.79 – 1.90 (m, 1H), 3.37 (s, 3H), 3.49 – 3.77 (m, 43H), 3.83 – 3.94 (m, 3H), 4.17 (t, *J* = 4.9 Hz, 2H), 4.30 (t, *J* = 6.6 Hz, 2H), 4.41 (d, *J* = 11.9 Hz, 2H), 6.64 – 6.72 (m, 2H), 6.86 (s, 1H), 6.94 (s, 1H)

^{13}C NMR (100 MHz, $CDCl_3$, δ in ppm): 19.40, 25.40, 29.42, 30.54, 58.98, 62.21, 68.50, 68.81, 69.65, 69.83, 70.50, 70.61, 71.87, 97.58, 114.50, 116.13, 121.08, 132.70, 147.42, 149.28

MS (ESI-TOF) *m/z*: distribution centered at 875.6 ± 44, $[M+H]^+$

Compound 71

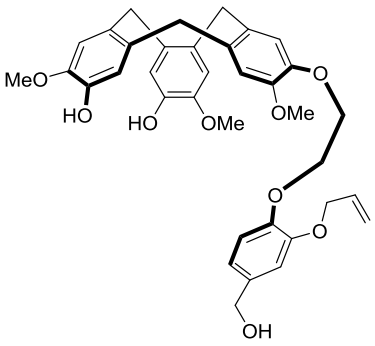

$C_{36}H_{38}O_9$

Mw = 614.69

71

Compound **37** (0.35 g, 1.22 mmol) was added in one portion to a stirred solution of **25** (1 g, 2.45 mmol) and cesium carbonate (1.6 g, 4.90 mmol) in dry DMF (63 mL). The solution was heated for 18 h at 80 °C under nitrogen. After cooling, the dark mixture was poured into water and the product was extracted with ethyl acetate. The combined organic layers were washed several times with brine and then dried over $MgSO_4$. The solvent was stripped off by rotary evaporation and the residue was purified by chromatography on silica gel (cyclohexane / ethyl acetate 50 : 50 → 0 : 100). 277 mg of expected product **31** was obtained (30 % yield based on recovered starting material).

White solid

^{1}H NMR (400 MHz, $CDCl_3$, δ in ppm): 3.43 – 3.55 (m, 3H), 3.72 (s, 3H), 3.79 – 3.85 (m, 6H), 4.25 – 4.42 (m, 4H), 4.54 (d, *J* = 5.1 Hz, 2H), 4.59 (s, 2H), 4.65 – 4.79 (m, 3H), 5.21 (dd, *J1* = 10.5 Hz, *J*2= 1.2 Hz, 1H), 5.36 (dd, *J1* = 17.2 Hz, *J*2= 1.2 Hz, 1H), 5.94 – 6.08 (m, 1H), 6.74 – 7.00 (m, 9H)

^{13}C NMR (100 MHz, $CDCl_3$, δ in ppm): 36.21, 36.26, 36.36, 55.99, 56.02, 56.13, 65.23, 67.66, 68.14, 70.49, 110.92, 112.15, 113.68, 113.73, 115.48, 115.52, 116.73, 118.17, 119.39, 131.15, 131.22, 131.92, 132.20, 132.48, 133.05, 133.49, 134.31, 144.06, 144.09, 145.21, 146.62, 147.55, 148.48, 149.62

MS (ESI-TOF) *m/z*: 597.4, $[M+H-H_2O]^+$; 1193.9, $[2M+1]^+$

Compound 72

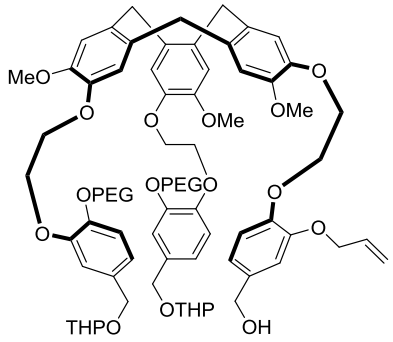

$C_{110}H_{166}O_{39}$

Mw = 2112.50

72

Compound **58** (0.42 g, 0.51 mmol) was added to a stirred solution of **71** (78 mg, 0.13 mmol) and cesium carbonate (0.17 g, 0.51 mmol) in dry DMF (6 mL). The solution was heated for 18 h at 80 °C under nitrogen. The solvent was stripped off and the residue was extracted with dichloromethane / water. The combined organic layers were washed with brine, dried over Mg_2SO_4 and evaporated to leave an oily residue. A purification by chromatography on silica gel (dichloromethane / methanol 100 : 0 → 90 : 10) afforded product **72** in 60 % yield (164 mg).

Yellow oil

^{1}H NMR (400 MHz, $CDCl_3$, δ in ppm): 1.46 – 1.66 (m, 8H), 1.68 – 1.77 (m, 2H), 1.78 – 1.90 (m, 2H), 3.37 (s, 6H), 3.48 – 3.70 (m, 88H), 3.71 – 3.76 (m, 6H) 3.77 – 3.85 (m, 4H), 3.86 – 3.95 (m, 2H), 4.17 (t, *J* = 5.0 Hz, 4H), 4.24 – 4.37 (m, 12H), 4.40 (d, *J* = 11.6 Hz, 2H), 4.54 (d, *J* = 5.4 Hz, 2H), 4.57 (s, 2H), 4.63 – 4.78 (m, 7H), 5.20 (dd, *J1* = 10.5 Hz, *J*2= 1.3 Hz, 1H), 5.35 (dd, *J1* = 17.3 Hz, *J*2= 1.3 Hz, 1H), 5.93 – 6.08 (m, 1H), 6.77 – 7.00 (m, 15H)

^{13}C NMR (100 MHz, $CDCl_3$, δ in ppm): 19.32, 25.33, 30.47, 36.31, 56.07, 58.89, 60.86, 62.09, 64.47, 66.49, 67.86, 68.45, 68.66, 69.54, 70.41, 70.61, 71.79, 97.45, 113.68, 113.74, 113.85, 114.50, 114.59, 114.82, 116.29, 118.17, 121.10, 131.70, 131.82, 132.76, 132.85, 133.49, 134.87, 135.13, 146.69, 147.76, 147.82, 148.03, 148.19, 148.38, 148.47, 148.54, 148.60, 148.71, 148.80, 148.90

MS (ESI-TOF) *m/z*: distribution centered at 968.1 ± 22, $[(M+2H-2THPOH-H_2O)/2]^+$, irregular mass caused by an ionisation problem

Compound 73

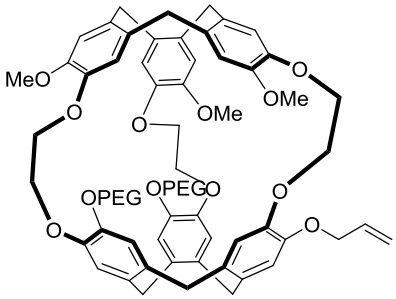

$C_{100}H_{144}O_{34}$

Mw = 1890.24

73

Compound **72** (0.1 g, 0.039 mmol) was dissolved in chloroform (50 mL), and then formic acid (50 mL) was added to the solution. The mixture was heated at 60 °C for 3 h. The cooled reaction mixture was evaporated to afford a crude material, which was then purified by silica gel chromatography (dichloromethane / methanol 100 : 0 → 90 : 10) to afford compound **73** in 60 % yield (44 mg).

Yellow oil

^{1}H NMR (400 MHz, $CDCl_3$, δ in ppm): 3.37 (s, 6H), 3.48 – 3.71 (m, 92H), 3.72 (s, 6H), 3.82 (t, *J* = 4.9 Hz, 4H), 4.17 (t, *J* = 4.9 Hz, 4H), 4.23 – 4.44 (m, 12H), 4.58 (d, *J* = 5.2 Hz, 2H), 4.74 (d, *J* = 13.8 Hz, 3H), 5.24 (d, *J* = 10.1 Hz, 1H), 5.38 (d, *J* = 17.3 Hz, 1H), 5.99 – 6.11 (m, 1H), 6.75 – 7.00 (m, 12H)

^{13}C NMR (100 MHz, $CDCl_3$, δ in ppm): 27.78, 29.60, 31.51, 31.87, 36.32, 36.59, 50.09, 58.90, 63.32, 65.47, 67.70, 67.82, 68.59, 68.73, 69.52, 69.78, 69.94, 70.31, 70.56, 71.74, 113.32, 113.85, 114.54, 114.76, 115.13, 116.29, 117.51, 117.75, 119.81, 120.11, 121.79, 122.00, 128.64, 131.79, 133.07, 133.25, 135.07, 146.59, 147.74, 148.35, 148.75

MS (ESI-TOF) *m/z*: distribution centered at 968.1 ± 22, $[(M+2H)/2]^+$

Compound 79

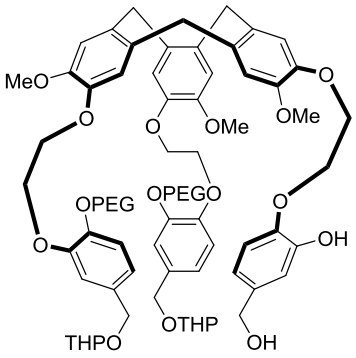

79

$C_{107}H_{162}O_{39}$

Mw = 2072.43

A solution of **72** (40 mg, 0.019 mmol), palladium acetate (0.4 mg, 1.8 µmol), triphenylphosphine (0.6 mg, 2.3 µmol), diethylamine (0.2 mL), THF (0.3 mL), and H_2O (0.1 mL) was stirred at 80 °C under an argon atmosphere for 3 h. The dark solution was then stripped off under reduced pressure and the product was extracted with ethyl acetate. The organic layer was washed with water followed by filtration with filter paper to remove insoluble dark material. The combined organic layers were washed three times with brine and then dried over Mg_2SO_4. A purification by chromatography on silica gel (dichloromethane / methanol 100 : 0 → 90 : 10) afforded product **68** in 63 % yield (25 mg).

Yellow oil

^{1}H NMR (400 MHz, $CDCl_3$, δ in ppm): 1.46 – 1.66 (m, 8H), 1.67 – 1.77 (m, 2H), 1.78 – 1.90 (m, 2H), 3.37 (s, 6H), 3.48 – 3.70 (m, 85H), 3.72 (s, 1H), 3.74 (s, 1H), 3.75 (s, 1H), 3.77 – 3.83 (m, 4H), 3.86 – 3.94 (m, 2H), 4.16 (t, *J* = 5.0 Hz, 4H), 4.21 – 4.37 (m, 12H), 4.40 (d, *J* = 11.7 Hz, 2H), 4.55 (s, 2H), 4.63 – 4.79 (m, 7H), 6.75 – 6.98 (m, 15H)

^{13}C NMR (100 MHz, $CDCl_3$, δ in ppm): 19.32, 25.33, 30.47, 36.31, 56.07, 58.89, 60.86, 62.09, 64.47, 66.49, 67.86, 68.45, 68.66, 69.54, 70.41, 70.61, 71.79, 97.45, 113.68, 113.74, 113.85, 114.50, 114.59, 114.82, 116.29, 121.10, 131.70, 131.82, 132.76, 132.85, 134.87, 135.13, 146.69, 147.76, 147.82, 148.03, 148.19, 148.38, 148.47, 148.54, 148.60, 148.71, 148.80, 148.90

MS (ESI-TOF) *m/z*: distribution centered at 1850.4 ± 44, $[M+H-2THPOH-H_2O]^+$, irregular mass caused by an ionisation problem

Compound 80

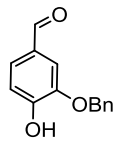

$C_{14}H_{12}O_3$

Mw = 228.25

80

To a suspension of NaH 95 % (0.36 g, 14.5 mmol) in anhydrous DMF (3 mL), it was slowly added at 0 °C a solution of 3,4-dihydroxybenzaldehyde (1 g, 7.24 mmol) in anhydrous DMF (3 mL). After 30 min of stirring, a solution of benzyl bromide (0.9 mL, 7.24 mmol) in anhydrous DMF (3 mL) was added. The reaction was kept at room temperature with stirring for 18 h. The reaction was quenched with water and a solution of HCl 1N was added until reaching pH 2. An extraction water / ethyl acetate was carried out and the organic phase was dried over $MgSO_4$ and concentrated under vacuum. A purification by chromatography on silica gel (cyclohexane / ethyl acetate 90 : 10 → 70 : 30) afforded the product **80** in 39 % yield (0.64 g).

White Solid

^{1}H NMR (400 MHz, $CDCl_3$, δ in ppm): 5.15 (s, 2H), 6.51 (s, 1H), 7.06 (d, *J* = 8.1 Hz, 1H), 7.33 – 7.46 (m, 6H), 7.51 (d, *J* = 1.4 Hz, 1H), 9.80 (s, 1H)

^{13}C NMR (100 MHz, $CDCl_3$, δ in ppm): 70.05, 112.56, 114.01, 126.52, 127.29, 128.08, 128.64, 130.75, 137.63, 149.02, 155.24, 190.72

MS (ESI-TOF) *m/z*: 229.2, $[M+H]^+$

Compound 81

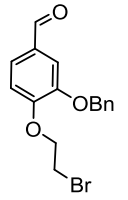

$C_{16}H_{15}BrO_3$

Mw = 335.20

81

Compound **80** (0.59 g, 2.6 mmol) was dissolved in DMF (5 mL) and then K_2CO_3 (0.43 g, 3.1 mmol) and 1,2-dibromoethane (0.9 mL, 10.4 mmol) were added into the solution. The reaction was heated at 80 °C with stirring for 16 h. After cooling, diethyl ether was added and it was washed with a solution of HCl 1N. The organic phase was dried over $MgSO_4$ and concentrated under vacuum. A purification by chromatography on silica gel (cyclohexane / ethyl acetate 80 : 20 → 50 : 50) afforded product **81** in 50 % yield (0.43 g).

White Solid

^{1}H NMR (400 MHz, $CDCl_3$, δ in ppm): 3.69 (t, *J* = 6.6 Hz, 2H), 4.42 (t, *J* = 6.6 Hz, 2H), 5.19 (s, 2H), 7.00 (d, *J* = 8.1 Hz, 1H), 7.29 – 7.53 (m, 7H), 9.84 (s, 1H)

^{13}C NMR (100 MHz, $CDCl_3$, δ in ppm): 28.49, 68.78, 70.01, 112.66, 113.01, 126.51, 127.29, 128.02, 128.54, 130.75, 136.30, 149.02, 153.54, 190.71

MS (ESI-TOF) *m/z*: 335.3, $[M+H]^+$

Compound 82

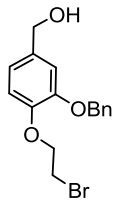

$C_{16}H_{17}BrO_3$

Mw = 337.21

82

Compound **81** (0.43 g, 1.27 mmol) was dissolved in THF (5 mL). The solution was cooled to 0 °C with an ice bath and then $NaBH_4$ (58 mg, 1.52 mmol) and methanol (0.5 mL) were added. The reaction was kept at 0 °C with stirring for 30 minutes and then quenched with a solution of HCl 1N and extracted with dichloromethane. The organic phase was dried over $MgSO_4$ and concentrated under vacuum. Product **82** was obtained in 99 % yield (0.43 g).

White solid

^{1}H NMR (400 MHz, $CDCl_3$, δ in ppm): 3.64 (t, *J* = 6.4 Hz, 2H), 4.33 (t, *J* = 6.4 Hz, 2H), 4.57 (s, 2H), 5.13 (s, 2H), 6.85 – 6.95 (m, 2H), 7.00 (d, *J* = 0.9 Hz, 1H), 7.29 – 7.51 (m, 5H)

^{13}C NMR (100 MHz, $CDCl_3$, δ in ppm): 29.30, 64.93, 69.58, 71.18, 114.02, 115.70, 112.10, 127.31, 127.84, 128.47, 135.23, 136.91, 147.62, 149.14

MS (ESI-TOF) *m/z*: 337.3, $[M+H]^+$

Compound 83

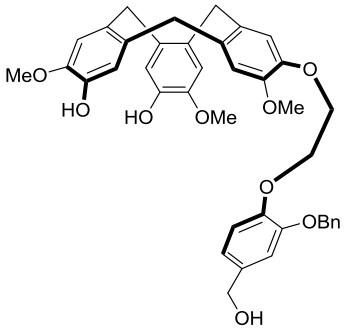

$C_{40}H_{40}O_9$

Mw = 664.75

83

Compound **82** (195 mg, 0.52 mmol) was added in one portion to a stirred solution of **25** (423 mg, 1.03 mmol) and cesium carbonate (674 mg, 2.07 mmol) in dry DMF (26 mL). The solution was then heated for 18 h at 80 °C under argon. After cooling, the dark mixture was poured into water and the product was extracted with ethyl acetate. The combined organic layers were washed several times with brine and then dried over $MgSO_4$. The solvent was stripped off by rotary evaporation and the residue was purified by chromatography on silica gel (cyclohexane / ethyl acetate 50 : 50 → 0 : 100). 118 mg of expected product **83** was thus obtained (43 % yield based on recovered starting material).

White solid

^{1}H NMR (400 MHz, $CDCl_3$, δ in ppm): 3.42 – 3.56 (m, 3H), 3.67 (s, 3H), 3.79 (s, 3H), 3.84 (s, 3H), 4.27 – 4.41 (m, 4H), 4.57 (s, 2H), 4.70 (d, *J* = 13.7 Hz, 3H), 5.09 (s, 2H), 6.70 – 7.00 (m, 9H), 7.20 – 7.33 (m, 3H), 7.39 (d, *J* = 7.0 Hz, 2H)

^{13}C NMR (100 MHz, $CDCl_3$, δ in ppm): 36.21, 36.26, 36.36, 55.99, 56.02, 56.13, 65.23, 67.66, 68.14, 71.17, 110.92, 112.15, 113.68, 113.73, 115.48, 115.52, 116.73, 119.39, 127.06, 127.59, 128.88, 131.15, 131.22, 131.92, 132.20, 132.48, 133.05, 134.31, 136.72, 144.06, 144.09, 145.21, 146.62, 147.55, 148.48, 149.62

MS (ESI-TOF) *m/z*: 664.8, $[M+H]^+$

Compound 84

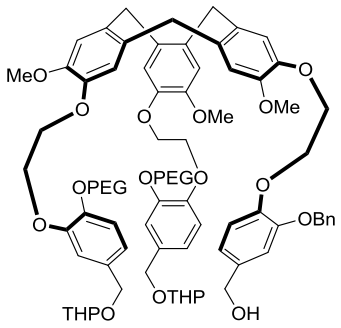

$C_{114}H_{168}O_{39}$

Mw = 2162.56

84

Compound **58** (0.36 g, 0.43 mmol) was added to a stirred solution of **83** (115 mg, 0.17 mmol) and cesium carbonate (0.23 g, 0.69 mmol) in dry DMF (7 mL). The solution was then heated for 18 h at 80 °C under nitrogen. The solvent was stripped off and the residue was extracted with dichloromethane / water. The combined organic layers were washed with brine, dried over Mg_2SO_4 and evaporated to leave an oily residue. A purification by chromatography on silica gel (dichloromethane / methanol 100 : 0 → 90 : 10) afforded product **84** in 76 % yield (279 mg).

Yellow oil

^{1}H NMR (400 MHz, $CDCl_3$, δ in ppm): 1.46 – 1.66 (m, 8H), 1.67 – 1.77 (m, 2H), 1.78 – 1.90 (m, 2H), 3.37 (s, 6H), 3.48 – 3.72 (m, 91H), 3.74 (s, 3H), 3.77 – 3.86 (m, 4H), 3.86 – 3.96 (m, 2H), 4.17 (t, *J* = 5.2 Hz, 4H), 4.23 – 4.46 (m, 14H), 4.56 (s, 2H), 4.63 – 4.78 (m, 7H), 5.08 (s, 2H), 6.74 – 7.02 (m, 15H), 7.20 – 7.32 (m, 3H), 7.38 (d, *J* = 7.0 Hz, 2H)

^{13}C NMR (100 MHz, $CDCl_3$, δ in ppm): 19.32, 25.33, 30.47, 36.31, 56.07, 58.89, 60.86, 62.09, 64.47, 66.49, 67.86, 68.45, 68.66, 69.54, 70.61, 71. 16, 71.79, 97.45, 113.68, 113.74, 113.85, 114.50, 114.59, 114.82, 116.29, 121.10, 127.13, 127.58, 128.93, 131.70, 131.82, 132.76, 132.85, 134.87, 135.13, 136.66, 146.69, 147.76, 147.82, 148.03, 148.19, 148.38, 148.47, 148.54, 148.60, 148.71, 148.80, 148.90

MS (ESI-TOF) *m/z*: distribution centered at 971.0 ± 22, $[(M+2H-2THPOH-H_2O)/2]^+$, irregular mass caused by an ionisation problem

Compound 85

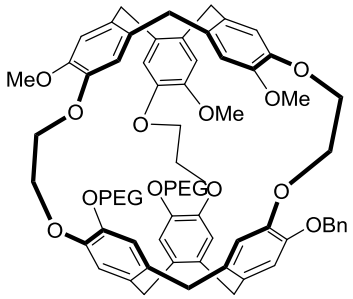

$C_{104}H_{146}O_{34}$

Mw = 1940.28

85

Compound **84** (78 mg, 0.036 mmol) was dissolved in chloroform (40 mL), and then formic acid (40 mL) was added to the solution. The mixture was heated at 60 °C for 3 h. The cooled reaction mixture was evaporated to afford a crude material, which was then purified by silica gel chromatography (dichloromethane / methanol 100 : 0 → 90 : 10) to afford compound **85** in 67 % yield (46 mg).

Yellow oil

^{1}H NMR (400 MHz, $CDCl_3$, δ in ppm): 3.37 (s, 6H), 3.48 – 3.71 (m, 95H), 3.72 (s, 3H), 3.79 – 3.84 (m, 4H), 4.16 (t, *J* = 4.6 Hz, 4H), 4.26 – 4.43 (m, 12H), 4.64 – 4.79 (m, 3H), 5.10 (s, 2H), 6.74 – 7.01 (m, 12H), 7.20 – 7.32 (m, 3H), 7.39 (d, *J* = 6.9 Hz, 2H)

^{13}C NMR (100 MHz, $CDCl_3$, δ in ppm): 27.78, 29.60, 31.51, 31.87, 36.32, 36.59, 50.09, 58.90, 63.32, 65.47, 67.70, 67.82, 68.59, 68.73, 69.52, 69.78, 69.94, 70.31, 71.30, 71.74, 113.32, 113.85, 114.54, 114.76, 115.13, 116.29, 117.51, 119.81, 120.11, 121.79, 122.00, 127. 21, 127.70, 128.64, 129.02, 131.79, 133.07, 135.07, 136.57, 146.59, 147.74, 148.35, 148.75

MS (ESI-TOF) *m/z*: distribution centered at 971.0± 22, $[(M+2H)/2]^+$

Compound 88

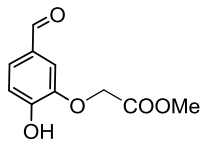

$C_{10}H_{10}O_5$

Mw = 210.19

88

To a suspension of NaH 95 % (2.2 g, 90.6 mmol) in anhydrous DMF (17 mL), it was slowly added at 0 °C a solution of 3,4-dihydroxybenzaldehyde (5 g, 36.2 mmol) in anhydrous DMF (17 mL). After 30 min of stirring, a solution of methyl bromoacetate (3.4 mL, 36.2 mmol) in anhydrous DMF (17 mL) was added. The reaction was kept at room temperature with stirring for 18 h. The reaction was quenched with water and a solution of HCl 1N was added until reaching pH 2. An extraction water / ethyl acetate was carried out and the organic phase was dried over $MgSO_4$ and concentrated under vacuum. A purification by chromatography on silica gel (cyclohexane / ethyl acetate 90 : 10 → 70 : 30) afforded the product **88** in 67 % yield (5.1 g).

White Solid

^{1}H NMR (400 MHz, $CDCl_3$, δ in ppm): 3.78 (s, 3H), 4.71 (s, 2H), 7.04 (d, *J* = 8.2 Hz, 1H), 7.38 (d, *J* = 1.7 Hz, 1H), 7.46 (dd, *J1* = 8.2 Hz, *J2* = 1.7 Hz, 1H), 9.76 (s, 1H)

^{13}C NMR (100 MHz, $CDCl_3$, δ in ppm): 52.60, 67.49, 113.90, 116.09, 128.65, 129.58, 146.22, 153.17, 170.08, 190.47

MS (ESI-TOF) *m/z*: 210.9, $[M+H]^+$

Compound 89

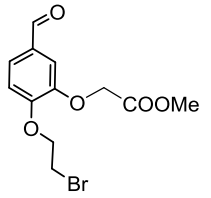

$C_{12}H_{13}BrO_5$

Mw = 317.14

89

Compound **88** (3.96 g, 18.9 mmol) was dissolved in DMF (45 mL) and then K_2CO_3 (3.13 g, 22.6 mmol) and 1,2-dibromoethane (12.9 mL, 0.15 mol) were added into the solution. The reaction was heated at 80 °C with stirring for 16 h. After cooling, diethyl ether was added and it was washed with a solution of HCl 1N. The organic phase was dried over $MgSO_4$ and concentrated under vacuum. A purification by chromatography on silica gel (cyclohexane / ethyl acetate 100 : 0 → 75 : 25) afforded product **89** in 52 % yield (3.1 g).

White Solid

^{1}H NMR (400 MHz, $CDCl_3$, δ in ppm): 3.65 (t, *J* = 6.5 Hz, 2H), 3.74 (s, 3H), 4.37 (t, *J* = 6.5 Hz, 2H), 4.71 (s, 2H), 6.97 (d, *J* = 8.1 Hz, 1H), 7.32 (d, *J* = 1.9 Hz, 1H), 7.45 (dd, *J1* = 8.1 Hz, *J2* = 1.9 Hz, 1H), 9.77 (s, 1H)

^{13}C NMR (100 MHz, $CDCl_3$, δ in ppm): 28.31, 52.10, 66.02, 68.77, 113.18, 113.28, 126.98, 130.48, 147.94, 153.25, 168.66, 190.29

MS (ESI-TOF) *m/z*: 316.9, $[M+H]^+$

Compound 90

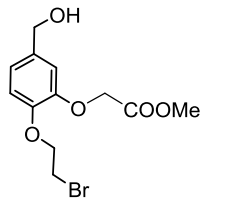

$C_{12}H_{15}BrO_5$

Mw = 319.15

90

Compound **89** (3.1 g, 9.8 mmol) was dissolved in THF (33 mL). The solution was cooled to 0 °C with an ice bath and then $NaBH_4$ (0.37 g, 9.8 mmol) and methanol (4 mL) were added. The reaction was kept at 0 °C with stirring for 30 minutes and then it was quenched with a solution of HCl 1N and extracted with dichloromethane. The organic phase was dried over $MgSO_4$ and concentrated under vacuum. A purification by chromatography on silica gel (cyclohexane / ethyl acetate 50 : 50 → 100 : 0) afforded the product **90** in 77 % yield (2.4 g).

White solid

^{1}H NMR (400 MHz, $CDCl_3$, δ in ppm): 3.62 (t, *J* = 6.4 Hz, 2H), 3.75 (s, 3H), 4.30 (t, *J* = 6.4 Hz, 2H), 4.52 (s, 2H), 4.65 (s, 2H), 6.82 – 6.94 (m, 3H

^{13}C NMR (100 MHz, $CDCl_3$, δ in ppm): 29.15, 52.07, 64.33, 66.56, 69.44, 114.60, 115.54, 121.14, 135.28, 147.44, 147.93, 169.43

MS (ESI-TOF) *m/z*: 318.9, $[M+H]^+$

Compound 91

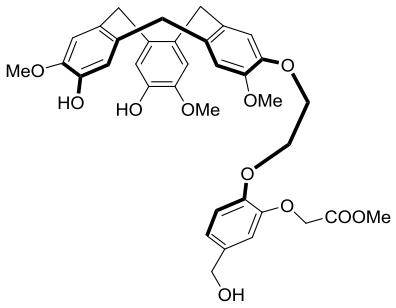

$C_{36}H_{38}O_{11}$

Mw = 646.69

91

Compound **90** (0.39 mg, 1.22 mmol) was added in one portion to a stirred solution of **25** (1 g, 2.45 mmol) and cesium carbonate (1.6 g, 4.90 mmol) in dry DMF (60 mL). The solution was then heated for 18 h at 80 °C under nitrogen. After cooling, the dark mixture was poured into water and the product was extracted with ethyl acetate. The combined organic layers were washed several times with brine and then dried over Na_2SO_4. The solvent was stripped off by rotary evaporation and the residue was purified by chromatography on silica gel (cyclohexane / ethyl acetate 50 : 50 → 0 : 100). 157 mg of expected product **91** was obtained (25 % yield based on recovered starting material).

Pale yellow solid

^{1}H NMR (400 MHz, $CDCl_3$, δ in ppm): 3.40 – 3.51 (m, 3H), 3.67 (s, 3H), 3.70 (s, 3H), 3.75 – 3.82 (m, 6H), 4.23 – 4.39 (m, 4H), 4.54 (s, 2H), 4.60 (s, 2H), 4.62 – 4.73 (m, 3H), 6.72 – 6.98 (m, 9H)

^{13}C NMR (100 MHz, $CDCl_3$, δ in ppm): 35.05, 51.58, 54.70, 54.97, 55.09, 62.93, 67.18, 67.47, 112.29, 112.59, 112.78, 113.36, 115.60, 115.88, 119.84, 130.45, 131.48, 132.08, 133.18, 134.84, 143.66, 143.74, 143.83, 144.88, 145.42, 146.41, 146.78, 170.39

MS (ESI-TOF) *m/z*: 664.6, $[M+H+H_2O]^+$

Compound 93

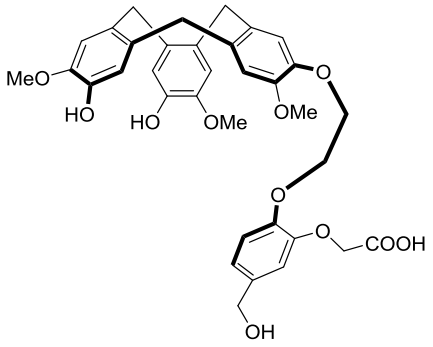

$C_{35}H_{36}O_{11}$

Mw = 632.66

93

Compound **90** (0.39 mg, 1.22 mmol) was added in one portion to a stirred solution of **25** (1 g, 2.45 mmol) and cesium carbonate (1.6 g, 4.90 mmol) in dry DMF (60 mL). The solution was then heated for 18 h at 80 °C under nitrogen. After cooling, the dark mixture was poured into water and the product was extracted with ethyl acetate. The combined organic layers were washed several times with brine and then dried over $MgSO_4$. The solvent was stripped off by rotary evaporation and the residue was purified by chromatography on silica gel (dichloromethane / methanol 100 : 0 → 80 : 20). 192 mg of product **93** was obtained (29 % yield based on recovered starting material).

Brown solid

^{1}H NMR (400 MHz, $CDCl_3$, δ in ppm): 3.40 – 3.51 (m, 3H), 3.70 (s, 3H), 3.75 – 3.82 (m, 6H), 4.23 – 4.39 (m, 4H), 4.54 (s, 2H), 4.60 (s, 2H), 4.62 – 4.73 (m, 3H), 6.72 – 6.98 (m, 9H)

^{13}C NMR (100 MHz, $CDCl_3$, δ in ppm): 35.05, 54.70, 54.97, 55.09, 62.93, 67.18, 67.47, 112.29, 112.59, 112.78, 113.36, 115.60, 115.88, 119.84, 130.45, 131.48, 132.08, 133.18, 134.84, 143.66, 143.74, 143.83, 144.88, 145.42, 146.41, 146.78, 174.39

MS (ESI-TOF) *m/z*: 650.4, $[M+H+H_2O]^+$

Compound 94

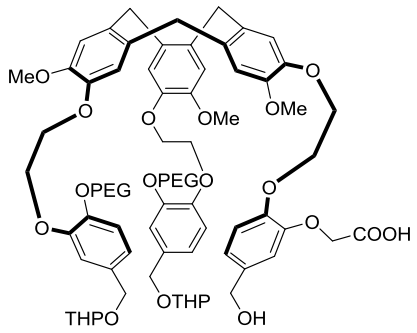

$C_{109}H_{164}O_{41}$

Mw = 2130.47

94

Compound **58** (400 mg, 0.482 mmol) was added to a stirred solution of **93** (122 mg, 0.193 mmol) and cesium carbonate (377 mg, 1.157 mmol) in dry DMF (5 mL). The solution was then heated for 18 h at 80 °C under nitrogen. The solvent was stripped off and the residue was extracted with dichloromethane / water. The combined organic layers were washed with brine, dried over Mg_2SO_4 and evaporated to leave an oily residue. A purification by chromatography on silica gel (dichloromethane / methanol 100 : 0 → 90 : 10) afforded product **94** in 30 % yield (122 mg).

Yellow oil

^{1}H NMR (400 MHz, $CDCl_3$, δ in ppm): 1.43 – 1.64 (m, 8H), 1.64 – 1.75 (m, 2H), 1.76 – 1.88 (m, 2H), 3.35 (s, 6H), 3.47 – 3.74 (m, 94H), 3.74 – 3.84 (m, 4H), 3.84 – 3.93 (m, 2H), 4.05 - 4.18 (m, 4H), 4.20 – 4.34 (m, 14H), 4.36 (s, 2H), 4.39 (s, 2H), 4.57 – 4.73 (m, 3H), 6.68 – 7.05 (m, 15H)

^{13}C NMR (100 MHz, $CDCl_3$, δ in ppm): 36.31, 56.07, 58.89, 60.86, 62.09, 64.47, 66.49, 67.86, 68.45, 68.66, 69.54, 70.61, 71. 16, 71.79, 97.45, 113.68, 113.74, 113.85, 114.50, 114.59, 114.82, 116.29, 121.10, 131.70, 131.82, 132.76, 132.85, 134.87, 135.13, 146.69, 147.76, 147.82, 148.03, 148.19, 148.38, 148.47, 148.54, 148.60, 148.71, 148.80, 148.90, 169.40

MS (ESI-TOF) *m/z*: distribution centered at 1065.5 ± 22, $[(M+2H-2THPOH-H_2O)/2]^+$, irregular mass caused by an ionisation problem

Compound 76

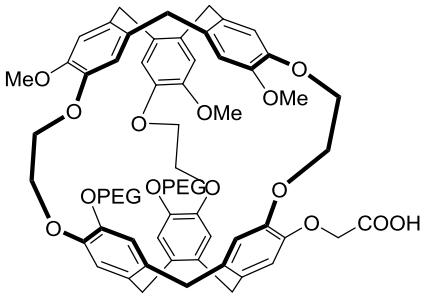

$C_{99}H_{142}O_{36}$

Mw = 1908.19

76

Compound **94** (120 mg, 0.036 mmol) was dissolved in a minimum of chloroform, and then formic acid (120 mL) was added to the solution. The mixture was heated at 60 °C for 3 h. The cooled reaction mixture was evaporated to afford a crude material, which was then purified by silica gel chromatography (dichloromethane / methanol 100 : 0 → 90 : 10) to afford compound **76** in 80 % yield (54 mg).

Yellow oil

^{1}H NMR (400 MHz, $CDCl_3$, δ in ppm): 3.36 (s, 6H), 3.47 – 3.88 (m, 102H), 4.04 – 4.37 (m, 16H), 4.46 – 4.77 (m, 5H), 6.53 – 7.01 (m, 12H)

^{13}C NMR (100 MHz, $CDCl_3$, δ in ppm): 29.59, 36.20, 36.27, 55.89, 56.03, 56.09, 58.90, 64.37, 64.44, 67.84, 67.90, 68.59, 69.52, 69.60, 69.70, 69.81, 69.87, 69.97, 70.05, 70.31, 71.77, 113.54, 113.69, 113.84, 114.87, 114.93, 116.15, 116.23, 120.01, 131.81, 135.17, 146.54, 147.55, 147.67, 148.29, 148.75, 169.96

MS (ESI-TOF) *m/z*: distribution centered at 1065.5 ± 22, $[(M+2H)/2]^+$

Compound 97

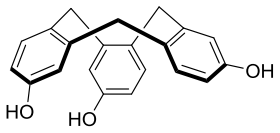

$C_{21}H_{18}O_3$

Mw = 318.37

97

Boron tribromide (200 mL of a 1 N solution of BBr_3 in CH_2Cl_2) was added dropwise to a suspension of 2,7,12-Trimethoxy-10,15-dihydro-5H-tribenzo[a,d,g]cyclononene **99** (10 g, 28 mmol) in dry CH_2Cl_2 (40 mL) at 0 °C. The solution was warmed to room temperature and stirred overnight. Then it was poured onto an ice and H_2O slurry. The aqueous solution was neutralized to pH 6 and filtered. The solid residue was washed with 120 mL of hot water and dried to provide a slightly colored powder. The powder was poured into 30 mL of acetonitrile and sonicated for 20 min. The precipitate was filtered, washed with 45 mL of acetonitrile and dried to furnish 8.8 g (100 % yield) of pure **97**.

White powder

^{1}H NMR (400 MHz, acetone-d6, δ in ppm): 3.54 (d, *J* = 13.4 Hz, 3H), 4.77 (d, *J* = 13.4 Hz, 3H), 6.54 (dd, *J1* = 8.0 Hz, *J2* = 2.6 Hz, 3H), 6.87 (d, *J* = 2.6 Hz, 3H), 7.21 (d, *J* = 8.0 Hz, 3H), 7.99 (s, 3H)

^{13}C NMR (100 MHz, acetone-d6, δ in ppm): 30.79, 113.55, 116.16, 130.58, 130.92, 141.56, 155.78

HRMS-ESI (*m/z*): 317.1190, $[M–H]^-$

Compound 100

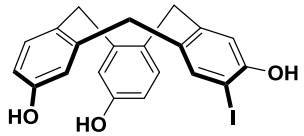

$C_{21}H_{17}IO_3$

Mw = 444.27

100

In a 250 mL round-bottom flask equipped with a septum and a magnetic stirrer under nitrogen atmosphere, cyclotriphenolene **97** (300 mg, 0.942 mmol) was dissolved in acetonitrile (100 mL). *N*-iodosuccinimide (212 mg, 0.942 mmol) was added and the reaction mixture was stirred for 30 min at room temperature. Then, the orange solution was quenched with water and concentrated *in vacuo*. The resulting residue was dissolved in ethyl acetate (50 mL), washed with water (20 mL) and the organic layer was separated. The aqueous layer was extracted with ethyl acetate (3x15 mL), the combined organic layers were washed with brine, dried over $MgSO_4$ and concentrated *in vacuo* to afford a brownish solid. The resulting crude product was purified by column chromatography on silica gel (cyclohexane / ethyl acetate) to afford **100** (184 mg, 72%, yield based on recovered starting material).

White powder

^{1}H NMR (400 MHz, acetone-d6, δ in ppm): 3.55 (m, 3H), 4.74 (d, *J* = 13.3 Hz, 3H), 6.56 (dd, *J* = 2.6 Hz, *J* = 8.2 Hz, 1H), 6.58 (dd, *J1* = 2.6 Hz, *J2* = 8.2 Hz, 1H), 6.88 (d, *J1* = 2.4 Hz, 1H), 6.92 (d, *J2* = 2.6 Hz, 1H), 7.00 (s, 1H), 7.16 (d, *J* = 8.4 Hz, 1H), 7.22 (d, *J* = 8.4 Hz, 1H), 7.74 (s, 1H)

^{13}C NMR (100 MHz, acetone-d6, δ in ppm): 156.9, 155.9, 143.3, 142.6, 141.9, 141.0, 134.3, 132.0, 131.7, 131.6, 131.0, 117.2, 117.0, 114.8, 114.6, 82.0, 36.7, 36.4, 36.1

HRMS-ESI (*m/z*): 445.0294, $[M+H]^+$

Compound 105

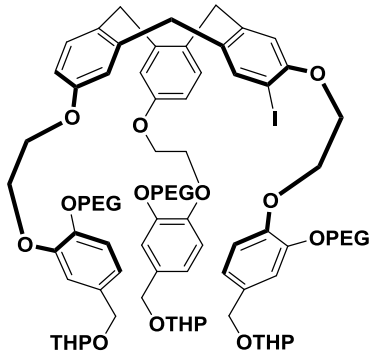

105

$C_{132}H_{209}IO_{48}$

Mw = 2690.98

In a 25 mL round-bottom flask equipped with a septum and a magnetic stirrer under nitrogen atmosphere, **100** (20.0 mg, 0.045 mmol) and cesium carbonate (58.6 mg, 0.180 mmol) were dissolved in DMF (7 mL). The pale yellow suspension was stirred at 80 °C for 15 min. Then, **18** (130.7 mg, 0.158 mmol) previously dissolved in DMF (1 mL), was added dropwise and the reaction mixture was strirred at 80 °C for 24 hours. Upon completion, the mixture was cooled to room temperature and concentrated *in vacuo*. The resulting residue was taken up in CH_2Cl_2, filtered through a pad of Celite® and the filtrate was concentrated *in vacuo* to afford a brownish oil. The crude was purified by preparative TLC (CH_2Cl_2 / MeOH 95:5) and the expected compound **105** was obtained (90.9 mg, 74%).

Yellow oil

^{1}H NMR (400 MHz, acetone-d6, δ in ppm): 7.71 (s, 1H), 7.27 - 7.20 (m, 2H), 7.03 - 6.85 (m, 12H), 6.69 - 6.54 (m, 2H), 4.73 - 4.58 (m, 9H), 4.41 (d, *J* = 11.9 Hz, 3H), 4.36 - 4.15 (m, 12H), 3.90 - 3.80 (m, 9H), 3.63 - 3.54 (m, 120H), 3.37 (s, 9H), 1.86 - 1.52 (m, 18H)

^{13}C NMR (100 MHz, acetone-d6, δ in ppm): 157.5, 157.4, 149.1, 148.2, 141.6, 141.1, 140.6, 140.4, 134.6, 134.1, 132.2, 132.1, 131.9, 131.4, 131.3, 130.9, 121.5, 121.3, 121.0, 116.3, 115.5, 115.3, 115.1, 114.8, 114.5, 114.3, 113.0, 97.7, 93.4, 84.6, 71.9, 71.5, 70.6, 69.7, 69.6, 68.8, 68.7, 68.2, 66.5, 62.3, 59.1, 36.5, 36.2, 30.6, 29.8, 25.5, 19.5

MS (ESI-TOF) *m/z*: distribution centered at 1347.6 ± 22, $[(M+2H-3THPOH)/2]^+$, irregular mass caused by an ionisation problem

Compound 106

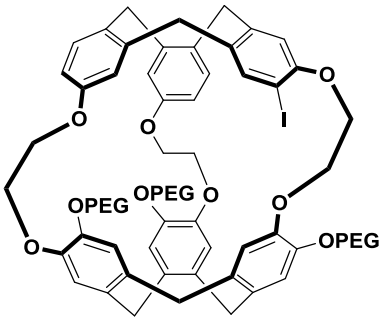

106

$C_{117}H_{179}IO_{42}$

Mw = 2384.58

In a 50 mL round-bottom flask equipped with a septum and a magnetic stirrer, **105** (40.0 mg, 0.015 mmol) was dissolved in formic acid (20 mL). The reaction mixture was slowly stirred at 60 °C for 3 hours. Subsequently, the colorless solution was allowed to cool down to room temperature and concentrated *in vacuo*. The brownish crude oil was purified by preparative HPLC (water / acetonitrile 100 : 0 → 0 : 100) to afford expected product **20** (14.5 mg, 41%).

Yellow oil

^{1}H NMR (400 MHz, $CDCl_3$, δ in ppm): 3.37 (s, 9H), 3.41 – 3.97 (m, 141H), 4.03 – 4.44 (m, 12H), 4.47 – 4.64 (m, 3H), 6.39 – 7.21 (m, 12H)

^{13}C NMR (100 MHz, $CDCl_3$, δ in ppm): Not enough products to achieve a satisfying resolution

MS (ESI-TOF) *m/z*: distribution centered at 1347.6± 22, $[(M+2H)/2]^+$

Compound 107

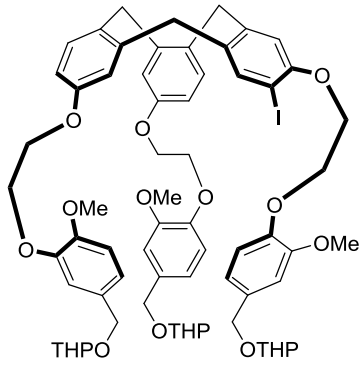

107

$C_{66}H_{77}IO_{15}$

Mw = 1237.23

Compound **34** (465 mg, 1.35 mmol) was added to a stirred solution of **100** (100 mg, 0.23 mmol) and cesium carbonate (440 mg, 1.35 mmol) in dry DMF (15 mL). The solution was heated for 3 days at 80 °C under nitrogen. The solvent was stripped off and the residue was extracted with dichloromethane / water. The combined organic layers were washed with brine, dried over Mg_2SO_4 and evaporated to leave an oily residue. A purification by chromatography on silica gel (cyclohexane / ethyl acetate 100 : 0 → 70 : 30) afforded product **107** in 73 % yield (207 mg).

Pale yellow solid

^{1}H NMR (400 MHz, $CDCl_3$, δ in ppm): 1.47 – 1.68 (m, 12H), 1.68 – 1.78 (m, 3H), 1.79 – 1.92 (m, 3H), 3.50 – 3.58 (m, 3H), 3.58 – 3.66 (m, 3H), 3.85 (s, 3H), 3.86 (s, 3H), 3.88 (s, 3H), 3.89 – 3.97 (m, 3H), 4.21 – 4.41 (m, 12H), 4.44 (d, *J* = 11.8 Hz, 3H), 4.63 - 4.77 (m, 9H), 6.64 (dd, *J1* = 8.5 Hz, *J2* = 2.5 Hz, 1H), 6.69 (dd, *J1* = 8.5 Hz, *J2* = 2.5 Hz, 1H), 6.85 – 6.96 (m, 11H), 6.99 (d, *J* = 8.0 Hz, 1H), 7.21 (d, *J* = 8.4 Hz, 1H), 7.24 – 7.30 (m, 1H), 7.72 (s, 1H)

^{13}C NMR (100 MHz, $CDCl_3$, δ in ppm): 19.37, 25.34, 30.49, 35.98, 36.29, 55.79, 55.92, 62.16, 66.20, 67.57, 68.05, 68.59, 84.47, 97.47, 111.92, 111.96, 112.82, 112.92, 113.77, 113.84, 114.00, 114.31, 116.15, 120.36, 120.51, 130.63, 131.01, 131.18, 131.59, 133.99, 140.16, 140.35, 140.91, 141.36, 147.43, 149.50, 156.02, 157.26

MS (ESI-TOF) *m/z*: 930.7, $[M+H-3THPOH]^+$, irregular mass caused by an ionisation problem

Compound 108 - anti

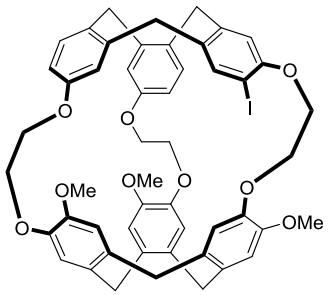

$C_{51}H_{47}IO_9$

Mw = 930.83

108 - anti

In a 250 mL round-bottom flask equipped with a septum and a magnetic stirrer, **107** (105 mg, 0.085 mmol) was dissolved in formic acid (100 mL). The reaction mixture was slowly stirred at 55 °C for 5 hours and kept stirring in the room temperature for 18 h. Subsequently, the colorless solution was cooled to room temperature and concentrated *in vacuo*. The crude product was purified by chromatography on silica gel (cyclohexane / chloroform 100 : 0 → 50 : 50) afforded product **108 - anti** in 44 % yield (35 mg).

^{1}H NMR (400 MHz, $CDCl_3$, δ in ppm): 3.36 – 3.57 (m, 6H), 3.78 (s, 3H), 3.83 (s, 3H), 3.85 (s, 3H), 3.89 – 3.99 (m, 2H), 4.04 – 4.42 (m, 10H), 4.46 - 4.69 (m, 6H), 4.44 (t, *J* = 9.4 Hz, 2H), 6.62 (s, 1H), 6.66 (s, 3H), 6.70 (s, 1H), 6.72 – 6.79 (m, 2H), 6.82 (s, 1H), 6.86 (s, 1H), 7.07 (d, *J* = 8.4 Hz, 1H), 7.12 (d, *J* = 8.4 Hz, 1H), 7.56 (s, 1H)

^{13}C NMR (100 MHz, $CDCl_3$, δ in ppm): 35.88, 36.14, 36.30, 55.87, 56.47, 56.72, 65.07, 65.36, 66.60, 77.68, 87.65, 111.75, 112.00, 113.10, 114.02, 114.78, 116.51, 116.62, 119.03, 119.09, 120.06, 122.01, 130.61, 130.78, 131.47, 132.23, 132.67, 132.92, 134.32, 136.20, 139.91, 140.25, 140.97, 141.79, 146.47, 146.95, 147.23, 148.42, 148.71, 156.29, 156.46, 157.41

MS (ESI-TOF) *m/z*: 948.7, $[M+H+H_2O]^+$

Compound 108 - syn

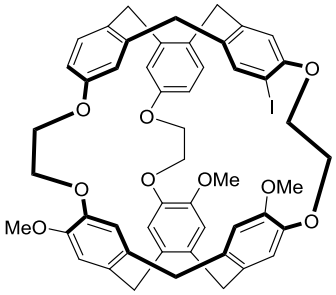

$C_{51}H_{47}IO_9$

Mw = 930.83

108 - syn

In a 250 mL round-bottom flask equipped with a septum and a magnetic stirrer, **107** (105 mg, 0.085 mmol) was dissolved in formic acid (100 mL). The reaction mixture was slowly stirred at 55 °C for 5 hours and kept stirring in the room temperature for 18 h. Subsequently, the colorless solution was cooled to room temperature and concentrated *in vacuo*. The crude product was purified by chromatography on silica gel (cyclohexane / chloroform 100 : 0 → 50 : 50). Then the fraction containing targeted product was purified by preparative TLC (chloroform / ethyl acetate 90 : 10) and the expected compound **108 - syn** was obtained in 2 % yield (2 mg).

^{1}H NMR (400 MHz, $CDCl_3$, δ in ppm): 3.37 – 3.52 (m, 6H), 3.53 – 3.61 (m, 1H), 3.68 – 3.76 (m, 1H), 3.80 (s, 3H), 3.82 (s, 3H), 3.85 (s, 3H), 3.91 – 4.05 (m, 2H), 4.06 – 4.15 (m, 1H), 4.17 – 4.45 (m, 7H), 4.46 - 4.69 (m, 6H), 6.61 (d, *J* = 2.4 Hz, 1H), 6.64 – 6.76 (m, 6H), 6.77 (d, *J* = 2.4 Hz, 1H), 6.80 (s, 1H), 6.87 (s, 1H), 7.07 (d, *J* = 8.6 Hz, 1H), 7.13 (d, *J* = 8.6 Hz, 1H), 7.60 (s, 1H)

^{13}C NMR (100 MHz, $CDCl_3$, δ in ppm): 157.66, 156.98, 156.56, 150.06, 149.49, 149.31, 147.16, 146.31, 146.18, 141.72, 140.69, 140.03, 139.96, 137.59, 134.69, 134.25, 133.97, 132.21, 132.09, 131.52, 131.34, 130.81, 130.73, 128.78, 121.82, 121.48, 121.30, 119.25, 118.87, 118.57, 114.15, 113.97, 113.62, 112.83, 88.11, 71.37, 71.24, 70.68, 69.24, 68.14, 65.84, 56.11, 38.71, 36.15, 30.94, 30.35, 29.70, 28.91, 23.73, 22.99, 14.06, 10.96

MS (ESI-TOF) *m/z*: 948.6, $[M+H+H_2O]^+$

Compound 111

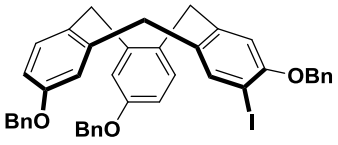

$C_{42}H_{35}IO_3$

Mw = 714.64

111

In a 100 mL round-bottom flask equipped with a septum and a magnetic stirrer under nitrogen, **100** (280 mg, 0.63 mmol), potassium carbonate (1.74 g, 12.6 mmol) and tetrabutylammonium iodide (69.8 mg, 0.189 mmol) were dissolved in DMF (55 mL). Subsequently, benzyl bromide (1.48 mL, 12.6 mmol) was added and the reaction mixture was stirred overnight at room temperature. The pale yellow suspension was diluted with ethyl acetate (70 mL) and water (30 mL). The aqueous layer was separated and extracted with ethyl acetate (3 x 20 mL). The combined organic layers were washed with brine, dried over $MgSO_4$ and concentrated *in vacuo*. The resulting yellow crude oil was purified by column chromatography on silica gel (cyclohexane / ethyl acetate) to afford product **111** (414.2 mg, 92%).

White solid

^{1}H NMR (400 MHz, $CDCl_3$, δ in ppm): 7.76 (s, 1H), 7.50-7.33 (m, 15H), 7.21 (d, *J* = 8.6 Hz, 1H), 7.00 - 6.97 (m, 2H), 6.95 (d, *J* = 2.6 Hz, 1H), 6.78 (s, 1H), 6.74 (dd, *J1* = 2.6 Hz, *J2* = 8.6 Hz, 1H), 6.64 (dd, *J1* = 2.6 Hz, *J2* = 8.6 Hz, 1H), 5.22 - 5.02 (m, 6H), 4.69 (m, 3H), 3.58 (m, 3H)

^{13}C NMR (100 MHz, acetone-d6, δ in ppm): 157.6, 157.5, 155.8, 141.3, 140.8, 140.5, 140.3, 137.1, 137.0, 136.7, 133.6, 131.8, 131.1, 130.6, 128.6, 128.5, 128.0, 127.8, 127.7, 127.5, 127.3, 126.8, 116.4, 116.2, 114.3, 113.2, 113.1, 84.5, 71.0, 70.1, 69.9, 36.4, 36.1

HRMS-ESI (*m/z*): 715.1705, $[M+H]^+$

Compound 112

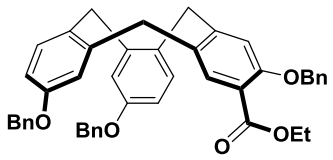

112

$C_{45}H_{40}O_5$

Mw = 660.81

In a 25 mL round-bottom flask equipped with a septum and a magnetic stirrer under nitrogen atmosphere, **111** (20 mg, 0.028 mmol) was dissolved in THF (4.25 mL). The reaction mixture was cooled to -78 °C and *n*-BuLi (2.5 M in THF, 56 µL, 0.140 mmol) was added dropwise. The resulting yellow solution was stirred at -78 °C for 15 min. Then, freshly distilled ethyl chloroformate (80 µL, 0.840 mmol) was added and the mixture was stirred 2 h at -78 °C and 2 h at room temperature. The pale yellow solution was quenched with a saturated NH_4Cl aqueous solution at 0 °C. The mixture was diluted with ethyl acetate and the organic layer was separated. The aqueous layer was extracted with ethyl acetate (3x10 mL). The combined organic layers were washed with brine, dried over $MgSO_4$ and concentrated *in vacuo*. The crude oil was purified by column chromatography on silica gel (cyclohexane / ethyl acetate) to afford product **112** (11.3 mg, 62%).

White solid

^{1}H NMR (400 MHz, $CDCl_3$, δ in ppm): 7.85 (s, 1H), 7.49 - 7.30 (m, 15H), 7.19 (d, *J* = 8.6 Hz, 1H), 7.03 (d, *J* = 2.6 Hz, 1H), 6.98 (d, *J* = 8.6 Hz, 1H), 6.94 (d, *J* = 2.6 Hz, 1H), 6.93 (s, 1H), 6.72 (dd, *J1* = 2.6 Hz, *J*2 = 8.4 Hz, 1H), 6.63 (dd, *J1* = 2.7 Hz, *J2* = 8.6 Hz, 1H), 5.25 - 5.02 (m, 6H), 4.75 (m, 3H), 4.35 (q, *J* = 7.0 Hz, 2H), 3.65 (m, 3H), 1.34 (t, *J* = 7.1 Hz, 3H)

^{13}C NMR (100 MHz, acetone-d6, δ in ppm): 166.2, 157.7, 157.6, 156.7, 145.5, 141.1, 140.4, 137.0, 133.6, 131.8, 131.4, 131.1, 130.8, 130.7, 128.6, 128.5, 128.0, 127.9, 127.7, 127.6, 127.4, 126.9, 119.6, 116.3, 116.2, 115.6, 113.3, 113.2, 70.9, 70.0, 60.8, 36.7, 36.5, 36.4, 14.3

HRMS-ESI (*m/z*): 661.2950, $[M+H]^+$

Compound 110

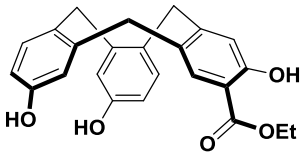

$C_{24}H_{22}O_5$

Mw = 390.44

110

A solution of **112** (11.2 mg, 0.017 mmol) and palladium (10% wt. on carbon, 1.8 mg, 0.002 mmol) in ethyl acetate (2 mL) was stirred under an atmospheric pressure of hydrogen at room temperature for 96 h, until complete disappearance of starting material (monitored by TLC). Upon completion, the reaction mixture was filtered through a pad of Celite® and the filtrate was concentrated *in vacuo* to afford **9** (6.5 mg, quantitative) without need for further purification.

White solid

^{1}H NMR (400 MHz, $CDCl_3$, δ in ppm): 10.47 (s, 1H), 8.09 (s, 1H), 8.07 (s, 1H), 7.90 (s, 1H), 7.30 (d, *J* = 8.4 Hz, 1H), 7.23 (d, *J* = 8.4 Hz, 1H), 7.04 (s, 1H), 6.90 (d, *J* = 2.6 Hz, 1H), 6.88 (d, *J* = 2.5 Hz, 1H), 6.60 (d, *J* = 1.1 Hz, 1H), 6.58 (d, *J* = 1.1 Hz, 1H), 4.81 (m, 3H), 4.39 (m, 2H), 3.62 (m, 3H), 1.39 (t, *J* = 7.1 Hz, 3H)

^{13}C NMR (100 MHz, acetone-d_6, δ in ppm): 170.7, 160.9, 157.1, 157.0, 150.5, 142.8, 141.8, 132.3, 132.2, 132.1, 131.8, 130.2, 119.0, 117.2, 117.1, 114.9, 114.8, 111.9, 62.2, 36.9, 36.8, 36.6, 14.6

HRMS-ESI (*m/z*): 391.1540, $[M+H]^+$

Compound 113

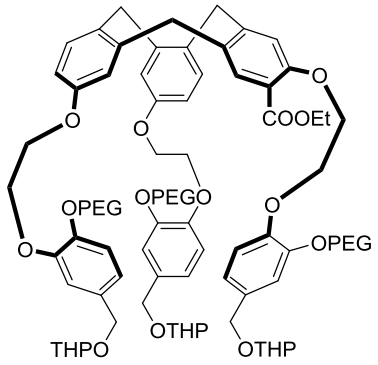

113

$C_{135}H_{214}O_{50}$

Mw = 2637.15

Compound **58** (128 mg, 0.154 mmol) was added to a stirred solution of **110** (15 mg, 0.039 mmol) and cesium carbonate (75 mg, 0.231 mmol) in dry DMF (1.5 mL). The solution was heated overnight at 80 °C under nitrogen. The solvent was stripped off and the residue was extracted with dichloromethane / water. The combined organic layers were washed with brine, dried over Mg_2SO_4 and evaporated to leave an oily residue. A purification by chromatography on silica gel (dichloromethane / methanol 100 : 0 → 90 : 10) afforded product **113** in 51 % yield (52 mg).

Yellow oil

^{1}H NMR (400 MHz, $CDCl_3$, δ in ppm): 1.28 (t, *J* = 7.1 Hz, 3H), 1.46 – 1.66 (m, 12H), 1.67 – 1.79 (m, 3H), 1.78 – 1.90 (m, 3H), 3.36 (s, 9H), 3.48 – 3.75 (m, 126H), 3.77 – 3.96 (m, 11H), 4.15 (t, *J* = 5.2 Hz, 6H), 4.19 – 4.37 (m, 12H), 4.41 (d, *J* = 11.7 Hz, 3H), 4.62 - 4.82 (m, 9H), 6.61 (dd, *J1* = 8.5 Hz, *J2* = 2.4 Hz, 1H), 6.67 (dd, *J1* = 8.5 Hz, *J2* = 2.4 Hz, 1H), 6.85 – 6.97 (m, 11H), 6.99 (s, 1H), 7.20 (d, *J* = 8.8 Hz, 1H), 7.25 (d, *J* = 8.8 Hz, 1H), 7.78 (s, 1H)

^{13}C NMR (100 MHz, $CDCl_3$, δ in ppm): 14.01, 18.67, 24.32, 28.87, 30.54, 36.01, 36.44, 59.03, 60.78, 62.19, 66.43, 68.02, 68.49, 69.43, 69.56, 70.45, 71.26, 71.79, 92.83, 96.58, 111.43, 113.28, 114.12, 114.38, 114.65, 115.02, 115.23, 115.32, 116.10, 120.56, 121.04, 121.32, 130.78, 131.56, 131.68, 131.90, 132.04, 134.11, 134.58, 140.00, 141.18, 141.65, 148.18, 149.06, 157.35, 157.50, 164.97

Compound 115

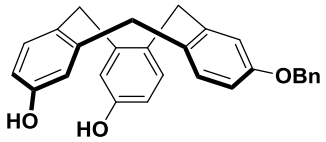

$C_{28}H_{24}O_3$

Mw = 408.50

115

In a 100 mL round-bottom flask equipped with a septum and a magnetic stirrer under nitrogen atmosphere, **97** (150 mg, 0.47 mmol), potassium carbonate (1.3 g, 9.42 mmol) and tetrabutylammonium iodide (52 mg, 0.14 mmol) were dissolved in DMF (40 mL). Subsequently, benzyl bromide (1.1 mL, 9.42 mmol) was added and the reaction mixture was stirred overnight at room temperature. The pale yellow suspension was diluted with ethyl acetate and water. The aqueous layer was separated and extracted with ethyl acetate. The combined organic layers were washed with brine, dried over $MgSO_4$ and concentrated *in vacuo*. The resulting yellow crude oil was purified by column chromatography on silica gel (cyclohexane / ethyl acetate 100 : 0 → 25 : 75) to afford product **115** in 55 % yield (105 mg).

White solid

^{1}H NMR (400 MHz, $CDCl_3$, δ in ppm): 3.50 – 3.66 (m, 3H), 4.76 – 4.86 (m, 3H), 5.06 (s, 2H), 6.51 - 6.60 (m, 2H), 6.73 (dd, *J1* = 2.6 Hz, *J2* = 8.6 Hz, 1H), 6.89 (dd, *J1* = 2.6 Hz, *J2* = 8.6 Hz, 2H), 7.07 (d, *J* = 2.6 Hz, 1H), 7.23 (dd, *J1* = 4.9 Hz, *J2* = 8.4 Hz, 2H), 7.27 – 7.40 (m, 4H), 7.40 – 7.48 (m, 2H), 8.05 (s, 2H)

^{13}C NMR (100 MHz, acetone-d6, δ in ppm): 37.66, 71.26, 114.72, 115.51, 117.81, 117.99, 128.31, 129.28, 129.44, 130.20, 132.30, 132.53, 132.82, 132.87, 132.93, 133.93, 139.56, 143.18, 143.44, 143.53, 157.67, 159.26

MS (ESI-TOF) *m/z*: 426.3, $[M+H+H_2O]^+$

Compound 114

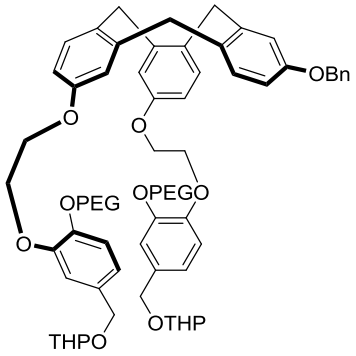

114

$C_{102}H_{152}O_{33}$

Mw = 1906.31

Compound **58** (173 mg, 0.208 mmol) was added to a stirred solution of **115** (34 mg, 0.083 mmol) and cesium carbonate (109 mg, 0.333 mmol) in dry DMF (3 mL). The solution was then heated overnight at 80 °C under nitrogen. The solvent was stripped off and the residue was extracted with dichloromethane / water. The combined organic layers were washed with brine, dried over Mg_2SO_4 and evaporated to leave an oily residue. A purification by chromatography on silica gel (dichloromethane / methanol 100 : 0 → 90 : 10) afforded product **114** in 96 % yield (150 mg).

Yellow oil

^{1}H NMR (400 MHz, $CDCl_3$, δ in ppm): 1.45 – 1.68 (m, 8H), 1.68 – 1.77 (m, 2H), 1.78 – 1.92 (m, 2H), 3.36 (s, 6H), 3.48 – 3.77 (m, 85H), 3.77 – 3.95 (m, 8H), 4.11 – 4.19 (m, 4H), 4.19 – 4.34 (m, 6H), 4.41 (d, *J* = 11.8 Hz, 2H), 4.67 - 4.78 (m, 7H), 4.98 (s, 2H), 6.61 – 6.72 (m, 2H), 6.84 – 7.00 (m, 11H), 7.18 (d, *J* = 8.5 Hz, 1H), 7.24 (s, 1H), 7.28 – 7.41 (m, 5H)

^{13}C NMR (100 MHz, $CDCl_3$, δ in ppm): 20.96, 24.14, 36.50, 42.21, 59.02, 66.52, 68.36, 68.77, 69.70, 70.54, 70.74, 71.91, 112.86, 112.92, 115.90, 115.96, 116.12, 116.18, 121.79, 131.12, 131.80, 133.24, 141.17, 146.46, 146.93, 148.96, 157.38

Compound 118

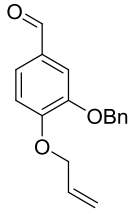

$C_{17}H_{16}O_3$

Mw = 268.31

118

Compound **67** (205 mg, 1.15 mmol) was dissolved in DMF (2 mL) and then K_2CO_3 (191 mg, 1.38 mmol) and benzyl bromide (0.55 mL, 4.61 mmol) were added into the solution. The reaction was heated at 80 °C with stirring for 16 h. After cooling, ethyl acetate was added and it was washed with a solution of HCl 1N. The organic phase was dried over $MgSO_4$ and concentrated under vacuum. A purification by chromatography on silica gel (cyclohexane / ethyl acetate 80 : 20 → 50 : 50) afforded product **118** in 95 % yield (292 mg).

White Solid

^{1}H NMR (400 MHz, $CDCl_3$, δ in ppm): 4.71 (d, *J* = 5.1 Hz, 2H), 5.20 (s, 2H), 5.33 (dd, *J1* = 10.5 Hz, *J2* = 1.3 Hz, 1H), 5.45 (dd, *J1* = 17.3 Hz, *J2* = 1.3 Hz, 1H), 6.01 – 6.16 (m, 1H), 7.00 (d, *J* = 8.5 Hz, 1H), 7.29 – 7.54 (m, 7H), 9.82 (s, 1H)

^{13}C NMR (100 MHz, $CDCl_3$, δ in ppm): 70.41, 71.01, 108.88, 113.71, 118.02, 124.51, 127.29, 127.62, 128.64, 130.55, 133.55, 136.70, 150.23, 153.54, 190.81

MS (ESI-TOF) *m/z*: 269.3, $[M+H]^+$

Compound 119

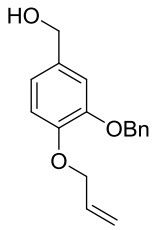

$C_{17}H_{18}O_3$

Mw = 270.33

119

Compound **118** (0.29 g, 1.08 mmol) was dissolved in THF (4 mL). The solution was cooled to 0 °C with an ice bath and then $NaBH_4$ (49 mg, 1.30 mmol) and methanol (0.44 mL, 10.82 mmol) were added. The reaction was kept at 0 °C with stirring for 30 minutes and then it was quenched with a solution of HCl 1N and extracted with dichloromethane. The organic phase was dried over $MgSO_4$ and concentrated under vacuum. Product **119** was obtained in 96 % yield (0.28 g).

White solid

^{1}H NMR (400 MHz, $CDCl_3$, δ in ppm): 4.58 (s, 2H), 4.62 (d, *J* = 5.5 Hz, 2H), 5.16 (s, 2H), 5.27 (dd, *J1* = 10.5 Hz, *J2* = 1.3 Hz, 1H), 5.41 (dd, *J1* = 17.3 Hz, *J2* = 1.3 Hz, 1H), 6.00 – 6.15 (m, 1H), 6.89 (s, 2H), 6.98 (s, 1H), 7.27 - 7.51 (m, 5H)

^{13}C NMR (100 MHz, $CDCl_3$, δ in ppm): 64.85, 70.49, 71.25, 114.14, 117.44, 118.26, 121.37, 112.56, 127.08, 127.56, 128.88, 133.62, 136.55, 146.69, 149.86

MS (ESI-TOF) *m/z*: 271.3, $[M+H]^+$

Compound 120

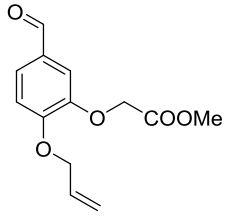

$C_{13}H_{14}O_5$

Mw = 250.25

120

Compound **67** (1.73 g, 9.68 mmol) was dissolved in DMF (20 mL) and then K_2CO_3 (1.6g, 11.6 mmol) and benzyl bromide (3.68 mL, 38.8 mmol) was added into the solution. The reaction was heated at 80 °C with stirring for 16 h. After cooling, ethyl acetate was added and it was washed with a solution of HCl 1N. The organic phase was dried over $MgSO_4$ and concentrated under vacuum. A purification by chromatography on silica gel (cyclohexane / ethyl acetate 70 : 30 → 50 : 50) afforded product **120** in 97 % yield (2.34 g).

White Solid

^{1}H NMR (400 MHz, $CDCl_3$, δ in ppm): 3.80 (s, 3H), 4.71 (d, *J* = 5.1 Hz, 2H), 4.76 (s, 2H), 5.34 (dd, *J1* = 10.5 Hz, *J2* = 1.3 Hz, 1H), 5.45 (dd, *J1* = 17.3 Hz, *J2* = 1.3 Hz, 1H), 6.01 – 6.16 (m, 1H), 7.01 (d, *J* = 8.2 Hz, 1H), 7.33 (d, *J* = 1.7 Hz, 1H), 7.48 (dd, *J1* = 8.2 Hz, *J2* = 1.7 Hz, 1H), 9.82 (s, 1H)

^{13}C NMR (100 MHz, $CDCl_3$, δ in ppm): 52.31, 65.91, 69.81, 112.05, 112.66, 118.64, 127.40, 129.93, 132.07, 147.96, 153.89, 168.81, 190.54

MS (ESI-TOF) *m/z*: 250.8, $[M+H]^+$

Compound 121

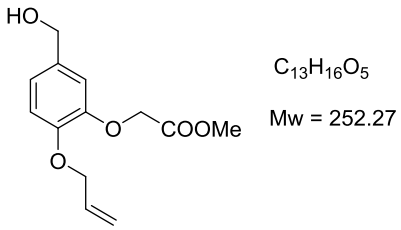

$C_{13}H_{16}O_5$

Mw = 252.27

121

Compound **120** (1.95 g, 7.8 mmol) was dissolved in THF (25 mL). The solution was cooled to 0 °C with an ice bath and then $NaBH_4$ (296 mg, 7.8 mmol) and methanol (3.2 mL, 78 mmol) were added. The reaction was kept at 0 °C with stirring for 10 minutes and then it was quenched with a solution of HCl 1N and extracted with dichloromethane. The organic phase was dried over $MgSO_4$ and concentrated under vacuum. A purification by chromatography on silica gel (cyclohexane / ethyl acetate 50 : 50 → 0 : 100) afforded the product **121** in 61 % yield (1.20 g).

White solid

^{1}H NMR (400 MHz, $CDCl_3$, δ in ppm): 3.80 (s, 3H), 4.59 (s, 2H), 4.61 (d, *J* = 5.4 Hz, 2H), 4.71 (s, 2H), 5.28 (dd, *J1* = 10.5 Hz, *J2* = 1.3 Hz, 1H), 5.41 (dd, *J1* = 17.3 Hz, *J2* = 1.3 Hz, 1H), 6.00 – 6.14 (m, 1H), 7.85 - 7.97 (m, 3H)

^{13}C NMR (100 MHz, $CDCl_3$, δ in ppm): 52.19, 65.01, 66.61, 69.99, 114.21, 117.87, 121.20, 133.15, 133.95, 147.73, 148.22, 169.52

MS (ESI-TOF) *m/z*: 252.8, $[M+H-H_2O]^+$

Compound 124

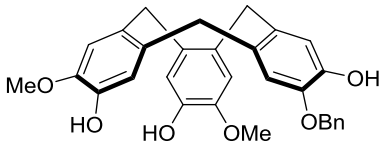

$C_{30}H_{28}O_6$

Mw = 484.55

124

To a solution of alcohol **44** (40 mg, 0.207 mmol) and alcohol **119** (28 mg, 0.104 mmol) in methanol (0.4 mL), cooled in an ice bath and magnetically stirred, was added dropwise 0.2 mL of 70 % perchloric acid, and the resulting pink solution was stirred under nitrogen at room temperature for 18 h. The formed precipitate was dissolved by adding dichloromethane and the organic phase was thoroughly washed with water until neutral pH. The dichloromethane solution was dried over magnesium sulfate and evaporated under vacuum, affording a crystalline residue (68 mg). This residue was dissolved with THF (2 mL) and then palladium acetate (1.3 mg, 5.8 µmol), triphenylphosphine (5 mg, 0.019 mmol), diethylamine (0.5 mL), and H_2O (0.5 mL) were added. The resulting solution was stirred at 80 °C under a nitrogen atmosphere for 3 h. The dark solution was then stripped off under reduced pressure and the product was extracted with ethyl acetate. The organic layer was washed once with water followed by filtration with filter paper to remove insoluble dark material. The combined organic layers were washed three times with brine and then dried over Mg_2SO_4. A purification by chromatography on silica gel (cyclohexane / ethyl acetate 50 : 50 → 0 : 100) afforded the product **124** in 25 % overall yield for two steps (12 mg).

Pale yellow solid

^{1}H NMR (400 MHz, acetone-D_6, δ in ppm): 3.42 – 3.55 (m, 3H), 3.85 (s, 6H), 4.70 (d, *J* = 14.1 Hz, 3H), 5.06 (d, *J* = 3.8 Hz, 2H), 5.41 (s, 1 H), 5.44 (s, 1 H), 5.48 (s, 1 H), 6.78 (s, 1 H), 6.79 (s, 1 H), 6.81 (s, 1 H), 6.87 (s, 1 H), 6.89 (s, 1 H), 6.97 (s, 1 H), 7.28 – 7.47 (m, 5H)

^{13}C NMR (100 MHz, $CDCl_3$, δ in ppm): Not enough products to achieve a satisfying resolution

MS (ESI-TOF) *m/z*: 502.3, $[M+H+H_2O]^+$

Compound 127

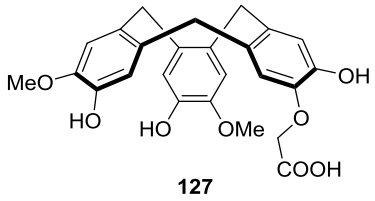

127

$C_{25}H_{24}O_8$

Mw = 452.46

To a solution of alcohol **44** (1.23 g, 6.35 mmol) and alcohol **121** (200 mg, 0.794 mmol) in methanol (10 mL), cooled in an ice bath and magnetically stirred, was added dropwise 5 mL of 70 % perchloric acid, and the resulting pink solution was stirred under nitrogen at room temperature for 18 h. The formed precipitate was dissolved by adding dichloromethane and the organic phase was thoroughly washed with water until neutral. The dichloromethane solution was dried over magnesium sulfate and evaporated under vacuum, affording a crystalline residue (1.47 g). This residue was dissolved with THF (50 mL) and then palladium acetate (30 mg, 0.13 mmol), triphenylphosphine (5 mg, 0.39 mmol), diethylamine (10 mL), and H_2O (10 mL) were added. The resulting solution was stirred at 80 °C under a nitrogen atmosphere for 3 h. The dark solution was then stripped off under reduced pressure and extracted with water / ethyl acetate. The aqueous layer was evaporated under reduced pressure to leave a dark residue. A purification by reversed-phase chromatography (water / acetonitrile 100 : 0 → 0 : 100) afforded the product **127** in 14 % overall yield for two steps (50 mg).

Pale yellow solid

^{1}H NMR (400 MHz, methanol-D_4, δ in ppm): 3.28 – 3.39 (m, 3H), 3.74 (s, 6H), 4.32 – 4.65 (m, 5H), 6.69 – 6.93 (m, 6H)

^{13}C NMR (100 MHz, $CDCl_3$, δ in ppm): Not enough sample kept to achieve a satisfying ^{13}C NMR spectrum

MS (ESI-TOF) *m/z*: 470.1, $[M+H+H_2O]^+$

Compound 129

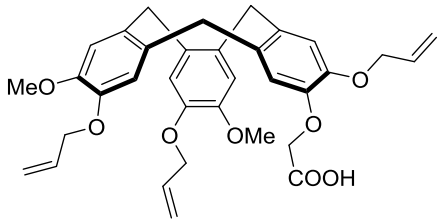

129

$C_{34}H_{36}O_8$

Mw = 572.65

To a solution of alcohol **44** (308 mg, 1.59 mmol) and alcohol **121** (200 mg, 0.794 mmol) in methanol (3 mL), cooled in an ice bath and magnetically stirred, was added dropwise 1.5 mL of 70 % perchloric acid, and the resulting pink solution was stirred under nitrogen at room temperature for 18 h. The formed precipitate was dissolved by adding dichloromethane and the organic phase was thoroughly washed with water until neutral. The dichloromethane solution was dried over magnesium sulfate and evaporated under vacuum, affording a crystalline residue (444 mg). To this residue, ethanol (1.5 mL) and a solution of 2N NaOH (1.5 mL) were added. The resulting yellow suspension was heated to reflux under a nitrogen atmosphere overnight. The solvent was stripped off under reduced pressure and the residue was extracted with 1N HCl / ethyl acetate. The organic layer was dried over $MgSO_4$ and concentrated under vacuum. A purification by chromatography on silica gel (dichloromethane / methanol 100 : 0 → 90 : 10) afforded the product **129** in 14 % overall yield for two steps (63 mg).

Pale yellow solid

^{1}H NMR (400 MHz, $CDCl_3$, δ in ppm): 3.44 – 3.55 (m, 3H), 3.83 (s, 6H), 4.51 – 4.65 (m, 8H), 4.67 – 4.78 (m, 3H), 5.21 – 5.31 (m, 3H), 5.33 – 5.45 (m, 3H), 5.98 – 6.12 (m, 3H), 6.76 – 6.97 (m, 6H)

^{13}C NMR (100 MHz, $CDCl_3$, δ in ppm): Not enough sample kept to achieve a satisfying ^{13}C NMR spectrum

MS (ESI-TOF) *m/z*: 573.3, $[M+H]^+$

Compound 131

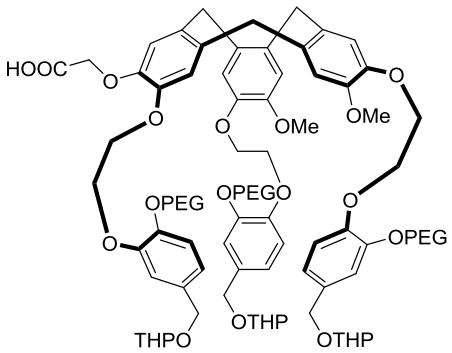

131

$C_{136}H_{216}O_{53}$

Mw = 2699.17

A solution of **129** (24 mg, 0.045 mmol), palladium acetate (0.5 mg, 2.3 µmol), triphenylphosphine (2 mg, 7.6 µmol), diethylamine (0.2 mL), THF (1 mL), and H_2O (0.2 mL) was stirred at 80 °C under a nitrogen atmosphere for 4 h. The dark solution was then stripped off under reduced pressure and the residue was dissolved with DMF (1 mL). The solution was filtered to remove insoluble dark material and then cesium carbonate (138 mg, 0.425 mmol) was added. After heating at 80 °C for 1 h with stirring, a solution of compound **58** (176 mg, 0.212 mmol) in DMF (1 mL) was added. The resulting orange solution was heated at 80 °C overnight. The solvent was evaporated under reduced pressure followed by an extraction with dichloromethane / water. The organic layer was washed with brine and dried over $MgSO_4$. After evaporation of solvent, the residue was purified by chromatography on silica gel (dichloromethane / methanol 100 : 0 → 90 : 10) afforded the product **131** in 49 % overall yield for two steps (59 mg).

Yellow oil

^{1}H NMR (400 MHz, $CDCl_3$, δ in ppm): 1.44 – 1.64 (m, 12H), 1.65 – 1.76 (m, 4H), 1.76 – 1.89 (m, 4H), 3.35 (s, 9H), 3.40 – 3.74 (m, 132H), 3.75 – 3.94 (m, 9H), 4.05 – 4.20 (m, 8H), 4.21 – 4.46 (m, 15H), 4.57 – 4.76 (m, 9H), 6.72 – 7.00 (m, 15H)

^{13}C NMR (100 MHz, $CDCl_3$, δ in ppm): Not enough sample kept to achieve a satisfying ^{13}C NMR spectrum

MS (ESI-TOF) *m/z*: distribution centered at 1307.8 ± 22, $[(M+2H-3THPOH)/2]^+$, irregular mass caused by an ionisation problem

Compound 132

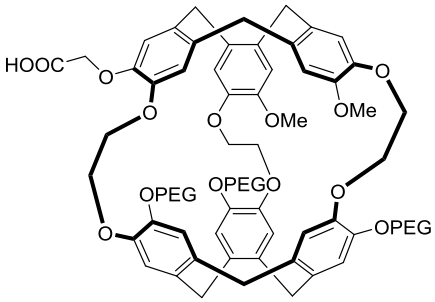

$C_{121}H_{186}O_{47}$

Mw = 2392.77

132

In a 100 mL round-bottom flask equipped with a septum and a magnetic stirrer, **131** (50 mg, 0.018 mmol) was dissolved in formic acid (50 mL). The reaction mixture was slowly stirred at 60 °C for 3 h. Subsequently, the colorless solution was cooled to room temperature and concentrated *in vacuo*. The brownish crude oil was purified by chromatography on silica gel (dichloromethane / methanol 100 : 0 → 90 : 10) to afford expected product **132** (29 mg, 65 %).

Yellow oil

^{1}H NMR (400 MHz, $CDCl_3$, δ in ppm): 3.37 (s, 9H), 3.48 – 3.90 (m, 141H), 3.98 – 4.40 (m, 16H), 4.48 – 4.77 (m, 7H), 6.56 – 7.05 (m, 12H)

^{13}C NMR (100 MHz, $CDCl_3$, δ in ppm): Not enough sample kept to achieve a satisfying ^{13}C NMR spectrum

MS (ESI-TOF) *m/z*: distribution centered at 1307.8 ± 22, $[(M+2H)/2]^+$

ÉCOLE DOCTORALE
Sciences chimiques : molécules, matériaux, instrumentation et biosystèmes

Titre : Conception et synthèse de nouveaux cryptophanes pour des applicationss en l'imagerie moléculaire par RMN du xénon

Mots clés : cryptophane, hydrosolubilisation et mono-functionalisation

Résumé : Entre tous les techniques de l'imagerie, imagerie par résonance magnétique (IRM) offre plusieurs avantages en raison de sa faible invasivité, son innocuité et sa résolution spatiale en profondeur, mais souffre d'une mauvaise sensibilité. Pour résoudre ce problème, différentes stratégies ont été proposées, y compris l'utilisation de l'espèce hyperpolarisée comme 129Xe.

Le xénon est un gaz inerte avec un nuage d'électrons polarisable qui est très sensible à son environnement chimique. Sa capacité d'être hyperpolarisée permet d'obtenir un gain significatif de la sensibilité. Néanmoins, le xénon n'a aucune spécificité à une cible biologique, par conséquent, il a besoin d'être encapsulé et vectorisée. Des cages moléculaires différentes ont été proposées et nous sommes particulièrement intéressés à cryptophane qui est l'un des meilleurs candidats pour l'encapsulation du xénon.

Dans ce contexte, l'objectif de cette thèse est de concevoir des nouveaux cryptophanes qui peuvent être utilisés comme les plates-formes moléculaires pour construire des nouvelles bio-sondes de ^{129}Xe IRM utilisables pour l'imagerie *in vivo*. Pour cette raison, ces cryptophanes devraient être hydrosoluble et mono-fonctionnalisable.

Dans cette thèse, le polyéthylène glycol (PEG) est utilisé pour améliorer la faible solubilité de la cage moléculaire hydrophobe. Il y a également une discussion systématique des façons de casser la symétrie des cryptophanes et les stratégies différentes ont été tentées pour synthétiser cryptophanes mono-fonctionnalisé.

En conséquence, plusieurs cryptophanes PEGylés et mono-fonctionnalisés ont été obtenus et leurs propriétés d'encapsulation du xénon ont été testées.

Title : Conception and synthesis of the new cryptophane for the applications in xenon NMR molecular imaging

Keywords : cryptophane, hydrosolubilization and mono-functionalization

Abstract: Among all the imaging techniques, magnetic resonance imaging (MRI) offers several advantages owing to its low invasiveness, its harmlessness and its spatial in-depth resolution but suffers from poor sensitivity. To address this issue, different strategies were proposed, including the utilization of hyperpolarizable species such as ^{129}Xe.

Xenon is an inert gas with a polarizable electronic cloud which leads to an extreme sensitivity to its chemical environment. Its capacity of being hyperpolarized makes it possible to obtain a significant gain of sensitivity. Nevertheless, xenon has no specificity to any biological target therefore it needs to be encapsulated and vectorized. Different molecular cages were proposed and we are particularly interested in cryptophane.

In this context, the objective of this thesis is to design new cryptophanes which can be used as molecular platforms to construct novel ^{129}Xe MRI biosensors usable for *in vivo* imaging. To meet this demand, these cryptophanes should be mono-functionalizable and enough soluble in water.

In this thesis, the polyethylene glycol (PEG) group is used to improve the poor solubility of the hydrophobic molecular cage. And there is a systematic discussion of how to break the symmetry of cryptophanes and different strategies were attempted to synthesize mono-functionalized cryptophanes.

As a result, several PEGylated mono-functionalized cryptophanes were obtained and their properties for encapsulating xenon were tested.